# Studies in Palladium and Rhodium Catalysis: Synthetic Strategies for C–C Bond Formation


**Mark Power, B. Sc.**

A thesis presented for the degree of

Doctor of Philosophy

to

NATIONAL UNIVERSITY OF IRELAND, CORK

School of Chemistry

University College Cork

Supervisor: Dr Gerard P. McGlacken

Head of School: Prof. Anita R. Maguire

**2024**

# Table of Contents

# Declaration

This is to certify that the work I am submitting is my own and has not been submitted for another degree, either at University College Cork or elsewhere. All external references and sources are clearly acknowledged and identified within the contents. I have read and understood the regulations of University College Cork concerning plagiarism.

X _____

Mark Power 08 May 2024

# Preface

This thesis contains work which has been published after peer-review, or which is in the process of publication. Publications arising from this thesis are provided in the Appendix.

Chapter 1 of this thesis has been published (doi: 10.1002/ejoc.202300790). A further publication involving the one-pot Buchwald-Hartwig, C−H Activation process will emanate from Chapter 1. A publication involving the asymmetric addition of free N−H indoles to enones will be based on Chapter 2, and is in preparation. A further publication based on Chapter 2 will involve the subsequent addition of the indole N−H to the carbonyl to form novel tetracyclic compounds. In addition, I also spent some time during my PhD working on the alkylation of ketones in flow (doi: 10.1039/D3RE00229B) and writing a review article on organolithiums in flow (doi: 10.1021/acs.oprd.0c00090). This work has not been included in my PhD submission. All three publications are included in the Appendix of this thesis.

Yield is specified throughout, either as an isolated yield or a $^{1}$H NMR yield determined *via* 1,3,5-trimethoxybenzene as an internal standard. Conversion is used in cases where product and starting material $^{1}$H NMR peaks are measured relatively. When discussing asymmetric protocols, enantiomeric excess (e.e.) is used throughout the Introduction as is done so by the referenced publications. In the case our own work in Results & Discussion, the term enantiomeric ratio (e.r.) is used.

# Acknowledgments

Firstly, I want to thank my supervisor Dr Ger McGlacken for his supervision and guidance during the course of my PhD. Your mentorship and advice was always appreciated and I am extremely grateful for the opportunities I have had during my time in your research group. I would like to sincerely thank Prof Jonathan Burton and Dr Humphrey Moynihan for examining this thesis. I would like to thank the IRC and HEA for funding this research.

I would like to acknowledge the Administration Staff of the School of Chemistry, particularly Imelda, Claire, Mark and Donal for everything you've done to keep things running smoothly over the years. Thanks to Dr Dan McCarthy, Dr Lorraine Bateman and Dr Denis Lynch for NMR services and thanks to Dr Florence McCarthy, Dr Denis Lynch and Dr Ryan Alam for Mass Spec services. Thanks to Noel Browne for solvents, gases and elemental analysis. To Fran, thank you for the many weird, wonderful and practical discussions. You've been a fantastic person to have around for your tips, tricks and comprehensive knowledge on any equipment I ask you about. I'm looking forward to seeing how long it takes before you can make a glass swan. Thanks to Anna for always being such a friendly face around the Kane and for being so incredibly helpful for all things equipment related. Thanks to Ian & Trevor for always uplifting the spirits of postgrads and being great craic. Special thanks to Trevor for contacting me whenever Everton are playing awful, which means we talk far too often. Thanks to Tina & Denis for keeping the place ticking over, being incredibly helpful and always up for a chat. You are an excellent addition to the School of Chemistry and my time here wouldn't have been the same without your chats. Thanks to Nuala for stopping a mental fracture on more than one occasion. You are extremely generous and without your help I would still be changing methods on the HPLC only to see one peak! Thanks to Tom for everything you've done for me over the years. From helping me with every instrument I can name, to hammering me on the golf course, you've always made the bad stuff fun! You seem to have an encyclopaedic knowledge of all things sport and I would have gone off my rocker much sooner without you to chat with. Finally from the School Staff, I want to thank Derry Kearney for making me laugh whether it was appropriate to or not. You were extremely kind and patient in showing me all things glass blowing. You possess a phenomenal skill that will be fondly remembered.

I would like to thank Ryan for being such an enthusiastic early supporter of Reaction of the Week and for setting up Organic Discussions. You have an affection for chemistry that made

me laugh and learn, and for that I will always be grateful. Thanks to Denis for everything you do for everyone. I don't think I would be able to summarise all you do for the postgrads even if my acknowledgments were as long as my thesis, but thank you for making sure I stayed sane and that I always got my data! Your advice on all topics life and lab related was always appreciated. Thanks to Davy for being so welcoming when I joined the group. I learned so much from time spent in the lab with you and I think my appreciation is shown solely from the comments I put up with. Thanks for always making time during my PhD, no matter how 'hard-hatted' the question. Thanks to Kat for being an excellent person to learn from. Showing me how to do two columns at once will be a day I'll never forget! You were a great mentor to have and thank you for always answering every question, no matter how abstract. I would also like to thank Manuel for all the training, excellent advice, unparalleled patience and always being up for the craic.

Thanks to Ella for all your help with everything flow and lab related. You were a great person to work alongside. Thanks to Robyn for all the TBAA support and trauma, and for understanding that to get crystals to grow simply means dissolve them in DCM! To Dave, Muireann, Si Lok, Conor, MC, Emma, Ben, James, Geoffrey and Kishore and all members of 413, thank you for making the lab a wonderful place to come in to. Thanks to Michelle for making my uncle diabetic through the amount of honey he ordered. Thanks to Kev for the many times you made me cry with laughter, especially *the* F1 video. Thanks to Michelle O'D for taking up the mantle for Organic Discussions and always answering every question I have about every aspect of your sporting career. Thanks for Dara for enabling my obsessive following of the PGA tour and for being my playing partner to the formidable duo of Tom and Aidan multiple times. Also a special thanks to Aoife, Conor, Louise, Olga, Deirbhile, Josh, Emily, Rachel, Michael, Fiona, Becky, Eabha and Evan for making the place so entertaining and welcoming.

Emma, thank you for welcoming me to the PhD with unwillingly open arms. I don't think we could have got off on a funnier foot than our trip to Bury before I had even started. Looking back now, you had the patience of Mother Teresa. I had a fantastic time with you throughout our overlap in 413. You were always understanding, helpful, and you were often the only one to laugh at any of my jokes. To Aobha, thank you for all the necessary tough love – you will always be the one to show the way of *feerse*. I don't think there was anyone I turned to in time of panic more than you and thank for always offering, help, laughs and/or pistachio. I really don't think I would have got through the start of my PhD without both of your

presence in the lab, the constant voice notes, group laughter therapy and most importantly, the constant baked goods.

Edel, thank you for being such a good friend during our overlap on the 4th floor. You are the most positive person and thank you for always laughing at even the most terrible jokes. The tolerance you had for terrible chemistry humour should be studied. Orla, thank you for always being up for every trip to Sicilian, the spang new Bollés and for the one million times I was allowed look at your LabCup. More importantly, thank you for validating all complaints I had, no matter how wrong I was in the matter. Amy, thanks for making every problem fun. I think the best skill I learned from my time here was coping through laughter with you and your memes. Aidan, thanks for always being there since day dot when we got ridiculed for Reaction of the Week and I blamed the entire thing on you. I couldn't have asked for a better pal to awkwardly attend conferences with and I think that Lisbon tram will forever haunt our memories. You've been a great friend both in and outside the lab, and my time here would have been very different without you.

To Katie, Ciara and Eimear, thank you for being the best possible bunch of people. Katie, thank you firstly, for your inability to not find things funny. It may have put a strain on your relationship with Eimear, but it certainly strengthened ours! Thank you for your countless hours of advice about all things PhD – from presentation slide making to picking a place for coffee. Our combined inability to make a French press will live forever in my mind. Ciara, you are simply the funniest person I have ever met. I think your eyebrows could be a language on Duolingo. Thank you for all the listening you put up with (which is a lot) about mine and *everyone's* problems. I think you'll have a lifelong fear of polarimeters from association of my giving out. I loved offering vino, even unplanned coffee, to have your side-eye confirm yes to the plans. Eimear, you are the best person I could have been put beside on day one of this PhD. I cannot possibly summarise everything you have done for me during my time here. You are honestly a Swiss-army knife of a student, with a tongue as sharp as one. You have been a crucial pillar of getting through this weird journey and I know I have made a lifelong friend. I also know you enjoy my singing despite how quickly you turn the speaker on once I start. Thank you for every trip to Sicilian, every evening of Lumineers, every Word trick and tip, every reaction plan, every Spotify recommendation, every conference attended, every glass of wine and pint of Beamish and thank you for always being there.

Finally, to my family and friends, thank you for always supporting me with all my pursuits. To the 6 members of Exodia who will probably never see this, thank you for all your patience

and support over the years with my constant struggles of being a student. Clare, thanks for always finding humour in the most abstract of things. You are one of the most positive people I know and your weird messages always made me laugh, even on the bad days. Mom and Dad, thank you sincerely for always prioritising the pursuit of education. I know it was not easy and I really appreciate everything you've done for me during all the years leading up to this. I also want to thank my grandparents for always being so loving, inquisitive and kind. I could not asked for a better family set-up to support me. A special thanks to Niall for always dropping off apple tarts and laptops during my time in college, whilst also purchasing enough honey to make us all question if we're in the wrong line of work. You really are a sound engineer. Thanks to Jess for always wagging whenever I complained, you always understood.

Finally, thanks to Holly for all the continuous support throughout these long, long years. You've also provided perspective on what really is a bad day at work! You have been a constant source of comfort and encouragement during my PhD and I will always be grateful for your help in getting me to finish line. You've kept me sane and I love you for it.

*For Mom & Dad*

# Table of Abbreviations

| | |
|---|---|
| $[\alpha]^{T}_{D}$ | Specific rotation |
| $^{13}C$ NMR | Carbon nuclear magnetic resonance |
| $^{19}F$ NMR | Fluorine nuclear magnetic resonance |
| $^{1}H$ NMR | Proton nuclear magnetic resonance |
| Å | Angstrom |
| Ac | Acetyl |
| acac | Acetylacetone |
| AcOH | Acetic acid |
| AMLA | Ambiphilic metal ligand activation |
| API | Active Pharmaceutical Ingredient |
| aq | Aqueous |
| BINAP | 2,2'-Bis-1,1'-binaphthalene |
| Bn | Benzyl |
| Boc | Tert-butyloxycarbonyl |
| BOX | Bisoxazoline |
| Bpin | Bis(pinacolato)diboron |
| bpy | 2,2’-bypyridine |
| br s | Broad singlet |
| Bu | Butyl |
| BuLi | Butyl lithium |
| c | Concentration (for optical rotation) |
| ℃ | Degrees Celsius |
| ca | Circa, approximately |
| Calcd. | Calculated |
| cat. | Catalytic |
| cod | 1,5-cyclooctadiene |
| CMD | Concerted metalation-deprotonation |
| COSY | Correlation spectroscopy |
| CPME | Cyclopentyl methyl ether |

| | |
|---|---|
| d | Doublet |
| DCM | Dichloromethane |
| dcype | 1,2-Bis(dicyclohexylphosphino)ethane |
| Dd | Doublet of doublets |
| Ddd | Doublet of doublet of doublets |
| DMA | Dimethylacetamide |
| DMSO | Dimethyl sulfoxide |
| Deg | Degree |
| DEPT | Distortionless enhancement by polarisation transfer |
| DFT | Density Functional Theory |
| e.g. | For example |
| dppb | 1,4-Bis(diphenylphosphino)butane |
| dppe | 1,2-Bis(diphenylphosphino)ethane |
| dppf | 1,1'-Bis(diphenylphosphino)ferrocene |
| dppp | 1,3-Bis(diphenylphosphino)propane |
| dq | Doublet of quartets |
| dr | Diastereomeric ratio |
| dt | Doublet of triplets |
| E | Electrophile |
| EDG | Electron donating group |
| e.e. | Enantiomeric excess |
| Equiv. | Equivalents |
| e.r. | Enantiomeric ratio |
| Et | Ethyl |
| EWG | Electron withdrawing group |
| g | Gram (s) |
| GC | Gas chromatography |
| h | Hour(s) |
| HFIP | Hexafluoroisopropanol |
| HMBC | Heteronuclear multiple-bond correlation spectroscopy |
| HPLC | High performance liquid chromatography |
| HRMS | High resolution mass spectrometry |

| | |
|---|---|
| HSQC | Heteronuclear single-quantum correlation spectroscopy |
| Hz | Hertz |
| i.e. | That is |
| IR | Infrared spectroscopy |
| I.S. | Internal standard |
| *J* | Coupling constant |
| *k* | Rate |
| K | Kelvin |
| L | Litre |
| LRMS | Low resolution mass spectrometry |
| *m* | Meta |
| M | Molarity |
| m/z | Mass-to-charge ratio |
| Max | Maximum |
| Me | Methyl |
| MeCN | Acetonitrile |
| mg | Milligram |
| MHz | Megahertz |
| MIDA | N-Methyliminodiacetic acid |
| Min | Minute(s) |
| mL | Millilitre |
| mmol | Millimole |
| mol% | Mole percent |
| M.p. | Melting Point |
| MS | Mass Spectrometry |
| M.S. | Molecular sieves |
| n.d. | Not determined |
| NMP | N-Methyl-2-pyrrolidone |
| NMR | Nuclear magnetic resonance |
| qNMR | Quantitative nuclear magnetic resonance |
| *o* | Ortho |
| OAc | Acetate |

| | |
|---|---|
| o/n | Overnight |
| *p* | Para |
| Ph | Phenyl |
| PhD | Doctorate of Philosophy |
| PivOH | Pivalic acid |
| $PPh_3$ | Triphenylphosphine |
| ppm | Parts per million |
| Pr | Propyl |
| Prof | Professor |
| PTS | Polyoxyethanyl-α-tocopheryl sebacate |
| PQS | Polyethyleneglycol ubiquinol succinate |
| q | Quartet |
| quin | Quintet |
| Rf | Retention factor |
| rt | Room temperature |
| s | Singlet |
| sat. | Saturated |
| SDS | Sodium dodecyl sulphate |
| $S_EAr$ | Electrophilic aromatic substitution |
| sept. | Septet |
| sext. | Sextet |
| SM | Starting material |
| t | Triplet |
| *t* | Tert |
| T | Temperature |
| td | Triplet of doublets |
| THF | Tetrahydrofuran |
| TIPS | Triisopropylsilyl ether |
| TLC | Thin layer chromatography |
| TMS | Tetramethylsilane |
| TMSCl | Trimethylsilyl chloride |
| TPGS | α-Tocopheryl polyethylene glycol succinate |

| | |
|---|---|
| tR | Retention time |
| UV | Ultraviolet |
| δ | Chemical shift |
| ν | Frequency of max absorption |

# Abstract

This thesis concerns studies in palladium and rhodium catalysis for carbon-carbon bond formation. Chapter 1 involves the synergistic use of tetrabutylammonium acetate ($NBu_4OAc$) with palladium catalysis to expand on the synthesis of dibenzofurans *via* C-H activation. Dibenzofuran and its derivatives are ubiquitous and important medicinal and natural products. Many contain electron-rich aryl rings. Previously, we found that the well-established conditions, which promote C−H functionalisation through Concerted Metalation-Deprotonation (CMD), proved unsatisfactory for electron-rich diarylether precursors. Herein, we report a Pd-catalysed C−H functionalisation protocol that works with electron-rich arenes. We suspect that tetrabutylammonium acetate can act as base, ligand and solvent, rendering this protocol a simple and efficient route to electron-rich dibenzofurans. A variety of functionalised dibenzofurans are successfully accessed through this protocol. The methodology can be applied to benzochromenes, with varying degrees of success. However, this protocol can be expanded to enable a robust, one-pot Buchwald-Hartwig, C–H activation sequence to access biologically relevant indoloquinoline scaffolds from simple building blocks.

In Chapter 2, rhodium-catalysed asymmetric conjugate additions are performed with indolyl boronic acids. The indole ring system represents one of the most abundant and important heterocycles in natural products, Active Pharmaceutical Ingredients (APIs), drugs and other materials. The prominence of indole compounds makes efficient protocols to derivatise the heterocycle highly desirable. A particular importance is placed on asymmetric protocols and utilising unprotected (NH) variants. Herein, we report a Hayashi-Miyaura-type Rh-catalysed asymmetric conjugate addition using free NH indole boronic acids and enones. Each position on the carbocyclic backbone of indole can be accessed, with a variety of enones. Yield of up to 94%, and e.r. values up to 99:1 can be achieved using mild reaction conditions. Furthermore, a 1,2-addition to benzil can be performed in excellent yield and e.r. Finally, a one-pot conjugate addition and intramolecular cyclisation of 7-indolyl boronic acid allows for the synthesis of a novel tetracyclic indole, similar to that found in natural products.

# Chapter 1

# Access to Electron-Rich Dibenzofurans through $NBu_4OAc$-Mediated Palladium Catalysis

*The path ahead*

*The path behind*

*It’s moon water*

# 1. Introduction

## 1.1. The Aryl–Aryl Bond

The aryl–aryl bond is a prominent molecular feature of compounds throughout the agrochemical, material chemistry and pharmaceutical industries. Some examples in natural products and active pharmaceutical ingredients (APIs) are depicted below in Figure 1. The ubiquity of this structure has inspired the development of a plethora of highly efficient synthetic methods to forge an aryl–aryl connection.[1,2]

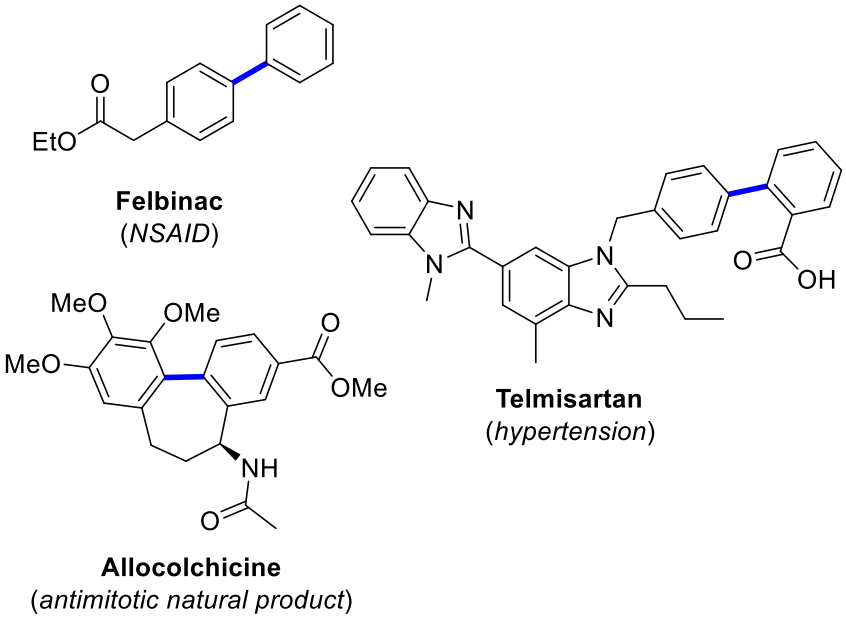


**Figure 1** Examples of the aryl–aryl bond in natural products and APIs

Organic chemistry went through a paradigm-shift between 1960-80's, where chemists globally began to realise the power of palladium (Pd). Initially, the field of organometallic chemistry was focused on the catalytic capabilities of nickel and copper. To chemists, palladium was considered 'useless' and was sold as a steel reinforcement. However, through the renowned pioneering work of Richard F. Heck and Pat Henry, palladium was put in the spotlight as an efficient metal catalyst for organic transformations. It was soon found that Pd could do a lot that Ni could not (and *vice versa*!) and through a short, publication-saturated timeline, palladium came to the forefront as the king of metals for organometallic catalysis.[3] Heck,[4] Neigishi,[5] Suzuki and many other excellent chemists led the way in this field, many similar bodies of work being published almost simultaneously, as a new research space was

well and truly opened. Even now, palladium-mediated processes continue to permeate the research space. While some work is dedicated to streamlining existing methodologies, even in recent months, new transformations have been discovered and published. A survey in Organic Process Research & Development highlighted how of 212 API syntheses, 92 of them contain at least one transition-metal catalysed step. Of these transition-metal catalysed steps, palladium accounted for over 81% of the transformations.[6] Consequently, the focus on continually developing palladium-catalysed protocols is of key significance.

Advancements in this field are mainly focused on reducing the drawbacks or prerequisites for the transformations to take place; namely the activation of coupling partners. Initially, coupling partners were restricted to organolithiums or Grignard reagents with aryl halides.[3] Through time, these reagents developed through different, more robust elements identified originally by Neigishi;[5] Tin (Stille), Zinc (Neigishi) and Boron (Suzuki). These traditional cross-couplings require two preactivated partners and are depicted in Scheme 1. Despite the effective and practical nature of these reactions, they do have associated drawbacks. The requirement to have both coupling partners pre-functionalised results in stoichiometric halide and organometallic waste, poor atom economy, a step-increase to the final product and an increase in cost.

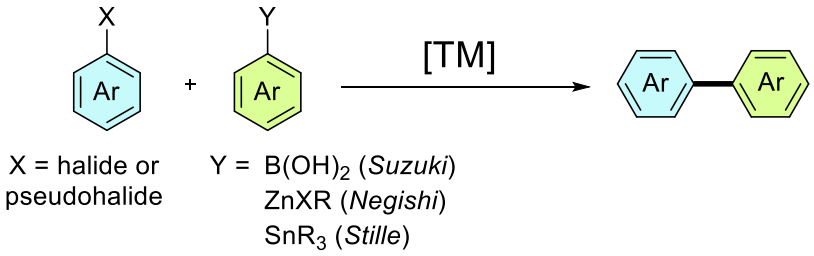


**Scheme 1** Traditional means of accessing an aryl–aryl bond

In recent years, advances have been made in the field to enable a potentially more environmentally benign and cost-effective approach. These advances generally concern one C–H activation event, which is referred to, in this case, as direct arylation.[2] Direct arylation involves the synthesis of a biaryl motif where the carbon–carbon bond formed arises from the cleavage of a C–H bond, aided by a transition metal. It is worth noting that the terms C–H activation and C–H functionalisation are used interchangeably. Direct arylation protocols aim to remove the prerequisite for functionalisation on one of the two coupling partners involved in aryl–aryl bond formation (Scheme 2a). This potentially, in turn, allows for a

reduction in waste generated and reduces the number of steps and cost of the reaction sequence.[1,2,7–9] This allows the waste by-products of traditional cross-couplings to be greatly decreased and as a result, modern methods to access molecular structures *via* C–H activation were published on the 'Wanted List' of top pharmaceutical companies.[10]

Ideally, this concept could be expanded to couple two C–H bonds, an approach referred to as double C–H activation, where the only by-products are potentially hydrogen gas or water (Scheme 2b). However, an inherent drawback to this transformation is the selectivity (and consequently, the efficiency) of the transformation, as there are often multiple C–H bonds present in any organic molecule. This approach also requires a stoichiometric oxidant to proceed. Additionally, the strength of C–H bonds means that this reaction is thermodynamically disfavoured.[11,12]

As such, a form of chemical compromise is reached where one partner is preactivated with a suitable handle (e.g. halide) and the other arene bears the C–H bond. The selectivity of this transformation can be controlled by employing specific ligand/catalyst systems or by the manipulation of steric effects and the inherent electronic properties of the substrates.[13]

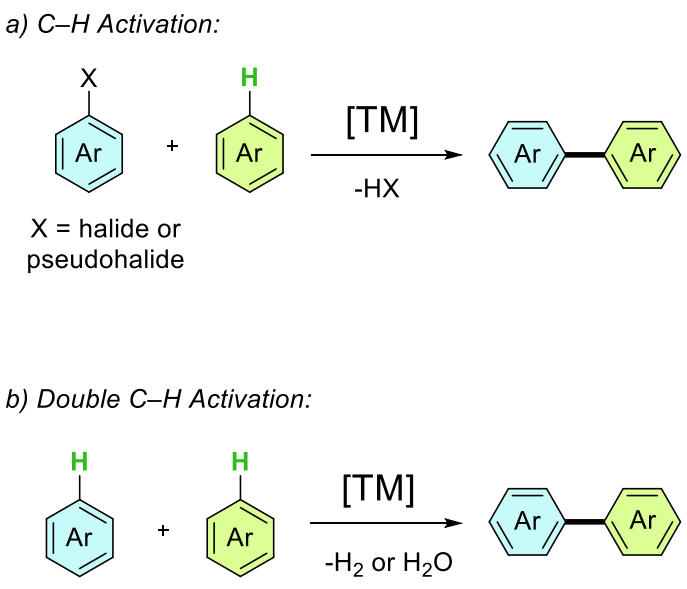


**Scheme 2** C–H Activation strategies as advancements in aryl–aryl bond formation

## 1.2. Direct arylation via C–H activation

The harsh conditions required, such as high temperatures, high loadings of transition-metals and the potential requirement for strong redox reagents[7,12] means that the functional group tolerance and applicability to substrates is often low. Efforts are being continuously made towards making the reaction conditions for C–H activation protocols milder to increase the scope of substrates and transformations.[7]

The mechanism by which aryl–aryl bonds are forged can be depicted generally as a three-step sequence, whether considering traditional cross-couplings or direct arylation protocols. Firstly, oxidative addition of the organohalide (or pseudohalide) to $Pd^0$ gives the $Pd^{II}$ species. This $Pd^{II}$ intermediate can then undergo transmetalation to give another $Pd^{II}$ species with a salt by-product, where the other aryl residue is installed at the metal centre. Finally, reductive elimination yields the biaryl product and regenerates the active $Pd^0$ species for another cycle (Figure 2).

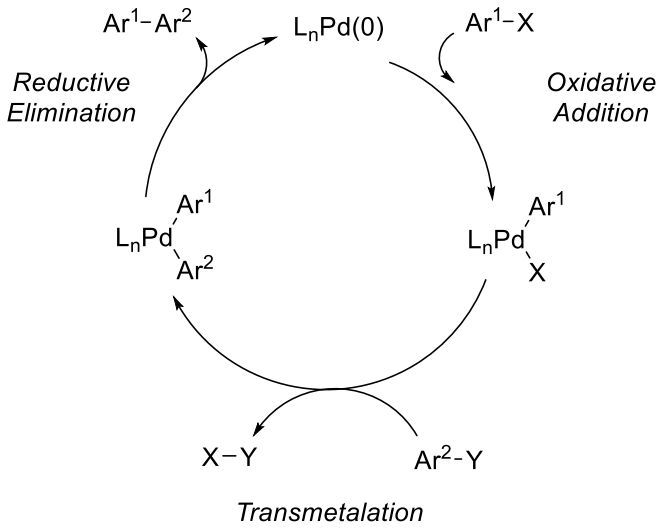


**Figure 2** Generic catalytic cycle for Pd-catalysed cross-couplings

Several general mechanistic modes for transition metal-mediated C–H activation processes have been proposed, such as electrophilic aromatic substitution ($S_EAr$)[14,15] concerted metalation-deprotonation (CMD),[16–24] and σ-bond metathesis.[25,26]

The generally accepted mechanism for a CMD-type process is illustrated below using an *o*-brominated diaryl ether to furnish a ring-closed dibenzofuran product (Scheme 3). Fagnou,

Echavarren and MacGregor, in particular, carried out pioneering work in the reporting and exploration of substrates applicable to CMD-type mechanisms. In 2005, MacGregor reported a new means of aryl–aryl bond formation mechanism, coined AMLA.[27] This report was within a year span of other analogous publications deciphering this mechanism. On top of proposing a new pathway for this chemistry, it offered an alternative means to how some electron-rich heterocycles underwent this transformation as it was generally accepted that these substrates worked *via* an $S_EAr$ mechanism. In 2012, Fagnou reported an investigation into the C–H cleavage step, resulting in the ability to classify aromatic C–H substrates.[18] This resulted in the creation of three classes, depending on what factors influenced the C–H cleavage. For Class I arenes, the regioselectivity of C–H bond functionalisation is controlled by the difference in the arene distortion energies. Class II includes the (hetero)arenes for which interaction energies with the metal catalyst are the determining factor. Class III arenes are the (hetero)arenes in which both the distortion and interaction energies influence the C–H bond functionalisation.

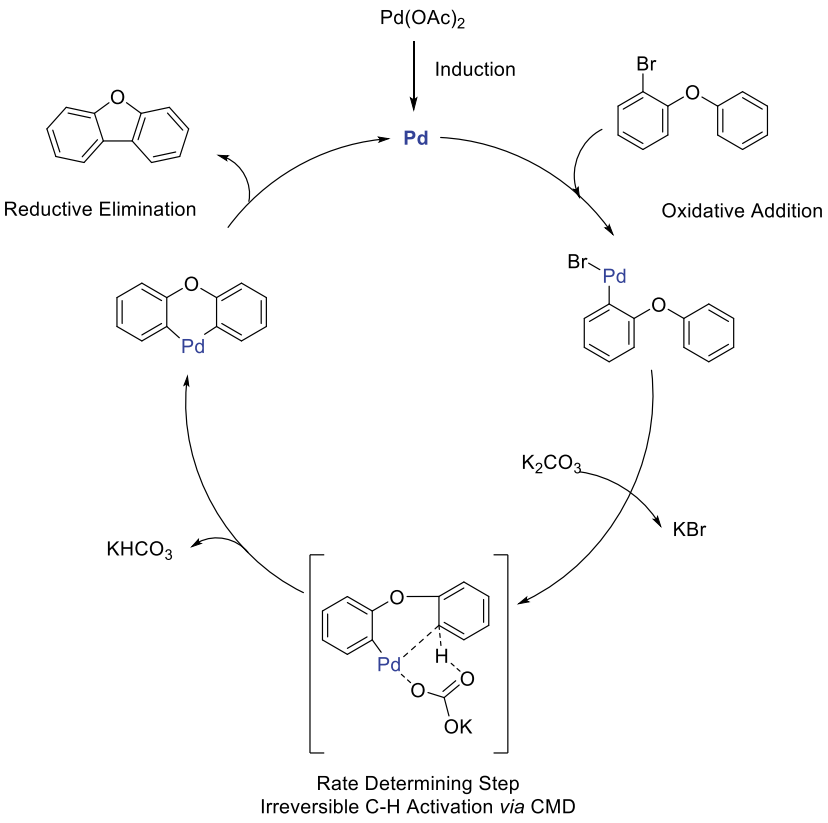


**Scheme 3** CMD mechanism proposed for *ortho*-halogenated diaryl ethers to generate dibenzofurans

Since this seminal work, a large volume of research has been reported describing transformations which occur *via* CMD mechanistic pathways.

## 1.3. Dibenzofurans

As mentioned previously, the aryl–aryl bond is a common molecular feature of a plethora of medicinally relevant and naturally occurring compounds.[28] Dibenzofuran is a molecular structure containing the biaryl feature. Despite its simplicity, the dibenzofuran motif is often a coveted framework due to its potential for biological activity.[29] Additionally, the field of organic semiconductors and electronics utilises dibenzofurans.[30–33] Dibenzofurans exhibit good charge-transport properties and high thermal stability, making them attractive targets for this field. Dibenzofurans have also been of use in coordination chemistry, acting as ligands.[34] Finally, this framework has a large breadth of biological activity, with reports of structures containing the motif providing anti-inflammatory,[35,36] anti-bacterial,[37,38] and anti-cancer [39,40] abilities, to name a few. Throughout the last decade, there has been a plethora of research published to expand the routes which allow access to dibenzofurans.[41] They examine new methodologies utilising previously unreported functionalities and reagents to access these structures. To access the dibenzofuran skeleton, a variety of different transformations are available. A C–O bond can be formed using C–H activation or through the displacement of leaving groups, or when considering C–C bond formation, direct arylation by displacement of various leaving groups or dehydrogenative coupling utilising double C–H activation.[41] A prominent protocol involves the use of *o*-halogenated diarylethers with Pd catalysis to furnish dibenzofuran through cyclisation. Select examples of these common routes are depicted in Scheme 4. There exists a myriad of methodologies to access this framework. In over 120 publications from the last 15 years, 50 different, distinctive means of accessing this scaffold have been reported.[41]

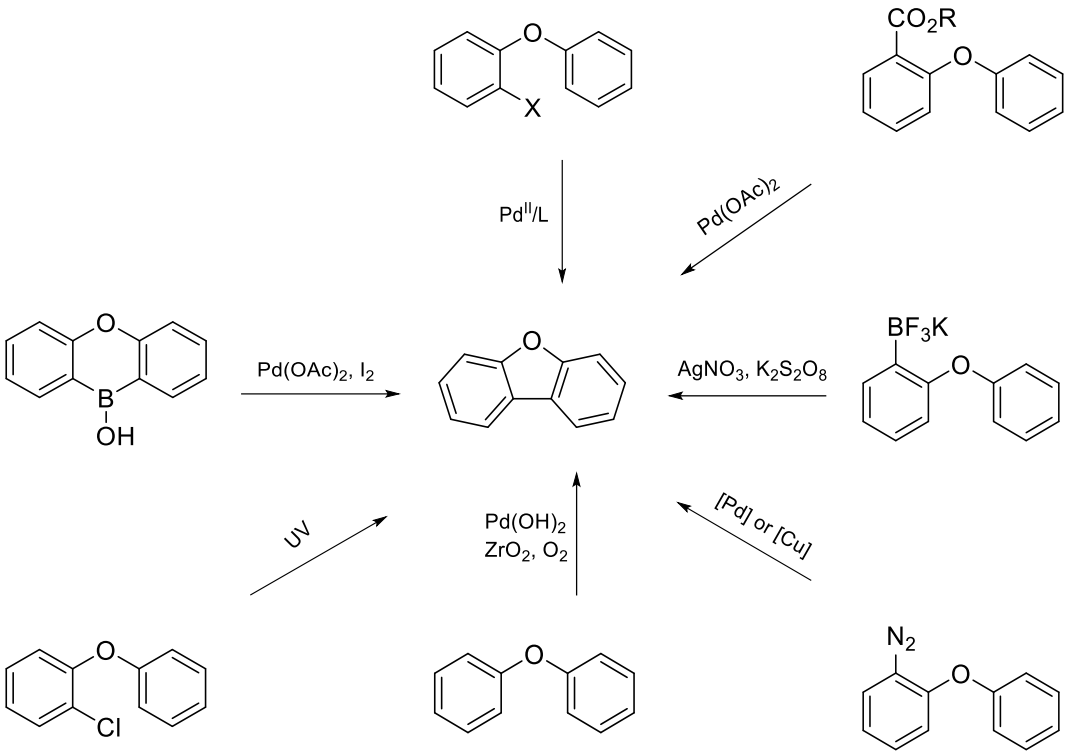


**Scheme 4** Routes to dibenzofuran from diarylethers

### 1.3.1. Dibenzofuran Synthesis *via* C–H Activation with *o*-Halogenated Diarylethers

This introduction aims to highlight the synthetic utility of the diaryl ether precursor as an entity to access dibenzofuran. Using an *ortho*-halogenated diaryl ether precursor is one of the most common protocols to synthesise dibenzofurans. The seminal work was reported by Ames and co-workers in 1983 (Scheme 5). Using $Pd(OAc)_2$ and $Na_2CO_3$ in DMA, these *o*-brominated diaryl ethers could be successfully ring closed under an inert atmosphere at high temperatures. However, the scope of substrates was very limited and only 8 successful substrates were reported.[42]

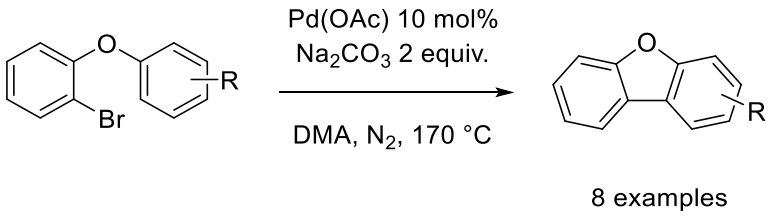


**Scheme 5** Seminal work in the synthesis of dibenzofurans from *o*-halogenated diarylethers

In 2005, Fagnou and co-workers reported the use of *N*-heterocyclic carbene ligands to enable ring closure of diarylethers using aryl chloride functional groups and low loadings of palladium catalyst (Scheme 6).[43] Using this methodology, the scope of *o*-halogenated diaryl ethers suitable for cyclisation to dibenzofuran was significantly expanded. Additionally, this work permitted the use of aryl chlorides rather than aryl bromides as synthetic precursors. Despite an increase in functional group tolerance, high temperatures and an inert atmosphere were still required.

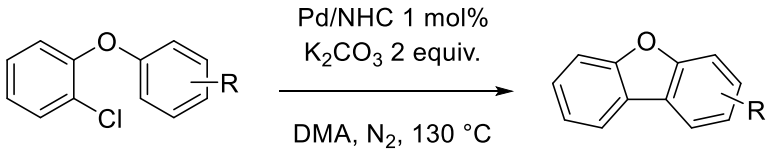


**Scheme 6** Expansion of diarylether substrates by employing NHC ligands for Pd-catalysed ring closures

In a subsequent publication, Fagnou showcased how the addition of a phosphine ligand to the system could facilitate the intramolecular cyclisation of *o*-halo benzyloxy ethers to form six-membered rings (Scheme 7).[44] This methodology was successfully applied using aryl chloride, bromide and iodide starting materials. The work was also extended to include the synthesis of dibenzofurans through the use of *o*-iodo diaryl ether, when silver salt additives were added. Through the work of Fagnou, it is evident that the choice of ligand has a fundamental effect on the reaction success. The use of a phosphine ligand in this case allowed the breadth of substrate functional groups to be significantly broadened. However, these strategies required an inert atmosphere.

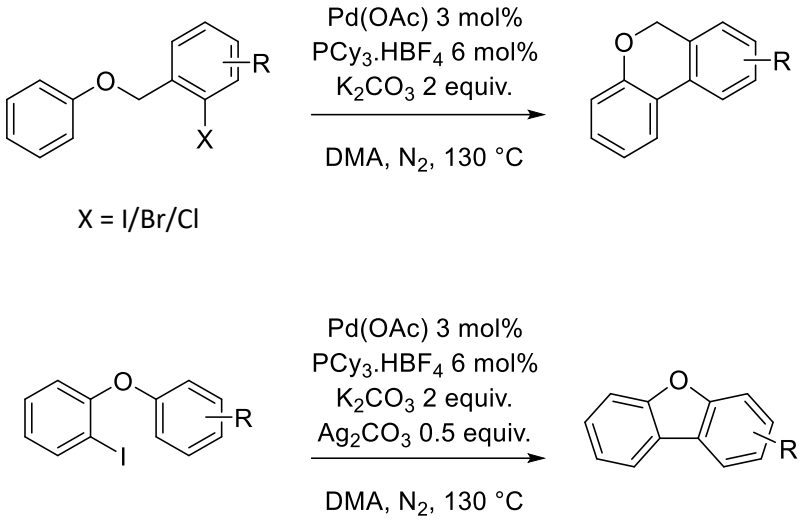


**Scheme 7** The use of phosphine ligands in the intramolecular C–H activation cyclisation of diarylethers

As mentioned previously, the common mechanism which underpins most of this C–H activation chemistry is a CMD pathway. This mechanism usually relies on the 'acidity' of the aryl C–H bond and thus, is less applicable to electron-rich substrates. Therefore, an inherent limitation to this traditional chemistry is the lack of efficiency found when the aryl rings of the precursor bear electron-donating substituents. However, naturally occurring and medicinally relevant dibenzofuran derivatives frequently contain electron-rich aryl rings and electron-donating groups (Scheme 8). The desire for chemists to synthesise dibenzofuran rings is to apply them medicinally and expand the space of drug discovery. Thus, a protocol which could intramolecularly cyclise electron-rich diarylethers to their corresponding dibenzofurans is highly coveted.

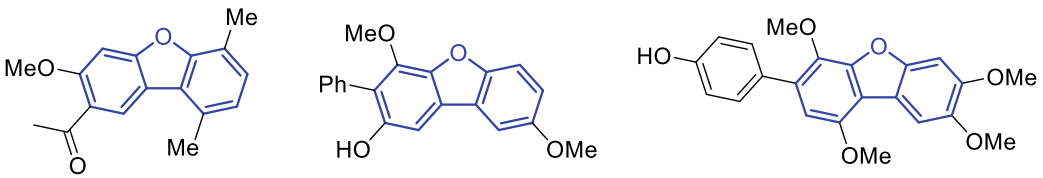

Ruscodibenzofuran Kehokorin *E* 3,4-dimethoxycandidusin

**Scheme 8** Examples of naturally occurring, electron-rich dibenzofurans

Along with of the lack of substrate scope compatibility, many of the existing methodologies suffer from:

i) High catalyst loadings

ii) Inert atmosphere requirement

iii) Additional additives

iv) Difficult purification

Previous work within our group has contributed to improving the synthetic protocols for dibenzofuran synthesis. One report details a palladium-mediated intramolecular direct arylation reaction that uses a readily available quinoline ligand (Scheme 9).[45] A decent range of dibenzofurans was accessed using this chemistry. However, when electron-rich substates were tried, the methodology was less efficient. Attempts to investigate electron-donating functionalities on the aryl-ring bearing the bromide atom led to a mixture of degradation products. A large optimisation study, using harsh, forcing conditions was required to get even moderate yield of the desired electron-rich dibenzofurans. It was postulated that oxidative addition into the C–Br bond for these substrates would be particularly sluggish due to the electron-rich nature of the aryl rings. It is understood that electron-poor aryl halides undergo oxidative addition with palladium metal much more readily than their electron-rich counterparts.[46] Thus, slow oxidative addition was likely a cause of reaction failure as this gave the catalyst time to fall off-cycle and degrade to Pd-black. This was observed even when bulky phosphines, which are known to promote oxidative addition, were used.

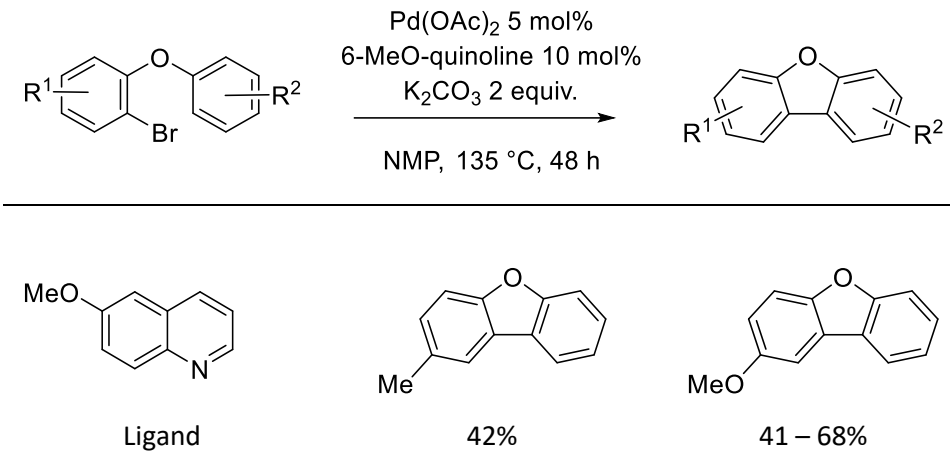


**Scheme 9** Previous work within the McGlacken Group

Other efforts towards advancing the use of *o*-halogenated diarylethers in the synthesis of dibenzofurans have been published in recent years. Panda and co-workers describe a more traditional approach to accessing dibenzofuran structures.[47] This publication depicts a facile method to synthesise *o*-iodo diarylethers from phenols (Scheme 10). Initially, the authors utilise a novel means to access these halogenated diarylethers through coupling electron-poor phenols with aryl iododiacetates. Subsequently, a C–H activation event on these substrates allows access to dibenzofurans. In particular, the authors show how very low loadings of Pd/C can be used in the reaction to achieve a high reaction efficiency. Additionally, the authors highlight how the Pd/C can be removed by filtration and reused in subsequent reactions. Despite the high yields observed using this protocol, this chemistry is limited to electron-withdrawing group functionalities, like many of the existing C–H activation methods.

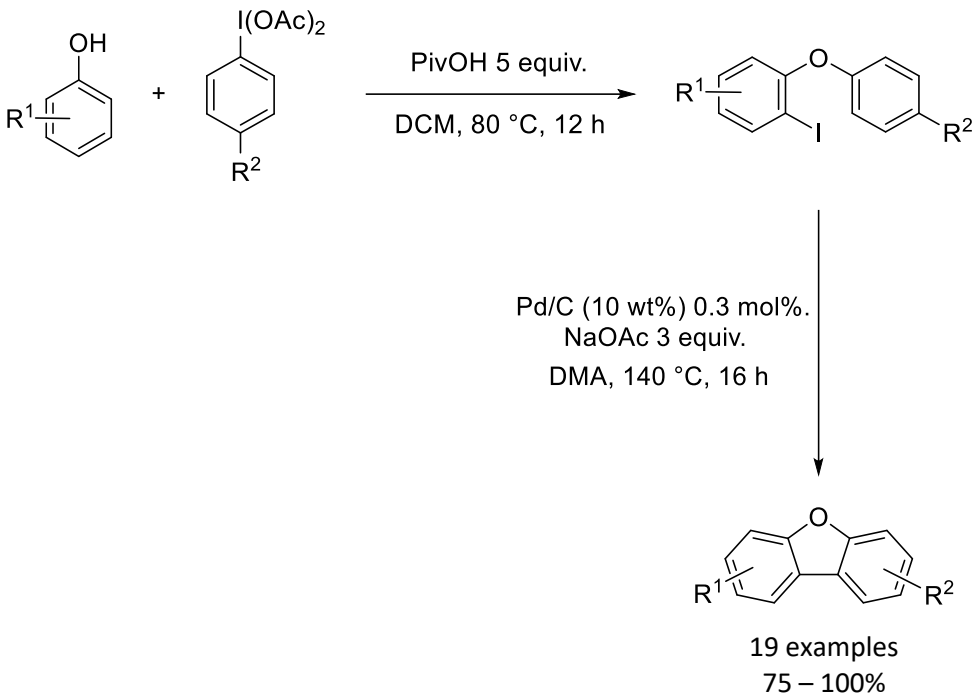


**Scheme 10** The one-pot synthesis of dibenzofurans from phenols and iododiacetates

Xu and Fan described a one-pot procedure to access dibenzofurans by reacting aryl halides with *o*-bromophenols.[48] Initially, an $S_NAr$ reaction occurs to forge the C–O bond which then undergoes a Pd-catalysed intramolecular cyclisation to afford the desired dibenzofuran (Scheme 11). A simple ligand ($PPh_3$) was used in conjunction with $Pd(OAc)_2$ for C–H activation. Very short reaction times (0.75 h) were required for this step. Excellent yields

were realised with this protocol although there are some limitations with substrate scope, as many of the arene precursors required *o*- or *p*-$NO_2$ groups.

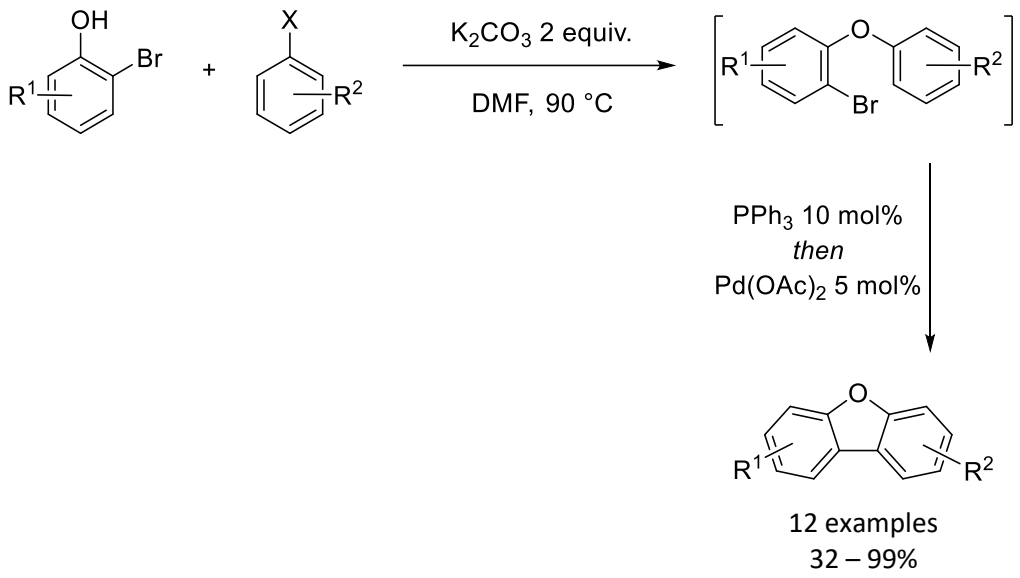


**Scheme 11** The one-pot synthesis of dibenzofurans from a $S_NAr$ followed by an intramolecular palladium-catalysed cyclisation

The remainder of this Introduction will summarise existing means of accessing the dibenzofuran scaffold and derivatives thereof. These protocols can be simply subdivided into carbon–oxygen or carbon–carbon bond formation. The associated drawbacks and advantages of each methodology will be highlighted. For the methods concerning carbon–carbon bond formation *via* C–H activation, the inability to employ electron-rich starting materials is a recurring theme.

### 1.3.2. Dibenzofuran Synthesis via Carbon–Carbon Bond Formation

Forging a carbon–carbon bond using C–H activation of an *ortho*-functionalised diarylether in the synthesis of dibenzofurans is perhaps the most common means of accessing this scaffold. The leaving group installed in this precursor is commonly a halide (as discussed earlier) but can also include carboxylic acids, tosylates, mesylates, pivalates, silanes or boron functionalities. For the purpose of this Introduction, select examples of leaving groups used in C–H activation to construct dibenzofurans will be highlighted.

In 2020, McGlacken and co-workers reported a palladium-catalysed intramolecular arylation *via* C–H activation using quinoline ligands, rather than the traditional phosphine ligand pairing for palladium chemistry (Scheme 12).[45] Using simple reaction conditions and a 6-methoxy quinoline ligand, dibenzofurans were afforded in excellent yields without the requirement for a phosphine ligand additive. However, despite the success of this protocol, again only electron-withdrawing diarylether precursors were tolerated.

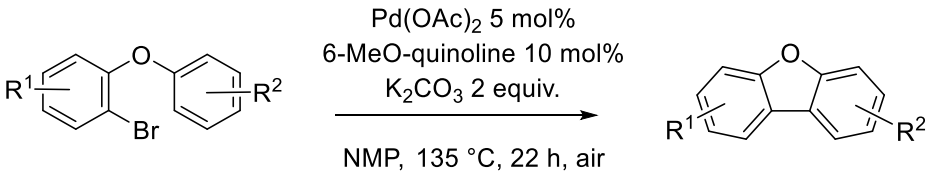


**Scheme 12** Phosphine-free synthesis of dibenzofurans via C–H activation of *ortho*-bromo diarylethers

Baran and co-workers describe a robust radical cyclisation of aryl boron species to furnish fluorenones and dibenzofurans.[49] This Pschorr-type or borono-Pschorr reaction uses boronic acid or trifluoroboronate salt precursors with catalytic silver nitrate and stoichiometric potassium persulfate to generate tricyclic scaffolds (Scheme 13). These reactions are operationally practical as they can take place in water and air and can be performed effectively on gram scale. The authors report a small scope of dibenzofurans, in moderate yields. The mechanism of action is still being investigated but it is thought that silver cation mediates decomposition of $S_2O_8^{2-}$ to give two radical species of $SO_4^{\bullet-}$. This radical subsequently attacks boron followed by homolysis of the weak carbon–boron bond. The aryl radical formed can then undergo cyclisation through the C–H bond of the other arene.

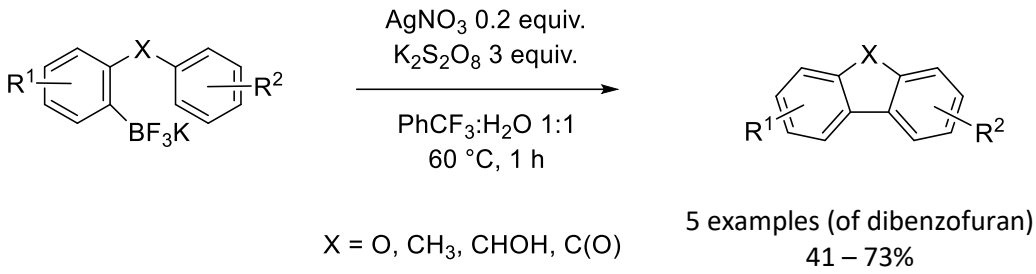


**Scheme 13** The synthesis of dibenzofurans using a Pschorr-type reaction

Glorius and co-workers published a unique route to dibenzofurans from benzoic acids using a tandem decarboxylation, C–H activation strategy (Scheme 14).[50] The authors postulated a transition-metal catalysed decarboxylation to start the mechanistic cycle which enables a typical C–H activation pathway. The addition of Cu or Ag salts was envisaged to assist the decarboxylation while also acting as suitable oxidants for the C–H activation step. Using harsh conditions of 15 mol% $Pd(TFA)_2$, DMSO additive and 150 ˚C, a good range of electron-poor and electron-rich dibenzofurans were accessed in good yields and impressive selectivity.

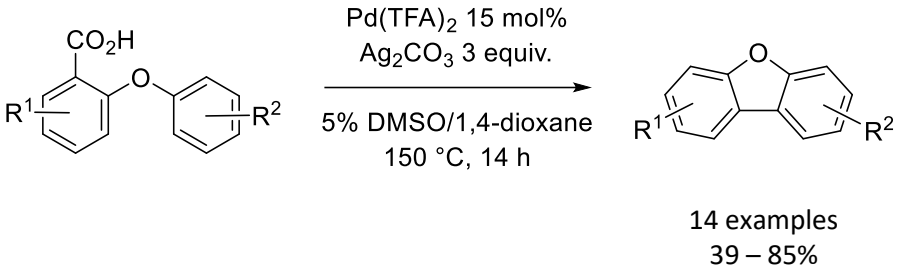


**Scheme 14** The decarboxylative cyclisation of benzoic acid diaryl ethers to furnish dibenzofurans

Fu and co-workers showcase the use of borylation to access dibenzofurans through a stepwise synthesis of dibenzoxaborininols from diarylethers followed by a palladium-catalysed intramolecular C–C bond formation (Scheme 15).[51] The obvious limitations of this process reside in the practicality of the synthesis as inert conditions, cryogenic temperatures and hazardous reagents such as alkyllithiums are required. Despite these inherent drawbacks, this chemistry does open up other synthetic avenues as the dibenzoxaborininols are valuable reactive intermediates for other transformations. Additionally, the scope of dibenzofurans accessed was large and high yielding regardless of substituent type.

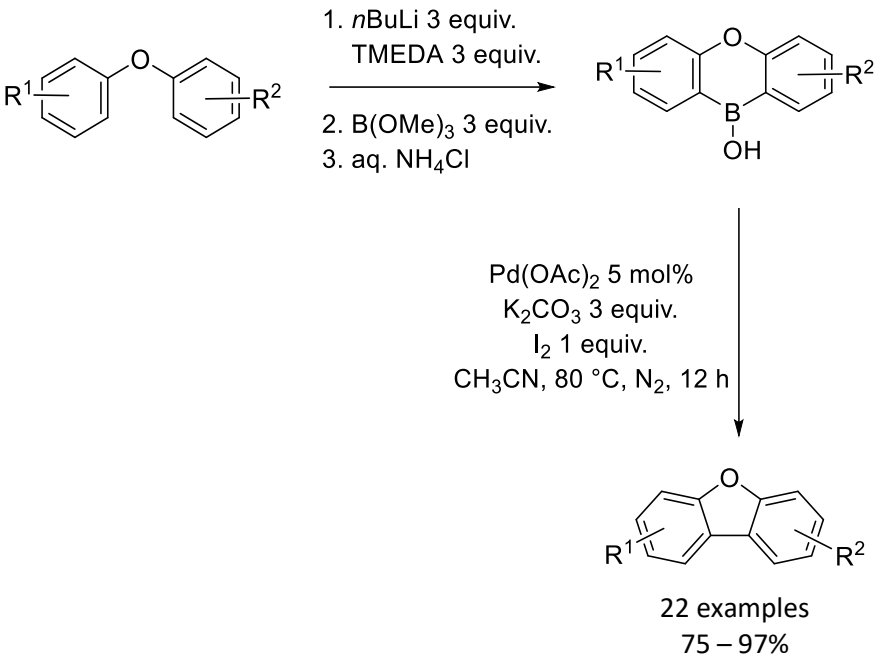


**Scheme 15** The synthesis of dibenzofurans from dibenzoxaborininols

Kalyani has described numerous reaction protocols where tosylates[52] mesylates[52,53] and pivalates[54] can be employed as leaving groups in the C–H activation of diarylethers. By employing a $Pd(OAc)_2$ catalyst, dcype as a ligand and with $Cs_2CO_3$ and CsOPiv as a base and additive, the authors could prepare a series of dibenzofurans from tosylated precursors with both electron-rich and electron-poor functionalities (Scheme 16). Excellent selectivity was observed under these conditions, in favour of the least sterically hindered site on the substrate. The cyclisation of mesylate compounds was also investigated (Scheme 17). For successful cyclisation using these mesylate compounds, the catalyst and ligand loadings had to be doubled, in comparison to the tosylated diarylethers. The base also had to be changed to $Rb_2CO_3$ from $Cs_2CO_3$. Under these conditions, the mesylated precursors could also be ring closed in high yields. Additionally, the authors showcased how a one-pot tosylation or mesylation of phenols, followed by a subsequent cyclisation, could be performed to furnish dibenzofurans in good yields. The work was also expanded to diarylamines which could be cyclised to afford carbazole products.

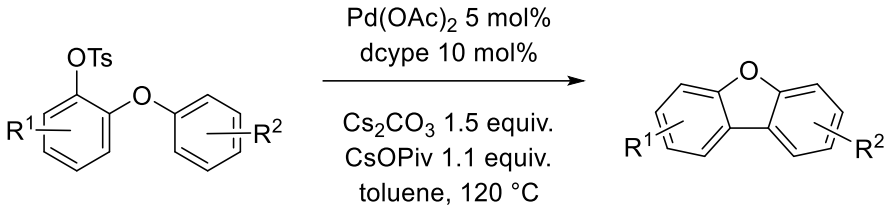


**Scheme 16** The use of tosylates as leaving groups in the C–H Activation cyclisation of diarylethers

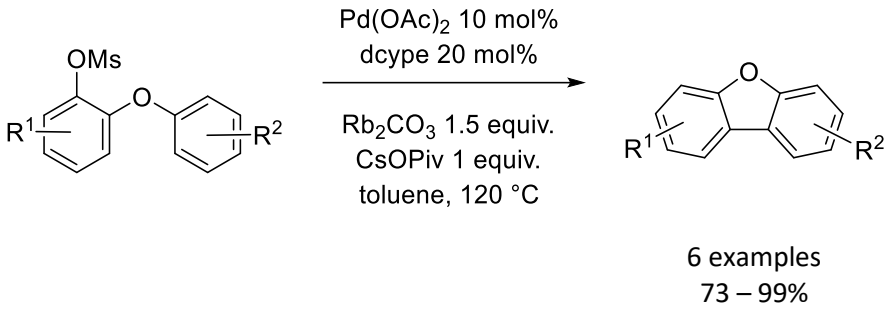


**Scheme 17** The use of mesylates as leaving groups in the C–H Activation cyclisation of diarylethers

Kalyani also reported on the use of pivalates as substrates in C–H activation cyclisations of diarylethers.[54] However, this reaction was facilitated by nickel rather than palladium catalysis. Using $Ni(COD)_2$, dcype and $Cs_2CO_3$ in xylene, the diarylethers bearing internal pivalates were successfully cyclised to furnish dibenzofurans (Scheme 18). Both electron-donating and electron-withdrawing substituents were tolerated under these conditions. However, the yields of the protocol were often reduced due to the persistent formation of proto-deoxygenated diarylethers. Other leaving groups were also explored, but gave substantially lowered yields.

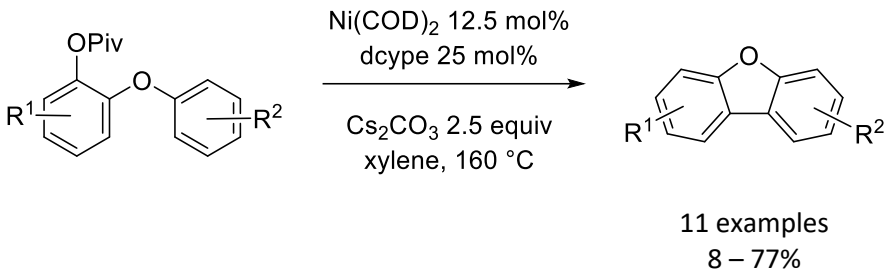


**Scheme 18** The use of pivalates as leaving groups for nickel catalysed cyclisations of diarylethers

### 1.3.3. Dibenzofuran Synthesis via Carbon–Oxygen Bond Formation

In 2011, Liu and co-workers showcased the first example of accessing dibenzofurans through C–O bond formation using a C–H activation approach. The protocol reported exceptional yields for a comprehensive scope of substrates, natural products and pharmaceutically relevant intermediates (Scheme 19).[55] The chemistry relies on a specific choice of oxidant. As mentioned, up to this point, intramolecular coupling of phenols with C–H bonds had not been reported. This was due to the fact that reductive elimination from the C–O Pd(II) intermediate is difficult to induce and phenols are not stable to strong oxidants. In fact, the authors noted that the reaction success was a serendipitous discovery when one of the reactions was unintentionally trialled in air. Interestingly, the authors were able to isolate a four-coordinate Pd(II) complex carrying an anionic pivalate ligand (Scheme 20). Key to reaction optimisation was the identification and isolation of this intermediate. The authors report the use of a myriad of phenolic precursors, which exhibited exceptional tolerance to electronic and steric hurdles.

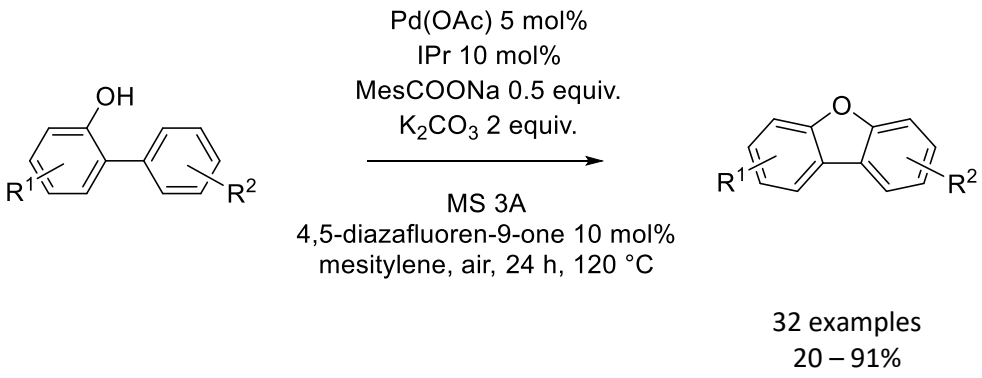


**Scheme 19** The synthesis of dibenzofurans from biaryl phenolic precursors

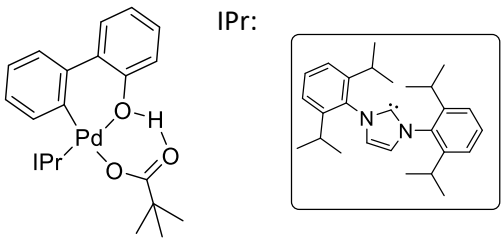


**Scheme 20** The key Pd-intermediate in the cyclisation of biaryl phenols

Using a similar approach, Wei and co-workers reported a means to oxidatively cyclise 2-arylphenols to their corresponding dibenzofurans *via* Pd(II)/peroxybenzoate catalysis (Scheme 21). The authors suggest that the use of peroxybenzoate enables a Pd(II) Pd(IV)

catalytic cycle. Using this system, a considerable range of dibenzofurans was efficiently synthesised in moderate yields. The work differs from that previously described in that Liu uses air as an oxidant (rather than peroxybenzoate) and that Liu's procedure requires additional additives, intricate ligands and molecular sieves. Interestingly, the work mechanistically follows what has been previously reported for these 2-arylphenol intramolecular cyclisations where the limiting step concerns the C–O bond cleavage. However, deuterium studies and KIE investigations by Wei show that their corresponding protocol is mechanistically different and unusually limited by the cleavage of the C–H bond.

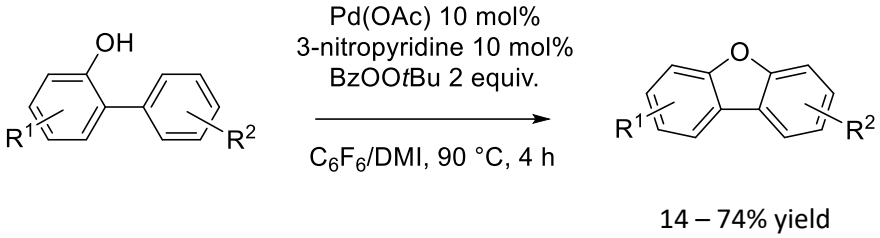


**Scheme 21** The synthesis of dibenzofurans from biarylphenols using Pd-catalysis

Liu and co-workers developed a procedure to synthesise dibenzofurans from cyclic diaryliodonium triflates and water (Scheme 22).[56] This work uses a phenanthroline ligand and copper catalyst to yield the product *via* oxygen-iodine exchange using water. This protocol is an example of how dibenzofurans can be synthesised *via* C–O bond formation. Good to excellent yields were observed for a range of simple dibenzofuran scaffolds. Substitution patterns at the *ortho*, *meta*, and *para* positions for electron-donating and electron-withdrawing groups were all tolerated. Fused tetra- and pentacyclic starting materials were also employed to yield interesting polycyclic products in moderate yield. Finally, when a thiophene-fused ring was employed, the corresponding sulfone product was afforded in a moderate 50% yield, giving access to organic field-effect transistor materials. Isotopic labelling studies using $H_2O^{18}$ showcased how the oxygen atom of the resulting dibenzofuran is derived from the water in the system. Additionally, when the reaction is performed in the absence of $H_2O$, no product is observed.

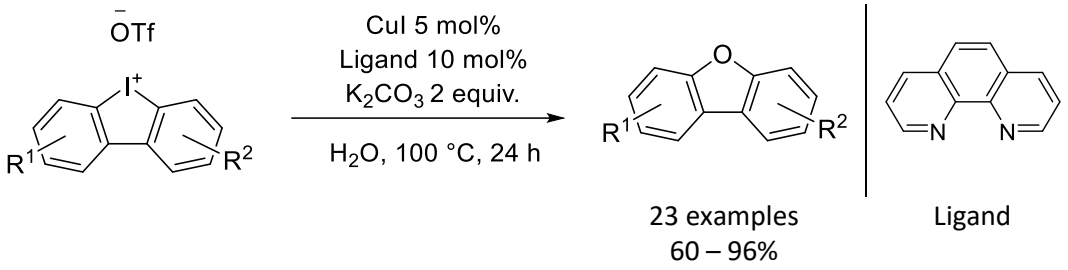


**Scheme 22** Synthesis of dibenzofurans via diaryliodonium triflates

More recently, Clarkson and Roesner described an effective synthesis of dibenzofurans by a metalation, Negishi cross-coupling and $S_NAr$ reaction sequence using aryl fluorides (Scheme 23).[57] Although a clever protocol, the reactions are only mildly tolerable to certain functionalisation on the aryl rings of the precursors in the case of dibenzofuran synthesis.[57] Despite this, the protocol is a true one-pot procedure and allows access to dibenzofurans, benzofuropyridines and benzothienopyridines. Overall, there is a large scope achieved using this one-pot procedure, with a range of substitution patterns exhibited.

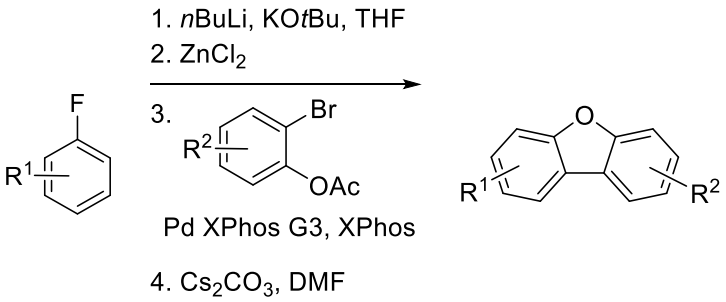


**Scheme 23** The one-pot synthesis of tricyclic carbolines from aryl fluoride precursors

Another multi-step protocol to access dibenzofuran and its heterocyclic derivatives was published by Liu and co-workers (Scheme 24).[58] The methodology comprises of a regioselective Suzuki-Miyaura reaction to generate a biaryl. The methoxy group is subsequently deprotected with $BBr_3$ which generates a phenol which can undergo a further copper-catalysed intramolecular cyclisation. A small scope of dibenzofurans is demonstrated with a relatively larger exhibition of heterocyclic dibenzofuran derivatives on display. This chemistry affords high yielding products for the substrates shown but does rely on the use of DMA at high temperatures.

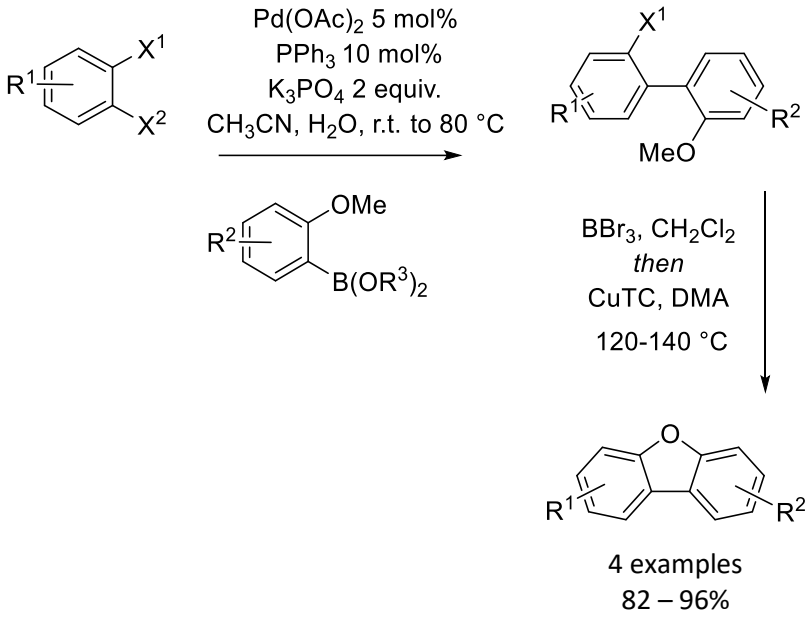


**Scheme 24** The synthesis of dibenzofurans via intermolecular C–O bond formation

Building on this C–O bond formation strategy, Zhao and co-workers reported a one-pot synthesis of dibenzofurans using a diazocyclohexenone precursor (Scheme 25).[59] This report utilises a familiar Pd-catalysed cross-coupling and subsequent Cu-catalysed Ullmann coupling to furnish a range of dibenzofurans with unique substitution patterns. This procedure is operationally simple and produced high yields of product across their respective scope. However, the methodology has inherent drawbacks by requiring use of hazardous diazo functionalised building blocks.

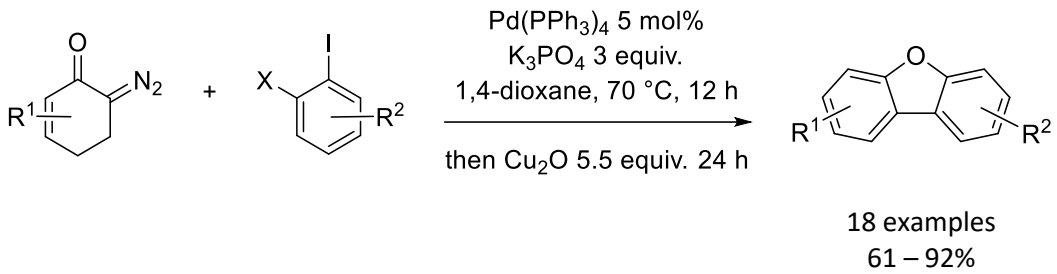


**Scheme 25** The synthesis of dibenzofurans from a palladium-catalysed cross-coupling followed by copper-catalysed Ullmann reaction

Recently, Hosoya and co-workers reported the synthesis of dibenzofurans by copper-catalysed deborylative ring contraction of dibenzoxaborins (Scheme 26).[60] This chemistry requires the independent preparation of a dibenzoxaborin starting material.

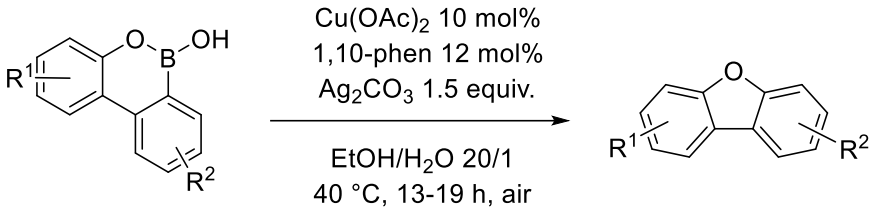


**Scheme 26** The synthesis of dibenzofurans from dibenzoxaborin starting materials

### 1.3.4. Alternative Routes for Dibenzofuran Synthesis

Thus far, common approaches used to build the dibenzofuran scaffold through C–C or C–O bond formation have been discussed. However, it would remiss to not mention alternative routes of dibenzofuran synthesis reported in the chemical literature and a select few examples of such protocols will be discussed in the following section.

Chatani and co-workers showcased how intramolecular arylation through C–CN bond cleavage *via* Rh-catalysed silylation can yield dibenzofurans (Scheme 27).[61] High loadings of $[RhCl(cod)]_2$ (10 mol%) along with 20 mol% of $P(p\text{-}CF_3C_6H_4)_3$ and two equivalents of hexamethyldisilane were required to furnish the desired dibenzofurans from the *ortho-ortho'* substituted diarylethers in moderate to good yields. A large range of functional groups were successfully employed including esters, amides, amines boronic acids and different heterocycles among many others. The authors proposed that the hexamethyldisilane reacts with the Rh catalyst to produce a $RhSiMe_3$ species alongside TMSCl. There then is a migration of the $SiMe_3$ group to the nitrogen atom of the *ortho* nitrile substituent. The nitrile ligates the rhodium which is followed by insertion of Rh into the aryl-nitrile bond. When the *ortho* substituent is a chlorine atom, the rhodium centre migrates to the C–Cl bond to form a 6-membered rhodacycle which generates dibenzofuran after reductive elimination of the rhodium catalyst.

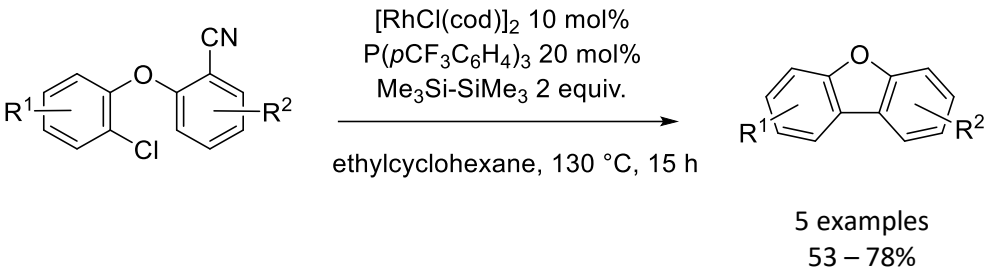


**Scheme 27** The cyclisation of *ortho-ortho'* diarylethers using Rh-catalysed silylation

Another common approach to constructing dibenzofuran involves dehydrogenative coupling using double C–H Activation of diphenylether. Seminal work in this field was reported by Akermark[62] and Shiotani.[63] In 1975, Akermark showcased how diphenyl ethers can be cyclised into dibenzofurans by using 2 to 4 equivalents of $Pd(OAc)_2$ in acidic solvent (Scheme 28a). Shiotani provided an update on this work in the following year by showcasing how the $Pd(OAc)_2$ loading could be lowered to 0.2 mol% when acetylacetone (0.2 mol%) was used as an additive in ethylene glycol (Scheme 28b). However, the reaction had to occur in a rocking autoclave containing $O_2/N_2$ (1:1) at 150 °C. The state-of-the-art dehydrogenative coupling is exhibited in a report by Fagnou.[64] Using mild conditions of pivalic acid in air and at room temperature with $Pd(OAc)_2$ and catalytic quantities of carbonate base, the diarylethers could be successfully cyclised to the corresponding dibenzofurans (Scheme 28c). This reaction occurred by a CMD-type mechanism and tolerated a range of functional groups on the diarylether precursor. Using this protocol, diarylamines could also be converted to carbazoles in good yields.

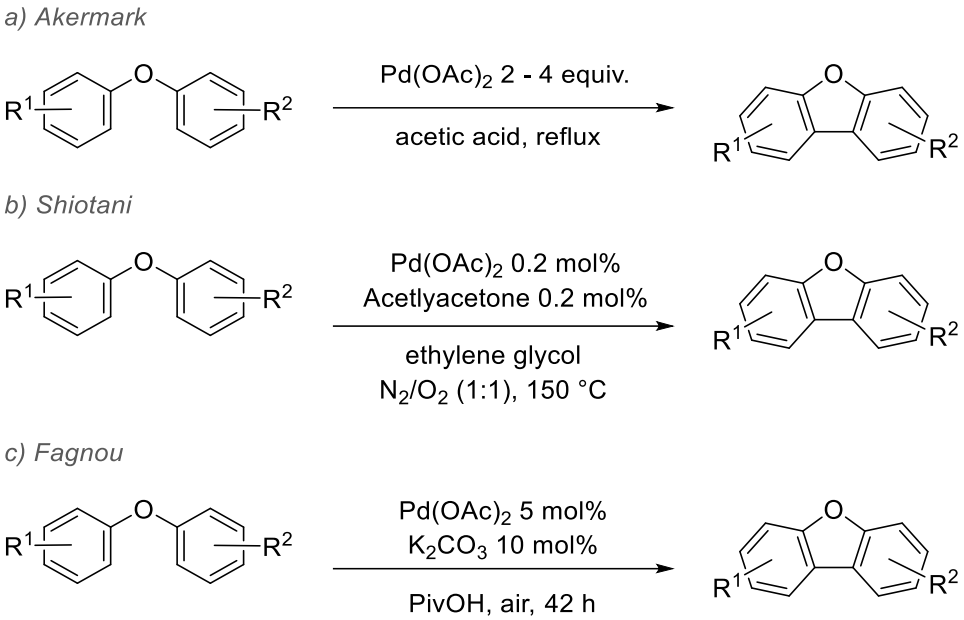


**Scheme 28** Dehydrogenative couplings to access dibenzofuran

Finally, in recent years the use of benzofuran or phenol precursors to access dibenzofurans through Diels-Alder or cyclisation reactions has become increasingly common. One selected example to highlight the power of this strategy is depicted in Scheme 29. Langer and co-workers describe a domino Heck-Mizoroki reaction followed by 6π-electrocyclisation of bromobenzofurans to furnish substituted dibenzofurans.[65]

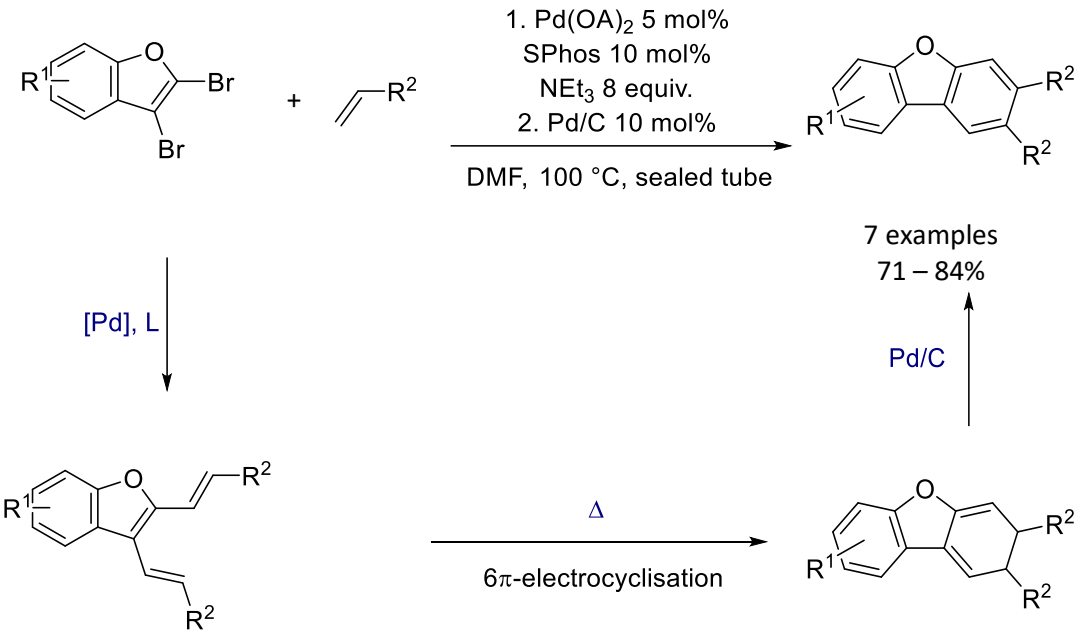


**Scheme 29** The synthesis of dibenzofurans from a double-Heck reaction followed by intramolecular cyclisation

## 1.4. The Use of Quaternary Ammonium Salts in Pd-Catalysis

Within the realm of palladium catalysis for aryl–aryl bond formation, the use of quaternary ammonium salts as organic bases has been reported in a variety of systems. The role of these quaternary ammonium salts is multifaceted. Jeffery's seminal work in this space employed tetrabutyl ammonium chloride ($NBu_4Cl$) with sodium carbonate to expand the substrates of the Heck-Mizoroki reaction and lower the temperature. This combination of a quaternary ammonium halide salt being used concurrently with an inorganic base became referred to as 'Jeffrey's conditions' and found prominent use, particularly with the Heck reaction. This section of the Introduction aims to summarise the relevant literature where Pd-catalysed cross-couplings are enabled by the use of quaternary ammonium salts. It is worth noting that there exist many names for these quaternary ammonium salts. In the case of tetrabutylammonium acetate, other titles like TBAA, $NBu_4OAc$ and TBAE, to name a few, are often used. There exist many examples of anionic Pd catalysts in cross-coupling reactions[66–68] and an excellent review by Dupont exhibits the range of carbon–carbon bond forming reactions facilitated by quaternary organic salts.[69] Some selected examples of the use of quaternary ammonium salts within Pd-catalysis are outlined below.

### 1.4.1. Pd-catalysed reactions using quaternary ammonium salts

Hull and co-workers demonstrate a palladate catalyst that enables an *anti*-Markovnikov selective aza-Wacker oxidation (Scheme 30).[70] The authors hypothesise that an anionic palladium species is generated upon reaction of the Pd(II) pre-catalyst with quaternary ammonium salts. This palladate species can then undergo a ligand-exchange step which is dubbed as the turnover-limiting step in the proposed cycle. The relevant step of the catalytic cycle is depicted in Scheme 31. Additionally, the authors also independently prepare the suspected palladate species [Pd], which is shown to be catalytically active within the transformation.

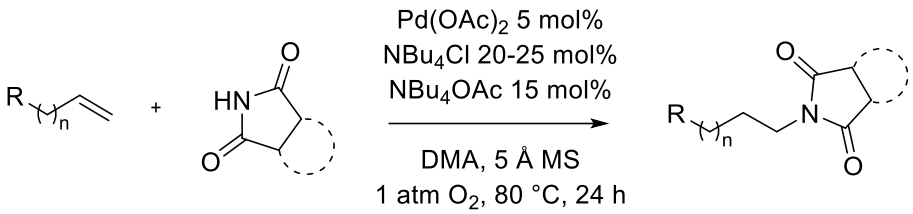


**Scheme 30** The palladium-catalysed selective anti-Markovnikov aza-Wacker oxidation

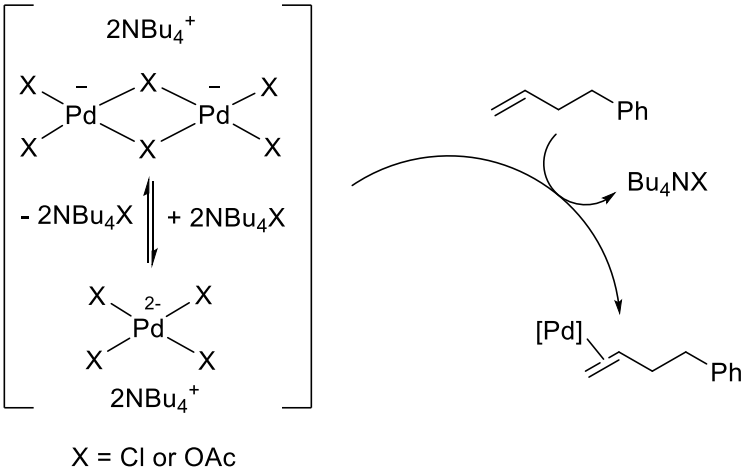


**Scheme 31** First-step of the proposed catalytic cycle for the transformation

Rothenberg and co-workers investigated the mechanism of Pd-nanoparticles formation in a Sonogashira cross-coupling where $NBu_4OAc$ was employed.[71] Their studies indicated that the $NBu_4OAc$ additive had a stabilising influence on the Pd-metal, allowing small clusters to form and remain catalytically active. No Pd-black was observed under these conditions. When the

reaction was trialled with $K_2CO_3$ instead of $NBu_4OAc$, Pd-black was observed in the reaction mixture. Two mechanisms of nanoparticle formation were identified, involving the leaching of Pd (0) or Pd(II).

Reetz and Westermann investigated the role of Pd-nanoparticles in the phosphine free, Pd-catalysed Heck reaction.[72] A standard Heck reaction using an aryl bromide was compared to a Heck reaction with $NBu_4OAc$ which used an aryl iodide. The authors noted that in the case of the quaternary ammonium salt, the reaction had no induction period and started immediately, while the standard Heck reaction conditions required an induction period of an hour. In previous studies by Reetz[73] and Beller,[74] it was demonstrated that preformed $R_4N^+X^-$ stabilised Pd colloids are catalytically active species. It was hypothesised that these Pd-colloids, stabilised by ammonium salts, were the catalytically active species.

### 1.4.2. Pd-catalysed direct arylation using quaternary ammonium salts

Bellina and co-workers report the use of $NBu_4OAc$ to mediate the mild direct arylation of azoles (Scheme 32).[75] The authors postulate that the role of $NBu_4OAc$ may be of relevance in the anionic ligand exchange step of the catalytic cycle (Pd-species **I** to **II**) (Scheme 33). DFT calculations by the authors suggest that the CMD pathway depicted is a more probable mechanism than the sigma-bond metathesis, where the bromine ligand would be in place of the acetate. It was then hypothesised that the Br/OAc exchange could be a rate-limiting step in the catalytic cycle, meaning poorly soluble bases would correspond with sluggish product formation. The increased solubility of the organic base $NBu_4OAc$ perhaps explains its efficiency in this reaction.

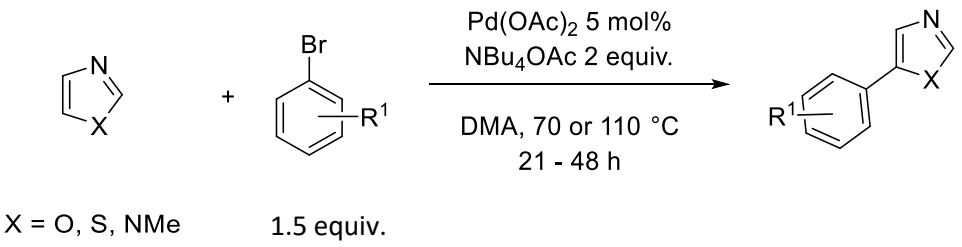


**Scheme 32** The direct arylation of azoles using $NBu_4OAc$

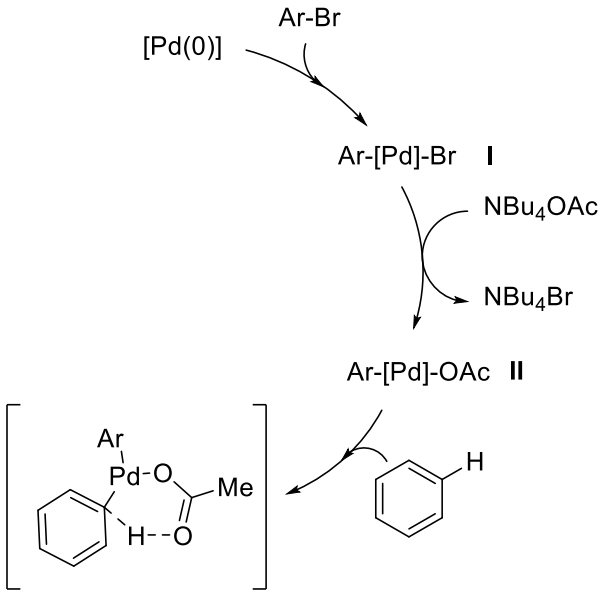


**Scheme 33** The CMD mechanism enabled by $NBu_4OAc$ ligand exchange

Langer and co-workers reported the diarylation of *N*-methyl- and *N*-phenylpyrrole by employing ligand-free Pd-catalysis using $NBu_4OAc$.[76] The authors demonstrate how electron-poor arenes can be coupled with protected pyrroles when $NBu_4OAc$ is used as the solvent (Scheme 34). Again, it was postulated that Pd-nanoparticles were forming. It is known that Polyvinylpyrrolidone (PVP) stabilised Pd-nanoparticles are oxidised to palladates in the presence of ammonium salts,[77] explaining the selective activity of the nanoparticles with $NBu_4OAc$. The authors also suggested that the tetrabutylammonium salt and $Pd(OAc)_2$ formed an anionic palladate species which are known to furnish Pd(0) in the presence of acetate anions at high temperatures.[78] A proposed catalytic cycle is depicted in Scheme 35. Additionally, the authors identified trace amounts of tributylamine formed at elevated temperatures. This tributylamine was derived from $NBu_4OAc$ undergoing Hoffman elimination. The amine formed could reduce the palladate species to the catalytically active Pd(0) species.[69] Therefore, the authors conclude that the $NBu_4OAc$ is crucial to the reactions success as it: i) stabilises the active Pd(0) species by preventing the formation of Pd-black and ii) increases the solubility of the organometallic complex. The formed ammonium palladate species represents a 'resting state' of the catalytically active Pd(0) species.

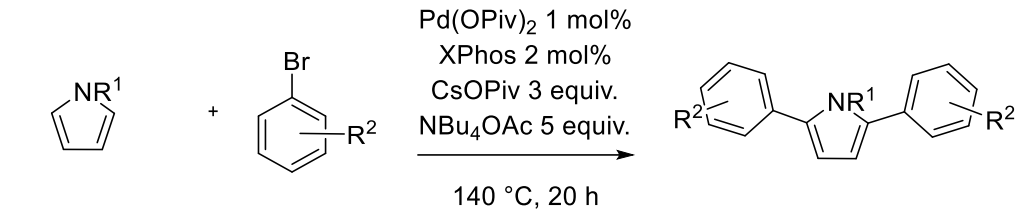


R = Me or Ph 3 equiv.

**Scheme 34** The diarylation of pyrroles using $NBu_4OAc$ and Pd-catalysis

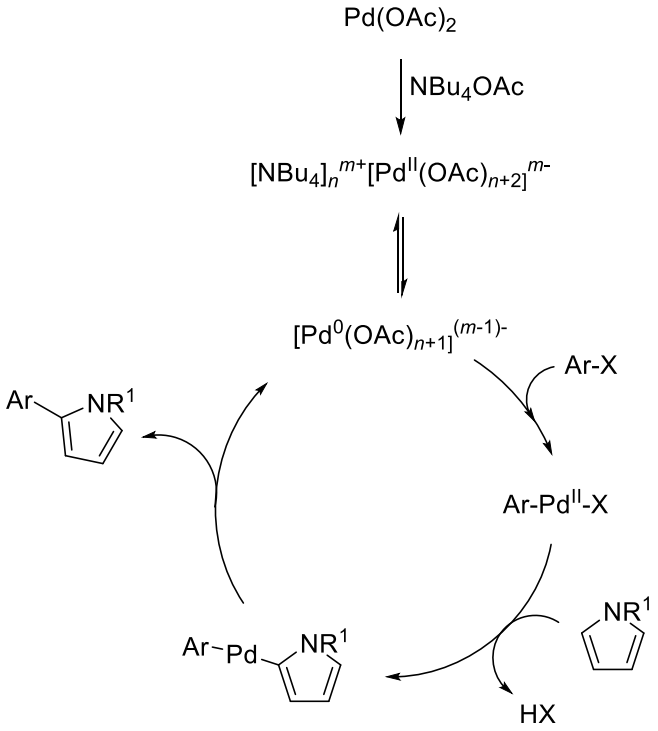


**Scheme** 35 Proposed catalytic cycle for the arylation of pyrroles using $NBu_4OAc$

Yang and Hong describe the Pd-catalysed direct arylation of arenes with aryl bromides by using quaternary ammonium salts.[79] The authors found that the ammonium salt generates an anionic palladium complex which facilitates arylation by a CMD process. They also found that this protocol was successful using substoichiometric quantities of the quaternary ammonium salt. An anionic Pd-species was also independently prepared and was shown to be catalytically active within their system, even in the absence of additional ammonium salt (Scheme 36). Using previous literature reports and their own mechanistic investigations, the authors proposed a catalytic cycle (Scheme 37).

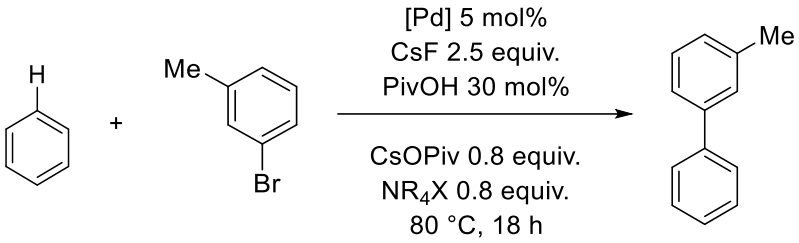


**Scheme 36** The use of anionic palladate catalysts in the reaction

| ***Entry*** | ***[Pd]*** | ***$NR_4X$*** | ***Yield*** |
|---|---|---|---|
| *1* | $Pd(OAc)_2$ | *n*-$Bu_4NBr$ | >99% |
| *2* | $PdBr_2$ | *n*-$Bu_4NBr$ | 91% |
| *3* | $PdBr_4(nBu_4N)_2$ | *n*-$Bu_4NBr$ | 46% |
| *4* | $PdBr_4(nBu_4N)_2$ | - | 92% |

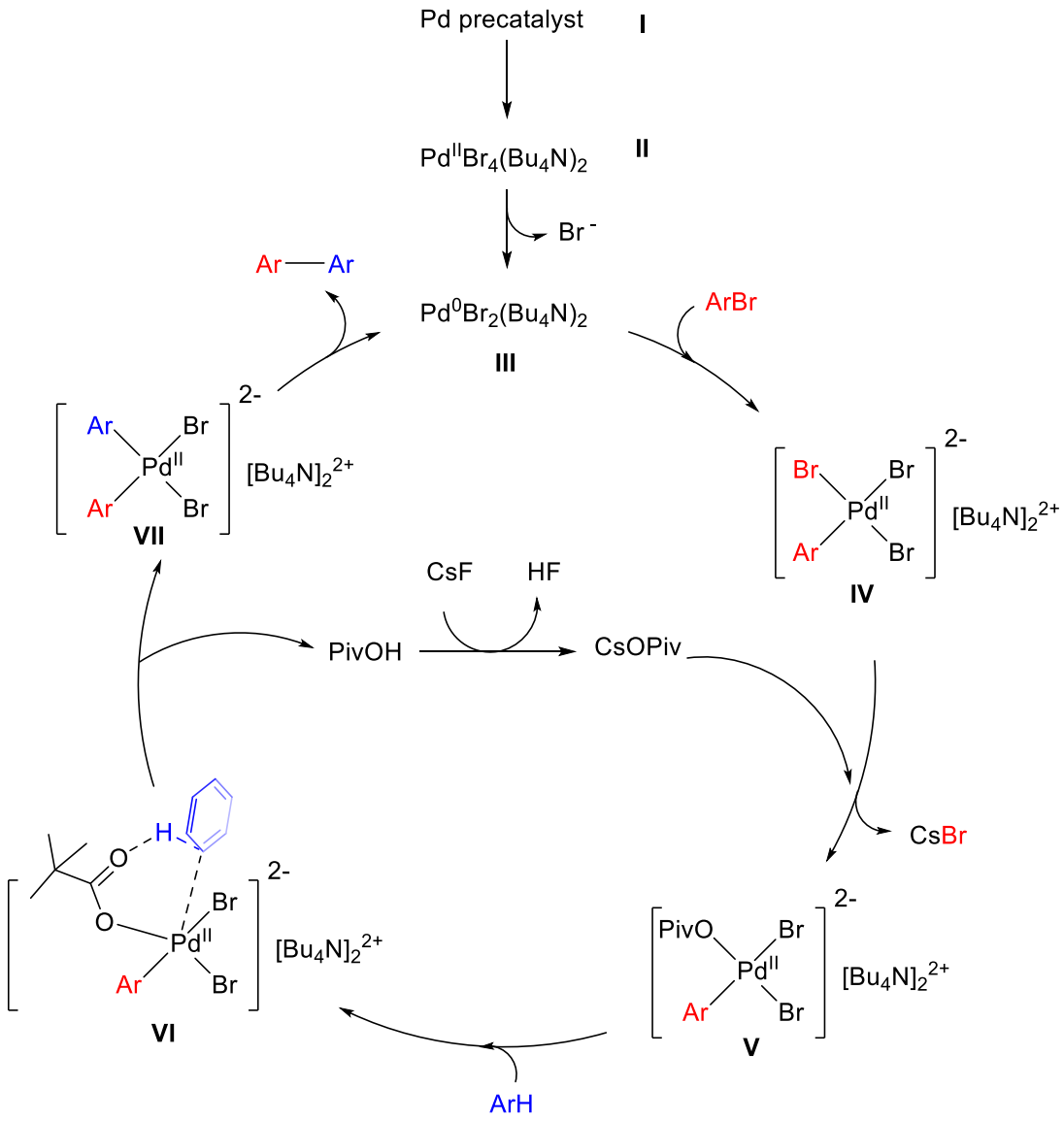


**Scheme 37** Proposed catalytic cycle for the quaternary ammonium salt facilitated arylation *via* a CMD process

### 1.4.3. Roles of Quaternary Ammonium Salts

Another potential role of organic salts in palladium-catalysis concerns the reoxidation of catalytically inactive Pd-black to the active monomeric Pd-species. Work by de Vries exhibits how halide salts can reoxidise palladium black to allow improved catalyst turnover in the Heck reaction.[80] The halide salts added can rescue off-cycle 'catalyst' and thus, keep the reaction turning over. Similar to silver salt additives, it is postulated that these organic halide salts may also play this role.

In these reactions, it is often $NBu_4OAc$ employed as the quaternary ammonium salt additive. In the case of the direct arylations using this additive, the increased availability in solution of

the acetate anion could be facilitating this mechanistic pathway. The availability of the acetate anion is key to the success of the CMD mechanism.[81] In some cases, the colour of the reaction solutions is noticeably different between the organic and inorganic base variants, potentially as a consequence of the improved solubility of the acetate additive.[75]

As a whole, the function of $NBu_4OAc$ within a Pd-catalysed reaction is multifaceted and depends on the nature of the reaction. $NBu_4OAc$ can simply be a more organic soluble base, giving rise to a greater availability of acetate anion in solution. It can solubilise organometallic intermediates. It can stabilise Pd-colloids and create Pd-nanoparticles which remain catalytically active. It can facilitate key ligand exchange steps in a catalytic cycle. It can create catalytically active palladate complexes. It can generate small quantities of tributylamine which reactivates Pd-catalyst in a redox process. It may even be possible that the halide salts of tetrabutyl ammonium cations can reoxidise the Pd-black off-cycle catalyst to aid catalytic turnover. It can also act as a solvent for the reaction as it is an ionic liquid.

It is clear that there is a large literature precedent for the use of these bases within Pd-catalysed reactions. There are many organometallic reports, since the seminal work of Jeffery, attempting to characterise the catalytic species generated by these quaternary ammonium salts. As a whole, the reactions which employ these additives showcase milder reaction conditions (either in time or temperature) than the corresponding inorganic variant. Alternatively, these quaternary ammonium additives can facilitate new substrates to be incorporated into protocols which previously could not tolerate them, or offer alternative selectivity.

## 1.5. Conclusion

To conclude, there is a myriad of synthetic procedures available to chemists to access the dibenzofuran framework. Of these, one of the most traditional and robust methodologies utilises palladium catalysis to cyclise *o*-halogenated diaryl ether precursors. The principal limitation to this route is its inherent incompatibility with electron-rich substrates. Electron-rich substitution patterns are recurrent features of naturally occurring dibenzofuran molecules, of which many are biologically active. Thus, being able to employ the robust Pd-catalysis methodology with electron-rich starting materials would be a highly valuable protocol to synthetic chemists. Pd-catalysis is often used in a synergistic means with quaternary ammonium salts, which can enable tolerance to new substrate classes which struggle under alternative conditions.

# 2. Results & Discussion

## 2.1. Objectives

This Chapter aims to describe an efficient construction of dibenzofuran motifs through Pd-catalysed intramolecular direct arylation of *ortho*-bromo diarylethers. In particular, advances in expanding the scope of this chemistry to medicinally important electron-rich arenes were investigated by the synergistic use of tetraalkylammonium salts with Pd-catalysis. The role of the quaternary ammonium salt was investigated alongside insight into the reaction mechanism. Attempts at expanding the protocol to more chemically diverse substrates were also undertaken.

## 2.2. Background Chemistry

As discussed in the Introduction Section of this Chapter, a number of useful methods have emerged for the synthesis of dibenzofurans. The metal-catalysed intramolecular cyclisation of *ortho*-halogenated diarylethers *via* C–H activation is an attractive route to target, pioneered by Ames and co-workers in the 1980's.[42] Subsequent developments have improved access to dibenzofurans.[43,44,47] In recent years, the McGlacken Group has published an update on this reaction, allowing efficient diarylether cyclisation *via* Pd-catalysis without the requirement for phosphine ligands.[45] Despite these advances, numerous issues still remain, particularly concerning the range of substrates amenable to the chemistry. As outlined in the Introduction, there is a keen interest in the dibenzofuran scaffold due to the breadth of biological activity displayed by naturally occurring dibenzofurans.[29,37,82] However, these natural occurring compounds are usually heavily decorated with electron-donating substituents.[29,83] Attempts to use the Pd-catalysed C–H Activation route on electron-rich precursors usually resulted in poor yields of product and degraded starting material. Perhaps, this is a result of sluggish oxidative addition to these electron-rich arenes. This Chapter describes attempts to access these important compounds as well as the optimisation and development of an efficient set of reaction conditions enhanced by a tetraalkylammonium salt, for the intramolecular cyclisation of electron-rich *ortho*-bromo diarylethers.

### 2.2.1. Proof-of-Principle

As outlined in the Introduction to this Chapter, tetraalkylammonium salts have a rich history of synergistic use with Pd-catalysis to increase reaction conversion, with seminal work reported by Jeffrey.[84,85] Following this, multiple reports using a variety of organic salts with transition metals to furnish organic products have been published.[14,69,72,75,76,79,86–93]

It is worth noting that in the case of palladium catalysis with tetraalkylammonium salts, the majority of transformations involve the Heck reaction, stemming from Jeffrey's original work. In the initial work on dibenzofuran synthesis within the McGlacken Group it was found that when electron-rich substrates were trialled under the optimised reaction conditions, starting material degradation or poor reaction efficiency was observed (

Scheme ***38***).[45]

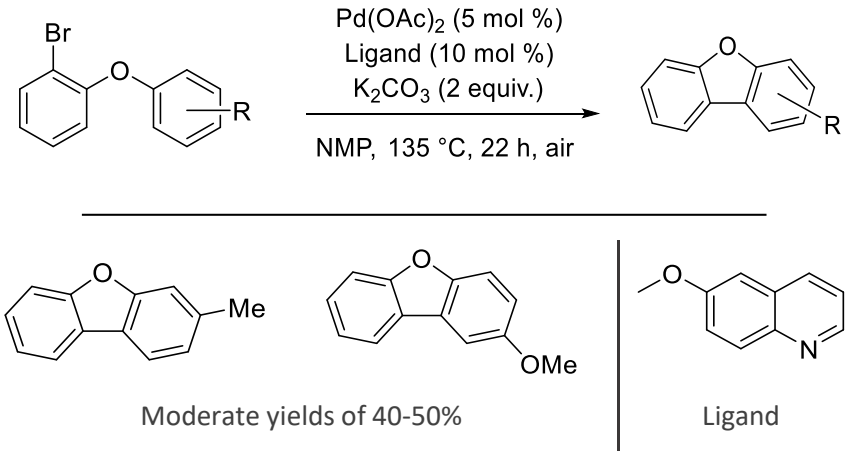


**Scheme 38** Previous work in the McGlacken Group

In these initial reaction attempts to cyclise diarylethers containing electron-donating groups, formation of a black precipitate was observed at the high temperatures. Despite alternative ligands, solvents or temperatures, the reaction failed to provide a clean conversion to product. It was hypothesised that the electronic nature of these arenes meant that the pivotal oxidative addition step was sluggish, and consequently, catalytically inactive palladium black aggregates were allowed to form. This catalytic dead-end removes active palladium from the reaction and results in poor product conversion. Given the breadth of literature involving organic bases with metal catalysis and the fact that organic ionic bases are known to have good solubility and fully ionize in organic solvents,[89] we hypothesised that

use of an organic soluble base like tetrabutylammonium acetate ($NBu_4OAc$) could allow more efficient oxidative addition by reducing the quantity of palladium falling off-cycle. This increased amount of active catalyst could possibly improve the yield of the desired product.

## 2.3. Optimisation of Reaction Conditions

To begin initial investigations, an appropriate model substrate was synthesised. Using a Chan-Lam-Evans coupling, the *p*-methoxy brominated phenol **1** was coupled with phenyl boronic acid using triethylamine as a base and stoichiometric quantities of copper acetate. Purification *via* silica gel column chromatography afforded the desired *o*-brominated model substrate **2** in 69% yield (Scheme 39).

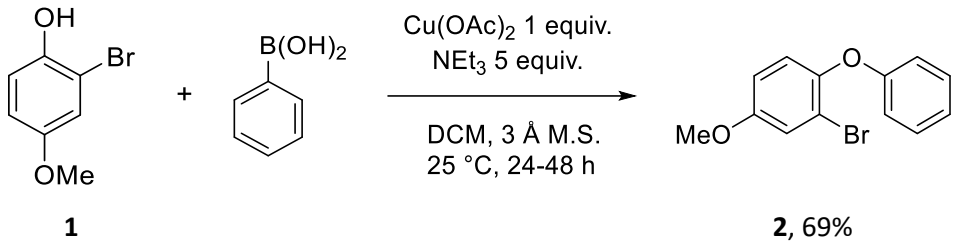


**1** **2**, 69%

**Scheme 39** The synthesis of the electron-donating model substrate

The model substrate **2** was then subjected to standard reaction conditions of $Pd(OAc)_2$ in dioxane, with $NBu_4OAc$ as a base (Table 1, Entry 1). Pleasingly, the employment of $NBu_4OAc$ in this system improved the conversion to product (70%). It was thought that an electron-rich phosphine ligand would facilitate the oxidative addition step of the catalytic cycle, which was postulated to be the problematic step of the catalytic cycle. Indeed, the addition of SPhos (Table 1, Entry 2) and $PCy_3.HBF_4$ (Table 1, Entry 3) increased the conversion to the desired dibenzofuran, with $PCy_3.HBF_4$ affording the product **3** in 96% isolated yield. With the success of this quaternary ammonium salt in the reaction, the loadings of catalyst and ligand were investigated (Table 1, Entries 4-7). It was found that reducing the catalyst loading to 2.5 mol% with 5 mol% of the phosphine ligand afforded the desired dibenzofuran **3** in 90% yield. When the optimal reaction conditions were trialled in the absence of $NBu_4OAc$, only trace amount of the desired product was observed (Table 1, Entry 8). The anhydrous 1,4-dioxane solvent was swapped to a greener and more sustainable option in cyclopentyl methyl ether (CPME)[94,95] but this also provided poor results, with only 40% conversion observed (Table 1,

Entry 9). Pleasingly, bulk (non-anhydrous) dioxane could be used in this reaction while still maintaining excellent yields (Table 1, Entry 10). Some reports showcase how milder reaction conditions can be achieved when Pd-catalysis is utilised with quaternary ammonium salts. Unfortunately, lowering the reaction temperature gave a sharp drop in yield to 41% (Table 1, Entry 11).

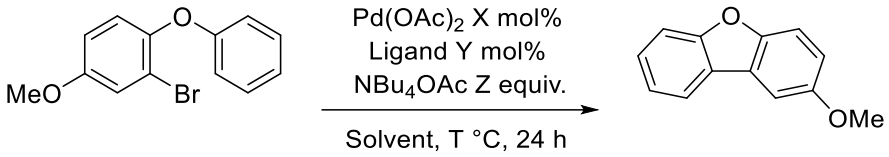


**2** **3**

| ***Entry*** | ***Pd(OAc)₂*** *(mol%)* | ***Ligand*** *(mol%)* | ***Solvent*** *(dried)* | ***NBu₄OAc*** *(equiv.)* | ***Temp*** *(°C)* | ***Yield*** [a] |
|---|---|---|---|---|---|---|
| *1* | 5.0 | - | 1,4-dioxane | 2 | 125 | 70% |
| *2* | 5.0 | SPhos (10) | 1,4-dioxane | 2 | 125 | 81% |
| *3* | 5.0 | $PCy_3.HBF_4$ (10) | 1,4-dioxane | 2 | 125 | [96%] |
| *4* | 5.0 | $PCy_3.HBF_4$ (05) | 1,4-dioxane | 2 | 125 | 67% |
| *5* | 2.0 | $PCy_3.HBF_4$ (10) | 1,4-dioxane | 2 | 125 | 25% |
| *6* | 1.0 | $PCy_3.HBF_4$ (02) | 1,4-dioxane | 2 | 125 | 8% |
| *7* | 2.5 | $PCy_3.HBF_4$ (05) | 1,4-dioxane | 2 | 125 | [90%] |
| *8* | 5.0 | $PCy_3.HBF_4$ (10) | 1,4-dioxane | 0 | 125 | <5% |
| *9* | 5.0 | $PCy_3.HBF_4$ (10) | CPME | 2 | 125 | 40% |
| *10* | 2.5 | $PCy_3.HBF_4$ (05) | 1,4-dioxane[b] | 2 | 125 | [92%] |
| *11* | 2.5 | $PCy_3.HBF_4$ (05) | 1,4-dioxane[b] | 2 | 100 | 41% |

[a] Yield refers to $^1H$ NMR yield which is calculated using 1,3,5-trimethoxybenzene as an internal standard
[b] Non-anhydrous solvent
Square brackets indicate that the yield is isolated

**Table 1** Optimisation of Pd-catalysed diaryl ether ring closure using $NBu_4OAc$

## 2.4. Investigation of Alternative Quaternary Organic Salts

Given the success of employing tetrabutylammonium acetate in the reaction, the use of alternative quaternary ammonium salts was also explored. The more atom economic quaternary ammonium salt, tetramethylammonium acetate ($NMe_4OAc$) was trialled under the optimal reaction conditions (Table 2, Entry 1 and 2). This salt did facilitate good

conversion to the desired dibenzofuran **3** at 74%, with a slight increase to 79% yield after 48 hours. Fagnou has demonstrated that carboxylate type anions can be key additives in C–H Activation reactions.[22] It was postulated that the tetraalkylammonium acetate salt could contain trace amounts of acetic acid, potentially mediating the reaction. Indeed, small additions of acetic acid did improve the use of $NMe_4OAc$ in the reaction, but still not to the level that $NBu_4OAc$ was successful (Table 2, Entry 3 and 4). Dimethylacetamide (DMA) is a popular solvent of choice for C–H Activation using palladium catalysis and it was observed that the use of $NMe_4OAc$ with DMA allowed for quantitative yields of the desired dibenzofuran to be achieved (Table 2, Entry 5). Furthermore, the use of Jeffrey's conditions was investigated where tetrabutylammonium bromide ($NBu_4Br$) and potassium carbonate were employed in unison, however, only moderate conversion was observed (Table 2, Entry 6).

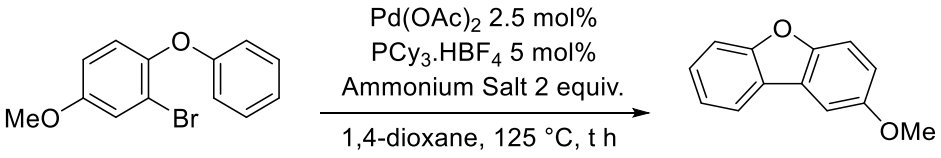


**2** **3**

| *Entry* | *Ammonium Salt* | *Additive* | *Time (h)* | *Yield* [a] |
|---|---|---|---|---|
| *1* | $NMe_4OAc$ | - | 24 | 74% |
| *2* | $NMe_4OAc$ | - | 48 | 79% |
| *3* | $NMe_4OAc$ | AcOH (10 mol%) | 24 | 82% |
| *4* | $NMe_4OAc$ | AcOH (10 mol%) | 48 | 81% |
| *5* | $NMe_4OAc$ | DMA (Solvent) | 24 | 98% |
| *6* | $NBu_4Br$ | $K_2CO_3$ (2 equiv.) | 24 | 45% |

[a] Yield refers to $^1H$ NMR yield which is calculated using 1,3,5-trimethoxybenzene as an internal standard

**Table 2** Investigation of alternative ammonium salts in the Pd-catalysed synthesis of dibenzofurans

As mentioned previously, several quaternary organic salts have been used in conjunction with transition-metal catalysts to mediate a variety of transformations. Previously, Liu and co-workers described the employment of quaternary organic salts used to facilitate a copper catalysed C–N coupling of aryl iodides.[86] They observed that the phosphonium salts, in

comparison to the corresponding ammonium variants, allowed the reaction to proceed under milder conditions, particularly when considering temperature and time. On this premise, the corresponding tetrabutylphosphonium acetate salt (**4**) was synthesised by a literature procedure[86] where an equimolar amount of tetra-*n*-butylphosphonium hydroxide and acetic acid were stirred in water for 3 hours under an atmosphere of $N_2$ (Scheme 40). The salt was adequately dried to yield tetrabutylphosphonium acetate.

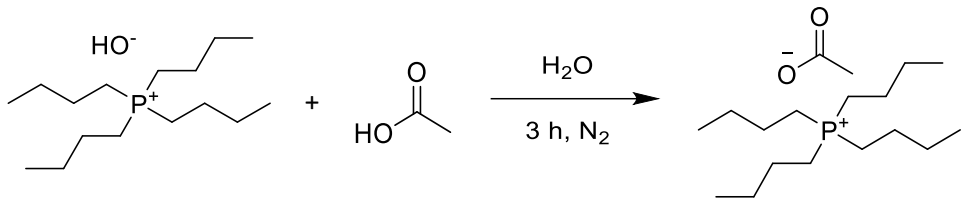


**4**

**Scheme 40** The synthesis of $PBu_4OAc$

With the resulting $PBu_4OAc$, attempts were made to improve the existing reaction conditions. Firstly, the reaction time was lowered to 2 hours from 24 hours. Pleasingly, the phosphonium salt enabled an 81% conversion to product after 2 hours (Table 3, Entry 1). Unfortunately however, even with $PBu_4OAc$, only a moderate conversion of 53% was observed when the reaction temperature was lowered from 125 °C to 90 °C (Table 3, Entry 2). Regardless, these results still indicate the power of employing phosphonium salts in Pd-catalysed processes but the corresponding $NBu_4OAc$ remained the organic base of choice for our particular transformation.

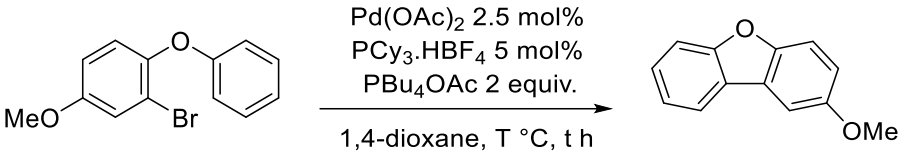


**2** **3**

| *Entry* | *Temperature* *(°C)* | *Time* *(h)* | *Yield* [a] |
|---|---|---|---|
| *1* | 125 | 2 | 81% |
| *2* | 90 | 24 | 53% |

[a] Yield refers to $^1$H NMR yield which is calculated using 1,3,5-trimethoxybenzene as an internal standard

**Table 3** The use of $PBu_4OAc$ in the Pd-catalysed dibenzofuran synthesis

## 2.5. The Synthesis of *ortho*-Brominated Diarylether Precursors

With optimal conditions to hand, a range of *ortho*-brominated diarylethers were synthesised *via* Chan-Lam-Evans coupling. It is worth noting that the yields of these compounds vary greatly and yields for each substrate is not optimised. This protocol served as a means to access enough material to apply each substrate to the methodology. In cases where the purification was difficult or the yield was low, efforts were not made to increase the yields of each diarylether.

As with any new chemical protocol, functional-group tolerance is key to the uptake of a new protocol. The Introduction to this Chapter has already highlighted the clear need to access electron-rich dibenzofuran scaffolds, on account of the breadth of their biological activity and the lack of existing protocols. However, we also aimed for the methodology to include electron-poor dibenzofuran derivatives. Accordingly, the fluorinated diarylethers **5** and **6**, alongside the pyridine (**7**) and acetyl (**8**) derivatives were prepared. It is also worth noting that the *ortho*-brominated diarylether (**9**) was synthesised by the same method, but was prepared by another member of the McGlacken Group. Furthermore, mono-substituted electron-rich arenes were synthesised where the *m*-methyl (**10**) and *m*-methoxy (**11**) derivatives, alongside the model substrate **2**, were all furnished in good yield. Furthermore, polyfunctionalised diarylethers were also prepared. Namely, the dimethyl (**12**), dimethoxy (**13**), trimethoxy (**14**) and tetramethoxy (**15**) diaryl ether derivatives were obtained, albeit in low yields (Scheme 41).

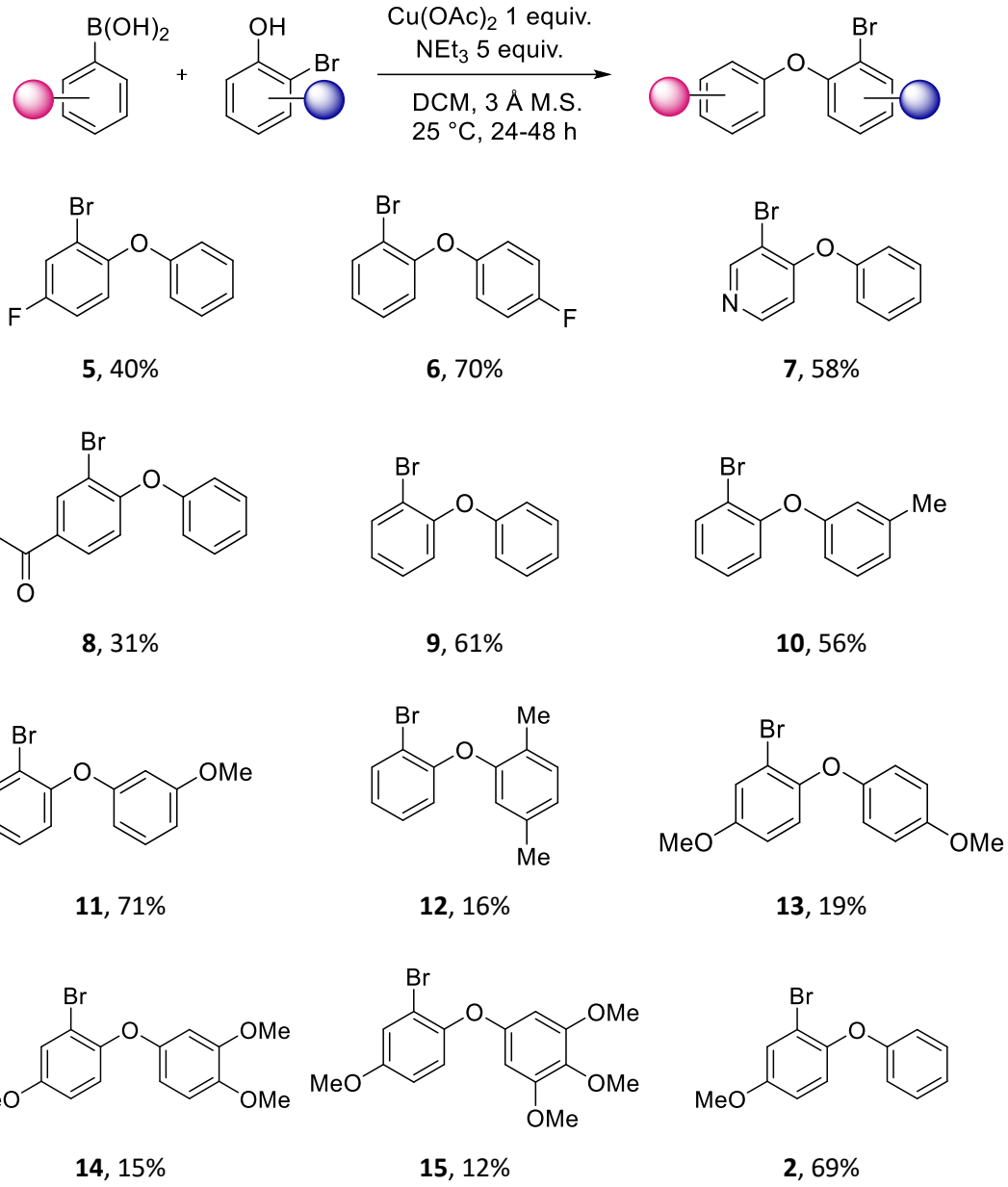


**Scheme 41** Substrate scope of diarylether synthesis

A general mechanism for the Chan-Lam-Evans arylation of phenols with phenyl boronic acids is outlined in Scheme 42. The first step involves deprotonation of the phenol followed by coordination of the phenoxide anion to a Cu(II) species to give **I**. Subsequently, transmetalation of the boronic acid with the Cu(II) species **I** gives an aryl Cu(II) phenoxide intermediate (**II**). This cuprous species **II** bears the two coupling partners and is believed to be the turnover limiting step in the cycle. This intermediate can then undergo reductive elimination or could be oxidised to Cu(III) *via* disproportionation with a second equivalent of $Cu(OAc)_2$, which is a more likely event.[96] This is followed by a reductive elimination step to

produce the diarylether product. Reductive elimination from a Cu(III) species is proposed to proceed faster than from a Cu(II) species. Completion of the catalytic cycle is achieved *via* oxidation to Cu(II) and this is proposed to be facilitated by $O_2$, $NEt_3$.AcOH and $BX(OH)_2$. This general mechanism is outlined based on investigative work by Watson and co-workers.[97]

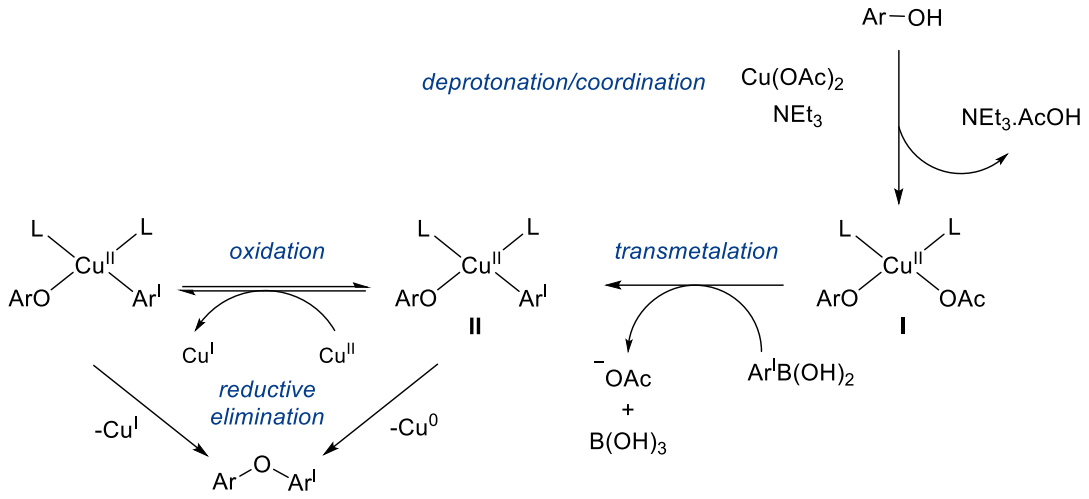


**Scheme 42** The general reaction mechanism for the Chan-Lam-Evans coupling of phenols with aryl boronic acids

### 2.5.1. Starting Material Synthesis Issues

As expected, some precursors were not amenable to coupling *via* this route. Some of the failed reactions are described below in Scheme 43. The coupling of **16** with several substituted boronic acids proved to be troublesome. The low nucleophilicity of some of these electron-poor arenes (**17**) is a possible explanation for their lack of reactivity towards forming diarylethers (**18**). It was thought that exploiting the large range of substituted phenols (**19**) available by using *ortho*-brominated boronic acid arenes (**20**) would be a nice way to access a larger range of products. However, these arenes performed very poorly in these reactions, presumably as a consequence of the steric nature of the substituent lowering their nucleophilicity (Scheme 44). It is worth noting that some of these reactions, such as the coupling of **16** with the trimethoxy boronic acid **21** to yield the diaryl ether **22**, furnished some product, but proved to be difficult to purify and so, were not pursued (Scheme 45). In an attempt to access a wider variety of dibenzofurans, the use of iodonium salts such as **23** was employed. Using 2-bromophenols in the presence of KO*t*-Bu is a known reaction used to access diarylethers.[98] However, in the case of the *p*-trifluoromethoxy substrate **24** (Scheme

46), only a small amount of material was observable in the crude reaction mixture and the purification proved to be arduous.

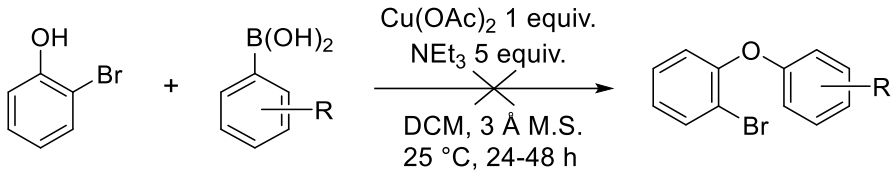


**16** **17** **18**

R = *p*-$OCF_3$, *p*-$CF_3$, *m*-$CF_3$

**Scheme 43** Failed boronic acid substrates for the Chan-Lam-Evans coupling

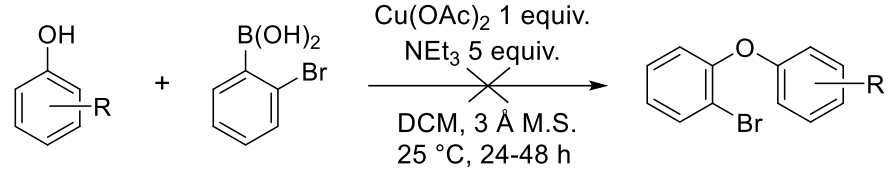


**19** **20** **18**

R = *m*-F, *m*-OMe, *m*-Me, *o*-Me

**Scheme 44** Failed phenol substrates for the Chan-Lam-Evans Coupling

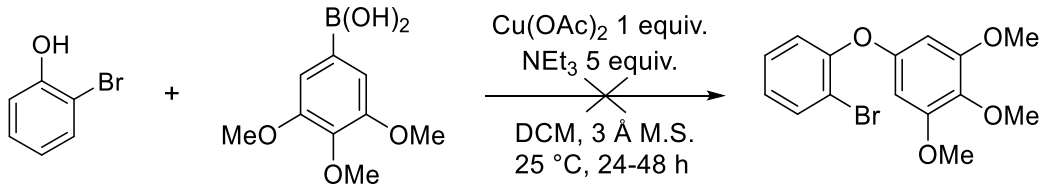


**16** **21** **22**

**Scheme 45** Failed Chan-Lam-Evans coupling

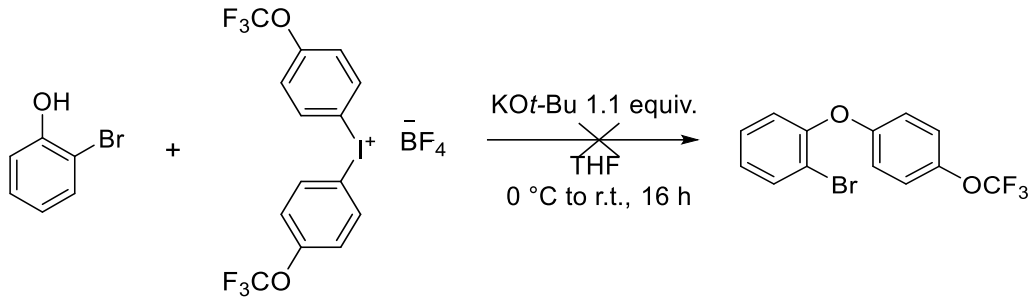


**16** **23** **24**

**Scheme 46** Failed synthesis of EWG-diaryl ether using iodonium salts

The Chan-Lam-Evans coupling provides advantages over alternative transition metal-catalysed process, particularly in the mildness of the reaction conditions. However, many substrates, including electron-poor or *ortho*-substituted arenes, are not well tolerated. Additionally, diminished yields can be compounded by the formation of several by-products, which are well documented to commonly occur in this coupling (Figure 3).[97,99,100] Oxidation of the phenyl boronic acid (**25**) by the competitive arylation of water, followed by oxidative homocoupling of the generated phenol to yield a diphenylether, are by-products commonly observed. Evans noted that a triphenylboroxine species formed from the phenyl boronic acid generates water in the system.[100] Evans also stated (and was later corroborated by Watson[97]), that performing the reaction under strictly anhydrous conditions does not suppress the formation of these undesired by-products. However, the addition of molecular sieves to the reaction mixture helps minimise the production of these by-products. Another by-product commonly found in the crude reaction mixture is the protodeboronation product from the phenyl boronic acid (**26**). From this protodeboronated product, Watson and co-workers also reported a homocoupled byproduct (**27**) which formed even under strictly anhydrous conditions. It is also reported that the Cu(I) species favours the formation of these undesired by-products and thus, slow oxidation of Cu(I) to Cu(II) will inherently lead to more by-products. In some case, using molecular oxygen as an external oxidant can be used to circumvent this issue, albeit with varying success.

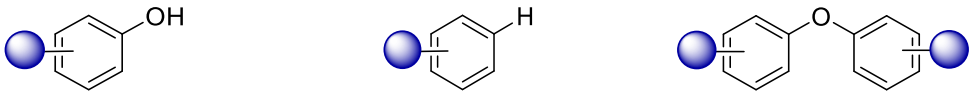


**25** - oxidation **26** - protodeboronation **27** - homocoupled

**Figure 3** The by-products of the Chan-Lam-Evans coupling reaction

To explore the synthetic applicability of our protocol, the *p*-methoxy substrate where the aryl halide is on a separate ring to the methoxy functional group was prepared. Unfortunately, obtaining this diaryl ether from a Chan-Lam-Evans route proved unsuccessful. However, a nucleophilic aromatic substitution protocol could be performed, where 1-bromo-2-fluorobenzene (**28**) was coupled with *p*-methoxy phenol (**29**) using sodium hydride as a base. Under an inert atmosphere at 120 °C, this procedure gratifyingly afforded the desired *p*-methoxy diarylether isomer **30** in 71% yield (Scheme 47).

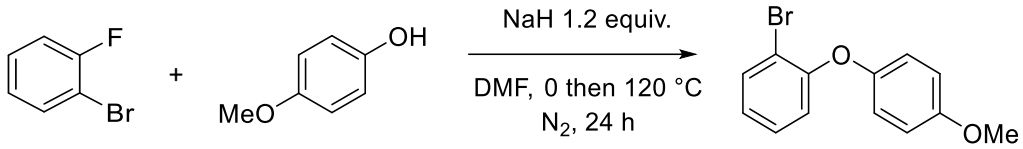


**28** **29** **30**, 71%

**Scheme 47** The synthesis of *p*-methoxy diaryl ether isomer by NAS

As well as the diaryl starting materials synthesised, a diaryl amine derivative, serving as a carbazole precursor, was also prepared. This work was carried out by another member of the McGlacken Group and is depicted in Scheme 48. Aniline (**31**) and 2-bromoiodobenzene (**32**) were coupled using a Buchwald-Hartwig reaction to yield the desired *ortho*-halogenated diaryl amine (**33**) in excellent yield.

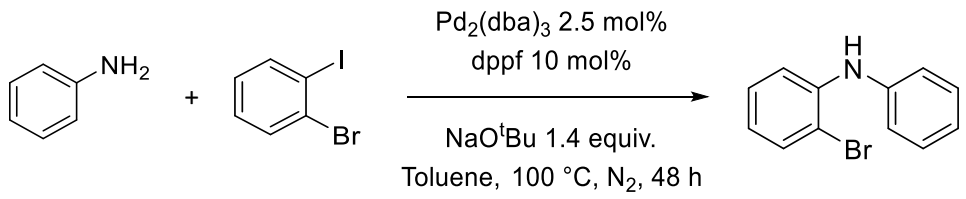


**31** **32** **33**, 96%

**Scheme 48** The synthesis of an *ortho*-brominated diaryl amine starting material *via* Buchwald-Hartwig coupling

## 2.6. Demonstration of Substrate Scope

With a range of diarylether starting materials successfully synthesised, and optimal reaction conditions realised, we turned our focus to appropriately employing this methodology (Scheme 49). The unfunctionalized diarylether (**9**) was successfully ring closed under these conditions in a good yield of 86% to give the unsubstituted dibenzofuran scaffold **34**. However, as the ultimate goal of this chemistry concerns the ability to access a wide variety of naturally occurring dibenzofurans, it is important that C−H functionalisation could occur on either ring, irrespective of the nature of the substituent. In light of this, two fluorinated analogues were employed to yield the same dibenzofuran, only differing in which C−H bond was activated prior to ring closure (**35** and **36**). Gratifyingly, both of these diarylether precursors underwent cyclisation in excellent yield using this protocol. The acetylated product **37** was formed in an excellent yield of 95%. This result showcases a tolerance to an acetyl group which is often present in naturally occurring dibenzofurans (e.g. ruscodibenzofuran). Pleasingly, the pyridyl (**38**) and carbazole (**39**) products were also formed in excellent yield using these conditions. The use of diaryl amines to yield carbazole products was a limitation in our previously published conditions. Furthermore, pyridine containing substrates can often pose issues in palladium-catalysed processes as a consequence of its ability to ligate to metals. In light of this, the results showcasing tolerance for heterocyclic products are particularly gratifying. The electron-rich *m*-methyl dibenzofuran **40** was furnished in excellent yield and regioselectivity (90% and 96:4 *m*:*o*) as was the corresponding *m*-methoxy derivative **41** (94% 97:3 *m*:*o*). The high yield achieved for **40** was satisfying to see as this substrate was classed as a limitation of our previous methodology. The high yield of the *p*-methoxy product **42** alongside the model substrate **3** once again exhibited how C−H functionalisation can be enacted on both the halogen-bearing and the halogen-free ring of the precursor. This highlights how the methodology can provide flexibility as a synthetic tool towards dibenzofuran targets.

Given that this protocol had clearly surpassed our previously published work and given the ubiquity of the dibenzofurans with multiple methoxy groups, we challenged our methodology with highly electron-rich diarylether precursors, reminiscent of naturally occurring dibenzofuran scaffolds. To a methodology relying on a CMD/AMLA mechanism, we suspected these substrates would represent a significant challenge given the associated sterics and electronics.[22] Two disubstituted precursors were prepared and excellent yields were observed for both the dimethyl (**43**) and dimethoxy (**44**) dibenzofuran scaffolds. Surprisingly, even the trimethoxy derivative (**45**) could be afforded in a superb yield of 90%. The ceiling of the systems tolerance was found with the tetramethoxy-substituted derivative **46** where a lower yield of 42% was observed. Nevertheless, this is a good, usable yield considering the electronic and steric challenges that this substrate poses.

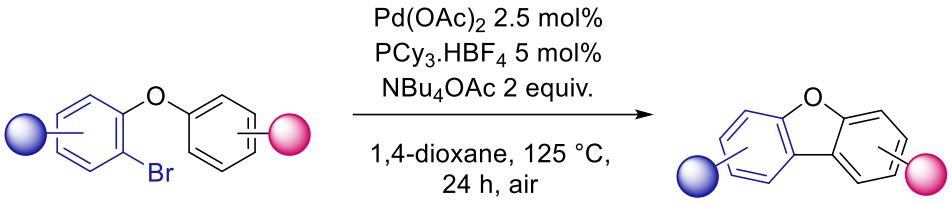


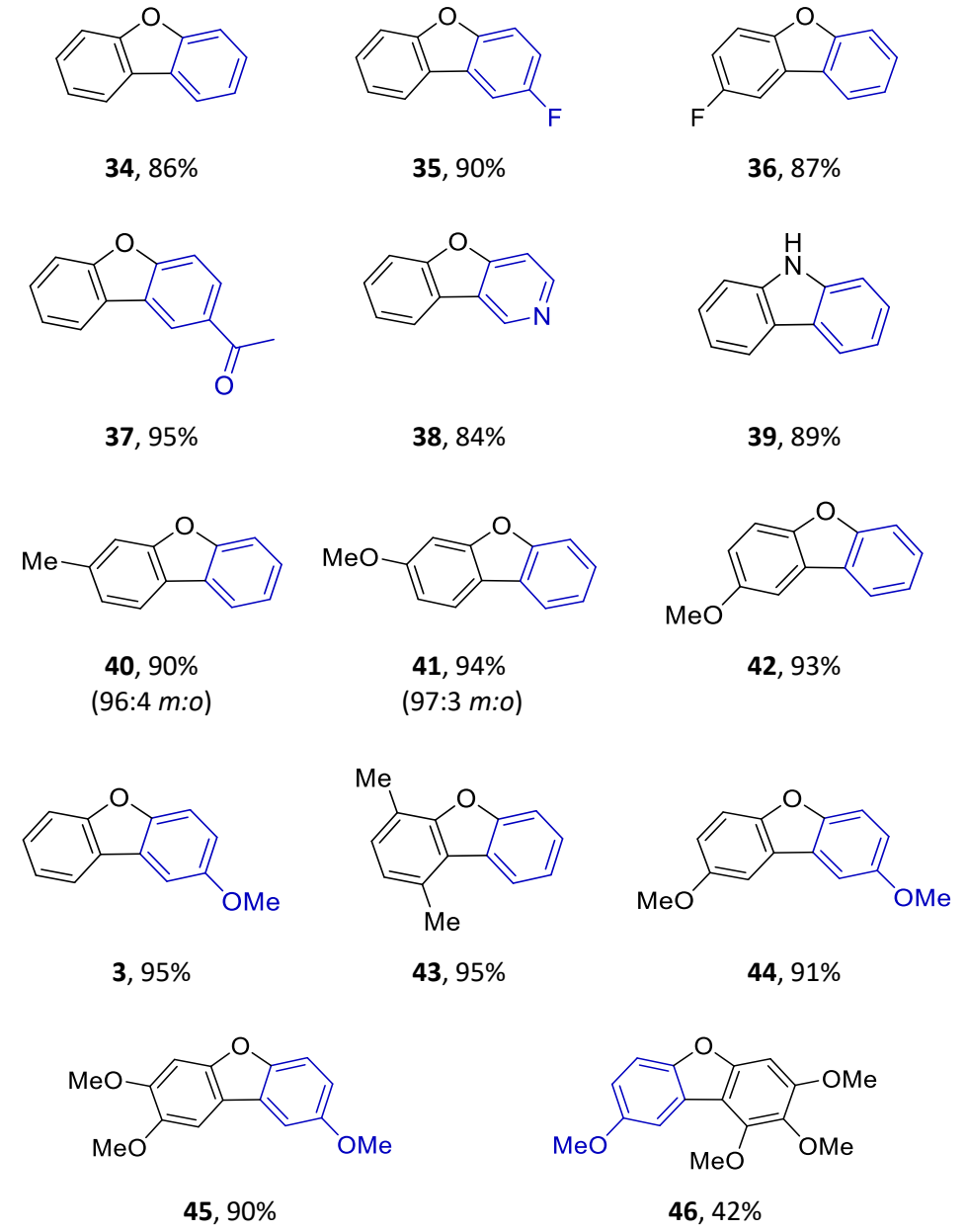


**Scheme 49** Substrate scope of dibenzofurans synthesised

The structures of the electron-rich derivatives **44** (Figure 4) and **45** (Figure 5) were confirmed by X-ray diffraction analysis of single crystals. These single crystals were obtained by vapour diffusion from a saturated solution of dichloromethane and toluene respectively, in hexane.

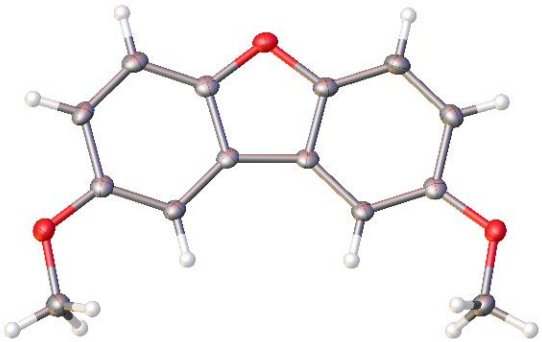

**Figure 4** Crystal structure of the dimethoxy dibenzofuran **44**

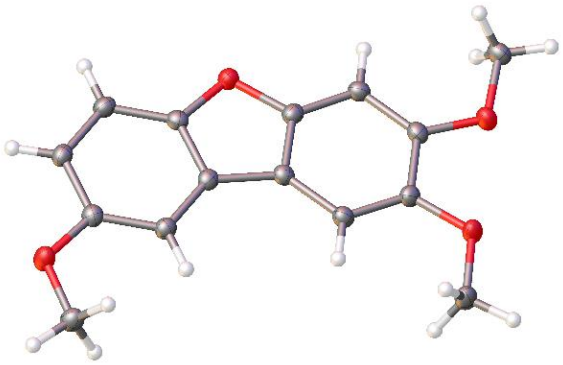

**Figure 5** Crystal structure of the trimethoxy dibenzofuran **45**

## 2.7. Investigation into 'Ligandless' Conditions

As outlined in the Introduction to this Chapter, the use of quaternary organic salts with transition-metal catalysis is a well reported means of increasing reaction efficiency. In the case of Pd metal, the function of quaternary ammonium salts is relatively well understood, particularly in the context of the Heck-Mizoroki reaction, as described earlier. These quaternary salts are known to stabilise Pd-clusters or form catalytically active species with Pd-precursors. Work by Hong,[79] Hull[70] and Muzart[101] all show how different Pd-catalysts can be reacted with quaternary ammonium salts to yield anionic Pd-species, which are catalytically active (Scheme 50). Hong and co-workers demonstrated how the isolated

anionic Pd-species remains catalytically active, even in the absence of additional ammonium salt, for the C–H functionalisation reaction depicted in Scheme 51.

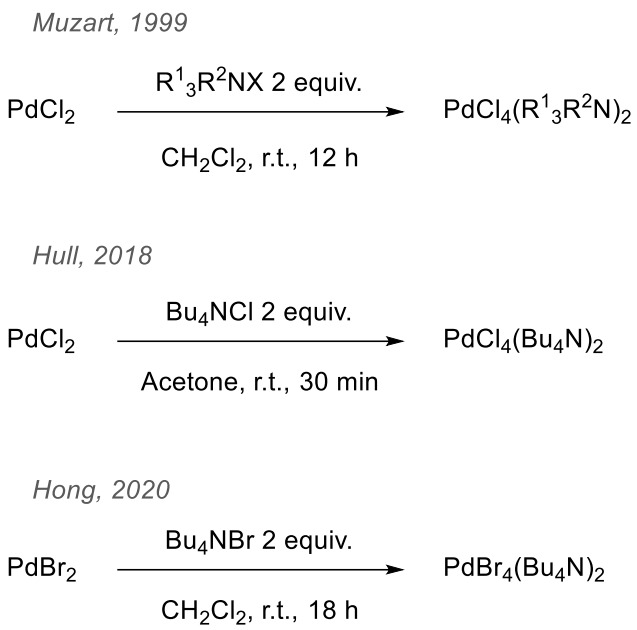


**Scheme 50** The different anionic Pd-species synthesised from quaternary ammonium salts

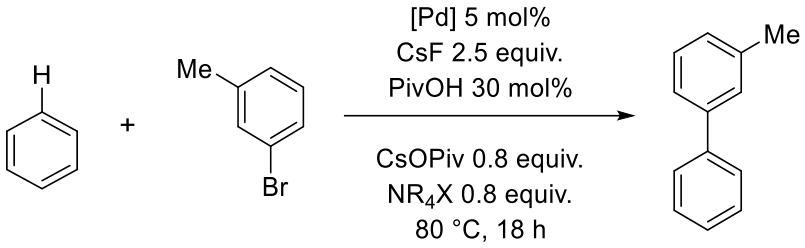


**47** **48** **49**

| *Entry* | *[Pd]* | *$NR_4X$* | *Yield* [a] |
|---|---|---|---|
| *1* | $Pd(OAc)_2$ | $Bu_4NBr$ | >99% |
| *2* | $PdBr_2$ | $Bu_4NBr$ | 91% |
| *3* | $PdBr_4(Bu_4N)_2$ | $Bu_4NBr$ | 46% |
| *4* | $PdBr_4(Bu_4N)_2$ | - | 92% |

[a] Yield determined by gas chromatography

**Scheme 51** The catalytic activity of the anionic Pd-species developed by Hong

Inspired by these bodies of work, we looked to independently generate an anionic Pd-species corresponding to our reaction conditions. Using conditions similar to Hull and co-workers,[70] two equivalents of $NBu_4OAc$ were added to one equivalent of $Pd(OAc)_2$ in dry acetone. The solution was then added to dry diethyl ether to crash out the desired palladate species **50** (Scheme 52). Once the palladate species was isolated, it was trialled in the model reaction. Using 5 mol% of the suspected palladate complex, and one equivalent of $NBu_4OAc$, the model diarylether **2** could be successfully ring closed in 34% yield (Scheme 53). This reaction demonstrates the catalytic activity of the proposed palladate species and thus, supports the hypothesis that this ammonium stabilised Pd-species is an active catalytic species in this system.

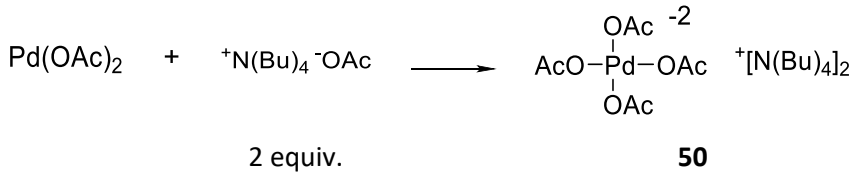


**Scheme 52** The synthesis of the ammonium acetate palladate complex

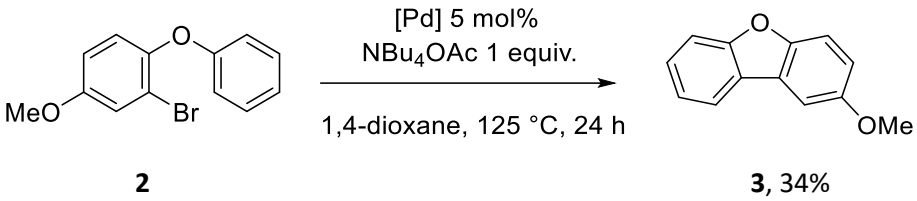


**Scheme 53** The catalytic capability of the palladate complex in our reaction

The strong precedent for quaternary ammonium salts stabilising Pd-clusters, or forming Pd nanoparticles, was a strong rationale for the conception of this project. We had also observed during the optimisation studies that the reaction performed well without the presence of phosphine ligand (70%, Table 1, Entry 1). Intrinsically, we wondered if an increase of quaternary ammonium salt would allow for higher yields to be achieved in the absence of any phosphine. Additionally, as the stoichiometry of the $NBu_4OAc$ increases, the requirement for solvent is circumvented as the quaternary salt becomes molten upon heating, allowing the reaction to be performed 'neat'. Pleasingly, with 2.5 mol% palladium and 5 equivalents of $NBu_4OAc$, a 81% yield was obtained. By doubling the $NBu_4OAc$ equivalents to 10, a 93% isolated yield was obtained for this reaction, highlighting the potentially stabilising effect that these ammonium salts can have on palladium.

These conditions allow for excellent yields of electron-rich dibenzofurans to be obtained without the requirement for organic solvent, phosphine ligand or inorganic base. It is this potential role of $NBu_4OAc$ acting as the reactions base, 'solvent' and ligand which makes the synergistic use of ammonium salts with palladium catalysis so powerful.

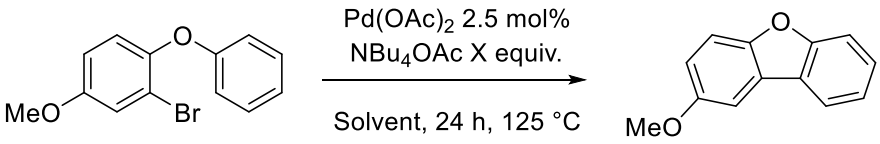


**2** **3**

| ***Entry*** | ***$NBu_4OAc$*** *(equiv.)* | ***Solvent*** | ***Yield*** [a] |
|---|---|---|---|
| *1* | 2 | 1,4-dioxane | 70% |
| *2* | 5 | Neat | 81% |
| *3* | 10 | Neat | [93%] |

[a] Yield refers to $^1H$ NMR yield using 1,3,5-trimethoxybenzene as an internal standard
Isolated yields are indicated by square brackets

**Table 4** The use of $NBu_4OAc$ to remove the requirement for phosphine ligands

Another potential role of organic salts in palladium-catalysis involves the reoxidation of catalytically inactive Pd-black to the active monomeric Pd-species. Work by de Vries[80] exhibits how halide salts can re-oxidise palladium black to allow improved catalyst turnover in the Heck reaction. Similarly, Sanford describes a Pd-catalysed reaction where the addition of a specific ligand can rescue off-cycle catalyst to keep the reaction turning over and improve the overall yield.[102] In our previous methodology to access dibenzofurans, we noticed rapid formation of Pd-black as outlined in Section 2.2. We decided to investigate whether our $NBu_4OAc$ could potential rescue some of the catalytically inactive Pd-black by oxidising the metal back to Pd (II). The Pd-catalyst ($Pd(OAc)_2$) was firstly stirred in 1,4-dioxane at 125 °C for 4 hours to degrade the metal to Pd-black, which was visibly observable. After this 4 hour period, the model substrate **2** was added to the flask, alongside 2 equivalents of $NBu_4OAc$, and left stir at reaction temperature for a further 24 hours. Interestingly, we saw a 15% conversion to the desired dibenzofuran **3**. When the parallel reaction was performed with $K_2CO_3$ as a base, only trace amounts of product was observed in the $^1H$ NMR spectrum. This experiment is not definitive but is certainly indicative towards the ability of $NBu_4OAc$ to

rescue active palladium catalysts, pointing towards another function of this organic salt in our reaction.

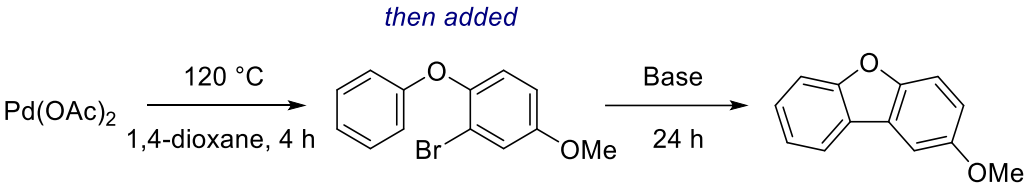


**2** **3**

| *Entry* | *Base* | *Yield* [a] |
|---|---|---|
| *1* | $NBu_4OAc$ | 15% |
| *2* | $K_2CO_3$ | <1% |

[a] Yield refers to $^1H$ NMR spectroscopy yield using 1,3,5-trimethoxybenzene as an internal standard

**Table 5** Investigation into the potential of Pd (II) regeneration from Pd-black

Liu and co-workers previously reported studies on the role of quaternary organic salts in copper-catalysed carbon–nitrogen bond formation.[86] In this report, the tetraalkylammonium or phosphonium cations undergo conductivity measurements to exhibit how these species are readily ionised in organic solvent. The authors showcase how the solubility and relative ionizations of these organic bases facilitates the reaction. Accordingly, we looked to demonstrate that the success of $NBu_4OAc$ in our protocol could not be attributed solely to improved solubility. A reaction scheme was designed where using our standard ligand and catalyst, we could employ an inorganic acetate base (KOAc) with a crown ether additive to provide improved solubility of the acetate anion (Scheme 54). However, when the crude NMR was analysed, no dibenzofuran product was observed. From this, we can rationalise that either i) the quaternary ammonium species is fundamental to the reactions success or ii) at some point in the catalytic cycle, an anionic species is formed which requires charge stabilisation which is inhibited by the presence of the crown ether additive. Regardless, we believe that the power of $NBu_4OAc$ within the protocol is not solely a result of improved reaction homogeneity and solubility. Corresponding reactions were trialled with $NMe_4OAc$ but they did not yield the same level of ring closure as achieved with $NBu_4OAc$ (Table 2).

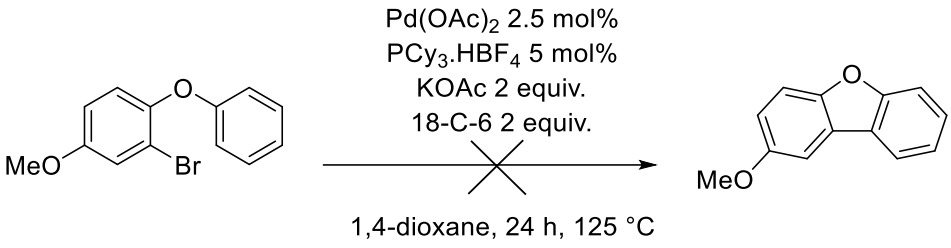


**2** **3**

**Scheme 54** The investigation into improved solubility of acetate anions using 18-C-6 additive

## 2.8. Mechanistic Considerations

As described previously, the mechanism of aryl-aryl bond formation by intramolecular direct arylation can occur by a variety of postulated mechanistic pathways (Scheme 55). This is dependent on reaction conditions and the substrate being considered. The predominant mechanistic pathway concerns a concerted metalation deprotonation CMD step and is depicted in Scheme 56. Our newly developed conditions allow previously unsuccessful substrate classes, in particular electron-rich diarylethers, to work exceedingly well by utilising $NBu_4OAc$. Considering this, we wondered could we gain a mechanistic insight into this transformation by comparing the reactivity and selectivity using our conditions with that using the standard conditions that facilitate a CMD step.

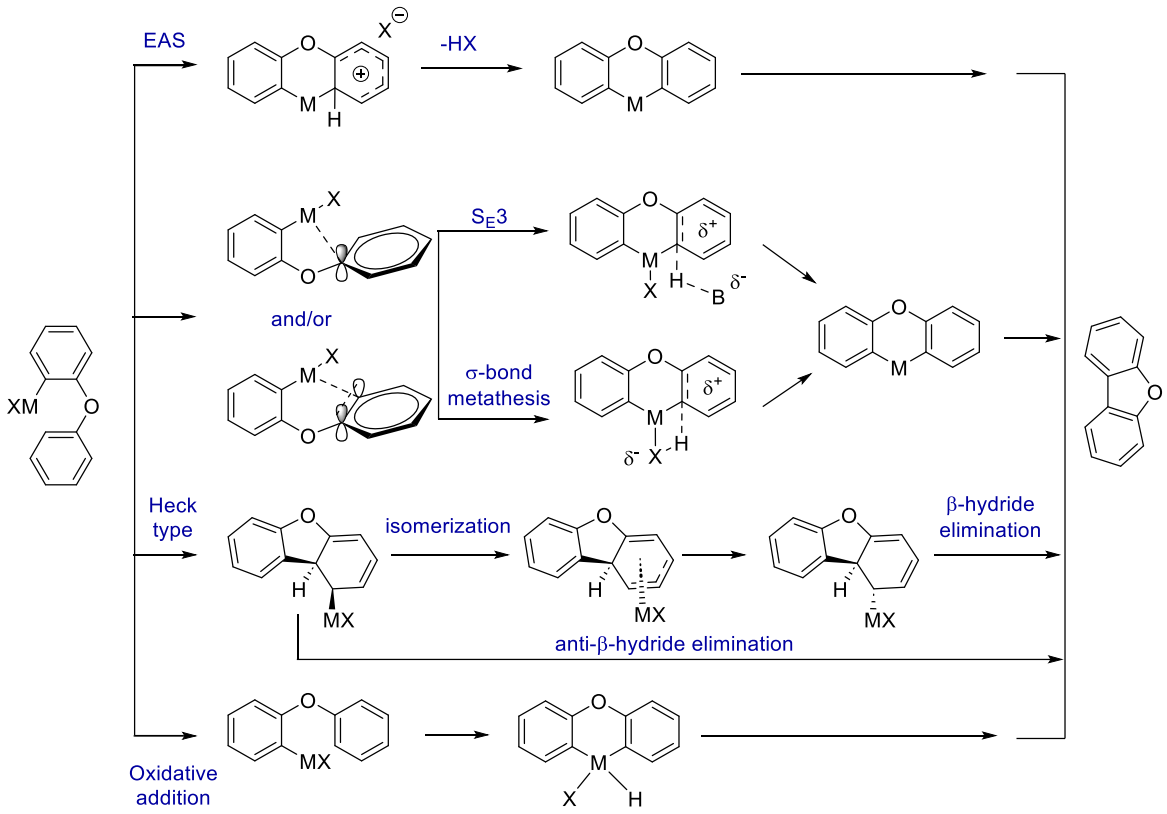


**Scheme 55** The potential mechanistic pathways available for diaryl ethers in forming dibenzofurans

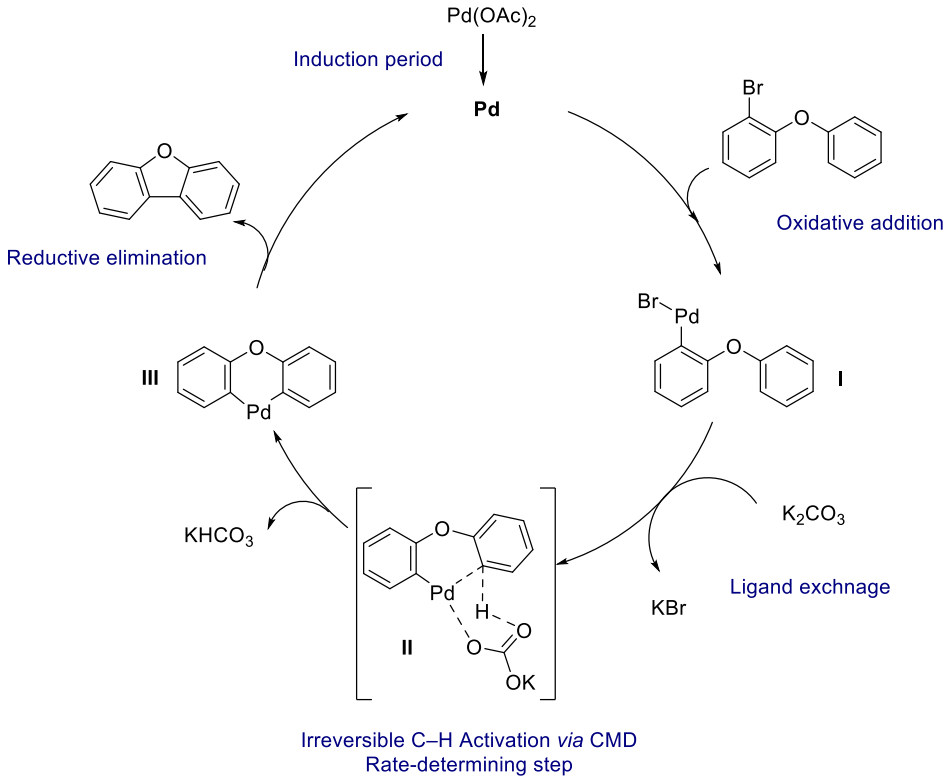


**Scheme 56** General CMD mechanism for Pd-catalysed direct arylation

Several potential reaction schemes were devised to investigate mechanistic differences between our newly developed conditions and existing literature protocols. The premise and results of each of these will be outlined below. However, many of the pathways explored proved to be inconclusive and these will be discussed before the successful attempts.

Firstly, a competition experiment between the *p*-F (**6**) and *p*-OMe (**30**) substrates was analysed (Scheme 57). Both substrates were added to the same flask under the standard reaction conditions. It was hypothesised that one of the electron-rich or electron-poor *ortho*-protons would react faster than the other. This preferential rate of reaction, dependent on the electronics of the arene, would ideally indicate a mechanism type for our conditions. When this approach was trialled at the standard temperature of 125 °C, the reaction rate was too fast and no preferential ring closure could be observed. Accordingly, the temperature was lowered to 100 °C to capture slower reaction progression. However, even with this reduced reactivity, the NMR shifts of the newly formed products **36** and **42** coincided with the signals of the diarylether starting materials.

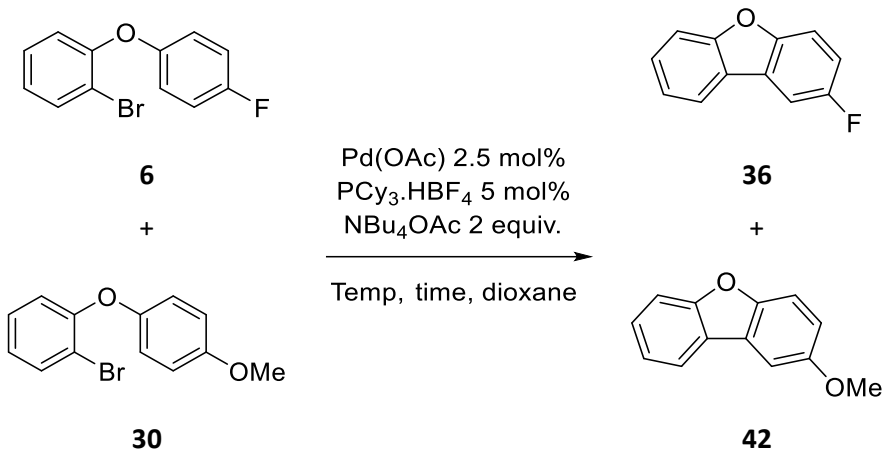


**Scheme 57** The competition experiment between *p*-F and *p*-OMe under our protocol

We then synthesised a diarylether substrate where a competition experiment could be performed on the one molecule in an intramolecular competition experiment. By using the 3-fluoro-5-methoxy phenyl boronic acid (**51**) and 2-bromophenol starting materials, the desired model compound (**52**) could be synthesised in moderate yield (Scheme 58). This substrate was designed to have one *ortho*-proton influenced by electron donating properties, and the alternative *ortho*-proton influenced by electron withdrawing properties.


**51** **16** **52**

**Scheme 58** The synthesis of a bifunctionalised model substrate for a competition experiment

Similarly, this substrate was subjected to the developed reaction conditions, where the products afforded (**53** and **54**) would be analysed to compare the arene site selectivity in the intramolecular ring closure (Scheme 59). The reaction was given the standard time of 24 hours to react but unfortunately, the crude NMR obtained gave a complex mixture of multiple products and was not definitive.

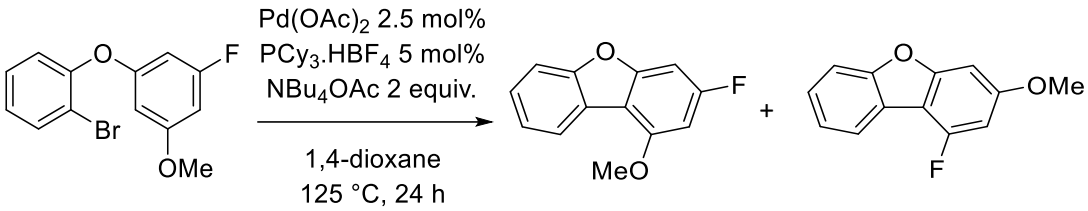


**52** **53** **54**

**Scheme 59** Intramolecular competition experiment

In a similar fashion, we investigated the use of a *meta*-substituted diarylether precursor. It was hoped that the discrimination displayed towards one of the *ortho*-C–H bonds would allow us to decipher a viable mechanistic switch from standard CMD-type conditions, to our ammonium salt conditions. The *m*-fluorinated boronic acid **55** was coupled with 2-bromophenol to yield the desired model diarylether starting material **56** (Scheme 60).

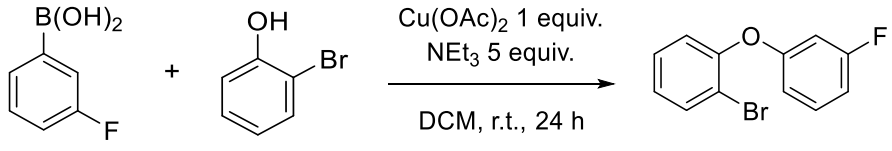


**55** **16** **56**

**Scheme 60** The synthesis of the *meta*-fluorinated diarylether

Subsequently, this precursor was subjected to literature 'CMD-type' conditions (obtained from Fagnou[19]) and the standard protocol we had developed using $NBu_4OAc$. The two potential products shown in Figure 6 have different $^{19}F$ NMR signals and so, $^{19}F$ qNMR was used as a measure of the relative ratios of product formed.[103] Using the 'CMD-type' conditions (Table 6, Entry 1) the ratio of *m*:*o* product was found to be 60:40. When our ammonium salt conditions were applied, the ratio of *m*:*o* product was found to be 70:30 (Table 6, Entry 2). This result is too small a difference to be considered a potential indicator for an alternative mechanism at play between these protocols. A large discrimination was seen between the *m*- and *o*-products for the *m*-substituted diarylether **11**, giving a ratio of 97:3 respectively (Scheme 61). However, the steric influence of this methoxy substituent is the likely factor.

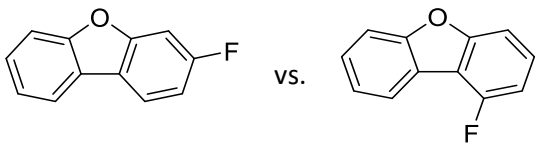


**57** **58**

δ -113.6 ppm δ -118.8 ppm

**Figure 6** The relative $^{19}F$ NMR shifts for each product

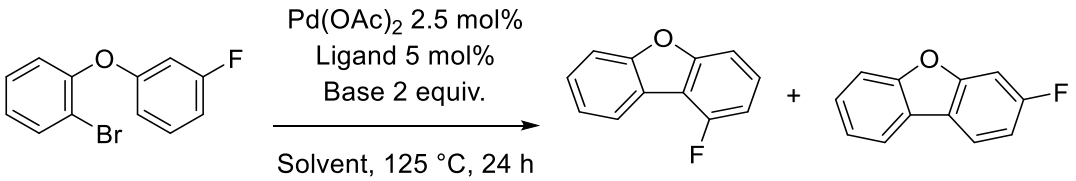


**56** **58** **57**

| *Entry* | *Ligand* | *Base* | *Solvent* | *Ratio [a] 58 : 57* |
|---|---|---|---|---|
| *1* | $P^tBu_2Me.HBF_4$ | $K_2CO_3$ | DMA | 40 : 60 |
| *2* | $PCy_3.HBF_4$ | $NBu_4OAc$ | 1,4-dioxane | 30 : 70 |

[a] Ratio determined by $^{19}F$ NMR spectroscopy

**Table 6** The electronic bias of different Pd-catalysed intramolecular direct arylation conditions for diarylethers

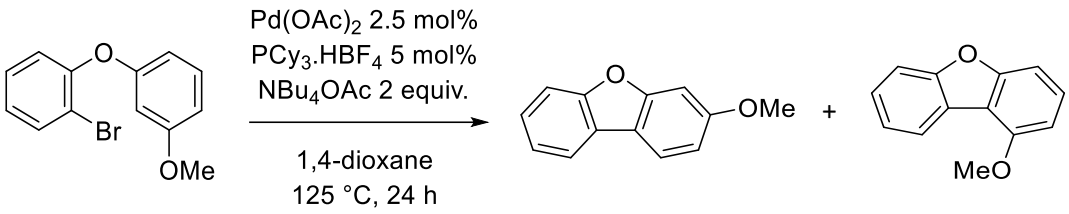


**11** **41** (97%) **59** (3%)

**Scheme 61** The electronic bias between *o* and *m* protons of a *m*-OMe substituted diarylether

Finally, in an attempt to directly compare literature CMD conditions to our protocol, the reaction reported by Fagnou and co-workers shown in Table 7 was examined.[44] Using this *meta*-fluorinated benzyloxy ether (**60**), Fagnou reports an electronic bias where the proton *ortho* to the fluorine atom (**61**) was preferential activated in a ratio of 4.3:1, when $PCy_3.HBF_4$ was employed as the ligand. When our conditions were applied to this substrate, a 1:1 ratio of both products was observed (Table 7). This change in selectivity may suggest a mechanistic switch for our protocol. However, it should be highlighted that when the phosphine ligand was changed in Fagnou's system, we observed varying ratios of the two constitutional isomers.

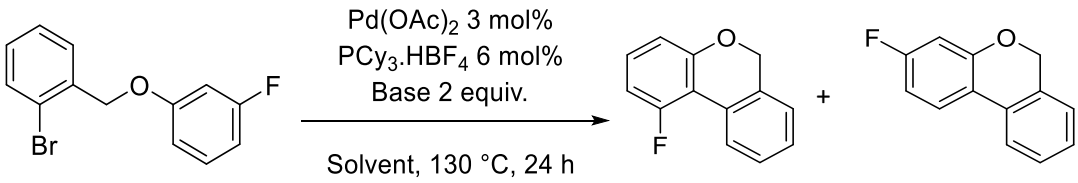


**60** **61** **62**

| *Entry* | *Base* | *Solvent* | *Ratio [a] 61 : 62* |
|---|---|---|---|
| *1* | $K_2CO_3$ | DMA | 4.3 : 1 |
| *2* | $NBu_4OAc$ | 1,4-dioxane | 1 : 1 |

[a] Ratio determined by $^1H$ NMR spectroscopy

**Table 7** The electronic bias of different Pd-catalysed intramolecular direct arylation conditions

## 2.9. Application to Six-Membered Ring Systems

Previously, within the McGlacken Group, the intramolecular direct arylation of benzyloxy ether substrates was investigated (Scheme 62).[104] With this work, the position of the halide

is fundamental to the success of the ring closure. Fagnou and co-workers previously described an excellent means of forming these benzochromene structures *via* intramolecular direct arylation.[105] Using this Pd-catalysed process, a range of steric and electronic effects was comprehensively explored. Catalytic loadings could be reduced to as low as 0.1 mol% while still retaining excellent yields of product. Additionally, the ethereal oxygen linker could be replaced with a nitrogen or carbon atom. Within the McGlacken Group, similar results were seen when the reaction was trialled with an alternative phosphine ligand. However, when the halide atom is on the phenolic fragment of the starting material, these conditions fail to yield any product. Furthermore, it was observed that when 'CMD-type' conditions were employed, only dehalogenated starting material was furnished.

*Fagnou*

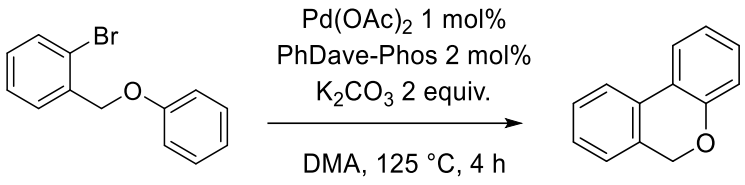


**63** **64**, 94%

*McGlacken*

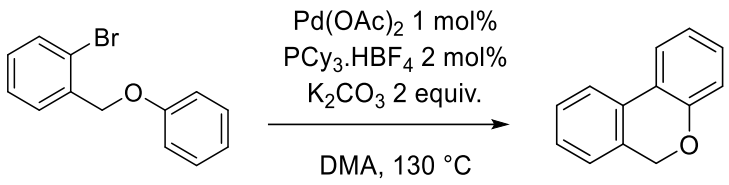


**63** **64**, 81%

*McGlacken*

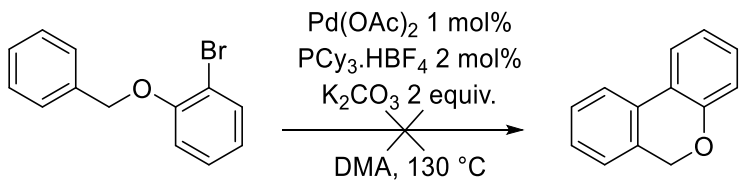


**65** **64**, 0%

**Scheme 62** Synthesis of benzochromenes performed by Fagnou and within the McGlacken Group

To date, the intramolecular direct arylation of benzyl ethers where the halide resides on the phenolic fragment, is unreported. With the successful use of $NBu_4OAc$ to effect ring closure

in dibenzofuran, we envisaged that this benzyl ether ring closure could be facilitated by the addition of quaternary ammonium salts. Using a variety of Pd catalysts and phosphine ligands, a number of reaction conditions were investigated for this substrate (Table 8). Using 5 mol% of $Pd(OAc)_2$, 10 mol% of $P^tBu_3.HBF_4$ and two equivalents of $NBu_4OAc$, the desired benzochromene could be generated in 55% yield after 48 h (Table 8, Entry 1). Unfortunately however, this result was not reproducible and the product yield varied significantly when the reaction was repeated. Alternative catalyst/ligand loadings, palladium catalysts, phosphine ligands, solvents and solvents were investigated alongside reaction temperature and time. Unfortunately, none of these initial attempts could provide good yields of the desired product. The use of added pivalic acid did not increase the yield of the reaction, despite the prominence found with employing pivalic acid as a key proton shuttle in CMD-type palladium-catalysed reactions (Table 8, Entry 4). The use of silver salt additives was also investigated, on the pretence that in C–H Activation events silver salts are well documented to facilitate key steps in the catalytic cycle. Unfortunately, the addition of silver carbonate did not increase the product yield (Table 8, Entry 7). Dimethylacetamide (DMA) (Table 8, Entries 8-10) and hexafluoro isopropanol (HFIP) (Table 8, Entry 12) were also trialled as solvents in the reaction, given the success observed when employing these solvents in C–H activation reactions. DMA gave good conversion to our desired benzochromene but disappointingly, only trace amounts of product were observed when HFIP was used as the reaction solvent. It is worth highlighting that in nearly all experiments, a moderate yield of the difficult-to-access benzochromene was observed, setting a proof-of-principle for further optimisation.

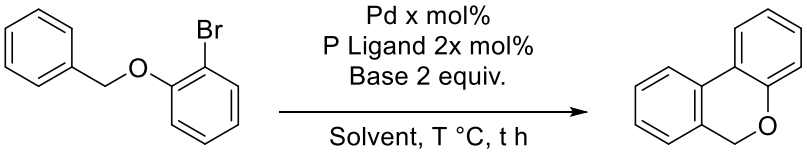


**65** **64**

| *Entry* | *Pd(OAc)₂ (mol%)* | *Ligand (mol%)* | *Additive (equiv.)* | *Base* | *Solvent* | *Time (h)* | *Yield* [a] |
|---|---|---|---|---|---|---|---|
| *1* | 5 | $P^tBu_3.HBF_4$ (10) | - | $NBu_4OAc$ | dioxane | 48 | 55% |
| *2* | 2.5 | $P^tBu_3.HBF_4$ (05) | - | $NBu_4OAc$ | dioxane | 24 | 34% |
| *3* | 2.5 | $PCy_3.HBF_4$ (05) | - | $NBu_4OAc$ | dioxane | 24 | 16% |
| *4* | 5 | $P^tBu_3.HBF_4$ (10) | PivOH[b] | $NBu_4OAc$ | dioxane | 24 | 21% |
| *5* | 5 | $P^tBu_3.HBF_4$ (10) | - | KOAc | dioxane | 24 | 10% |
| *6* | 5 | $P(pFC_6H_4)_3$ (10) | - | $NBu_4OAc$ | dioxane | 24 | 15% |
| *7* | 5 | $P^tBu_3.HBF_4$ (10) | $Ag_2CO_3$[b] | $NBu_4OAc$ | dioxane | 24 | 24% |
| *8* | 5 | $P^tBu_3.HBF_4$ (10) | - | $NBu_4OAc$ | DMA[c] | 24 | 39% |
| *9* | 5 | $PCy_3.HBF_4$ (10) | - | $NBu_4OAc$ | DMA | 24 | 43% |
| *10* | $Pd(OPiv)_2$ | $PCy_3.HBF_4$ (10) | - | $NBu_4OAc$ | DMA | 24 | 18% |
| *11* | $PdCl_2(MeCN)_2$ | $P^tBu_3.HBF_4$ (10) | - | $NBu_4OAc$ | dioxane | 24 | 23% |
| *12* | 5 | $PCy_3.HBF_4$ (10) | - | $NBu_4OAc$ | HFIP | 24 | 6% |
| *13* | 5 | $PCy_3.HBF_4$ (10) | - | $NBu_4OAc$[d] | DMA | 24 | 15% |

[a] Yield refers to $^1H$ NMR yield which is calculated using 1,3,5-trimethoxybenzene as an internal standard

[b] 30 mol% of the additive used

[c] Reaction performed at 140 °C

[d] 5 equivalents of base used

**Table 8** Optimisation for the synthesis of benzochromene using $NBu_4OAc$

Given the moderate success of DMA as a solvent for the reaction, a variety of phosphine ligands were screened in the reaction (Scheme 63). SPhos proved to be an excellent ligand when employed with $NBu_4OAc$, producing the product in 74% yield. However, like previous experiments with this reaction type, the yield varied significantly upon repetition.

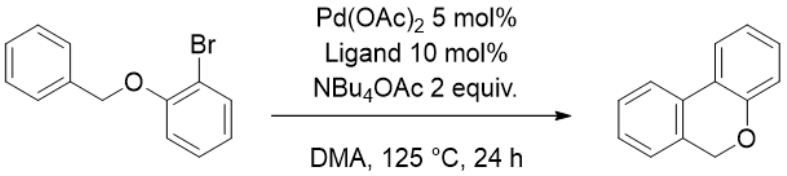


**65** **64**

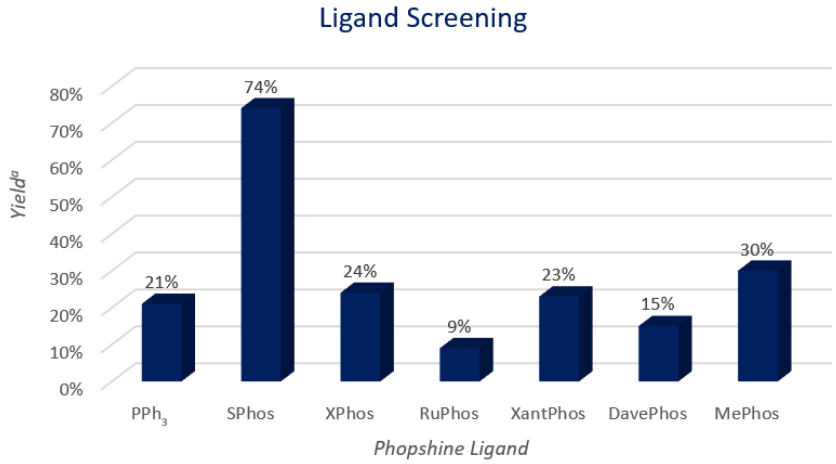


[a] Yield refers to $^1H$ NMR yield which is calculated using 1,3,5-trimethoxybenzene as an internal standard

**Scheme 63** Effect of ligand screening on the benzochromene synthesis

As a final attempt to enable this intramolecular direct arylation, we postulated that the tetrabutylphosphonium acetate that was developed during the dibenzofuran investigation, could produce higher yields in the reaction. Thus, two equivalents of $PBu_4OAc$ were used in DMA with our standard conditions (Scheme 64). However, only poor conversion to the product was observed.

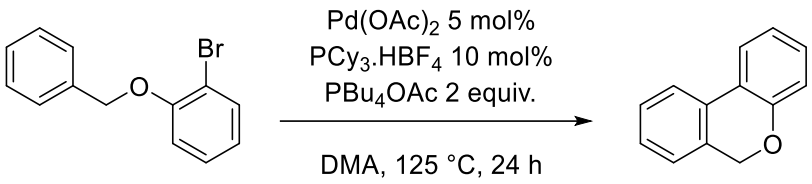


**65** **64**, 25%

**Scheme 64** The use of $PBu_4OAc$ in the intramolecular ring closure of benzoxyethers

Thus far, only poor to moderate yields of the benzochromene scaffold have been obtained from the intramolecular direct arylation of benzyloxy substrates with a halogenated phenol. The good yields obtained have been found to be somewhat irreproducible and inconsistent. However, to the best of our knowledge, this is the first time that this particular substrate has been successfully ring closed, albeit in moderate yields. The formation of any product, irrespective of the yield, showcases the potential for quaternary ammonium salts to facilitate difficult Pd-catalysed transformations. Further work is required to find a consistent reaction system that produces good yields of the desired substrate.

## 2.10. Application to Indoloquinoline Substrates

Many polycyclic alkaloids are found in traditional herbal medicines which have contributed to the discovery of new therapeutic agents.[106] The indoloquinoline structure is one such alkaloid found in the West African Climbing Shrub *Cryptolepis sanguinolenta*.[107,108] The roots of this plant have been used by traditional African healers for centuries in the treatment of a multitude of afflictions.[106,109] The indoloquinoline structure is termed a privileged scaffold due to the breadth of its therapeutic use. 11*H*-Indolo[3,2-*c*]quinoline (**66**) is an isomeric analogue of other naturally occurring indoloquinolines such as isocryptolepine, neocryptolepine and cryptolepine. An indoloquinoline scaffold is characterised by an indole and quinoline fused ring system. One can envisage a key C–H activation step to create this tetracyclic motif.

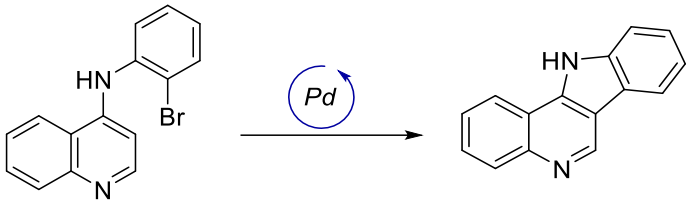


**66**

Previous work within the McGlacken group described a Pd-catalysed approach to yield a range of benzofuroquinolines.[110] Within this work, a two-step procedure was reported where a Buchwald-Hartwig amination and subsequent intramolecular direct arylation was detailed (Scheme 65). Initially, the brominated quinoline (**67**) and aniline (**68**) starting materials underwent a Buchwald-Hartwig amination to yield the diarylamine intermediate **69**. This intermediate then underwent a C–H activation event to yield the desired indoloquinoline product **66** in 61% yield over two-steps (Scheme 65).

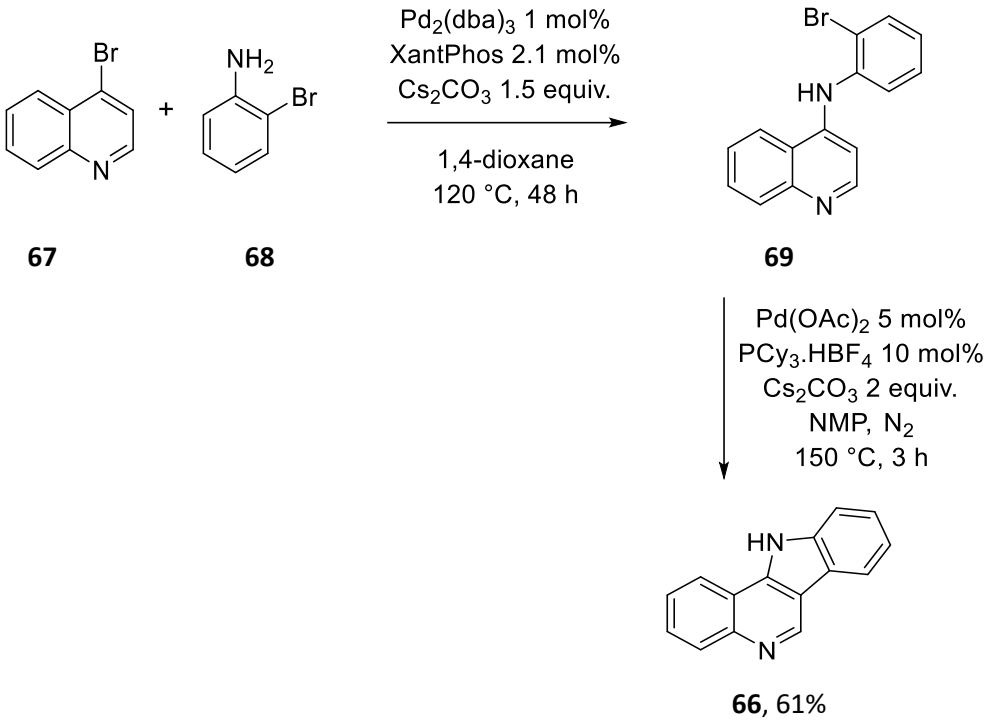


**67** **68** **69**

**66**, 61%

**Scheme 65** The synthesis of indoloquinoline via Buchwald-Hartwig coupling and subsequent direct arylation

At the time of this work, this indoloquinoline product was sent for biological evaluation for quorum sensing and yielded promising results as an antibacterial agent. Consequently, a more efficient route to target was desired as a range of these indoloquinolines would have to be synthesised. As depicted in Scheme 65, both steps share the features of high

temperature and Pd-catalysis. Given our success of employing $NBu_4OAc$ with Pd-catalysis in the synthesis of dibenzofurans, it was postulated that the organic base may improve this synthetic route. An initial problem with this route is the requirement for NMP in the C–H Activation step. NMP was required as the solvent to get acceptable yields of the desired product. However, NMP is highly toxic and required multiple steps of column chromatography to be removed. It is well documented that NMP can act as a ligand for Pd species in solution. It was thought that this potential ligation, or the increased solubility of Pd complexes in NMP relative to dioxane, was why NMP was required to obtain high yields of product.

However, it was hypothesised that the use of $NBu_4OAc$ may allow the transformation to occur in dioxane, removing the prerequisite for extensive purification. Pleasingly, when $NBu_4OAc$ was trialled in the reaction, complete consumption of starting material was observed after six hours. This success created parallels between both steps, namely; Pd catalyst, carboxylate base, dioxane solvent, inert atmosphere and high temperature. Accordingly, a one-pot approach employing $NBu_4OAc$ was attempted (Scheme 66). Pleasingly, with 3.5 equivalents of $NBu_4OAc$, the indoloquinoline could be generated in 98% yield in one-pot, with dioxane as the solvent (Table 9, Entry 1). The catalyst and ligand loading was lowered to 2.5 and 5 mol% respectively, but a drop in yield to 81% was observed (Table 9, Entry 2). Using loadings of 5 and 10 mol% for the catalyst and ligand, the loading of $NBu_4OAc$ could be reduced to 2 equivalents while retaining the high yield of 98% (Table 9, Entry 3). Similarly, an excellent yield of 90% was achieved when the ligand loading was lowered to 6 mol% (Table 9, Entry 4). Interestingly, $NBu_4OAc$ also enabled changing the solvent to cyclopentylmethyl ether (CPME) (Table 9, Entry 5 and 6). CPME is classed as a green solvent[94,95] and is a significant advancement from the original solvent of NMP. Furthermore, it was found that the reaction did not require an inert atmosphere under these conditions. Using 5 and 6 mol% of the catalyst and phosphine respectively, with 2 equivalents of $NBu_4OAc$ in CPME, the reaction could proceed in air to give an 86% isolated yield of the desired product (Table 9, Entry 8). However, it is worth noting that when the reaction was trialled in non-anhydrous solvent (Table 9, Entry 7), or in the absence of phosphine (Table 9, Entry 9) the yield was reduced.

To conclude, the indoloquinoline scaffold can be synthesised in excellent yields in one-pot from simple starting materials when $NBu_4OAc$ is employed in the reaction. Many previous syntheses utilise harsh reaction conditions, hazardous reagents or multi-step protocols to access these scaffolds. When using an excess of quaternary ammonium salt, a one-pot

procedure can be carried out to achieve high yields of the desired product without the need for phosphine ligand or additional solvent.

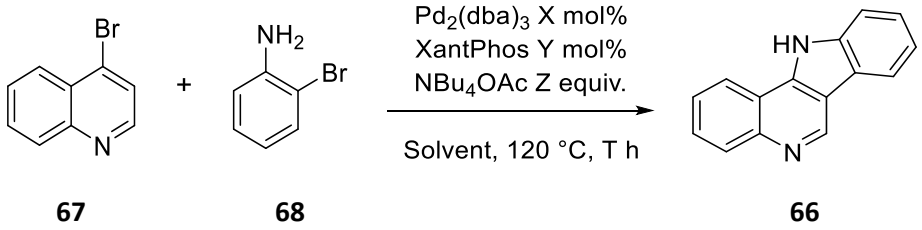


**67** **68** **66**

**Scheme 66** The one-pot optimisation of the synthesis of indoloquinoline

| ***Entry*** | ***$Pd_2(dba)_3$*** *(mol%)* | ***XantPhos*** *(mol%)* | ***$NBu_4OAc$*** *(equiv.)* | ***Time*** *(h)* | ***Solvent*** *(dried)* | ***Atmosphere*** | ***Yield*** [a] |
|---|---|---|---|---|---|---|---|
| *1* | 5 | 10 | 3.5 | 30 | dioxane | $N_2$ | 98%[a] |
| *2* | 2.5 | 5 | 3.5 | 30 | dioxane | $N_2$ | 81%[a] |
| *3* | 5 | 10 | 2 | 30 | dioxane | $N_2$ | 98%[a] |
| *4* | 5 | 6 | 2 | 30 | dioxane | $N_2$ | 90%[a] |
| *5* | 5 | 10 | 2 | 30 | CPME | $N_2$ | 93%[a] |
| *6* | 5 | 6 | 2 | 30 | CPME | $N_2$ | 90%[a] |
| *7* | 5 | 10 | 2 | 30 | CPME[b] | $N_2$ | 32%[a] |
| *8* | 5 | 6 | 2 | 30 | CPME | Air | [86%] |
| *9* | 5 | 0 | 2 | 48 | CPME | Air | 17%[a] |

[a] Yield refers to $^1H$ NMR yield which is calculated using 1,3,5-trimethoxybenzene as an internal standard
[b] Refers to non-anhydrous solvent used in the reaction

**Table 9** The optimisation of the one-pot synthesis of indoloquinoline

As showcased with the synthesis of dibenzofurans the use of excess quaternary ammonium salt can obviate the requirement for phosphine ligands. A similar investigation was performed with the one-pot synthesis of indoloquinoline (Scheme 67). To our delight, the desired tetracyclic product was formed in an excellent yield of 94% when 5 mol% of Pd catalyst was used with 10 equivalents of $NBu_4OAc$. As discussed earlier, $NBu_4OAc$ can be identified as an ionic liquid and so, when adding 10 equivalents of the salt to the reaction, the need for a solvent is removed. In this case, the $NBu_4OAc$ performs as the base, solvent and potentially a ligand in the system.

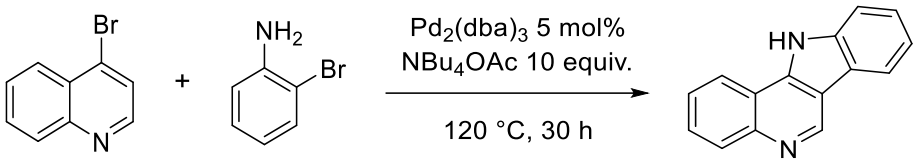


**67** **68** **66**, 94%

**Scheme 67** The use of excess $NBu_4OAc$ to allow removal of phosphine

## 2.11. Conclusions and Future Work

The intramolecular cyclisation of electron-rich diarylethers and diarylamines was successfully demonstrated. In the case of diarylether substrates, a range of dibenzofuran scaffolds were furnished in excellent yields by employing $NBu_4OAc$ in the Pd-catalysed C–H Activation event. A protocol where excess $NBu_4OAc$ could act as the base, solvent and ligand furnished the desired dibenzofuran in 93% yield. Investigations into the role of the $NBu_4OAc$ salt were explored. It was postulated that the quaternary ammonium salt can possibly stabilise palladium colloids, rescue off-cycle palladium or form active palladate species. These palladium-ammonium interactions are attributed to the successful C–H Activation performed on these difficult electron-rich substrates. Furthermore, the protocol was extended to indoloquinolines. A one-pot Buchwald-Hartwig, C–H activation procedure was devised where halogenated quinolines and anilines could be coupled using Pd-catalysis and $NBu_4OAc$. This improved protocol reduces the steps required to access indoloquinolines. Additionally, the requirement for hazardous reagents like NMP are circumvented when $NBu_4OAc$ was employed.

Future work on this project will involve synthesising a range of indoloquinolines to be biologically evaluated for their antibacterial properties. A key goal of future work is to better understand the palladium-ammonium complex which enables the transformation to take place.

# 3. Experimental

## 3.1. General Procedures

All solvents and reagents purchased from Sigma Aldrich, Fluorochem/Doug Discovery, Alfa Aesar, Tokyo Chemical Industry and Strem were used as obtained from commercial sources and without purification, unless otherwise noted. All experiments performed under inert conditions were done so under an atmosphere of nitrogen atmosphere, using flame-dried glassware and Schlenk set-up. When required, solvents were dried using activated 3Å molecular sieves (20% w/v) and stored inertly in a Young's flask.

Wet flash column chromatography was carried out using Kieselgel 60 Å (35-70 µm) silica gel (Merck). Thin Layer Chromatography (TLC) was carried out on pre-coated silica gel plates (Merck 60 PF254). Visualisation was achieved by UV light and staining with potassium permanganate staining. Melting points (m.p) were recorded on a uni-melt Thomas Hoover Capillary melting point apparatus or an Electrothermal IA9300 Digital Melting Point apparatus.

NMR spectra were run in $CDCl_3$ using tetramethylsilane (TMS) as the internal standard at 25 °C, unless otherwise specified. $^{1}H$ NMR (600 MHz spectra), $^{1}H$ NMR (500 MHz) spectra, $^{1}H$ NMR (400 MHz) spectra and $^{1}H$ NMR (300 MHz) spectra were recorded on Bruker Avance 600, Bruker Avance 500, Burker Avance 400 and Bruker Avance 300 NMR spectrometers respectively. $^{13}C$ (150 MHz) spectra, $^{13}C$ (125 MHz) spectra, $^{13}C$ (100 MHz) spectra and $^{13}C$ (75.5 MHz) spectra were recorded on Bruker Avance 600, Bruker Avance 500, Burker Avance 400 and Bruker Avance 300 NMR spectrometers respectively in proton decoupled mode. $^{19}F$ NMR (376 MHz) and $^{19}F$ NMR (282 MHz) spectra were recorded on a Bruker Avance 400 and Bruker Avance 300 NMR spectrometers respectively in proton decoupled mode. All spectra were recorded at University College Cork. Chemical shifts $\delta_H$ and $\delta_C$ are expressed as parts per million (ppm), positive shift being downfield from TMS; coupling constants (*J*) are expressed in hertz (Hz) as observed and are uncorrected. Splitting patterns in $^{1}H$ NMR spectra are designated as s (singlet), br s (broad singlet), d (doublet), dd (doublet of doublets), dt (doublet of triplets), t (triplet), q (quartet) and m (multiplet). For $^{13}C$ NMR spectra, the number of attached protons for each signal was determined using the DEPT pulse sequence run in the DEPT-90 and DEPT-135 modes. $^{1}H$-$^{1}H$ COSY, HSQC, and HMBC experiments were performed to aid the NMR assignment of novel chemical structures.

Nominal mass spectra (LRMS) were recorded on a Waters Quattro Micro Triple Quadrupole spectrometer (QAA1202) in ESI mode using 50% acetonitrile–water containing 0.1% formic acid as eluent. Samples were prepared in acetonitrile. High resolution mass spectra (HRMS) were recorded on a Waters LCT Premier Time of Flight (ToF LC-MS) spectrometer (KD160) or a Waters Vion IMS mass spectrometer (SAA055 K) with Waters Acquity I-class UPLC in electrospray ionisation (ESI) mode using 50% acetonitrile– water containing 0.1% formic acid as eluent and Leucine Enkephalin as a reference solution. Samples (max. 1 mg/mL) were dissolved in acetonitrile, methanol, water or 10% DMSO/acetonitrile.

The Microanalysis Laboratory, National University of Ireland, Cork, performed elemental analysis using a Perkin-Elmer 240 and Exeter Analytical CE440 elemental analysers.

$^{1}$H NMR spectra, $^{13}$C spectra, and LRMS analyses were recorded for all previously reported compounds. For novel compounds, in addition to the aforementioned analyses, HRMS and 2D $^{1}$H NMR spectra were also obtained. Crystal structures were also obtained for select substrates.

**2-bromo-4-methoxy-1-phenoxybenzene (2)**

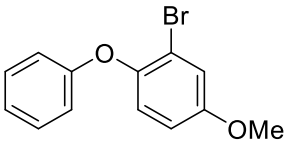


2-bromo-4-methoxy phenol (406 mg, 2 mmol, 1 equiv.), phenyl boronic acid (487 mg, 4 mmol, 2 equiv.), $Cu(OAc)_2$ (1 equiv.) and triethylamine (1.4 mL, 5 equiv.) were added to a 250 mL round-bottom flask containing DCM (20 mL) and 3 Å molecular sieves. The resulting mixture was stirred at room temperature until TLC analysis indicated complete consumption of starting material (48 h). The reaction mixture was then filtered through Celite® using hexanes (60 mL). The filtrate was then concentrated *in vacuo* and the resulting residue was purified by silica gel chromatography (7:3 hexane:DCM, gradient to 100% hexane) to yield the title product as a white solid (386 mg, 69%). M.P: 63 ˚ C (lit. 61–62 ˚ C).[111]

$^1$H NMR (300 MHz, $CDCl_3$) $\delta_H$; 7.34 – 7.26 (m, 2H), 7.17 (d, $J$ = 3.0 Hz, 1H), 7.09 – 6.94 (m, 2H), 6.93 – 6.78 (m, 3H), 3.80 (s, 3H) ppm. $^{13}$C NMR (75 MHz, $CDCl_3$) $\delta_C$; 157.9, 156.6, 146.6, 129.6, 122.5, 118.5, 116.7, 116.1, 114.6, 55.9 ppm. HRMS (ESI-TOF) m/z: $[M]^+$ calcd. for $C_{13}H_{11}BrO_2$: 279.0015, found: 279.0022.

**2-bromo-4-fluoro-1-phenoxybenzene (5)**

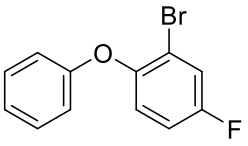


2-bromo-4-fluorophenol (382mg, 2 mmol, 1 equiv.), phenyl boronic acid (488 mg, 4 mmol, 2 equiv.), $Cu(OAc)_2$ (1 equiv., 2 mmol) and triethylamine (1.4 mL, 5 equiv., 10 mmol) were added to a 250 mL round-bottom flask containing DCM (20 mL) and 3 Å molecular sieves. The resulting mixture was stirred at room temperature until TLC analysis indicated complete consumption of starting material (48 h). The reaction mixture was then filtered through Celite® using hexanes (60 mL). The filtrate was then concentrated *in vacuo* and the resulting residue was purified by silica gel chromatography (7:3 DCM:Hexane) to yield the title product as a white solid (214 mg, 40%). MP: 63 °C (lit 60 – 61 ˚ C). Characterisation data is consistent with the literature.[45]

$^1$H NMR (400 MHz, $CDCl_3$) $\delta_H$; 7.44 – 7.31 (m, 3H), 7.16 – 7.10 (m, 1H), 7.07 – 6.93 (m, 4H) ppm. $^{13}$C NMR (125 MHz, $CDCl_3$) $\delta_C$; 158.7 (d, $J_{C\text{-}F}$ = 246 Hz), 157.2, 149.8 (d, $J_{C\text{-}F}$ = 3.0 Hz), 129.8, 123.3, 121.8 (d, $J_{C\text{-}F}$ = 9.0 Hz), 120.7 (d, $J_{C\text{-}F}$ = 26 Hz), 117.5, 115.6 (d, $J_{C\text{-}F}$ = 23.0 Hz), 115.5 ppm. $\delta_F$ (376 MHz, $CDCl_3$): -117.2 ppm

**1-bromo-2-(4-fluorophenoxy)benzene (6)**

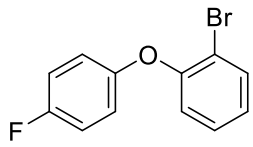


2-bromophenol (346 mg, 2 mmol, 1 equiv.), 4-fluorobenzne boronic acid (560 mg, 4 mmol, 2 equiv.), $Cu(OAc)_2$ (363 mg, 1 equiv., 2 mmol) and triethylamine (1,4 mL, 5 equiv., 10 mmol) were added to a 250 mL round-bottom flask containing DCM (20 mL) and 3 Å molecular sieves. The resulting mixture was stirred at room temperature until TLC analysis indicated complete consumption of starting material (48 h). The reaction mixture was then filtered through Celite® using hexanes (60 mL). The filtrate was then concentrated *in vacuo* and the resulting residue was purified by silica gel chromatography (7:3 hexane:DCM) to yield the title product as a colourless oil (374 mg, 70%). Characterisation data is consistent with the literature.[45]

$^1$H NMR (400 MHz, $CDCl_3$) $\delta_H$; 7.62 (dd, $J$ = 8.0, 1.4 Hz, 1H), 7.29 – 7.22 (m, 1H), 7.08 – 6.87 (m, 6H) ppm. $^{13}$C NMR (100 MHz, $CDCl_3$) $\delta_C$; 158.8 (d, $J_{C\text{-}F}$ = 243 Hz), 154.0, 152.7 (d, $J_{C\text{-}F}$ = 2.4 Hz), 133.9, 128.7, 124.9, 119.9 (2 x CH, d, $J_{C\text{-}F}$ = 11.5 Hz), 119.7, 116.3 (2 x CH, d, $J_{C\text{-}F}$ = 23.5 Hz), 114.5 ppm. $\delta_F$ (282 MHz, $CDCl_3$): -119.9 ppm. HRMS (ESI-TOF) m/z: $[M+Na]^+$ calcd. for $C_{12}H_8BrFONa$: 288.9634, found: 288.9625.

**3-bromo-4-phenoxypyridine (7)**

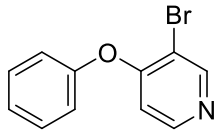


A mixture of 3-bromo-4-chloro pyridine (0.3 g, 1.56 mmol, 1 equiv.) and phenol (0.586 g, 6.23 mmol, 5 equiv.) were added to a 250 mL round bottomed flask and stirred neat at 130 °C in an oil bath until TLC analysis indicated complete consumption of starting material. The cooled reaction mixture was then diluted with 10% aq. NaOH (5 mL) and stirred at room temperature for 1 hour. The aqueous phase was extracted with DCM (3 × 10 mL). The combined organics were washed with 6M NaOH (3 × 10 mL), water (10 mL) and brine (10 mL) and then dried with MgSO4, filtered and concentrated in vacuo. The crude product was passed through a short pad of silica (hexanes:EtOAc, 3:1) to yield the title product as a yellow oil (0.345 g, 88%).

$^1$H NMR (300 MHz, $CDCl_3$) $\delta_H$; 8.70 (bs, 1H), 8.30 (bs, 1H), 7.49 – 7.40 (m, 2H), 7.31 – 7.24 (m, 1H), 7.14 – 7.07 (m, 2H), 6.62 (d, $J$ = 5.6 Hz, 1H) ppm. $^{13}$C NMR (75 MHz, $CDCl_3$) $\delta_C$; 161.4, 153.8, 153.3, 149.8, 130.3, 125.8, 120.6, 116.3 and 111.6 ppm. HRMS (ESI-TOF) m/z: $[M]^+$ calcd. for $C_{11}H_8BrNO$: 249.9862, found: 249.9861.

**1-(3-bromo-4-phenoxyphenyl)ethan-1-one (8)**

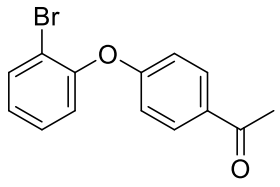

2-bromophenol (0.126 mL, 1.2 mmol, 1 equiv.), 4-acetyl phenyl boronic acid ( 399 mg, 2.4 mmol, 2 equiv.), $Cu(OAc)_2$ (218 mg, 1 equiv., 1.2 mmol) and triethylamine (0.84 mL, 5 equiv., 10 mmol) were added to a 250 mL round-bottom flask containing DCM (12 mL) and 3 Å molecular sieves. The resulting mixture was stirred at room temperature until TLC analysis indicated complete consumption of starting material (24 h). The reaction mixture was then filtered through Celite® using hexanes (60 mL). The filtrate was then concentrated *in vacuo* and the resulting residue was purified by silica gel chromatography (100% DCM) to yield the title product as a white solid (105 mg, 30%). MP: 61 °C.

$^1$H NMR (300 MHz, $CDCl_3$) $\delta_H$; 7.98 – 7.91 (m, 2H), 7.67 (dd, *J* = 7.9, 1.6 Hz, 1H), 7.35 (td, *J* = 15.6, 1.6 Hz, 1H), 7.16 – 7.06 (m, 2H), 6.97 – 6.91 (m, 2H), 2.57 (s, 3H) ppm$^{13}$C NMR (125 MHz, $CDCl_3$) $\delta_C$; 196.6, 161.3, 152.0, 134.1, 132.1, 130.6, 129.0, 126.4, 122.4, 116.5, 115.9, 26.4 ppm. HRMS (ESI-TOF) m/z: $[M]^+$ calcd. for $C_{14}H_{11}BrO_2$: 291.0015, found: 291.0027.

**1-bromo-2-phenoxybenzene (9)**

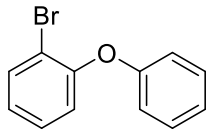

2-bromo phenol (0.117 mL, 1 mmol, 1 equiv.), phenyl boronic acid (244 mg, 2 mmol, 2 equiv.), $Cu(OAc)_2$ (181 mg, 1 mmol, 1 equiv.) and triethylamine (0.7 mL, 5 mmol, 5 equiv.) were added to a 250 mL round-bottom flask containing DCM (10 mL) and 3 Å molecular sieves. The resulting mixture was stirred at room temperature until TLC analysis indicated complete consumption of starting material (20 h). The reaction mixture was then filtered through Celite® using hexanes (60 mL). The filtrate was then concentrated *in vacuo* and the resulting residue was purified by silica gel chromatography (100% Hexane) to yield the title product as a colourless oil (151 mg, 61% yield). Characterisation data is consistent with the literature.[49]

$^1$H NMR (400 MHz, $CDCl_3$) $\delta_H$; 7.63 (dd, *J* = 7.9, 1.4 Hz, 1H), 7.36 – 7.29 (m, 2H), 7.28 – 7.22 (m, 1H), 7.14 – 7.07 (m, 1H), 7.05 – 6.93 (m, 4H). $^{13}$C NMR (100 MHz, $CDCl_3$) $\delta_C$; 156.9, 153.7, 133.8, 129.8, 129.7, 128.6, 124.9, 123.4, 120.6, 118.9, 118.1, 114.9 ppm. HRMS (ESI-TOF) m/z: $[M]^+$calcd. for 248.9909 found 248.9907.

**1-bromo-2-(*m*-tolyloxy)benzene (10)**

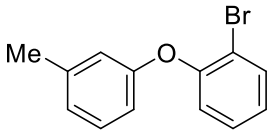


2-bromo phenol (0.23 mL, 2 mmol, 1 equiv.), 3-tolyl boronic acid (544 mg, 4 mmol, 2 equiv.), $Cu(OAc)_2$ (363 mg, 2 mmol, 1 equiv.) and triethylamine (1.4 mL, 10 mmol, 5 equiv.) were added to a 250 mL round-bottom flask containing DCM (20 mL) and 3 Å molecular sieves. The resulting mixture was stirred at room temperature until TLC analysis indicated complete consumption of starting material (48 h). The reaction mixture was then filtered through Celite® using hexanes (60 mL). The filtrate was then concentrated *in vacuo* and the resulting residue was purified by silica gel chromatography (7:3 DCM:Hexane) to yield the title product as a clear oil (294 mg, 56%).

$^1$H NMR (300 MHz, $CDCl_3$) $\delta_H$; 7.61 (dd, *J* = 7.9, 1.6 Hz, 1H), 7.28 – 7.15 (m, 2H), 7.01 –6.85 (m, 3H), 6.84 – 6.71 (m, 2H), 2.32 (s, 3H) ppm. $^{13}$C NMR (75 MHz, $CDCl_3$) $\delta_C$; 156.9, 153.8, 140.0, 133.8, 129.5, 128.6, 124.8, 124.3, 120.6, 118.9, 115.2, 114.9, 21.4 ppm. HRMS (ESI-TOF) m/z: $[M+H]^+$ calculated for $C_{13}H_{11}BrO$: 263.0066 found 263.0070.

**1-bromo-2-(3-methoxyphenoxy)benzene (11)**

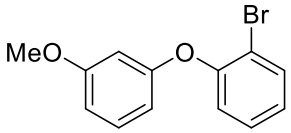


2-bromo phenol (0.105 mL, 1 mmol, 1 equiv.), 3-methoxy phenyl boronic acid (304 mg, 2 mmol, 2 equiv.), $Cu(OAc)_2$ (181 mg, 1 mmol, 1 equiv.) and triethylamine (0.7 mL, 5 mmol, 5 equiv.) were added to a 250 mL round-bottom flask containing DCM (10 mL) and 3 Å molecular sieves. The resulting mixture was stirred at room temperature until TLC analysis indicated complete consumption of starting material (24 h). The reaction mixture was then filtered through Celite® using hexanes (60 mL). The filtrate was then concentrated *in vacuo* and the resulting residue was purified by silica gel chromatography (1:1 Hexane:DCM) to yield the title product as a colourless oil (199 mg, 71%). Characterisation data consistent with the literature.[49]

$^1$H NMR (300 MHz, $CDCl_3$) $\delta_H$; 7.65 – 7.57 (m, 1H), 7.29 – 7.16 (m, 2H), 7.04 – 6.95 (m, 2H), 6.67 – 6.62 (m, 1H), 6.56 – 6.48 (m, 2H), 3.76 (s, 3H) ppm. $^{13}$C NMR (75 MHz, $CDCl_3$) $\delta_C$; 161.0, 158.1, 153.5, 133.8, 130.2, 128.7, 125.2, 120.9, 115.0, 110.1, 109.0, 104.2, 55.4 ppm. HRMS (ESI-TOF) m/z: $[M]^+$ calcd. for $C_{13}H_{11}BrO_2$: 279.0015, found: 279.0016.

**2-(2-bromophenoxy)-1,4-dimethylbenzene (12)**

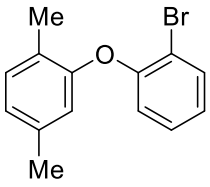


2-bromo phenol (0.23 mL, 2 mmol, 1 equiv.), 2,5-dimethyl phenyl boronic acid (600 mg, 4 mmol, 2 equiv.), $Cu(OAc)_2$ (383 mg, 2 mmol, 1 equiv.) and triethylamine (1.4 mL, 10 mmol, 5 equiv.) were added to a 250 mL round-bottom flask containing DCM (20 mL) and 3 Å molecular sieves. The resulting mixture was stirred at room temperature until TLC analysis indicated complete consumption of starting material (48 h). The reaction mixture was then filtered through Celite® using hexanes (60 mL). The filtrate was then concentrated *in vacuo* and the resulting residue was purified by silica gel chromatography (7:3 DCM:Hexane) to yield the title product as a yellow oil (189 mg, 34%).

$^1$H NMR (400 MHz, $CDCl_3$) $\delta_H$; 7.61 (dd, *J* = 8.0, 1.3 Hz, 1H), 7.22 – 7.16 (m, 1H), 7.13 (d, *J* = 7.7 Hz, 1H), 6.93 (td, *J* = 7.7, 1.3 Hz, 1H), 6.88 (d, *J* = 8.0 Hz, 1H), 6.72 (dd, *J* = 8.0, 1.3 Hz, 1H), 6.65 (s, 1H), 2.27 (s, 3H) and 2.20 (s, 3H) ppm. $^{13}$C NMR (125 MHz, $CDCl_3$) $\delta_C$; 154.4, 153.9, 137.1, 133.7, 131.2, 128.4, 126.3, 124.9, 123.7, 119.7, 118.1, 113.4, 20.9, 15.7 ppm. HRMS (ESI-TOF) m/z: $[M]^+$ calcd. for $C_{14}H_{13}BrO$: 277.0222, found: 277.0221.

**2-bromo-4-methoxy-1-(4-methoxyphenoxy)benzene (13)**

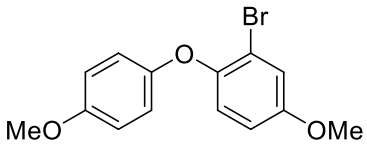


2-bromo-4-methoxy phenol (305 mg, 1.5 mmol, 1 equiv.), *p*-methoxy phenyl boronic acid (456 mg, 3 mmol, 2 equiv.), $Cu(OAc)_2$ (272 mg, 1.5 mmol, 1 equiv.) and triethylamine (1.05 mL, 7.5 mmol, 5 equiv.) were added to a 250 mL round-bottom flask containing DCM (15 mL) and 3 Å molecular sieves. The resulting mixture was stirred at room temperature until TLC analysis indicated complete consumption of starting material (48 h). The reaction mixture was then filtered through Celite® using hexanes (60 mL). The filtrate was then concentrated *in vacuo* and the resulting residue was purified by silica gel chromatography (8:2 $CHCl_3$:Hexane) to yield the title product as a colourless oil (88 mg, 19%).

$^1$H NMR (300 MHz, $CDCl_3$) $\delta_H$; 7.15 (d, *J* = 2.9 Hz, 1H), 6.92 – 6.76 (m, 6H), 3.77 (apparent doublet, 6H) ppm. $^{13}$C NMR (75 MHz, $CDCl_3$) $\delta_C$; 156.1, 155.4, 151.4, 147.9, 121.2, 119.5, 118.6, 118.5, 115.1, 114.8, 114.5, 55.9, 55.7 ppm. HRMS (ESI-TOF) m/z: $[M]^+$ calcd. for $C_{14}H_{13}BrO_3$: 309.0121, found: 309.0115.

**2-bromo-1-(3,4-dimethoxyphenoxy)-4-methoxybenzene) (14)**

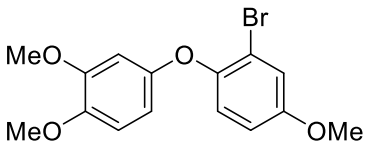


2-bromo-4-methoxy phenol (406 mg, 2 mmol, 1 equiv.), 3,4-dimethoxy phenyl boronic acid (728 mg, 4 mmol, 2 equiv.), $Cu(OAc)_2$ (363 mg, 2 mmol, 1 equiv.) and triethylamine (1.4 mL, 10 mmol, 5 equiv.) were added to a 250 mL round-bottom flask containing DCM (20 mL) and 3 Å molecular sieves. The resulting mixture was stirred at room temperature until TLC analysis indicated complete consumption of starting material (48 h). The reaction mixture was then filtered through Celite® using hexanes (60 mL). The filtrate was then concentrated *in vacuo* and the resulting residue was purified by silica gel chromatography (1:1 Hexane:DCM) to yield the title product as an off-white solid (100 mg, 15%) MP: 92 – 93 ˚ C.

$^1$H NMR (300 MHz, $CDCl_3$) $\delta_H$; 7.16 (d, *J* = 2.9 Hz, 1H), 6.94 – 6.87 (m, 1H), 6.84 – 6.87 (m, 2H) 6.61 (d, *J* = 2.8 Hz, 1H), 6.36 (dd, *J* = 8.7, 2.8 Hz, 1H), 3.85 – 3.82 (m, 6H), 3.79 (s, 3H) ppm. $^{13}$C NMR (75.5 MHz, $CDCl_3$) $\delta_C$; 156.2, 151.7, 149.9, 147.6, 144.9, 121.3, 118.5, 115.2, 114.5, 111.7, 108.1, 102.8, 56.3, 55.9, 55.8 ppm. HRMS (ESI-TOF) m/z: $[M]^+$ calcd. For $C_{15}H_{15}BrO_4$: 339.0226, found: 339.0222.

**5-(2-bromo-4-methoxyphenoxy)-1,2,3-trimethoxybenzene (15)**

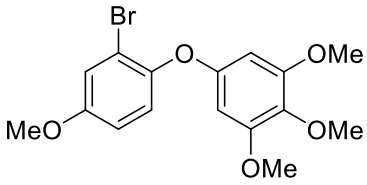


2-bromo-4-methoxy phenol (264 mg, 1.3 mmol, 1 equiv.), 3,4,5-trimethoxy phenyl boronic acid (551 mg, 2.6 mmol, 2 equiv.), $Cu(OAc)_2$ (236 mg, 1.3 mmol, 1 equiv.) and triethylamine (0.9 mL, 6.5 mmol, 5 equiv.) were added to a 250 mL round-bottom flask containing DCM (13 mL) and 3 Å molecular sieves. The resulting mixture was stirred at room temperature until TLC analysis indicated complete consumption of starting material (24 h). The reaction mixture was then filtered through Celite® using hexanes (60 mL). The filtrate was then concentrated *in vacuo* and the resulting residue was purified by silica gel chromatography (100% DCM) to yield the title product as a white solid (85 mg, 12%) MP: 129 – 130 ˚ C.

$^1$H NMR (300 MHz, $CDCl_3$) $\delta_H$; 7.17 (d, *J* = 2.9 Hz, 1H), 6.96 (d, *J* = 9.0 Hz, 1H), 6.84 (dd, *J* = 9.0, 2.9 Hz, 1H), 6.15, (s, 2H), 3.80 (s, 6H), 3.78 (s, 6H) ppm. $^{13}$C NMR (75 MHz, $CDCl_3$) $\delta_C$; 156.4, 154.0, 153.8, 146.9, 133.7, 121.8, 118.4, 115.5, 114.5, 94.9, 60.9, 56.1 (Cx2), 55.8 ppm. HRMS (ESI-TOF) m/z: $[M+H]^+$ calculated for $C_{16}H_{18}BrO_5$: 369.0332 found 369.0330.

**1-bromo-2-(4-methoxyphenoxy)benzene (30)**

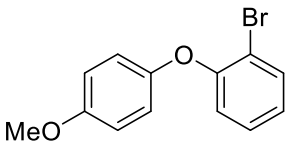


Sodium hydride (1.2 equiv., 60%) was added to a flask evacuated and refilled with nitrogen before DMF (2 mL/mmol) was added on ice. *p*-methoxy phenol (323 mg, 2.6 mmol, 1 equiv.) was added dropwise to the mixture stirring at 0 ˚ C. Once the phenol was added the mixture was left stir on ice for 1 hour. 2-bromofluorobenzene (0.29 mL, 2.6 mmol, 1 equiv.) was then added dropwise and the resulting mixture was left stir at 120 ˚ C for 24 hours under a nitrogen atmosphere. After 24 hours the reaction mixture was cooled to room temperature and quenched with water (10 mL). The organic layer was extracted with diethyl ether (3 x 10 mL) and brine (1 x 10 mL) before being dried over MgSO4. The mixture was then filtered and concentrated in vacuo. The resulting residue was purified by silica gel chromatography (9:1 Hexane:Ethyl acetate) to yield the title product as a yellow oil (515 mg, 71%). Characterisation data is consistent with the literature.[112]

$^{1}$H NMR(400 MHz, $CDCl_3$) $\delta_H$; 7.59 (dd, *J* = 8.0, 1.5 Hz, 1H), 7.22 – 7.15 (m, 1H), 6.98 – 6.90 (m, 3H), 6.90 – 6.85 (m, 2H), 6.82 (dd, *J* = 8.0, 1.5 Hz, 1H), 3.79 (s, 3H) ppm. $^{13}$C NMR (100 MHz, $CDCl_3$) $\delta_C$; 156.0, 154.9, 149.9, 133.7, 128.5, 124.1, 120.3, 118.8, 114.9, 113.7, 55.7 ppm. HRMS (ESI-TOF) m/z: $[M]^+$ calcd. for $C_{13}H_{11}BrO_2$: 279.0015, found: 279.0016.

**2-methoxydibenzo[*b,d*][furan (3)**

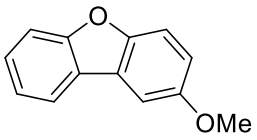


Diarylether **2** (70 mg, 0.25 mmol, 1 equiv.) or diarylether **30** (70 mg, 0.25 mmol, 1 equiv.) $Pd(OAc)_2$ (2.5 mol%), $PCy_3.HBF_4$ (5 mol%), $NBu_4OAc$ (2 equiv.) and 1,4-dioxane (2 mL/mmol) were added to a sealed reaction vial equipped with a magnetic stir bar. The reaction mixture was stirred at 125 ˚ C for 24 hours in a multi-reaction heating mantle. After 24 hours the reaction mixture was cooled to room temperature and diluted with DCM (15 mL), filtered through a pad of Celite® and the solvent was concentrated under reduced pressure. The resulting residue was then purified by column chromatography using 100% $CHCl_3$ as eluent on silica gel to elute the title product as a white solid (**3** 47 mg, 95% and **42** 46 mg 93%). MP: 45 – 46 °C (lit 46 – 47 °C). Characterisation data consistent with the literature.[113]

$^{1}$H NMR (300 MHz, $CDCl_3$) $\delta_H$; 7.92 (d, *J* = 7.7 Hz, 1H), 7.55 (d, *J* = 8.2 Hz, 1H), 7.50 – 7.40 (m, 3H), 7.33 (td, *J* = 7.5, 0.9 Hz, 1H), 7.06 (dd, *J* = 8.9, 2.6 Hz, 1H) and 3.92 (s, 3H) ppm. $^{13}$C NMR (75 MHz, $CDCl_3$) $\delta_C$; 156.9, 155.9, 150.9, 127.1, 124.7, 124.5, 122.4, 120.6, 115.2, 112.1, 111.7, 103.8 and 56.0 ppm. HRMS (ESI-TOF) m/z: $[M+H]^+$ calculated for $C_{13}H_{10}O_2$: 199.075356 found 199.07629.

**dibenzo[*b,d*]furan (34)**

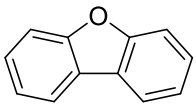

Diarylether **9** (50 mg, 0.2 mmol, 1 equiv.), $Pd(OAc)_2$ (2.5 mol%), $PCy_3.HBF_4$ (5 mol%), $NBu_4OAc$ (2 equiv.) and 1,4-dioxane (2 mL/mmol) were added to a sealed reaction vial equipped with a magnetic stir bar. The reaction mixture was stirred at 125 ˚ C for 24 hours in a multi-reaction heating mantle. After 24 hours the reaction mixture was cooled to room temperature and diluted with DCM (15 mL), filtered through a pad of Celite® and the solvent was concentrated under reduced pressure. The resulting residue was then purified by column chromatography using 100% Hexane as eluent on silica gel to elute the title product as a white solid (29 mg, 86%). MP: 78 – 79 °C (lit 78 – 80 °C).[57] Characterisation data consistent with the literature.[59]

$^1$H NMR (400 MHz, $CDCl_3$) $\delta_H$; 7.35 (t, *J* = 7.5 Hz, 2H), 7.46 (t, *J* = 7.5 Hz, 2H), 7.59 (d, *J* = 8.2 Hz, 2H), 7.97 (d, *J* = 7.7 Hz, 2H) ppm. $^{13}$C NMR (100 MHz, $CDCl_3$) $\delta_C$; 155.2, 126.1, 123.2, 121.6, 119.6, 110.6 ppm. HRMS (ESI-TOF) m/z: $[M+H]^+$ calculated for $C_{12}H_8O$: 169.0647 found 169.0640.

**2-fluorodibenzo[*b,d*]furan (35)**

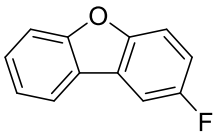

Diarylether **5** (187 mg, 0.7 mmol, 1 equiv.) or diarylether **6** (107 mg, 0.4 mmol, 1 equiv.) $Pd(OAc)_2$ (2.5 mol%), $PCy_3.HBF_4$ (5 mol%), $NBu_4OAc$ (2 equiv.) and 1,4-dioxane (2 mL/mmol) were added to a sealed reaction vial equipped with a magnetic stir bar. The reaction mixture was stirred at 125 ˚ C for 24 hours in a multi-reaction heating mantle. After 24 hours the reaction mixture was cooled to room temperature and diluted with DCM (15 mL), filtered through a pad of Celite® and the solvent was concentrated under reduced pressure. The resulting residue was then purified by column chromatography using 7:3 DCM:Hexane as eluent on silica gel to elute the title product as a white solid (**35** 115 mg, 87% and **36** 68 mg, 90%). MP: 89 ˚ C (lit. 90 – 91 ˚ C). Characterisation data is consistent with the literature.[49] $^1$H NMR (400 MHz, $CDCl_3$) $\delta_H$; 7.90 (d, *J* = 7.7 Hz, 1H) 7.64 - 7.53 (m, 2H) 7.52 – 7.42 (m, 2H) 7.33 (t, *J* = 7.6 Hz, 1H) 7.15 (td, *J* = 9.0, 2.6 Hz, 1H). $^{13}$C NMR (100 MHz, $CDCl_3$) $\delta_C$; 160.2 ($J_{C-F}$ = 239.1 Hz), 157.8, 157.2, 152.2, 127.7, 125.2 ($J_{C-F}$ = 10.2 Hz) , 124.0 ($J_{C-F}$ = 3.6 Hz), 122.7, 120.8, 114.5 ($J_{C-F}$ = 25.9 Hz), 112.3 ($J_{C-F}$ = 9.3 Hz), 111.9, 106.7 ($J_{C-F}$ = 25.1 Hz) ppm. $\delta_F$ (376 MHz, $CDCl_3$) -120.5 ppm. HRMS (ESI-TOF) m/z: $[M+Na]^+$ calculated for $C_{12}H_7FO$: 209.0373 found 209.0380.

**1-(dibenzo[*b,d*]furan-2-yl)ethan-1-one (37)**

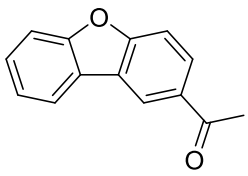

Diarylether **8** (58 mg, 0.2 mmol, 1 equiv.), $Pd(OAc)_2$ (2.5 mol%), $PCy_3.HBF_4$ (5 mol%), $NBu_4OAc$ (2 equiv.) and 1,4-dioxane (2 mL/mmol) were added to a sealed reaction vial equipped with a magnetic stir bar. The reaction mixture was stirred at 125 ˚ C for 24 hours in a multi-reaction heating mantle. After 24 hours the reaction mixture was cooled to room temperature and diluted with DCM (15 mL), filtered through a pad of Celite® and the solvent was concentrated under reduced pressure. The resulting residue was then purified by column chromatography using 100% DCM as eluent on silica gel to elute the title product as a pale yellow solid (40 mg, 95%). MP: 80 – 81 °C (lit. 84 – 85.5 °C). Characterisation data consistent with the literature.[114]

$^1$H NMR (400 MHz, $CDCl_3$) $\delta_H$; 8.59 (d, *J* = 1.6 Hz, 1H), 8.11 (dd, *J* = 8.6, 1.7 Hz, 1H), 8.01 (d, *J* = 7.7 Hz, 1H), 7.60 (d, *J* = 8.6 Hz, 2H), 7.51 (t, *J* = 7.7 Hz, 1H), 7.39 (t, *J* = 7.6 Hz, 1H), 2.71 (s, 3H) ppm. $^{13}$C NMR (100 MHz, $CDCl_3$) $\delta_C$; 197.3, 158.9, 156.9, 132.6, 128.0, 127.9, 124.6, 123.7, 123.4, 121.6, 120.9, 111.9, 111.6, 26.7 ppm. HRMS (ESI-TOF) m/z: $[M+H]^+$ calculated for $C_{14}H_{10}O_2$: 211.0754 found 211.0755.

**benzofuro[3,2-*c*]pyridine (38)**

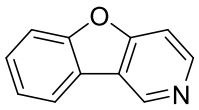

Diarylether **7** (88 mg, 0.35 mmol, 1 equiv.), $Pd(OAc)_2$ (2.5 mol%), $PCy_3.HBF_4$ (5 mol%), $NBu_4OAc$ (2 equiv.) and 1,4-dioxane (2 mL/mmol) were added to a sealed reaction vial equipped with a magnetic stir bar. The reaction mixture was stirred at 125 ˚ C for 24 hours in a multi-reaction heating mantle. After 24 hours the reaction mixture was cooled to room temperature and diluted with DCM (15 mL), filtered through a pad of Celite® and the solvent was concentrated under reduced pressure. The resulting residue was then purified by column chromatography using 100% DCM as eluent on silica gel to elute the title product as a clear oil (50 mg, 84%). Characterisation data is consistent with the literature.[115]

$^1$H NMR (400 MHz, $CDCl_3$) $\delta_H$; 9.26 (s, 1H), 8.65 (d, *J* = 5.5 Hz, 1H), 8.02 (d, *J* = 7.7 Hz, 1H), 7.62 (d, *J* = 8.2 Hz, 1H), 7.56 – 7.47 (m, 2H), 7.42 (t, *J* = 7.7 Hz, 1H) ppm. $^{13}$C NMR (125 MHz, $CDCl_3$) $\delta_C$; 160.9, 155.9, 147.4, 143.5, 128.3, 123.8, 121.6, 121.5, 121.1, 111.9, 107.4 ppm. HRMS (ESI-TOF) m/z: $[M+H]^+$ calculated for $C_{11}H_7NO$: 170.0600 found 170.0611.

**9*H*-carbazole (39)**

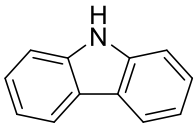

2-bromo-*N*-phenylaniline **33** (62 mg, 0.25 mmol, 1 equiv.), $Pd(OAc)_2$ (2.5 mol%), $PCy_3.HBF_4$ (5 mol%), $NBu_4OAc$ (2 equiv.) and 1,4-dioxane (2 mL/mmol) were added to a sealed reaction vial equipped with a magnetic stir bar. The reaction mixture was stirred at 125 ˚ C for 24 hours in a multi-reaction heating mantle. After 24 hours the reaction mixture was cooled to room temperature and diluted with DCM (15 mL), filtered through a pad of Celite® and the solvent was concentrated under reduced pressure. The resulting residue was then purified by column chromatography using 100% Hexane as eluent on silica gel to elute the title product as a pale white solid (37.5 mg, 89%). MP: 246 °C. Characterisation data consistent with the literature.[116]

$^1$H NMR (300 MHz, $(CD_3)_2SO$) $\delta_H$; 11.22 (bs, 1H), 8.10 (d, *J* = 7.9 Hz, 2H), 7.49 (m, 2H), 7.38 (ddd, *J* = 1.1, 7.4, 8.0 Hz, 2H), 7.16 (ddd, *J* = 1.1, 7.4, 8.0 Hz, 2H) ppm. $^{13}$C NMR (100 MHz, $(CD_3)_2SO$) $\delta_C$; 140.1, 125.9, 122.8, 120.6, 118.9, 111.3 ppm; m/z (ES+): 168 $[(M+H)]^+$, 100%.

**3-methyldibenzo[*b,d*]furan (40)**

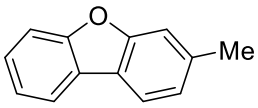

Diarylether **10** (52 mg, 0.2 mmol, 1 equiv.), $Pd(OAc)_2$ (2.5 mol%), $PCy_3.HBF_4$ (5 mol%), $NBu_4OAc$ (2 equiv.) and 1,4-dioxane (2 mL/mmol) were added to a sealed reaction vial equipped with a magnetic stir bar. The reaction mixture was stirred at 125 ˚ C for 24 hours in a multi-reaction heating mantle. After 24 hours the reaction mixture was cooled to room temperature and diluted with DCM (15 mL), filtered through a pad of Celite® and the solvent was concentrated under reduced pressure. The resulting residue was then purified by column chromatography using 100% DCM as eluent on silica gel to elute the title product as a white solid (33 mg, 90%). MP: 61 – 62 °C (lit. 62 – 63 °C). Characterisation data is consistent with the literature.[117]

$^1$H NMR (400 MHz, $CDCl_3$) $\delta_H$; 7.89 (d, *J* = 7.7 Hz, 1H), 7.81 (d, *J* = 7.8, 1H), 7.53 (d, *J* = 8.2 Hz, 1H) 7.44 – 7.35 (m, 2H), 7.31 (t, *J* = 7.8 Hz, 1H), 7.15 (d, *J* = 7.8 Hz, 1H), 2.52 (s, 3H) ppm. $^{13}$C NMR (100 MHz, $CDCl_3$) $\delta_C$; 156.6, 156.2, 137.6, 126.5, 124.3, 123.9, 122.5, 121.6, 120.3, 120.1, 111.9, 111.5, 21.9 ppm. HRMS (ESI-TOF) m/z: $[M+Na]^+$ calculated for $C_{13}H_{10}O$: 205.0624 found 205.0630.

**3-methoxydibenzo[*b,d*]furan (41)**

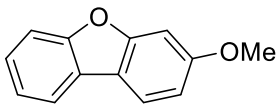


Diarylether **11** (112 mg, 0.4 mmol, 1 equiv.), $Pd(OAc)_2$ (2.5 mol%), $PCy_3.HBF_4$ (5 mol%), $NBu_4OAc$ (2 equiv.) and 1,4-dioxane (2 mL/mmol) were added to a sealed reaction vial equipped with a magnetic stir bar. The reaction mixture was stirred at 125 ˚ C for 24 hours in a multi-reaction heating mantle. After 24 hours the reaction mixture was cooled to room temperature and diluted with DCM (15 mL), filtered through a pad of Celite® and the solvent was concentrated under reduced pressure. The resulting residue was then purified by column chromatography using 1:1 Hexane:DCM as eluent on silica gel to elute the title product as a pale yellow solid (74 mg, 94%). MP: 94 – 95 ˚ C (lit. 95 – 96 ˚ C). Characterisation data is consistent with the literature.[117]

$^1$H NMR (300 MHz, $CDCl_3$) $\delta_H$; 7.85 (d, *J* = 7.4 Hz, 1H), 7.80 (d, *J* = 8.5 Hz, 1H), 7.52 (d, *J* = 8.1 Hz, 1H), 7.41 – 7.33 (m, 1H), 7.33 -7.26 (m, 1H), 7.09 (d, *J* = 2.2 Hz, 1H), 6.94 (dd, *J* = 8.5, 2.2 Hz, 1H), 3.90 (s, 3H) ppm. $^{13}$C NMR (75 MHz, $CDCl_3$) $\delta_C$; 160.3, 157.9, 156.7, 126.0, 124.7, 123.0, 121.3, 120.1, 117.7, 111.7, 111.3, 96.8, 56.0 ppm. HRMS (ESI-TOF) m/z: $[M+H]^+$ calculated for $C_{13}H_{10}O_2$: 199.0753 found 199.0746.

**1,4-dimethyldibenzo[*b,d*]furan (43)**

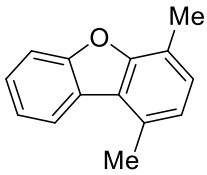


Diarylether **12** (83 mg, 0.3 mmol, 1 equiv.), $Pd(OAc)_2$ (2.5 mol%), $PCy_3.HBF_4$ (5 mol%), $NBu_4OAc$ (2 equiv.) and 1,4-dioxane (2 mL/mmol) were added to a sealed reaction vial equipped with a magnetic stir bar. The reaction mixture was stirred at 125 ˚ C for 24 hours in a multi-reaction heating mantle. After 24 hours the reaction mixture was cooled to room temperature and diluted with DCM (15 mL), filtered through a pad of Celite® and the solvent was concentrated under reduced pressure. The resulting residue was then purified by column chromatography using 100% Hexane as eluent on silica gel to elute the title product as a clear oil (56 mg, 95%).

$^1$H NMR (300 MHz, $CDCl_3$) $\delta_H$; 8.02 (d, *J* = 7.7 Hz, 1H), 7.59 (d, *J* = 8.2 Hz, 1H), 7.44 (t, *J* = 7.7, 1H), 7.33 (t, *J* = 7.6, 1H), 7.15 (d, *J* = 7.5 Hz, 1H), 7.01 (d, *J* = 7.5 Hz, 1H), 2.76 (s, 3H), 2.56 (s, 3H) ppm. $^{13}$C NMR (100 MHz, $CDCl_3$) $\delta_C$; 155.9, 154.9, 130.7, 127.8, 126.3, 125.3, 123.7, 122.5, 122.3, 122.2, 118.9, 111.5, 19.6, 14.9 ppm. HRMS (ESI-TOF) m/z: $[M+H]^+$ calculated for $C_{14}H_{12}O$: 197.0960 found 197.0958.

**2,8-dimethoxydibenzo[b,d]furan (44)**

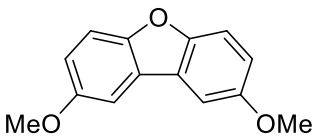


Diarylether **13** (74 mg, 0.24 mmol, 1 equiv.), $Pd(OAc)_2$ (2.5 mol%), $PCy_3.HBF_4$ (5 mol%), $NBu_4OAc$ (2 equiv.) and 1,4-dioxane (2 mL/mmol) were added to a sealed reaction vial equipped with a magnetic stir bar. The reaction mixture was stirred at 125 ˚ C for 24 hours in a multi-reaction heating mantle. After 24 hours the reaction mixture was cooled to room temperature and diluted with DCM (15 mL), filtered through a pad of Celite® and the solvent was concentrated under reduced pressure. The resulting residue was then purified by column chromatography using 7:3 DCM:Hexane as eluent on silica gel to elute the title product as a white solid (50 mg, 91%). MP: 89 °C. Characterisation data consistent with the literature.[61]

$^1$H NMR (600 MHz, $CDCl_3$) $\delta_H$; 7.43 (d, *J* = 8.9 Hz, 2H), 7.37 (d, *J* = 2.7 Hz, 2H), 7.03 (dd, *J* = 8.9, 2.7 Hz), 3.91 (s, 6H) ppm. $^{13}$C NMR (151 MHz, $CDCl_3$) $\delta_C$; 155.6, 151.6, 124.9, 115.2, 112.2, 103.5, 56.0 ppm. HRMS (ESI-TOF) m/z: $[M+H]^+$ calculated for $C_{14}H_{12}O_3$: 229.0859 found 229.0865.

**2,3,8-trimethoxydibenzo[*b,d*]furan (45)**

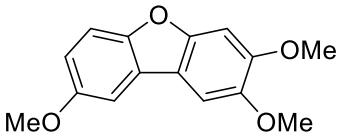


Diarylether **14** (68 mg, 0.2 mmol, 1 equiv.), $Pd(OAc)_2$ (2.5 mol%), $PCy_3.HBF_4$ (5 mol%), $NBu_4OAc$ (2 equiv.) and 1,4-dioxane (2 mL/mmol) were added to a sealed reaction vial equipped with a magnetic stir bar. The reaction mixture was stirred at 125 ˚ C for 24 hours in a multi-reaction heating mantle. After 24 hours the reaction mixture was cooled to room temperature and diluted with DCM (15 mL), filtered through a pad of Celite® and the solvent was concentrated under reduced pressure. The resulting residue was then purified by column chromatography using 7:3 DCM:Hexane as eluent on silica gel to elute the title product as an off-white solid (47 mg, 90%). MP: 100 °C.

$^1$H NMR (300 MHz, $CDCl_3$) $\delta_H$; 7.40 (d, *J* = 8.9 Hz, 1H), 7.32 (s, 1H), 7.29 (d, *J* = 2.6 Hz, 1H), 7.08 (s, 1H), 6.94 (dd, *J* = 8.9, 2.6 Hz, 1H), 3.98 (s, 3H), 3.96 (s, 3H), 3.89 (s, 3H) ppm. $^{13}$C NMR (100 MHz, $CDCl_3$) $\delta_C$; 155.8, 151.9, 151.0, 149.9, 146.1, 125.3, 115.8, 113.3, 111.8, 102.9, 102.2, 95.7, 56.6, 56.3, 56.0 ppm. HRMS (ESI-TOF) m/z: $[M+H]^+$ calculated for $C_{15}H_{14}O_4$: 259.0964 found 259.0956.

**1,2,3,8-tetramethoxydibenzo[*b,d*]furan (46)**

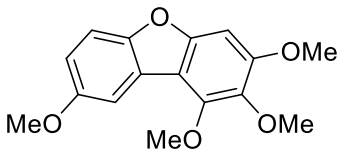


Diarylether (55 mg, 0.15 mmol, 1 equiv.), $Pd(OAc)_2$ (2.5 mol%), $PCy_3.HBF_4$ (5 mol%), $NBu_4OAc$ (2 equiv.) and 1,4-dioxane (2 mL/mmol) were added to a sealed reaction vial equipped with a magnetic stir bar. The reaction mixture was stirred at 125 ˚ C for 24 hours in a multi-reaction heating mantle. After 24 hours the reaction mixture was cooled to room temperature and diluted with DCM (15 mL), filtered through a pad of Celite® and the solvent was concentrated under reduced pressure. The resulting residue was then purified by column chromatography using 7:3 DCM:Hexane as eluent on silica gel to elute the title product as a yellow solid (18 mg, 42%). MP: 61 – 62 °C.

$^1$H NMR (300 MHz, $CDCl_3$) $\delta_H$; 7.50 (d, *J* = 2.7 Hz, 1H), 7.37 (d, *J* = 8.9 Hz, 1H), 6.94 (dd, *J* = 8.9, 2.7 Hz, 1H), 6.85 (s, 1H), 4.15 (s, 3H), 3.94 (s, 3H), 3.91 (apparent d, 6H) ppm. $^{13}$C NMR (75 MHz, $CDCl_3$) $\delta_C$; 155.9, 154.3, 153.6, 150.6, 148.1, 137.8, 124.3, 112.9, 111.2, 110.7, 105.3, 91.3, 61.5, 61.0, 56.4, 56.1 ppm. HRMS (ESI-TOF) m/z: $[M+H]^+$ calculated for $C_{16}H_{16}O_5$: 289.1071 found 289.1077.

**11*H*-indolo[3,2-*c*]quinoline**

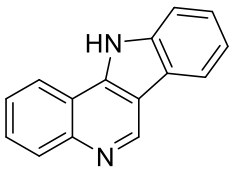


To a screw-cap vial equipped with a magnetic stir bar was added 4-bromo quinoline (42 mg, 0.2 mmol, 1 equiv.), 2-bromo aniline (38 mg, 0.22 mmol, 1.1 equiv.), $Pd(OAc)_2$ (5 mol%), XantPhos (6 mol%) and $NBu_4OAc$ (2 equiv.). 1,4-Dioxane or CPME (2 mL/mmol) was added and the reaction was heated to 120 °C for 30 hours. Upon reaction completion, the mixture was cooled and subsequently diluted with $CH_2Cl_2$ before being filtered through a pad of Celite®. The solvent was removed by rotary evaporation and the resulting residue was purified by silica gel column chromatography using DCM as eluent to afford the title product as an off-white solid (188 mg, 86%). Characterisation data is consistent with the literature.[118]

$^1$H NMR (300 MHz, DMSO-$d_6$) $\delta_H$; 12.74 (bs, 1H), 9.60 (s, 1H), 8.52 (d, *J* = 7.8 Hz, 1H), 8.32 (d, *J* = 7.8 Hz, 1H), 8.14 (d, *J* = 8.1 Hz, 1H), 7.80 – 7.65 (m, 3H), 7.50 (t, *J* = 7.6 Hz, 1H) and 7.35 (t, *J* = 7.6 Hz, 1H) ppm. $^{13}$C NMR (75.5 MHz, DMSO-$d_6$) $\delta_C$; 145.9, 145.3, 140.2, 139.2, 130.0, 128.4, 126.1, 125.9, 122.5, 122.3, 121.0, 120.5, 117.6, 114.8 and 112.3 ppm.

## 3.2. Crystal Data

| Compound | **6a** | **6b** |
|---|---|---|
| Formula | $C_{14}H_{12}O_3$ | $C_{15}H_{14}O_4$ |
| $D_{calc.}$/ g cm$^{-3}$ | 1.389 | 1.423 |
| $m$/mm$^{-1}$ | 0.798 | 0.103 |
| Formula Weight | 228.24 | 258.26 |
| Colour | clear colourless | clear colourless |
| Shape | prism-shaped | plate-shaped |
| Size/mm$^3$ | 0.33×0.06×0.04 | 0.36×0.16×0.04 |
| $T$/K | 100(2) | 100(2) |
| Crystal System | orthorhombic | triclinic |
| Flack Parameter | 0.13(14) | - |
| Hooft Parameter | 0.12(11) | - |
| Space Group | $P2_12_12_1$ | $P$-1 |
| $a$/Å | 4.74800(10) | 6.0439(2) |
| $b$/Å | 10.9125(2) | 9.6768(3) |
| $c$/Å | 21.0717(4) | 10.6997(3) |
| $a$/° | 90 | 88.835(2) |
| $b$/° | 90 | 78.123(3) |
| $g$/° | 90 | 79.937(2) |
| V/Å$^3$ | 1091.78(4) | 602.88(3) |
| $Z$ | 4 | 2 |
| $Z'$ | 1 | 1 |
| Wavelength/Å | 1.54184 | 0.71073 |
| Radiation type | Cu $K_a$ | Mo $K_a$ |
| $Q_{min}$/° | 4.196 | 1.945 |
| $Q_{max}$/° | 76.711 | 28.498 |
| Measured Refl's. | 10527 | 30327 |
| Indep't Refl's | 2206 | 3043 |
| Refl's I≥2 $s$(I) | 2115 | 2531 |
| $R_{int}$ | 0.0850 | 0.0413 |
| Parameters | 157 | 175 |
| Restraints | 0 | 0 |
| Largest Peak | 0.241 | 0.332 |

| | | |
|---|---|---|
| Deepest Hole | -0.261 | -0.192 |
| GooF | 1.084 | 1.071 |
| $wR_2$ (all data) | 0.1177 | 0.1052 |
| $wR_2$ | 0.1161 | 0.0994 |
| $R_1$ (all data) | 0.0434 | 0.0481 |
| $R_1$ | 0.0421 | 0.0383 |

CCDC:

**6a:** CCDC-2244127

**6b:** CCDC-2238733

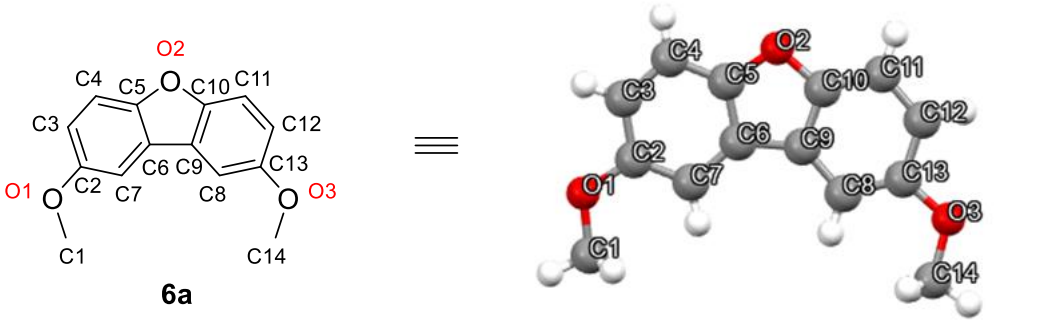


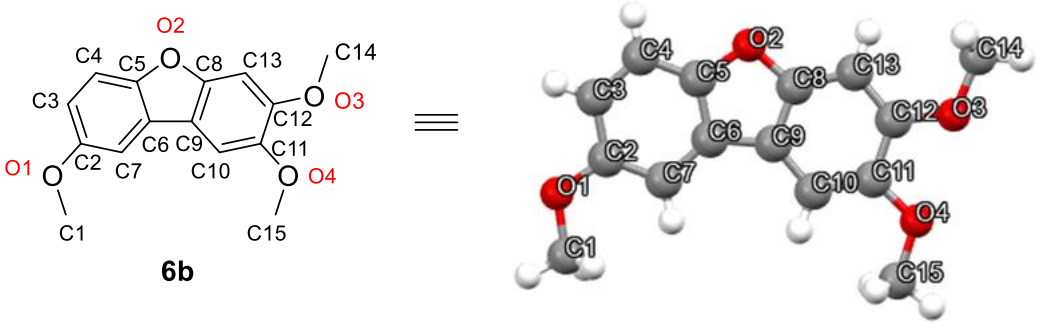

**Crystal Analysis Experimental:**

**6a**: Experimental. Single clear colourless prism-shaped crystals of **6a** recrystallised from DCM by slow evaporation. A suitable crystal with dimensions 0.33 × 0.06 × 0.04 $mm^3$ was selected and mounted on a MITIGEN holder with silicon oil on a ROD, Synergy Custom system, HyPix diffractometer. The crystal was kept at a steady T = 100(2) K during data collection. The structure was solved with the ShelXT 2014/5 (Sheldrick, 2014) solution program using dual methods and by using Olex2 1.5-alpha (Dolomanov *et al.,* 2009) as the graphical interface. The model was refined with ShelXL 2016/6 (Sheldrick, 2015) using full matrix least squares minimisation on $F^2$.

**6b**: Single clear colourless plate-shaped crystals of **6b** recrystallised from toluene by slow evaporation. A suitable crystal with dimensions 0.36 × 0.16 × 0.04 $mm^3$ was selected and mounted on a MITIGEN holder with silicon oil on a ROD, Synergy Custom system, HyPix diffractometer. The crystal was kept at a steady T = 100(2) K during data collection. The structure was solved with the ShelXT 2014/5 (Sheldrick, 2014) solution program using dual methods and by using Olex2 1.5-alpha (Dolomanov *et al*., 2009) as the graphical interface. The model was refined with ShelXL 2016/6 (Sheldrick, 2015) using full matrix least squares minimisation on $F^2$.

# 4. References


(1) Alberico, D.; Scott, M. E.; Lautens, M. *Chem. Rev.* **2007**, *107*, 174–238.

(2) Mc Glacken, G. P.; Bateman, L. M. *Chem. Soc. Rev.* **2009**, *38*, 2447–2464.

(3) Johansson Seechurn, C. C. C.; Kitching, M. O.; Colacot, T. J.; Snieckus, V. *Angew. Chem. Int. Ed.* **2012**, *51*, 5062–5085.

(4) Heck, R. F. *Synlett* **2006**, 2855–2860.

(5) Negishi, E.-I. *Acc. Chem. Res.* **1982**, *11*, 340 – 348.

(6) Farina, V. *Org. Process Res.Dev.* **2023**, *27*, 831–846.

(7) Gensch, T.; Hopkinson, M. N.; Glorius, F.; Wencel-Delord, J. *Chem. Soc. Rev.* **2016**, *45*, 2900–2936.

(8) Labinger, J. A.; Bercaw Arnold, J. E.; Beckman, M. *Nature* **2002**, *417*, 507–514.

(9) Godula, K.; Sames, D. *Science* **2006**, *312*, 67–72.

(10) Fairlamb, I. J. S. in *Green and Sustainable Medicinal Chemistry: Methods, Tools and Strategies for the 21st Century Pharmaceutical Industry*, Royal Society Chemistry, UK, **2016**, pp. 129–139.

(11) Xue, X. S.; Ji, P.; Zhou, B.; Cheng, J. P. *Chem. Rev.* **2017**, *117*, 8622–8648.

(12) Hartwig, J. F. *J. Am. Chem. Soc.* **2016**, *138*, 2–24.

(13) Kondrashov, M.; Provost, D.; Wendt, O. F. *Dalton Trans.* **2016**, *45*, 525–531.

(14) Lane, B. S.; Brown, M. A.; Sames, D. *J. Am. Chem. Soc.* **2005**, *127*, 8050–8057.

(15) Pivsa-Art, S.; Satoh, T.; Kawamura, Y.; Miura, M.; Nomura, M. *B. Chem. Soc. Jpn.* **1998**, *71*, 467–473.

(16) García-Cuadrado, D.; De Mendoza, P.; Braga, A. A. C.; Maseras, F.; Echavarren, A. M. *J. Am. Chem. Soc.* **2007**, *129*, 6880–6886.

(17) García-Cuadrado, D.; Braga, A. A. C.; Maseras, F.; Echavarren, A. M. *J. Am. Chem. Soc.* **2006**, *128*, 1066–1067.

(18) Gorelsky, S. I.; Lapointe, D.; Fagnou, K. *J. Org. Chem.* **2012**, *77*, 658–668.

(19) Lapointe, D.; Fagnou, K. *Chem. Lett.* **2010**, *39*, 1118–1126.

(20) Gorelsky, S. I.; Lapointe, D.; Fagnou, K. *J. Am. Chem. Soc.* **2008**, *130*, 10848–10849.

(21) Lafrance, M.; Gorelsky, S. I.; Fagnou, K. *J. Am. Chem. Soc.* **2007**, *129*, 14570–14571.

(22) Lafrance, M.; Fagnou, K. *J. Am. Chem. Soc.* **2006**, *128*, 16496–16497.

(23) Davies, D. L.; Macgregor, S. A.; McMullin, C. L. *Chem. Rev.* **2017**, *117*, 8649–8709.

(24) Boutadla, Y.; Davies, D. L.; Macgregor, S. A.; Poblador-Bahamonde, A. I. *Dalton Trans.* **2009**, 5820–5831.

(25) Hennessy, E. J.; Buchwald, S. L. *J. Am. Chem. Soc.* **2003**, *125*, 12084–12085.

(26) Thompson, M. E.; Baxter, S. M.; Ray Bulls, A.; Burger, B. J.; Nolan, M. C.; Santarsiero, B. D.; Schaefer, W. P.; Bereaw, J. E. *J. Am. Chem. Soc.* **1987**, *109*, 203–219.

(27) Davies, D. L.; Donald, S. M. A.; Macgregor, S. A. *J. Am. Chem. Soc.* **2005**, *127*, 13754–13755.

(28) McGlacken, G. P.; Bateman, L. M. *Chem. Soc. Rev.* **2009**, *38*, 2447–2464.

(29) Love, B. E. *Eur. J. Med. Chem.* **2015**, *97*, 377–387.

(30) Zhang, L.; Zhang, Y. X.; Hu, Y.; Shi, X. B.; Jiang, Z. Q.; Wang, Z. K.; Liao, L. S. *ACS Appl. Mater. Interfaces* **2016**, *8*, 16186–16191.

(31) Nakanishi, K.; Fukatsu, D.; Takaishi, K.; Tsuji, T.; Uenaka, K.; Kuramochi, K.; Kawabata, T.; Tsubaki, K. *J. Am. Chem. Soc.* **2014**, *136*, 7101–7109.

(32) Shyam Sundar, M.; Bedekar, A. V. *Org. Lett.* **2015**, *17*, 5808–5811.

(33) Nakahara, K.; Mitsui, C.; Okamoto, T.; Yamagishi, M.; Matsui, H.; Ueno, T.; Tanaka, Y.; Yano, M.; Matsushita, T.; Soeda, J.; Hirose, Y.; Sato, H.; Yamano, A.; Takeya, J. *Chem. Comm.* **2014**, *50*, 5342–5344.

(34) Itoh, K.; Sibi, M. P. *Org. Biomol. Chem.* **2018**, *16*, 5551–5565.

(35) Martel, R. R.; Rochefort, J. G.; Klicius, J.; Dorson, T. A. *Can. J. Physiol. Pharmacol.* **1974**, *52*, 669.

(36) Ye, Y. Q.; Negishi, C.; Hongo, Y.; Koshino, H.; Onose, J. I.; Abe, N.; Takahashi, S. *Bioorg. Med. Chem.* **2014**, *22*, 2442–2446.

(37) Patpi, S. R.; Pulipati, L.; Yogeeswari, P.; Sriram, D.; Jain, N.; Sridhar, B.; Murthy, R.; Anjana Devi, T.; Kalivendi, S. V.; Kantevari, S. *J. Med. Chem.* **2012**, *55*, 3911–3922.

(38) Wossa, S. W.; Beekman, A. M.; Ma, P.; Kevo, O.; Barrow, R. A. *Asian J. Org. Chem.* **2013**, *2*, 565–567.

(39) Oliveira, A. M. A. G.; Raposo, M. M. M.; Oliveira-Campos, A. M. F.; Machado, A. E. H.; Puapairoj, P.; Pedro, M.; Nascimento, M. S. J.; Portela, C.; Afonso, C.; Pinto, M. *Eur. J. Med. Chem.* **2006**, *41*, 367–372.

(40) Kaniwa, K.; Ohtsuki, T.; Yamamoto, Y.; Ishibashi, M. *Tetrahedron Lett.* **2006**, *47*, 1505–1508.

(41) Alami, M.; Provot, O. *Org. Biomol. Chem.* **2024**, *22*, 1323–1345.

(42) Ames, D. E.; Opalko, A. *Synthesis (Stuttg)* **1983**, *3*, 234–235.

(43) Campeau, L. C.; Thansandote, P.; Fagnou, K. *Org. Lett.* **2005**, *7*, 1857–1860.

(44) Campeau, L. C.; Parisien, M.; Jean, A.; Fagnou, K. *J. Am. Chem. Soc.* **2006**, *128*, 581–590.

(45) Mackey, K.; Jones, D. J.; Pardo, L. M.; McGlacken, G. P. *Eur. J. Org. Chem.* **2021**, *2021*, 495–498.

(46) Amatore, C.; Pflüger, F. *Organometallics*, **1990**, *8*, 2276 – 2282.

(47) Panda, N.; Mattan, I.; Nayak, D. K. *J. Org. Chem.* **2015**, *80*, 6590–6597.

(48) Xu, H.; Fan, L.-L. *Chem. Pharm. Bull.* **2008**, *56*, 1496 – 1498.

(49) Lockner, J. W.; Dixon, D. D.; Risgaard, R.; Baran, P. S. *Org. Lett.* **2011**, *13*, 5628–5631.

(50) Wang, C.; Piel, I.; Glorius, F. *J. Am. Chem. Soc.* **2009**, *131*, 4194–4195.

(51) Niu, L.; Yang, H.; Jiang, Y.; Fu, H. *Adv. Synth. Catal.* **2013**, *355*, 3625–3632.

(52) Nervig, C. S.; Waller, P. J.; Kalyani, D. *Org. Lett.* **2012**, *14*, 4838–4841.

(53) Ferguson, D. M.; Rudolph, S. R.; Kalyani, D. *ACS Catal.* **2014**, *4*, 2395–2401.

(54) Wang, J.; Ferguson, D. M.; Kalyani, D. *Tetrahedron* **2013**, *69*, 5780–5790.

(55) Xiao, B.; Gong, T. J.; Liu, Z. J.; Liu, J. H.; Luo, D. F.; Xu, J.; Liu, L. *J. Am. Chem. Soc.* **2011**, *133*, 9250–9253.

(56) Li, J.; Xu, Q. N.; Wang, Z. B.; Li, Y.; Liu, L. *ACS Omega* **2018**, *3*, 12923–12929.

(57) Clarkson, G. J.; Roesner, S. *J. Org. Chem.* **2023**, *88*, 684–689.

(58) Liu, J.; Fitzgerald, A. E.; Mani, N. S. *J. Org.Chem.* **2008**, *73*, 2951–2954.

(59) Zhao, H.; Yang, K.; Zheng, H.; Ding, R.; Yin, F.; Wang, N.; Li, Y.; Cheng, B.; Wang, H.; Zhai, H. *Org. Lett.* **2015**, *17*, 5744–5747.

(60) Sumida, Y.; Harada, R.; Sumida, T.; Johmoto, K.; Uekusa, H.; Hosoya, T. *Org. Lett.* **2020**, *22*, 6687–6691.

(61) Tobisu, M.; Kita, Y.; Ano, Y.; Chatani, N. *J. Am. Chem. Soc.* **2008**, *130*, 15982–15989.

(62) Akermark, B.; Eberson, L.; Jonsson, E.; Pettersson, E. *J. Org. Chem.* **1975**, *40*, 1365.

(63) Akinori Shiotani, B.; ltatani, H. *J. Chem. Soc., Perkin Trans. 1* **1976**, 1236.

(64) Liégault, B.; Lee, D.; Huestis, M. P.; Stuart, D. R.; Fagnou, K. *J. Org. Chem.* **2008**, *73*, 5022–5028.

(65) Hussain, M.; Hung, N. T.; Langer, P. *Tetrahedron Lett.* **2009**, *50*, 3929–3932.

(66) Silarska, E.; Trzeciak, A. M.; Pernak, J.; Skrzypczak, A. *Appl. Catal. A: General* **2013**, *466*, 216–223.

(67) Schroeter, F.; Soellner, J.; Strassner, T. *ACS Catal* **2017**, *7*, 3004–3009.

(68) Huynh, H. V.; Han, Y.; Ho, J. H. H.; Tan, G. K. *Organometallics* **2006**, *25*, 3267–3274.

(69) Prechtl, M. H. G.; Scholten, J. D.; Dupont, J. *Molecules* **2010**, *15*, 3441–3461.

(70) Kohler, D. G.; Gockel, S. N.; Kennemur, J. L.; Waller, P. J.; Hull, K. L. *Nat. Chem.* **2018**, *10*, 333–340.

(71) Thathagar, M. B.; Kooyman, P. J.; Boerleider, R.; Jansen, E.; Elsevier, C. J.; Rothenberg, G. *Adv. Synth. Catal.* **2005**, *347*, 1965–1968.

(72) Reetz, M. T.; Westermann, E. *Angew. Chem. Int. Ed.* **2000**, *39*, 165 – 168.

(73) Reetz, M. T.; Wannlnger, K. *Tetrahedron Lett.* **1996**, *37*, 4499–4502.

(74) Belier, M.; Fischer, H.; Kiihlein, K.; Reisinger, C.-P.; Herrmarm, W. A. *J. Organomet. Chem.* **1996**, *520*, 257–259.

(75) Bellina, F.; Lessi, M.; Manzini, C. *Eur. J. Org. Chem.* **2013**, 5621–5630.

(76) Ehlers, P.; Petrosyan, A.; Baumgard, J.; Jopp, S.; Steinfeld, N.; Ghochikyan, T. V.; Saghyan, A. S.; Fischer, C.; Langer, P. *ChemCatChem* **2013**, *5*, 2504–2511.

(77) Gniewek, A.; Trzeciak, A. M.; Ziółkowski, J. J.; Kępiński, L.; Wrzyszcz, J.; Tylus, W. *J. Catal.* **2005**, *229*, 332–343.

(78) Pryjomska-Ray, I.; Gniewek, A.; Trzeciak, A. M.; Ziółkowski, J. J.; Tylus, W. in *Top. Catal.*, **2006**, pp. 173–184.

(79) Yang, S.; Hong, S. H. *Asian J. Org. Chem.* **2020**, *9*, 1846–1851.

(80) De Vries, A. H. M.; Parlevliet, F. J.; Schmieder-van De Vondervoort, L.; Mommers, J. H. M.; Henderickx, H. J. W.; Walet, M. A. M.; De Vries, J. G. *Adv. Synth. Catal.* **2002**, *344*, 996–1002.

(81) Ackermann, L. *Chem. Rev.* **2011**, *111*, 1315–1345.

(82) Momotake, A.; Lindegger, N.; Niggli, E.; Barsotti, R. J.; Ellis-Davies, G. C. R. *Nat. Methods* **2006**, *3*, 35–40.

(83) Zhang, W.; Wei, W.; Shi, J.; Chen, C.; Zhao, G.; Jiao, R.; Tan, R. *Bioorg. Med. Chem. Lett.* **2015**, *25*, 2698–2701.

(84) Jeffery, T. *Tetrahedron* **1996**, *52*, 10113–10130.

(85) Jeffery, T. *J. Chem. Soc., Chem. Commun* **1984**.

(86) Yang, C. T.; Fu, Y.; Huang, Y. B.; Yi, J.; Guo, Q. X.; Liu, L. *Angew. Chem. Int. Ed.* **2009**, *48*, 7398–7401.

(87) Liu, L.; Frohn, M.; Xi, N.; Dominguez, C.; Hungate, R.; Reider, P. J. *J. Org. Chem.* **2005**, *70*, 10135–10138.

(88) Abdo, N. I.; El-Shehawy, A. A.; El-Barbary, A. A.; Lee, J. S. *Eur. J. Org. Chem.* **2012**, 5540–5551.

(89) Xu, H. J.; Zhao, Y. Q.; Zhou, X. F. *J. Org. Chem.* **2011**, *76*, 8036–8041.

(90) Trippé-Allard, G.; Lacroix, J. C. *Tetrahedron* **2013**, *69*, 861–866.

(91) Sugihara, T.; Satoh, T.; Miura, M. *Tetrahedron Lett.* **2005**, *46*, 8269–8271.

(92) Farina, V. *Adv. Synth. Catal.* **2004**, *346*, 1553–1582.

(93) Wong, N. W. Y.; Forgione, P. *Org. Lett.* **2012**, *14*, 2738–2741.

(94) Azzena, U.; Carraro, M.; Pisano, L.; Monticelli, S.; Bartolotta, R.; Pace, V. *ChemSusChem* **2019**, *12*, 40–70.

(95) De Gonzalo, G.; Alcántara, A. R.; Domínguez de María, P. *ChemSusChem* **2019**, *12*, 2083–2097.

(96) King, A. E.; Brunold, T. C.; Stahl, S. S. *J. Am. Chem. Soc.* **2009**, *131*, 5044–5045.

(97) Vantourout, J. C.; Miras, H. N.; Isidro-Llobet, A.; Sproules, S.; Watson, A. J. B. *J. Am. Chem. Soc.* **2017**, *139*, 4769–4779.

(98) Jalalian, N.; Ishikawa, E. E.; Silva, L. F.; Olofsson, B. *Org. Lett.* **2011**, *13*, 1552–1555.

(99) Chan, D. M. T.; Monaco, K. L.; Wang, R.-P.; Winters, M. P. *Tetrahedron Lett.* **1998**, *39*, 2933–2936.

(100) Evans, D. A.; Katz, J. L.; West, T. R. *Tetrahedron Lett.* **1998**, *39*, 2937–2940.

(101) Bouquillon, S.; Du Moulinet D'hardemare, A.; Averbuch-Pouchot, M.-T.; Henin, F.; Muzart, J. *Polyhedron,* **1999**, *18*, 3511 – 3516.

(102) Cabrera, P. J.; Lee, M.; Sanford, M. S. *J. Am. Chem. Soc.* **2018**, *140*, 5599–5606.

(103) Laali, K. K.; Borodkin, G. I. *J. Chem. Soc., Perkin Trans.* **2002**, *2*, 953–957.

(104) Eoin O Muimhneachain, PhD thesis, University College Cork, **2018**.

(105) Campeau, L. C.; Parisien, M.; Leblanc, M.; Fagnou, K. *J. Am. Chem. Soc.* **2004**, *126*, 9186–9187.

(106) Rishton, G. M. *Am. J. Cardiol.* **2008**, *101*, 43 – 49.

(107) Lavrado, J.; Moreira, R.; Paulo, A. *Curr. Med.Chem.* **2010**, *17*, 2348–2370.

(108) Thobokholt, E. N.; Larghi, E. L.; Bracca, A. B. J.; Kaufman, T. S. *RSC Adv* **2020**, *10*, 18978–19002.

(109) Oliver-Bever, B. *Medicinal Plants in Tropical West Africa*, Cambridge University Press, Cambridge, **1986**.

(110) Shanahan, R. M.; Hickey, A.; Reen, F. J.; O'Gara, F.; McGlacken, G. P. *Eur. J. Org. Chem.* **2018**, *2018*, 6140–6149.

(111) James Forrest, B. *J. Chem. Soc.* **1960**, 581–588.

(112) Ebisawa, M.; Ueno, M.; Oshima, Y.; Kondo, Y. *Tetrahedron Lett.* **2007**, *48*, 8918–8921.

(113) Maetani, S.; Fukuyama, T.; Ryu, I. *Org. Lett.* **2013**, *15*, 2754–2757.

(114) Bao, Y. S.; Bao, A.; Bao, Z.; Jia, M.; Baiyin, M. *Org. Biomol. Chem.* **2015**, *13*, 4179–4182.

(115) Hong, F.; Chen, Y.; Lu, B.; Cheng, J. *Adv. Synth. Catal.* **2016**, *358*, 353–357.

(116) Gao, H.; Xu, Q. L.; Yousufuddin, M.; Ess, D. H.; Kürti, L. *Angew. Chem. Int. Ed.* **2014**, *53*, 2701–2705.

(117) Zhu, D.; Li, M.; Wu, Z.; Du, Y.; Luo, B.; Huang, P.; Wen, S. *Eur. J. Org. Chem.* **2019**, *2019*, 4566–4571.

(118) Håheim, K. S.; Lund, B. A.; Sydnes, M. O. *Eur. J. Org. Chem.* **2023**, *26*, e202300137.

*So many foreign worlds*

*So relatively -*

*So ready for us*

*The Creature Fear*

# Chapter 2

# The Asymmetric Rh-Catalysed 1,4-Addition of *N*–H Indolyl Boronic Acids

# 5. Introduction

## 5.1. Introduction to C–C bond formation by Conjugate Addition

The ability to form carbon–carbon bonds efficiently and selectively is a key aspect of synthetic chemistry. The ability to do so in a regio- and enantioselective manner gives chemists the tools to create new targets and investigate novel chemical space. Many named reactions are excellent examples of this reaction type, such as the Diels-Alder,[1] Wittig[2,3] and many variants of the Pd-catalysed cross-coupling reactions.[4]

One such reaction is the conjugate addition reaction. This reaction has been known for nearly 150 years and is afforded a full chapter in Clayden's *Organic Chemistry*.[5] A conjugate addition is a type of reaction where a nucleophile adds to a particular C=C double bond in a conjugated molecule. This type of nucleophilic addition to a α,β-unsaturated system is also known as a Michael addition and consequently, these α,β-unsaturated compounds are known as Michael acceptors (Figure 7).

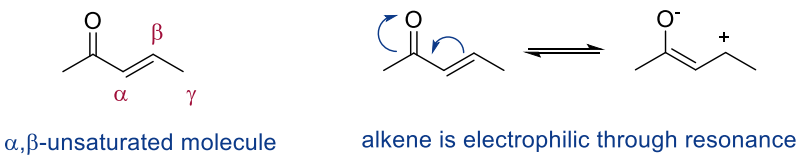


**Figure 7** α,β-unsaturated molecules and their affinity for nucleophilic conjugate addition

The earliest example of this reaction type was in 1883 where Komnenos reported the addition of sodium diethyl malonate to ethylidene malonate to give a symmetrical conjugate addition product (Scheme 68).[6]

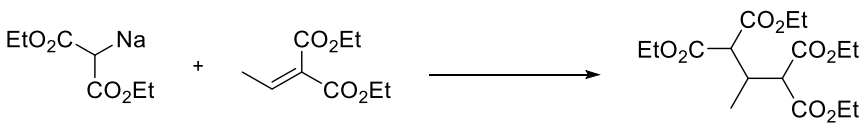


**Scheme 68** First report of a 1,4-conjugate addition reaction in 1883

Three years after this initial report, Michael reported the conjugate addition of the same sodium diethyl malonate to an acrylic bromide which yielded a cyclopropyl product (Scheme

69a).[7] Michael postulated that this product could only arise from a conjugate addition reaction to create an intermediate which could then cyclise. This hypothesis was confirmed when the coupling of sodium diethyl malonate with a linear enone was investigated and a conjugate addition product was formed (Scheme 69b).

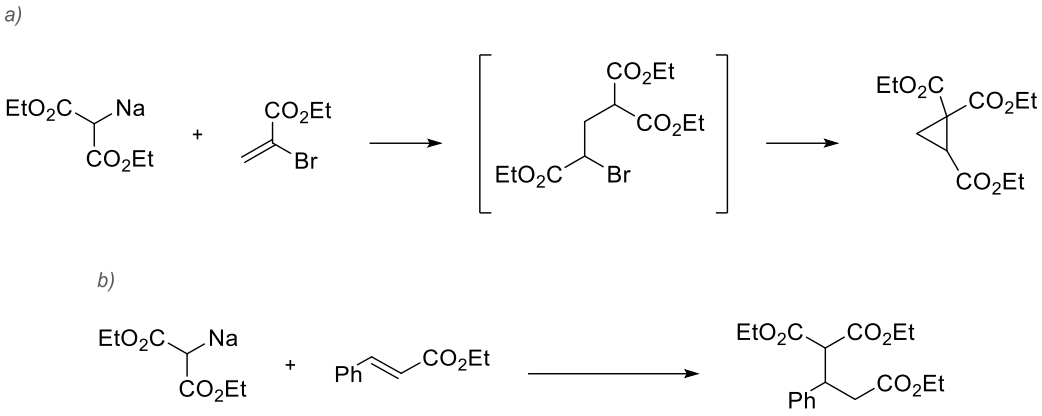


**Scheme 69** Seminal work by Michael involving the conjugate addition reaction

The first metal-catalysed variant of this reaction was published in 1941, when Kharasch used a catalytic quantity of copper to react a Grignard reagent with isophorone to give the conjugate addition product shown in Scheme 70.[8]

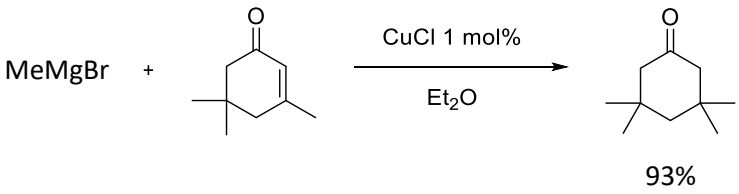


**Scheme 70** The first report of a metal catalysed conjugate addition reaction

From this initial reaction, many variants of this transformation were published, mainly using Cu,[9] Ni[10–12] or Pd[13,14] as the metal catalyst and Mg[15] or Li[16] organometallic nucleophile. The most common metals used to facilitate this transformation are, Co, Ni, Cu, Zn, Rh and Pd. All these metals have been employed successfully. However, when considering efficiency, selectivity, substrate scope, generality and catalyst availability, rhodium is the best performing metal. This thesis will include an introduction to rhodium-catalysed 1,4-additions.

## 5.2. Rhodium-Catalysed Conjugate Additions

The first example of a rhodium-catalysed conjugate addition was described by Ito in 1992 where α-cyano carboxylates could be asymmetrically added to vinyl ketones (Scheme 71).[17] It was found that the cyano group of the substrate was essential to the success of the transformation as it ligated the chiral rhodium catalyst. A good substrate scope was displayed, with high yields and enantioselectivities. The reaction proceeded under mild temperature and in a short time of 4 hours.

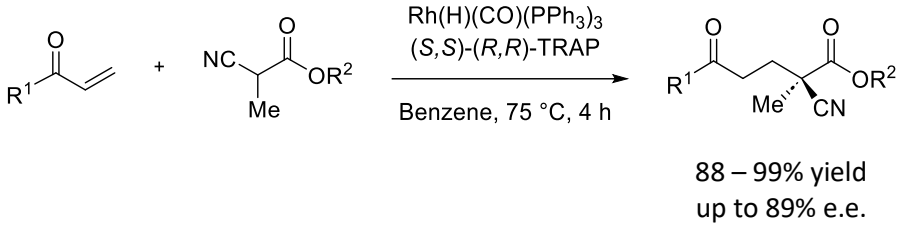


**Scheme 71** The first example of a Rh-catalysed conjugate addition reaction

The first example of the rhodium-catalysed 1,4-addition of a boronic acid to an enone was reported in 1997 by Hayashi and Miyaura (Scheme 72).[18] This work improved on previous protocols which employed Pd-catalysis with organoboronic acids in the presence of $SbCl_3$. Using $Rh(acac)(CO)_2$/dppb as a catalyst system, phenyl boronic acids could be successfully added to linear enones in excellent yields, setting the scene for this powerful transformation.

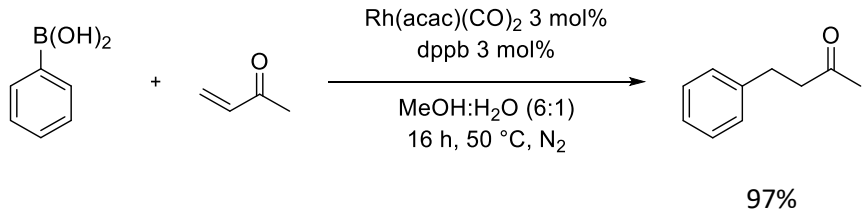


**Scheme 72** The first example of a Rh-catalysed 1,4-addition involving aryl boronic acids

### 5.2.1. The Development of Asymmetric Conjugate Additions

The success of this transformation was founded on the use of 1,4-bis(diphenylphosphino)butane (dppb) as a ligand.[18] Other ligands were screened, such as monodentate $AsPh_3$ and $PPh_3$, and bidentate phosphines such as dppp and dppe, which were all found to be less effective as ligands in the reaction. With the latter, the reaction

inefficiency was found to correlate to the size of the bite angle in the P-Rh-P complex. Despite the success observed with modifying the phenyl substituents, the reaction would not proceed when cyclohexenone was employed as the Michael-acceptor. However, in the following year, this hurdle was overcome when Hayashi and Miyaura utilised an alternative catalyst to access cyclic Michael-acceptors.[19] The key finding was to switch the Rh source to [Rh(acac)($C_2H_4$)$_2$] and to investigate the use of alternative phosphine ligands for the transformation. Through ligand screening, (*S*)-BINAP proved to be the most efficient ligand for the reaction. By altering the reaction solvent, temperature and time, in conjunction with the use of a new catalyst system, Hayashi could perform the first asymmetric 1,4-addition in quantitative yields and excellent enantioselectivities to afford the desired product (Scheme 73).

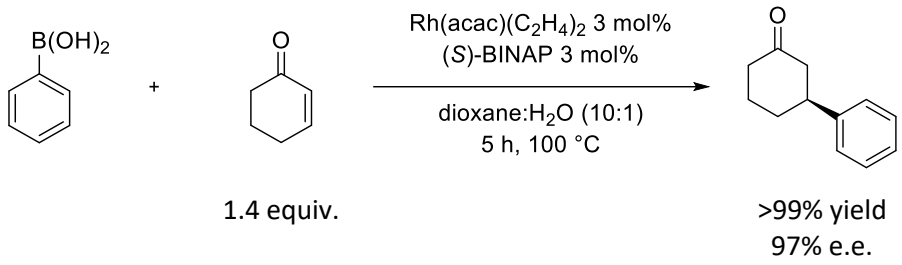


**Scheme 73** The asymmetric 1,4-addition of aryl boronic acids to cyclic enones

This methodology was suitable for a range of phenylboronic acids as well as cyclic and linear Michael-acceptors. The immediate expansion of this work was summarised by Hayashi in a report highlighting recent improvements.[20] Developments since then have included refining of the catalyst source, ligand type, reaction conditions and substrate tolerance. An excellent review on advances since Hayashi and Miyaura's seminal work was published by Fagnou and Lautens in 2003[21] which illustrates the many notable examples of how quickly the field was expanded by the chemistry community. The robustness of the chemistry allowed for rapid industrial uptake to synthesise enantioenriched products and manipulating the catalyst system allowed for much milder conditions to be employed, including reduced temperature and reaction time.[21]

A general catalytic cycle for this reaction is outlined below (Scheme 74).[22] The cycle begins with transmetalation between the aryl boronic acid and rhodium catalyst. This is then followed by the insertion of an unsaturated compound into the aryl−rhodium bond which subsequently undergoes hydrolysis giving a hydroarylation product and a hydroxorhodium species. In the elucidation of this catalytic cycle it became apparent that there is a more

direct route to product formation. The regeneration of the acac–H from the Ar-B(OH)$_2$ is a slow step in the cycle. However, if you start with a hydroxy rhodium precatalyst, the regeneration of the Rh-Ar species is much more efficient. This was demonstrated by Hayashi where milder conditions were employed to retain excellent enantioselectivities and yields (Scheme 75).[22]

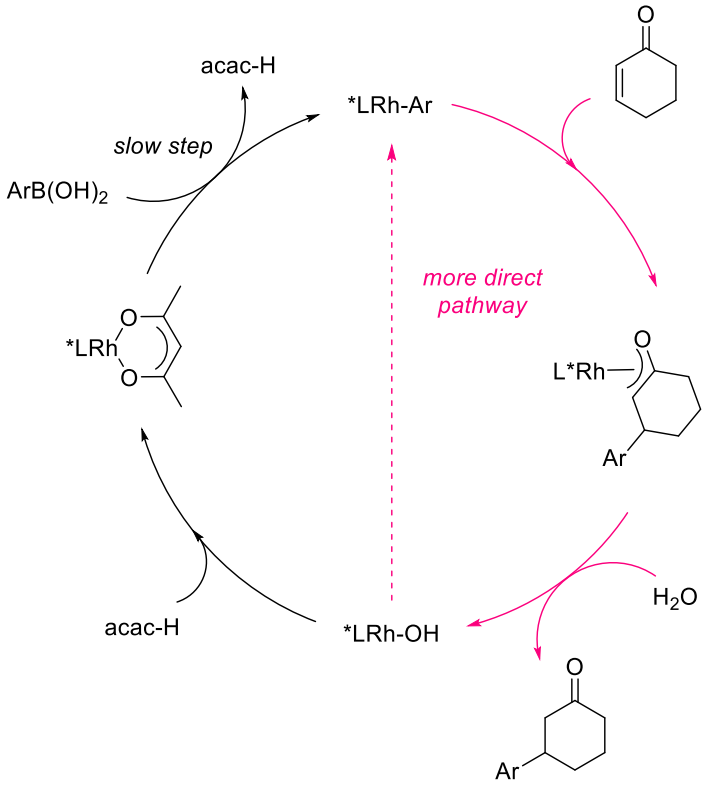


**Scheme 74** General catalytic cycle for the Rh-catalysed 1,4-addition of aryl boronic acids to enones

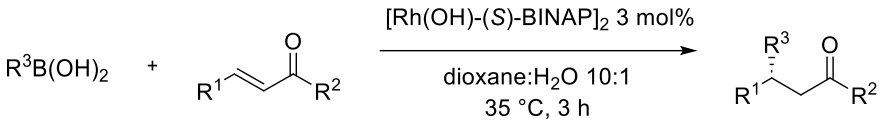


**Scheme 75** The use of a Rh-hydroxy precatalyst to create a more efficient catalytic cycle

### 5.2.2. Ligand Development for Asymmetric Conjugate Additions

The next advancement in the field of rhodium-catalysed 1,4-addition was in 2003 when Hayashi and Yoshida pioneered the use of chiral dienes as ligands for rhodium catalysis.[23] These dienes have a chiral environment which enables asymmetric transformations through the sterics existing between the phenyl (or benzyl) group and the hydrogen atom on the alkene(s) of the ligand. In the traditional BINAP-type ligands, the chirality is controlled by the

conformation taken once both phosphines have ligated the metal. In the case of chiral dienes, the metal is ligated in a rigid conformation and thus, the spacial discrimination is controlled by altering the size of the olefin substituent (Scheme 76).

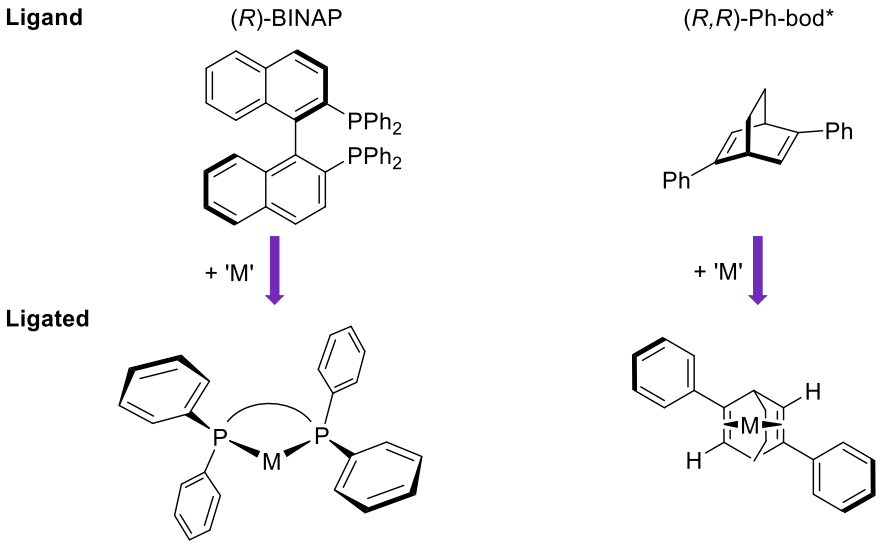


**Scheme 76** The chiral conformation of phosphine and diene catalytic systems

This new class of ligand was tested using literature standard Rh-catalysed 1,4-addition reactions and excellent yields and enantioselectivities (up to 99% e.e.) were observed.[23] One immediate advantage of having a new ligand class was that reactions which previously proceeded poorly with phosphine ligands could be trialled under new catalytic pretences. One example which highlights this advantage is in the case of utilising organostannane reagents.[23] The low catalytic activity of the phosphine complex can be overcome in this case by using a chiral diene ligand and the desired 1,4-addition product can be achieved in two-steps in 80% yield and 95% e.e. (Scheme 77).

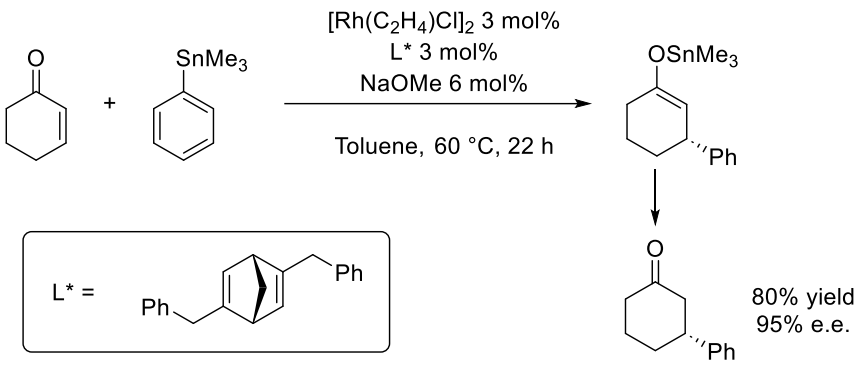


**Scheme 77** The use of chiral diene ligands to allow the use of organostananne reagents

Another example of the benefit of chiral diene catalysis is shown in the enantioenrichment of organosilicon compounds. With (*R*)-BINAP, this reaction proceeds with good yields and moderate enantioselectivities. However, when a chiral diene is employed in the case of (*R*,*R*)-Ph-bod* or (*R*,*R*)-Bn-bod*, the target 1,4-addition product is achieved in excellent yield, and an e.e. up to 99% (Scheme 78).[24] This dramatic improvement in enantioenrichment is also accompanied by the additional benefits of mild reaction conditions.

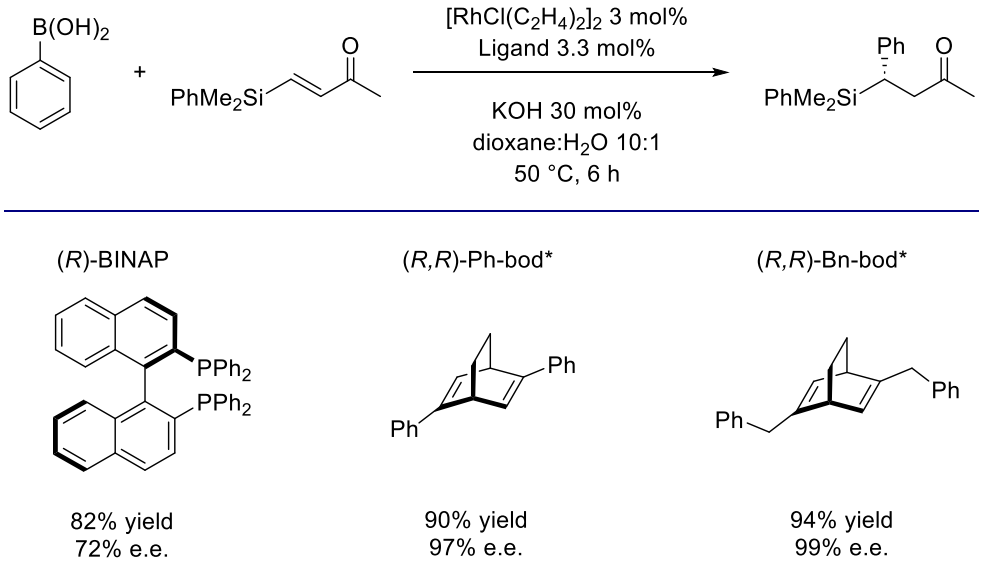


**Scheme 78** Comparative yields and enantioenrichment of organosilicon products with chiral ligands

Hayashi later reported that these diene ligands coordinate to transition-metals more weakly than the comparative phosphine ligands.[25] In an attempt to unify the two ligand classes, a phosphine-olefin hybrid ligand was designed (Scheme 79). This new ligand displayed an

efficiency comparable with the previous chiral dienes designed. Given the comparative results for this ligand against simpler dienes and phosphines, the arduous synthesis outweighs the potential benefit of using this compound in a catalytic system.

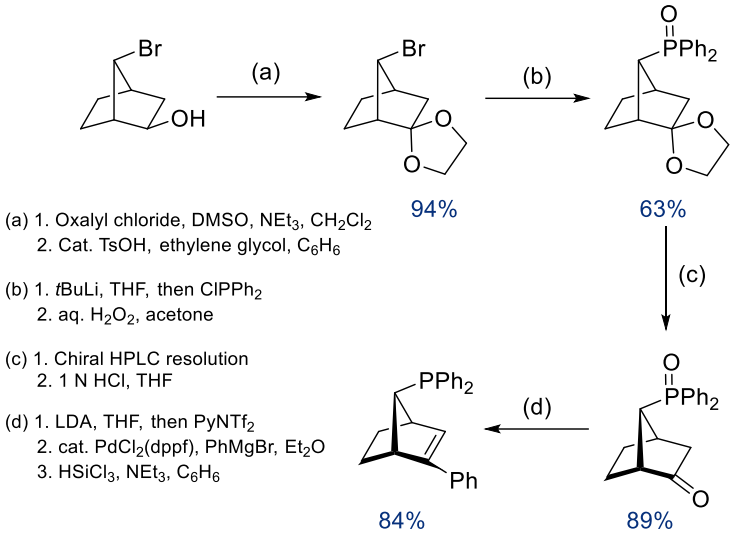


**Scheme 79** The route to access a hybrid phosphine-olefin class of ligand

In the years following Hayashi's publication of a chiral diene ligand, many reports from other groups emerged showcasing other types of chiral diene ligand suitable for this transformation. One such report was by Carreira where the chiral dienes of type **I** (Scheme 80) were synthesised. [26] An advantage of this new ligand is that it displays activity to a wider range of Michael-acceptors than previously shown by Hayashi. This list included cyclic and acyclic enones, lactones, esters, coumarins and amides, while these substrates showcased varying yields but excellent enantioselectivities (Scheme 80).

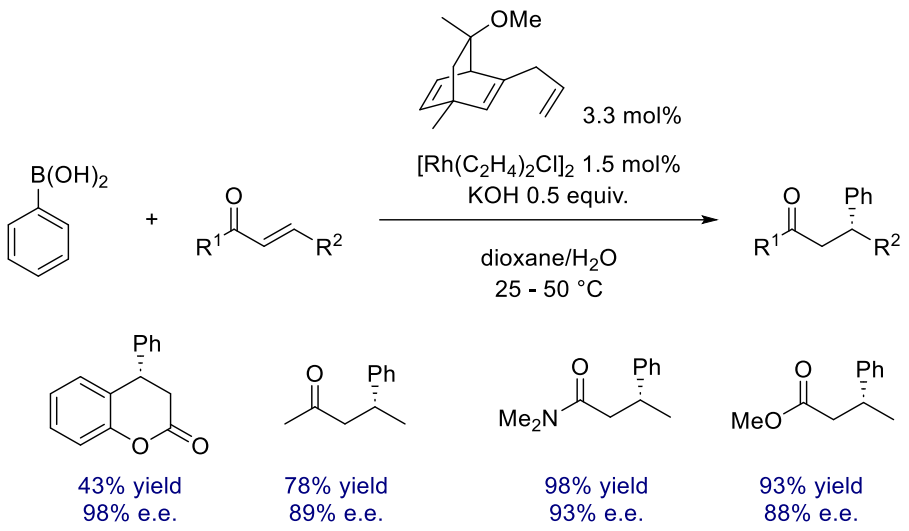


**Scheme 80** An alternative chiral diene ligand with broad substrate applicability

In 2011 a new class of ligands, mostly derived from Ellman's auxiliary, found widespread use in asymmetric catalysis. The majority of this initial work was by Lin and co-workers which was rooted in $SmI_2$-mediated asymmetric synthesis.[27–29] On the back of the rise in sulphur-based chiral ligands for asymmetric catalysis, Xu and co-workers aimed to fuse the success of chiral dienes in rhodium-catalysis with the popularity of chiral sulphur ligands. In 2011, Xu reported the first instance of a hybrid sulphur-olefin ligand which was employed to facilitate rhodium-catalysed 1,4-additions with cyclic α,β-unsaturated carbonyl compounds.[30] Excellent yields and enantioselectivities were observed, up to 99% and 98% e.e. respectively. The modularity afforded with this simple chiral building block readily enabled ligand derivatisation. In a rapid release of publications, many variations of these sulphur-olefin ligands were reported to facilitate rhodium-catalysed asymmetric 1,2- and 1,4-addition reactions (Scheme 81).

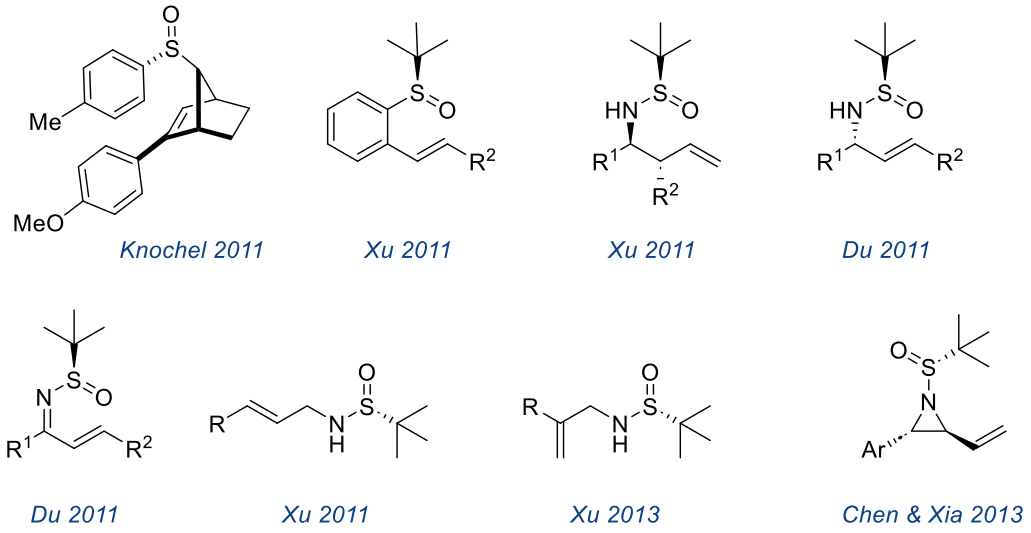


**Scheme 81** The range of sulphur-olefin ligands published between 2011-2013

## 5.3. Alternative Organometallic Reagents

A remaining challenge for rhodium-catalysed conjugate additions is the quantity of boronic acid required for efficient conversion, particularly when using heteroaromatic substrates. This is on account of competitive protodeboronation pathways. Boronate esters such as ethylene glycol, pinacol and 2-methyl-2,4-pentanediol derivatives are well-known entities used as viable alternatives to boronic acids in palladium cross-couplings. However, they are lesser used reagents for 1,4-additions in comparison to their boronic acid counterparts. However, a number of more suitable arylboronates can be used in 1,4-additions (Figure 8).

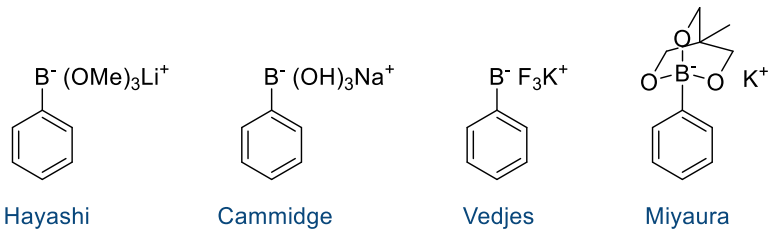


**Figure 8** Examples of published aryl boronate esters

The lithium trimethoxyboronate species shown in Figure 8 is the first example of an arylboronate being employed in rhodium-catalysed 1,4-additions.[31] Hayashi describes the *in situ* formation of the boronate ester by addition of *n*BuLi to the appropriate aryl bromide followed by subsequent treatment with trimethoxyborane to access the desired species

(Scheme 82). However, as expected, these boron species are sensitive reagents and a specific quantity of water was required to facilitate the conjugate addition while concurrently not accelerating the hydrolysis of the carbon–boron bond.

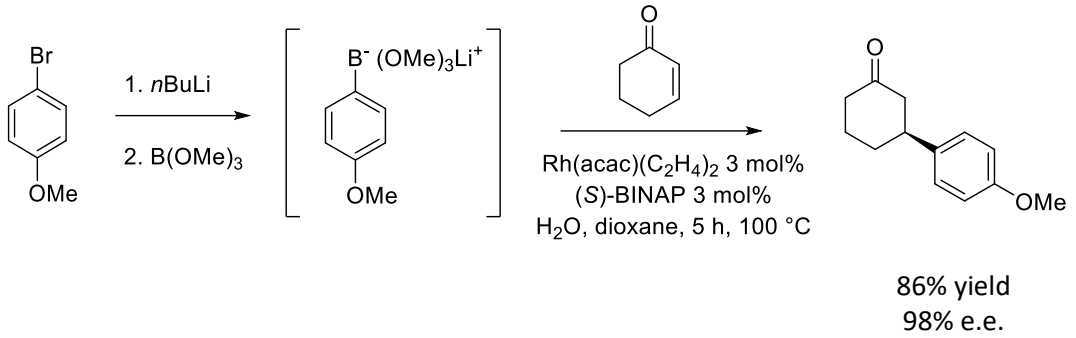


**Scheme 82** The first use of lithium trimethoxyboronates in Rh-catalysed 1,4-addition reactions

A report by Whitehead and co-workers in 2006 shows how aryl bromides (or boronic acids) can be simply turned into their corresponding trihydroxyborate sodium salts by treatment with sodium hydroxide solution in toluene or hexane.[32] The resulting salts were effectively deployed in Pd-catalysed cross-coupling reactions, allowing easy access to boronate reagents (Scheme 83). These trihydroxyborates have, to the best of our knowledge, not been used in Rh-catalysed conjugate additions.

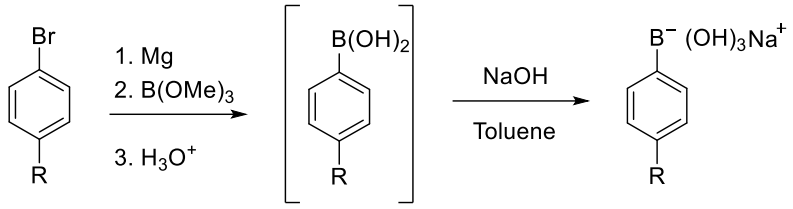


**Scheme 83** The formation of sodium aryltrihydroxyborates for cross-couplings

Other important arylboronate species are potassium organotrifluoroborates, which are currently the boronate reagent of choice for a variety of organometallic processes.[33] These species boast stability towards reagents that can be troublesome for other boron reagents. They are air and water stable, as first described by Thierig and Umland in 1967.[34] In the case of rhodium-catalysed 1,4-additions, these species were first introduced as suitable reagents in back-to-back publications by Genêt and co-workers.[35,36] The relative rate of reaction for

$BF_3K$ salts is faster than their boronic acid counterparts, which is thought to be due to a faster transmetalation step in the catalytic cycle. Genêt showcased how, when using the appropriate rhodium precatalyst, full conversion to the desired product could be obtained in 2 hours using this boron species, and excellent enantioselectivities were still observed (Scheme 84).

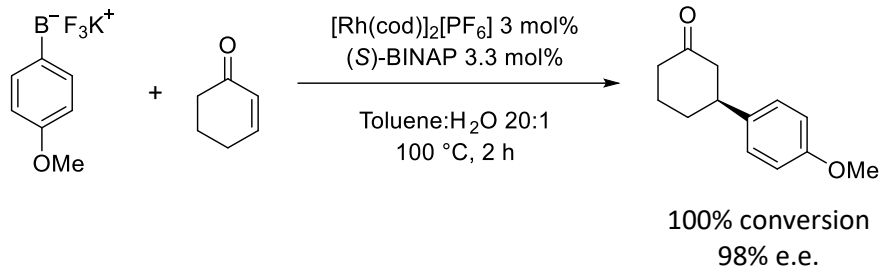


**Scheme 84** The use of potassium organotrifluoroborates in Rh-catalysed 1,4-addition reactions

Finally, Miyaura and co-workers have reported access to potassium and lithium cyclic triolboronate salts from various boronic acid starting materials.[37] Using the triol depicted in Scheme 85, alongside potassium or lithium bases, the desired cyclic triolborates can be readily prepared in excellent yields. The authors also show the application of these triolboronate salt species in Pd-catalysed cross-couplings. As with the sodium aryltrihydroxyborates, these species have yet to be exploited in Rh-catalysis for conjugate additions.

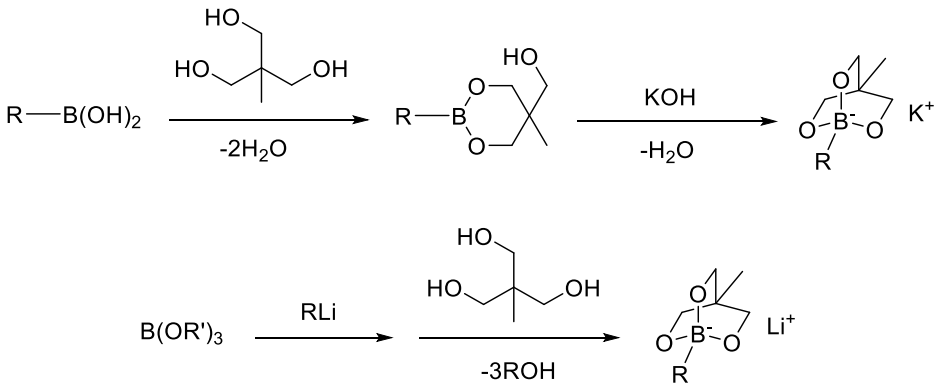


**Scheme 85** The synthesis of potassium and lithium cyclic triolborates

It is worth noting that this list of alternative boron reagents is not exhaustive. Many varieties of arylboronates exist as viable counterparts to traditional boronic acid coupling partners.

## 5.4. Substrate Scope of the Rh-Catalysed Conjugate Addition

So far within this introduction to the Rh-catalysed 1,4-addition reaction, the Michael-acceptors described have been variations on cyclic and acyclic enones. It would be remiss not to mention the array of Michael-acceptor type substrates which can be employed, such as: Alkenylphosphonates,[38] nitroalkenes,[39] 5,6-dihydro-2(1*H*)-pyridinones,[40] coumarins,[41] substituted malemides,[42] as well as many other α,β-unsaturated compounds (Scheme 86).

*Alkenylphosphonate Addition*

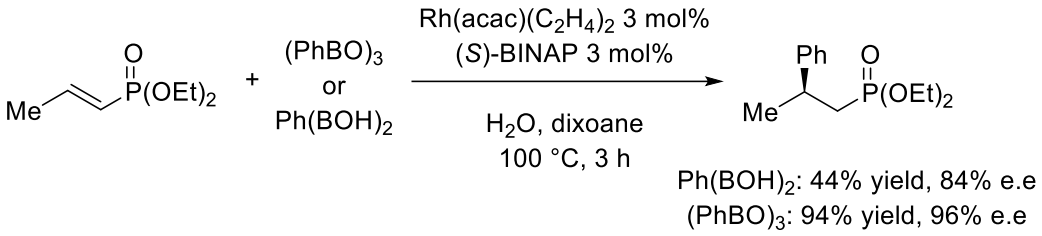


*Nitroalkene Addition*

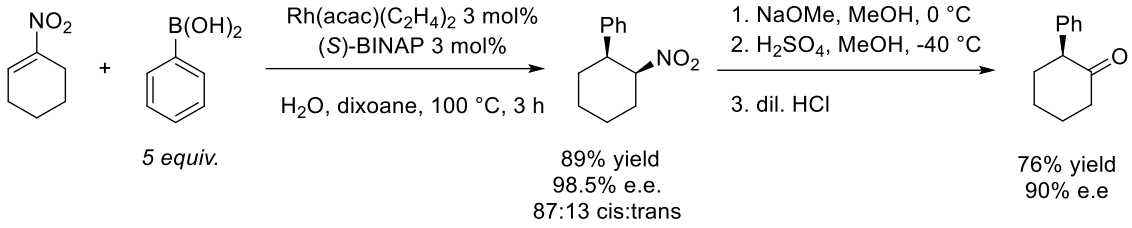


*Dihydropyridinone Addition*

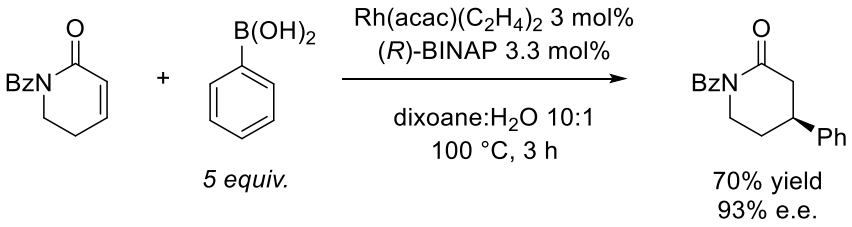

*Coumarin Addition*

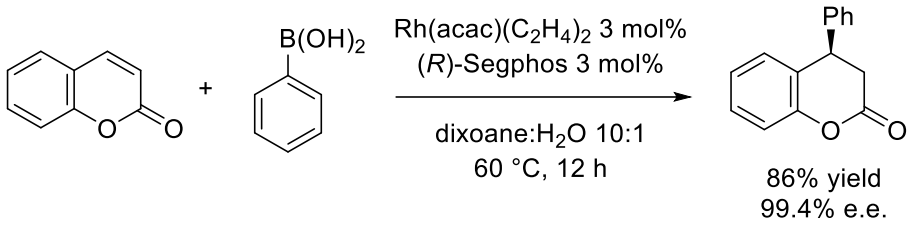


*Maleimide Addition*

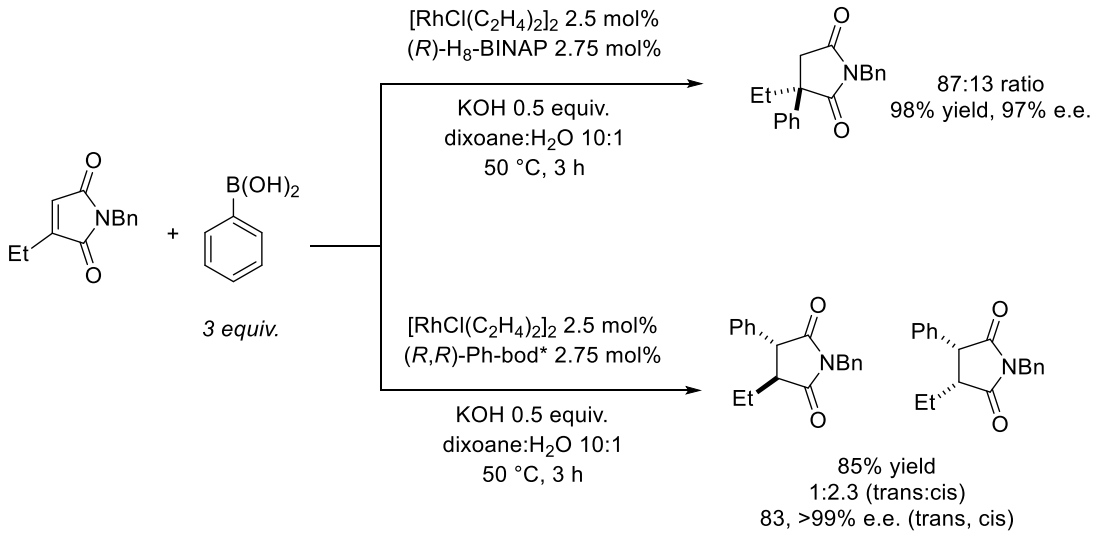


**Scheme 86** Select examples of Michael-acceptor substrates employed in the 1,4-addition reaction

Of the many examples of Michael acceptors subjected to Rh-catalysed conjugate additions, this Introduction will highlight some recent, and more exotic, examples of the variety of substrates available for this transformation.

Marek and co-workers reported an unusual Michael-acceptor type substrate in 2018.[43] Using small nonfunctionalized cyclopropenes, a variety of asymmetrically arylated cyclopropanes could be efficiently accessed *via* Rh-catalysis. Although a large range of phenyl boronic acids were trialled under the reaction conditions (as shown in Scheme 87). The cyclopropene substitution could also be efficiently altered from small to bulky substituents as well as tolerating bicyclic systems. It is worth highlighting that the heteroaromatic boronic acids of thiophene, furan or pyridine were not successfully employed in their reaction scope.

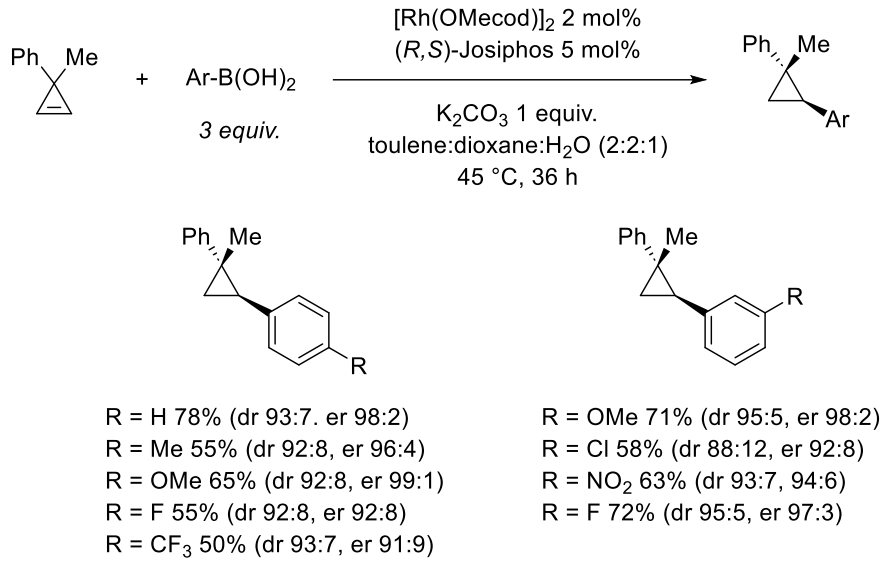


**Scheme 87** The Rh-catalysed conjugate addition of arylboronic acids to cyclopropene substrates

In 2021, Fletcher and co-workers reported a rhodium-catalysed approach to access complex enantioenriched cyclobutanes.[44] This comprehensive publication looks at the different reaction pathways available to this unique substrate. Once the cyclobutene is metalated with the rhodium catalyst, the reaction conditions and substitution pattern of the substrate can determine the fate of the product. A hydroarylation, 1,5-addition, reductive Heck or remote substitution *via* chain walking can all take place, giving rise to a myriad of products (Scheme 88). While this chemistry does not fall under the umbrella of conjugate addition reactions, it showcases the work still ongoing in the field of asymmetric rhodium catalysis and the plethora of Michael acceptor-type substrates to be exploited.

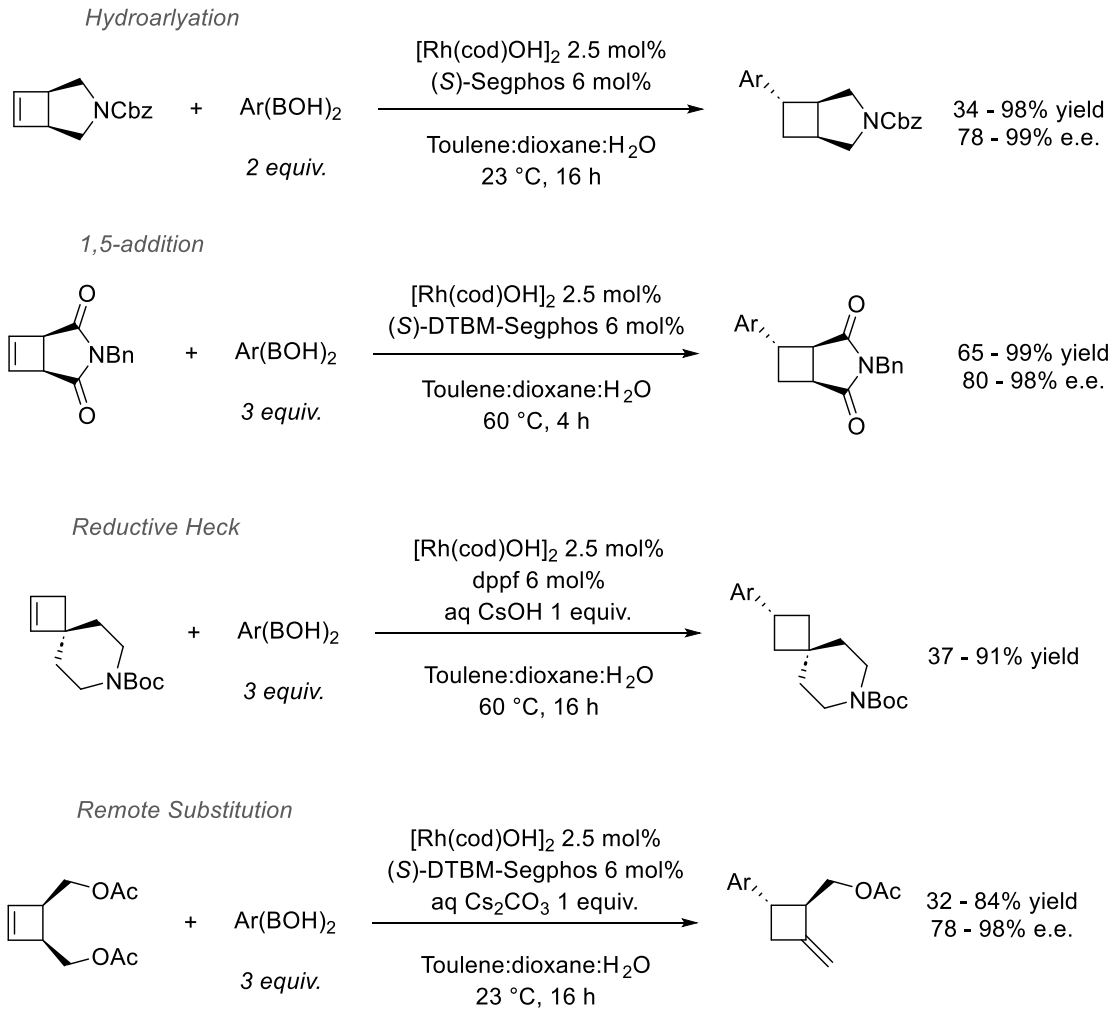


**Scheme 88** The various reaction pathways of metalated cyclobutenes

A recent, relevant example of Rh-catalysed 1,4-addition is the enantioselective synthesis of 3-piperidines from pyridine.[45] By reducing pyridine to the appropriate phenyl carbamate dihydropyridine, a suitable Michael-acceptor type substrate was unmasked to yield difficult-to-access enantioenriched 3-piperidines (Scheme 89). This work again highlights the array of substrates susceptible for conjugate addition. The dihydropyridine was synthesised by alkylating the pyridine nitrogen followed by reduction through a source of hydride. It was found that the alkylating group was fundamental to the success of this transformation and the phenyl carbamate-protected dihydropyridine was a substrate which could be easily isolated as a crystalline solid. The prevalence of chiral piperidines in APIs was a driving force for the development of this protocol and the authors showcase a broad substrate scope for the asymmetric conjugate additions to dihydropyridines.

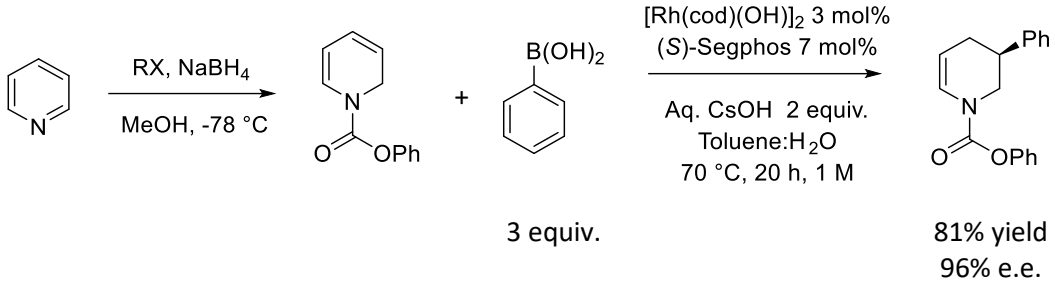


**Scheme 89** The synthesis of enantioenriched 3-piperidiens via asymmetric 1,4-addition

### 5.4.1. Heteroaryl Substrate Scope

As much as the Michael acceptor component of this reaction has varied throughout the years, the organometallic species has remained, by and large, phenyl boronic acid or derivatives thereof. Using a heteroaryl boron derivative in this chemistry is much less common. Few examples of these heteroaromatic boronic acids are used in reactions, namely: Furan, thiophene, protected pyrroles and recently, pyridine.[46] A large reason for the lack of success with heteroboron derivatives is due to the lability of the heteroarylboronic acid bond, and the associated rapid protodeboronation. This is especially problematic considering the prerequisite for water in many of the existing catalytic systems. Additionally, low reactivity can be observed with certain heteroaromatics due to their ability to poison metal catalysts. As mentioned, there are some examples of select heteroaryl groups being used in this chemistry to varying degrees of success. The substitution of the heteroaromatic group and the nature of the boron reagent are paramount when devising the use heterocycles in asymmetric Rh-catalysed conjugate additions.

In 2003, Hayashi reported the 1,4-addition of 3-thiopheneboronic acids to α,β-unsaturated compounds. A range of cyclic and acyclic enones were shown to undergo efficient asymmetric conjugate addition to give the heteroaromatic products in good yield and excellent enantioselectivity (Scheme 90).[47]

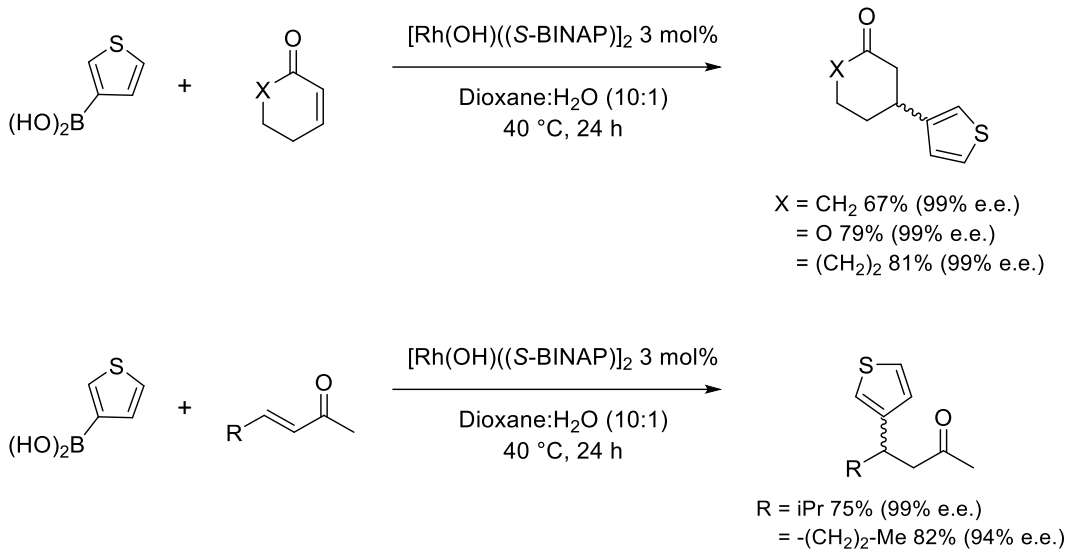


**Scheme 90** The coupling of 3-thiopheneboronic acids with α,β-unsaturated compounds

Examples like this coupling, where heteroaryl residues are transferred as a boronic acid are rare within this reaction type. A recent example which highlights the use of heteroaromatic boronic acids in conjugate additions was published by Chang and co-workers.[48] Evidently, this reaction is not a rhodium-catalysed transformation but instead, is a selected example of an magnesium-catalysed reaction which can also form enantioenriched conjugate addition products. Select substrate examples are depicted in Scheme 91. Like Hayashi's previous work, success was observed with the thiophene boronic acids. It is worth noting however, that the furan boronic acid and benzofuran boronic acid both gave a significant reduction in enantioenrichment.

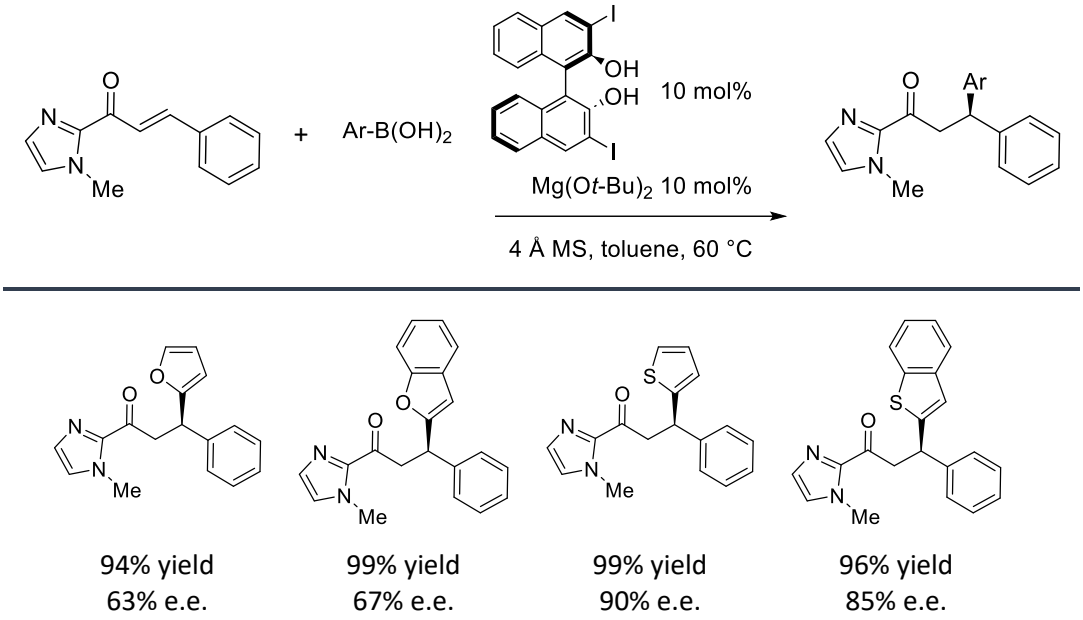


**Scheme 91** A chiral diol catalysed enantioselective conjugate addition

However, as mentioned previously, the few examples employing heteroaromatic substrates in rhodium-catalysed conjugate additions primarily require some form of a boronate ester.

Miyaura showcased how heteroaromatic triolborates can be used in Rh-catalysed conjugate additions.[49] A range of thiophene and pyridine triolborates underwent efficient asymmetric conjugate addition with various Michael-acceptors. However, some of these heteroaromatic substrates displayed poor yield and/or enantioenrichment (Scheme 92). It was concluded that the electronic character of the C–B bond determined the level of reactivity of the substrate. The lower nucleophilicity of unsubstituted pyridines and thiophenes lead to no product being formed and it was hypothesised that the competitive hydrolytic C–B bond cleavage outcompeted the conjugate addition.

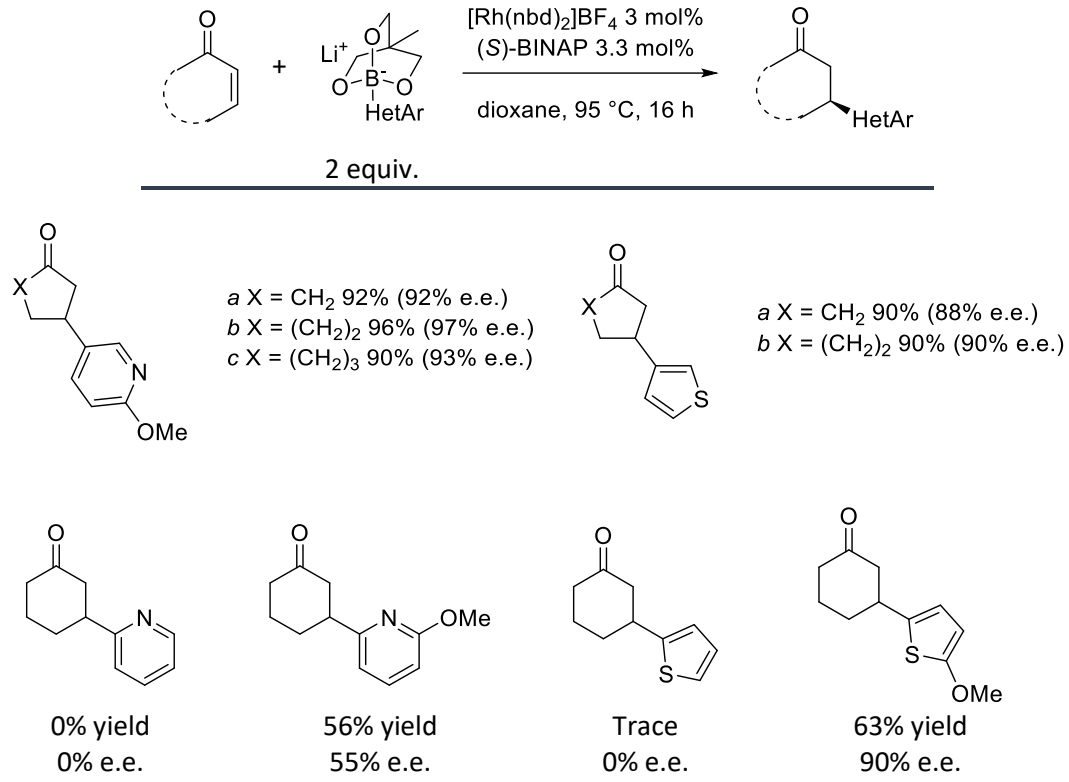


**Scheme 92** The use of heteroaromatic cyclic triolborates in conjugate additions

Boysen and co-workers have published a comprehensive study on the use of heteroarylboronates in rhodium-catalysed conjugate additions.[46] This work culminates what was previously reported in the literature, whereby the nucleophilic character of the C–B position determines the reaction success. Several heteroaryl substrates were trialled in their MIDA or pinacol boronate forms. Different pyridines, furans, thiophenes and pyrroles were investigated but it is worth noting that in the case of the pyrrole substrates, the N-H had to be protected in the form of a TIPS, Boc or methyl protecting group. The Boysen group concluded that the success of the reaction largely depends on the electronic nature of the boron species and thus, on the borylation position on the heteroaromatic ring. To efficiently couple these heteroaromatic residues in an asymmetric fashion required intense optimisation, particularly regarding ligand design. However, many substrates proved to be problematic. Only promising substrates were trialled in the asymmetric variant. Some successful examples of these heteroarylboronates are depicted in Scheme 93.

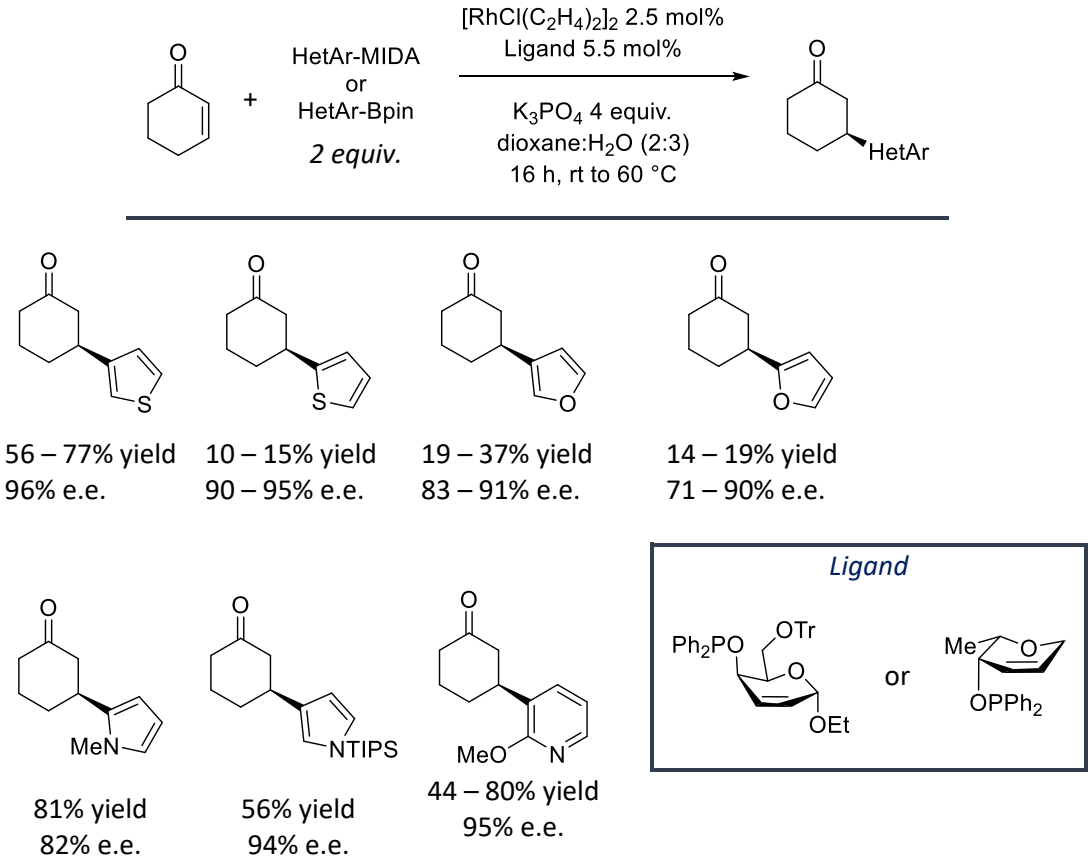


**Scheme 93** The use of MIDA or pinacol boronates in Rh-catalysed conjugate additions

A final, and recent, example concerning heteroaryl conjugate addition reactions was published by Dou and co-workers in 2022.[50] This work reports the rhodium-catalysed asymmetric conjugate pyridylation of α,β-unsaturated carbonyl compounds with pyridylboronic acids. This work was enabled by employing a bifunctional chiral amide-diene ligand. As well as acting as a chiral ligand for the reaction, the authors suggest that the ligand dramatically accelerated the rate of reaction *via* H-bonding, allowing the conjugate addition to outcompete the protodeboronation. The reaction was found to only proceed efficiently when carried out in aqueous ethanol, supporting this H-bonding hypothesis. A large range of Michael-acceptor substrates were showcased with various pyridylboronic acids. A select few examples are shown in Scheme 94. The H-bonding effect of the chiral amide-diene ligand was explored by the authors and when the amide proton was changed to a methyl group, a large reduction in rection rate was observed (Scheme 95).

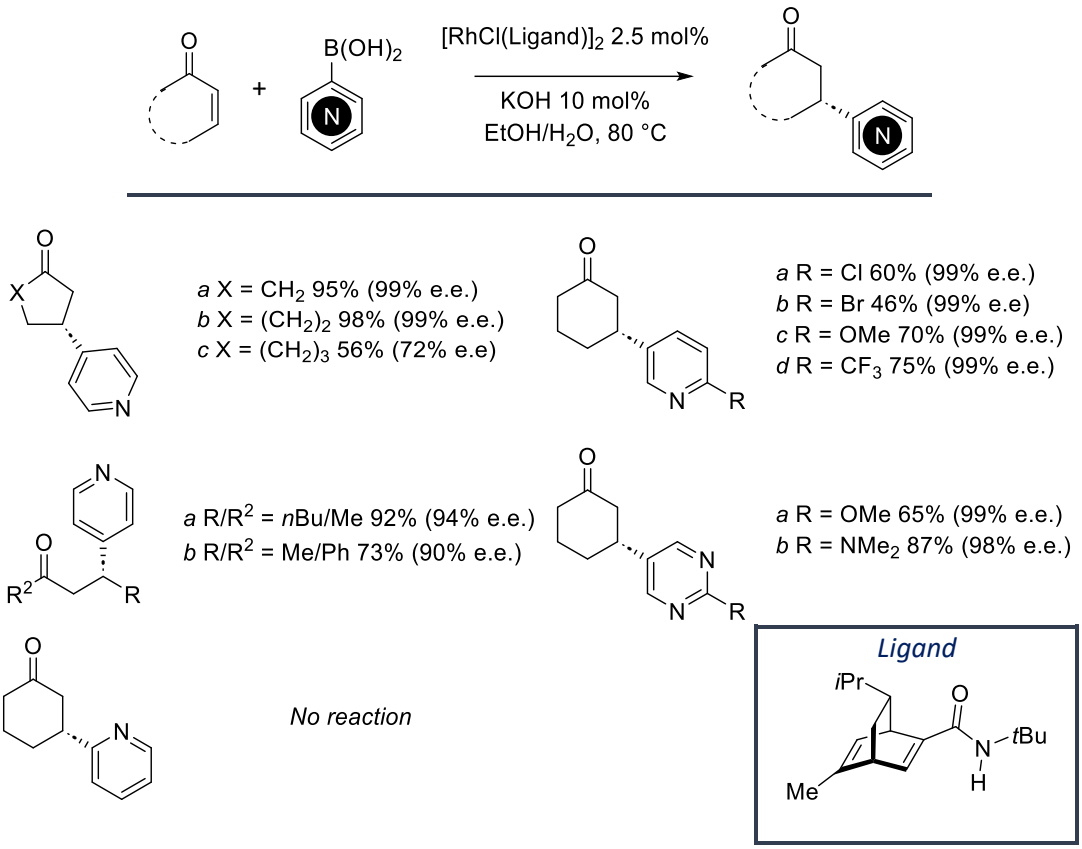


**Scheme 94** The asymmetric conjugate addition of pyridylboronic acids

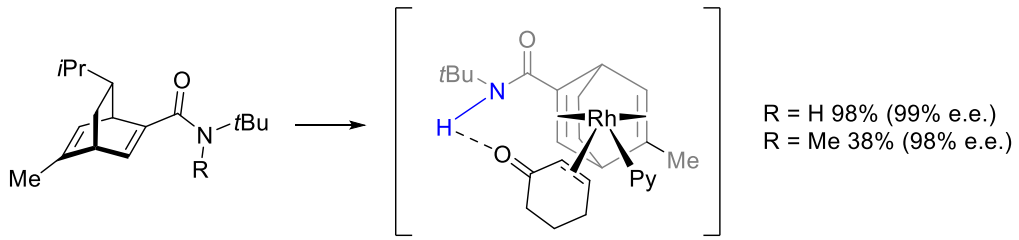


**Scheme 95** The potential H-bonding effect of the chiral amide-diene ligand

## 5.5. The Importance of Indole as a Heteroaromatic Scaffold

Despite the research in this space, it is clear that there is no general means for accessing heteroaryl conjugate addition products. Particularly for systems which are electron-deficient at boron. Using a heterocyclic boronic acid instead of a modified boronate ester is increasingly difficult for heteroaryl residues. Additionally, applying heteroaromatic groups with a free N-H bond is unreported. In fact, there is, to the best of our knowledge, only one example of indolyl boronic acids being employed in this transformation and it requires the

N-H bond to be suitably protected (N-Me).[51] The lack of reactivity observed is presumably a consequence of indoles propensity to undergo protodeboronation[52] and potentially interact with metal catalysts.[49] As a result, there has been no report of indolylboronic acids undergoing rhodium-catalysed conjugate addition reactions. This represents a significant gap in the scientific literature.

Indole represents one of the most abundant and important heterocycles in nature. For over a hundred years there has been a large scientific effort to explore the derivatisation of indole ring systems owing to their status as 'privileged biological structures'. The indole pharmacophore is critical to the function of a profusion of biologically active entities, ranging from large and complex natural products to simpler signalling molecules, like serotonin. Indole is central to the structure of many blockbuster APIs for the treatment of cancer, migraine, hypertension and other human diseases. In fact, it was reported that the indole-containing drugs sumatriptan, tadalafil, rizatriptan and fluvastatin accounted for total sales of $3.2 billion in 2010. An example of some of the many indole containing compounds is illustrated in Scheme 96 including common API's and signalling molecules.[53]

Derivatisation of the indole structure is commonly observed on the heterocyclic ring, particularly at the C3-position, owing to the inherent reactivity of that position towards electrophilic aromatic substitution.[54] The C2-poisition of the heterocycle is also commonly observed to be activated with appropriate transition-metal catalysts and the N-H bond itself is often exploited in alkylation or reductive amination protocols. Substitution processes on the phenyl backbone of indole is less commonly observed.[55]

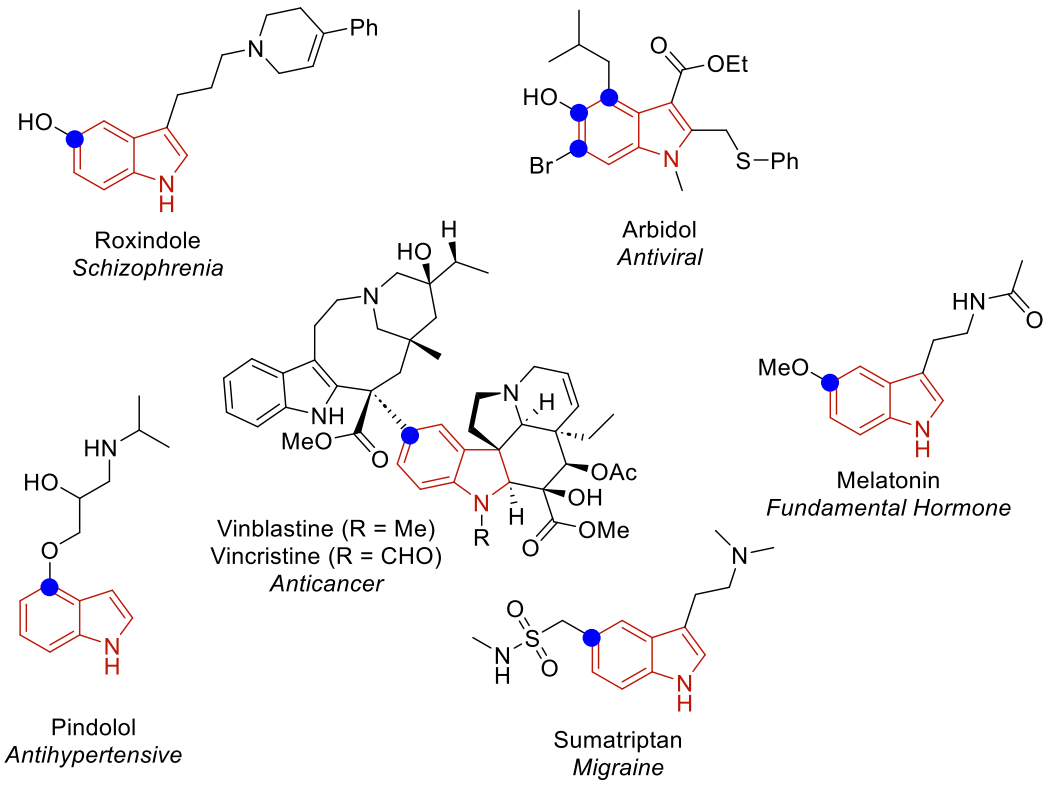


**Scheme 96** Indole containing APIs and natural occurring compounds

## 5.6. The use of Micellar Catalysis for Rh-Catalysed Conjugate Addition

As outlined previously, the utilisation of heteroaromatic coupling partners in 1,4-addition is limited by several factors. In some cases, their poor solubility in organic solvent and the additional problem of protodeboronation accelerated by base and water can create a roadblock when designing a reaction scheme. Micellar catalysis has, in recent years, come to the fore as viable alternative to organic solvent in chemical reactions, particularly through the work of Lipshutz.[56,57] The use of micellar catalysis has been successfully employed in the arena of Rh-catalysis, particularly in relation to asymmetric 1,4-additions.[58,59] This allows the benefit of aqueous solubility to be combined with the efficiency of an organic solvent for these transformations (Scheme 97). Micelles have associated potential benefits including; improving the green metrics of a reaction, allowing catalyst (or ligand) recyclability, milder reaction conditions and new reaction pathways as a consequence of the high concentrations associated with the use of micelles. Rhodium catalysis has, in particular, benefited from the use of micellar catalysis in recent years.

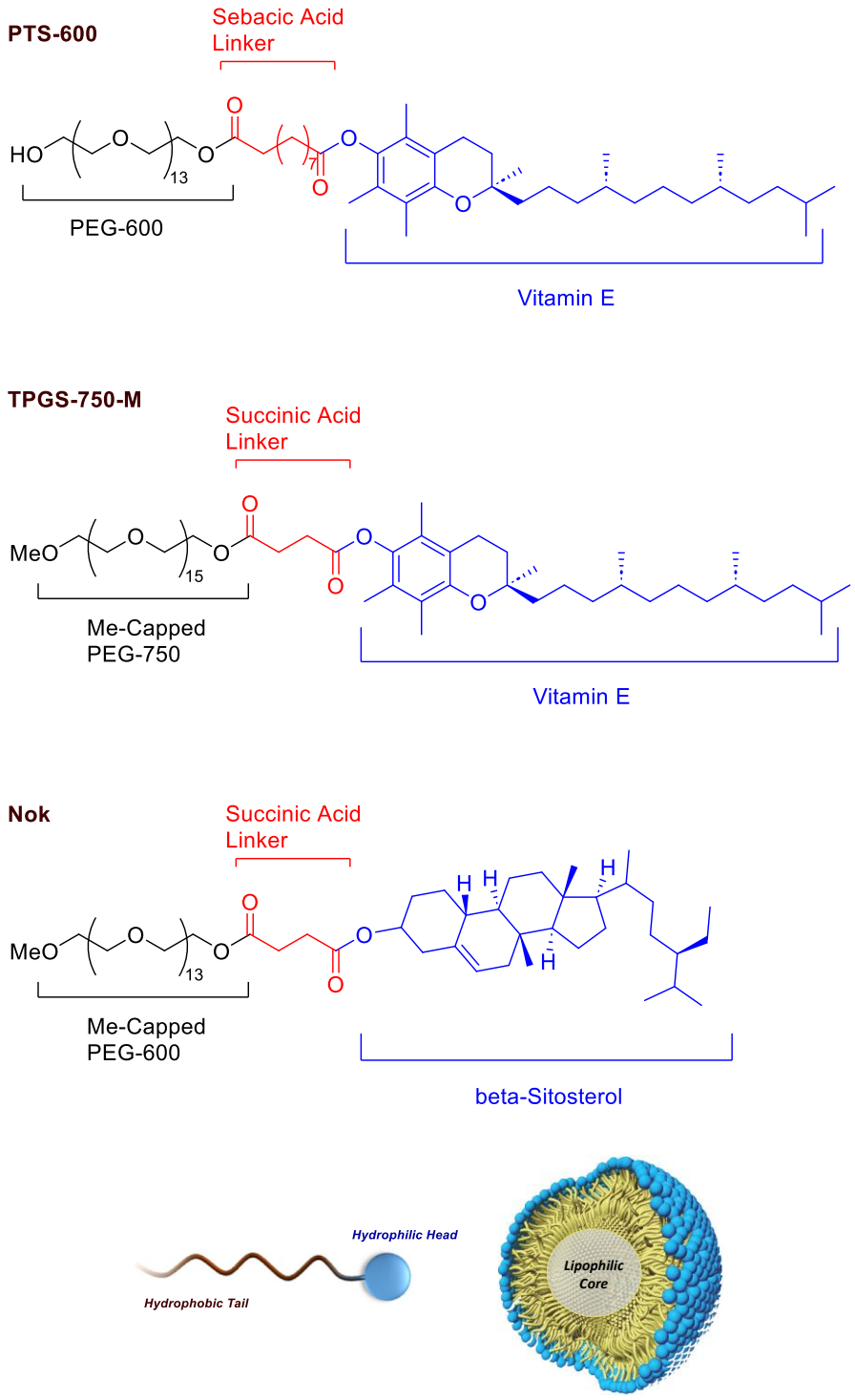


**Scheme 97** A summary of micelles and various surfactant[60]

In a report by Lipshutz, the benefit of aqueous micellar chemistry is highlighted by improved yields and enantioselectivities relative to those in organic solvent (Scheme 98).[58] Lipshutz and co-workers designed a micelle-catalyst system where the polyethyleneglycol ubiquinol succinate (PQS) surfactant was bound to the chiral ligand and could be premixed with a

suitable rhodium catalyst to create a chiral surfactant catalyst. The success of this reaction medium was showcased through employing different ring sizes of the Michael-acceptor and by alternating the arylboronic acid. In all cases, improved and more consistent yields and enantioselectivities were observed using aqueous micellar catalysis. It should be noted however, that the initial results in organic solvent were still excellent, for the most part. The synthesis of this simple surfactant ligand and catalyst system is shown in Scheme 99.

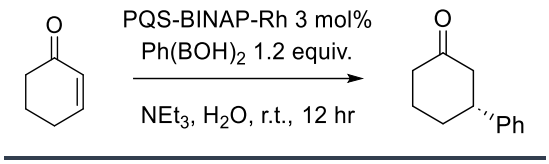


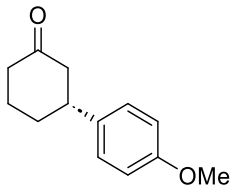


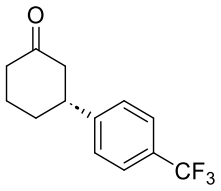


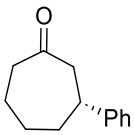


| | | | |
|---|---|---|---|
| aq miceller: | 99% yield, >99% e.e. | 87% yield, 99.9% e.e. | 83% yield, 96.3% e.e. |
| organic: | 99% yield, 94-97% e.e. | 70-84% yield, 99% e.e. | 40-83% yield, 89-93% e.e. |

**Scheme 98** Lipshutz's comparison of the solvent effect on Rh-catalysed asymmetric 1,4-additions

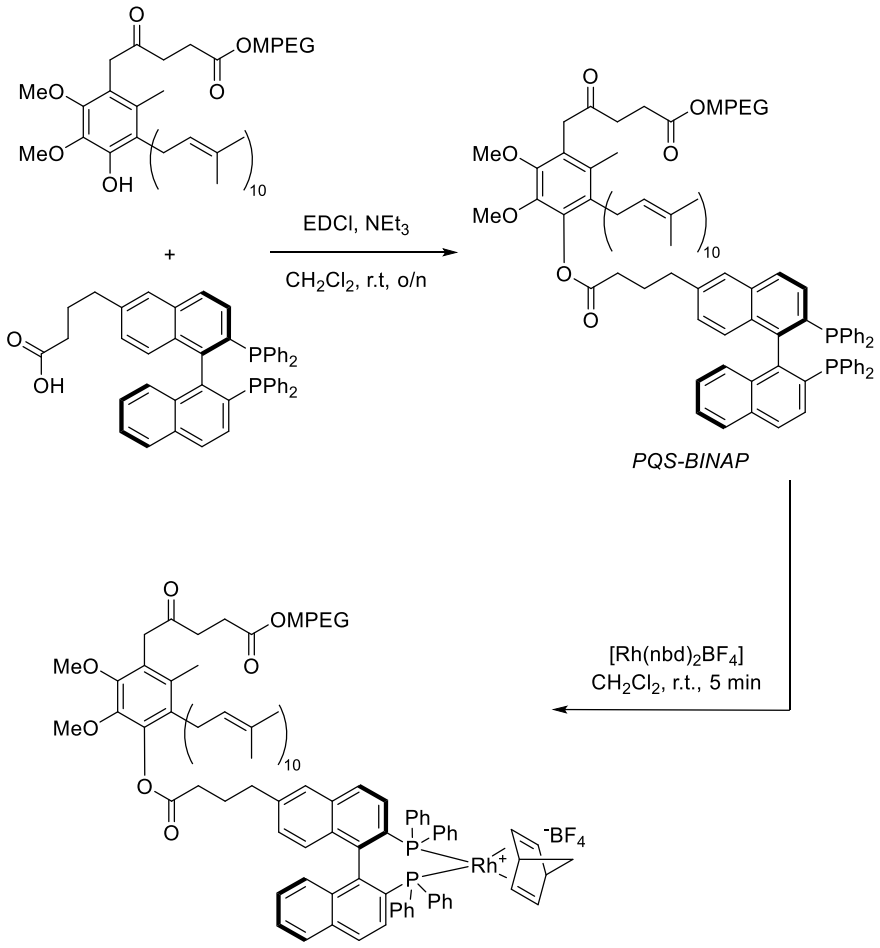


**Scheme 99** The synthesis of PQS-BINAP-Rh for asymmetric micellar catalysis

Similar work was carried out by Fernandez and co-workers,[59] where rather than pre-forming their chiral surfactant, they used a standard catalyst in a surfactant solvent for the reaction. A range of Michael-acceptors with phenylboronic acids was trialled in suitable surfactants to yield desired products in excellent yields and enantioselectivities (Scheme 100). Furthermore, using these developed reaction conditions, the corresponding 1,2-addition could also be performed in aqueous media. The structures of the PTS and SDS surfactants used are represented in Figure 9.

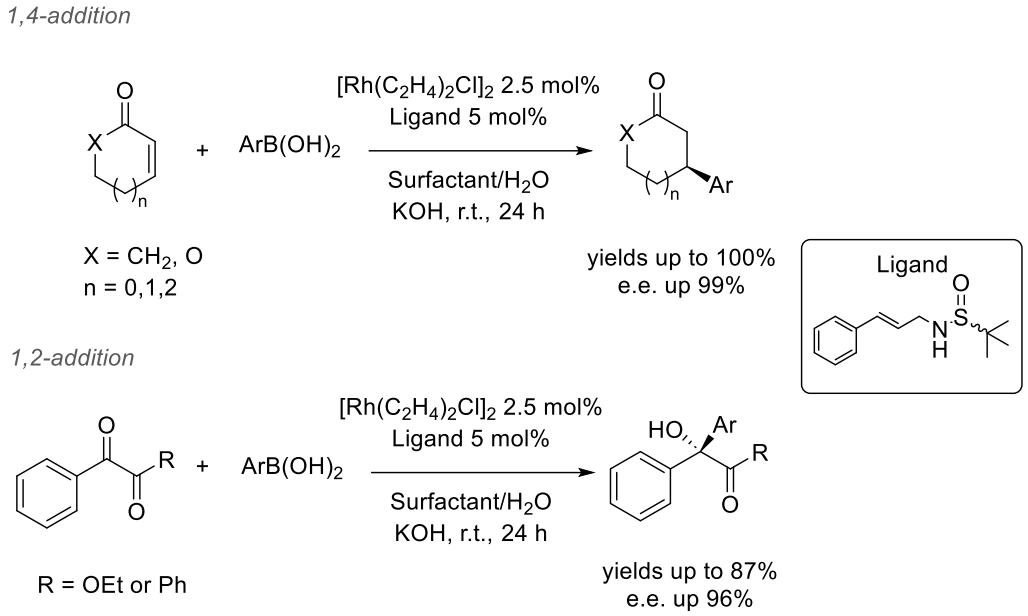


**Scheme 100** The use of surfactants in Rh-catalysed conjugate addition reactions

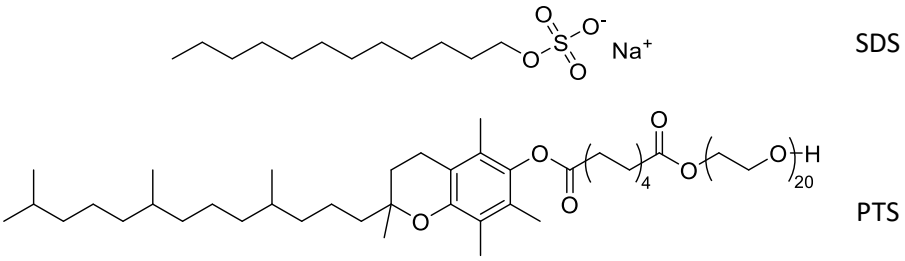


**Figure 9** Structures of common surfactants for micellar catalysis

The use of micelles as a reaction medium for Rh-catalysed 1,4-additions sets the stage for their application to heteroaryl boronic acids.

# 6. Results & Discussion

## 6.1. Objectives

Indole represents one of the most abundant and important heterocycles in nature. A straightforward approach to building molecular complexity on the indole backbone would be to employ indolyl boronic acids in asymmetric 1,4-addition reactions. As described in the Introduction, the use of heteroaryl boronic acids is under-reported in the literature as a consequence of their propensity to undergo protodeboronation, unwanted interaction with metal catalysts and engage in alternative reactive pathways. This section looks at utilising indolyl boronic acids in the asymmetric 1,4-addition reaction to yield enantioenriched, novel indole derived scaffolds. Ideally, this project would allow for a protecting-group-free strategy in aqueous media. The proof-of-principle reactions in this Chapter were carried out by another member of the McGlacken Group, Dr Katrina Mackey.

## 6.2. Background Chemistry

As this work was started by another member of the McGlacken group, some of the initial attempts to couple indoles with Michael-acceptors will be described to provide context for this thesis. This project was in collaboration with Eli Lilly, Indianapolis who required a route to access enantioenriched conjugate addition products from indole precursors. The initial reaction concept looked at employing an indole bromide with a suitable enone under transition metal catalysis to yield the conjugate addition product. The use of an aryl bromide could circumvent the foreseen issues with heteroaryl boronic acids. Many reactions were attempted using aryl halides with various palladium and rhodium catalysed protocols. However, any attempt to couple an indole halide with a enone failed to afford the desired product in a decent yield.

## 6.3. Initial Reaction Screening – Dr Katrina Mackey

On the premise that there was no obvious path to proceed with using indolyl halides, the idea of utilising Rh-catalysis and indole boronic acids for an asymmetric conjugate addition was conceptualised. As described in the Introduction of this Chapter, the precedent for using heteroaromatic boronic acids in this chemistry is limited, and the use of indolyl boronic acids is unreported. The state-of-the-art for this reaction would use mild reaction conditions, a chiral ligand and a simple Rh catalyst, as seen in seminal work by Hayashi and Miyaura

(Scheme 101).[19] More recent work by Fernandez and co-workers shows the power of using surfactants in unison with this chemistry, where at room temperature and in aqueous media, conjugate additions can be carried out in quantitative yields and in an e.e. up to 99% using a chiral sulphur-olefin ligand (Scheme 102).[61]

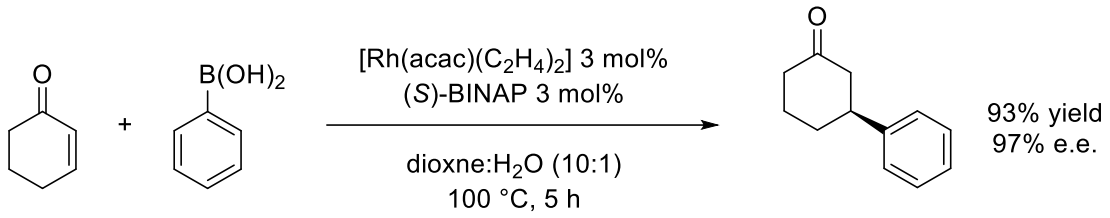


**Scheme 101** The first Rh-catalysed asymmetric addition using phenyl boronic acids

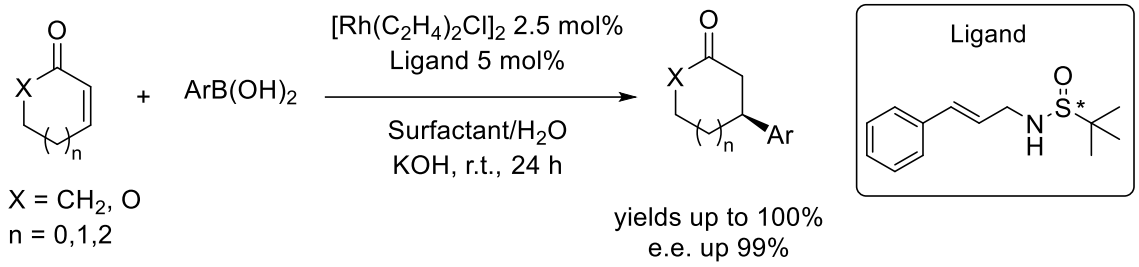


**Scheme 102** Modern advances in Rh-catalysed asymmetric additions

An initial reaction was trialled using 5-indolyl boronic acid in conjunction with (*R*)-BINAP, a standard rhodium catalyst and polyoxyethanyl-α-tocopheryl sebacate (PTS), which was the best performing surfactant for Fernandez and co-workers (Scheme 103).[59] The desired product was formed, albeit in low conversion of 31% and moderate enantiomeric ratio (e.r.) of 63:37.

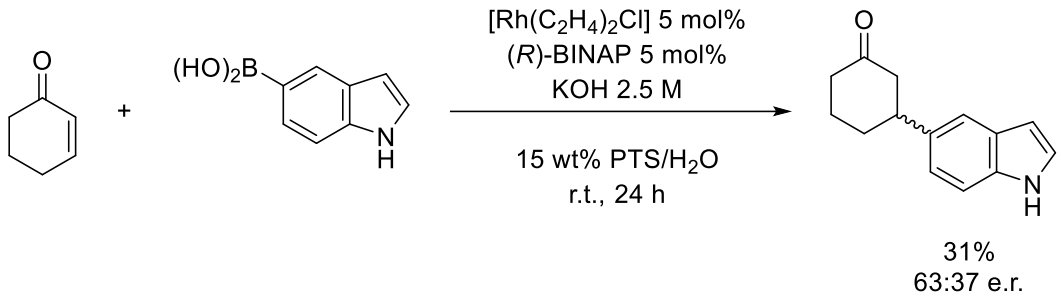


**Scheme 103** Initial reaction conditions for the Rh-catalysed conjugate addition of indolyl boronic acids

From this, the sulphur-olefin ligand **L1** employed by Fernandez was examined.[59] The ligand could be simply synthesised *via* reductive amination between cinnamaldehyde and Ellman's auxiliary.[59] The first step utilises titanium ethoxide as an activating agent[62] to form the imine intermediate which is subsequently reduced by sodium borohydride to furnish the desired amine product (Scheme 104). Both the racemic and enantiopure variants of the ligand were synthesised. The racemic reaction proceeded smoothly and provided access to a racemic product for HPLC method development (Scheme 105) (see Experimental for more information).

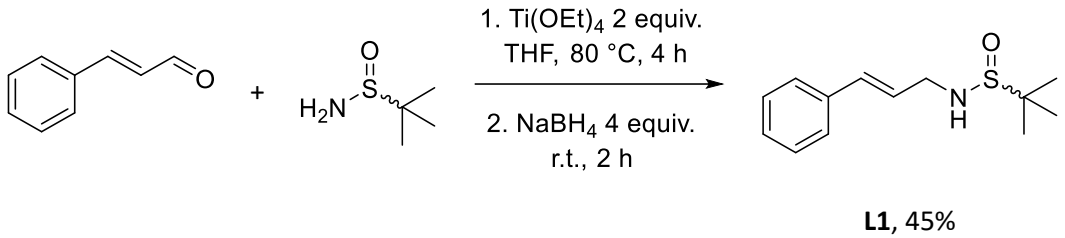


**L1**, 45%

**Scheme 104** The synthesis of chiral sulphur-olefin ligand by reductive amination

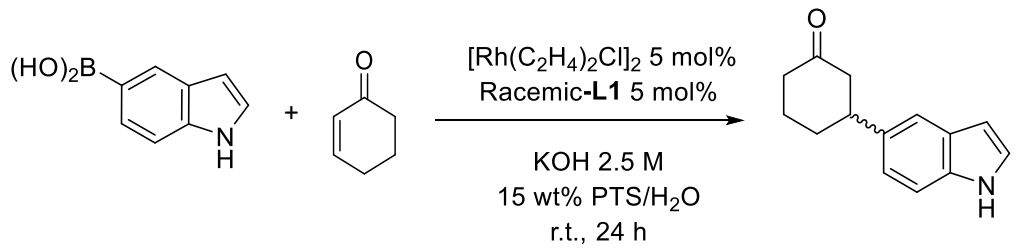


70%

**Scheme 105** The racemic Rh-catalysed reaction of 5-indolyl boronic acid with cyclohexenone

The corresponding asymmetric variant with the (*S*)-enantiomer ligand **L1** was then employed in the reaction. Under these initial reaction conditions, a yield of 70% was achieved with an enantiomeric ratio of 95:5.

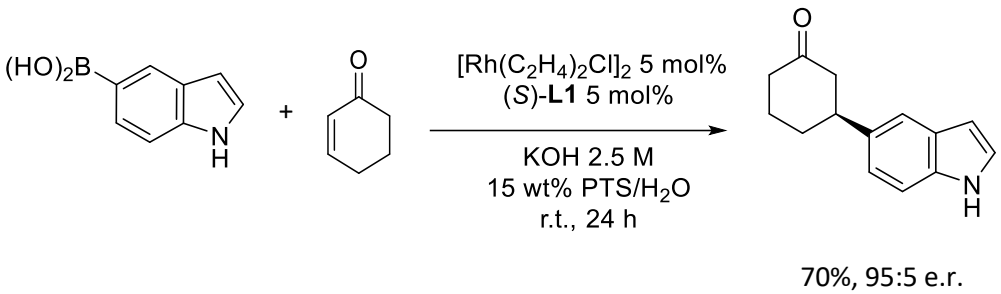


**Scheme 106** The asymmetric Rh-catalysed reaction of 5-indolyl boronic acid with cyclohexenone

The parallel reaction was also trialled initially in water rather than in a micellar solution and a comparable yield and enantioselectivity was obtained (Scheme 107). However, these conditions gave a more complex crude spectrum with additional side-products and was not as optimal as the corresponding version carried out in micelles.

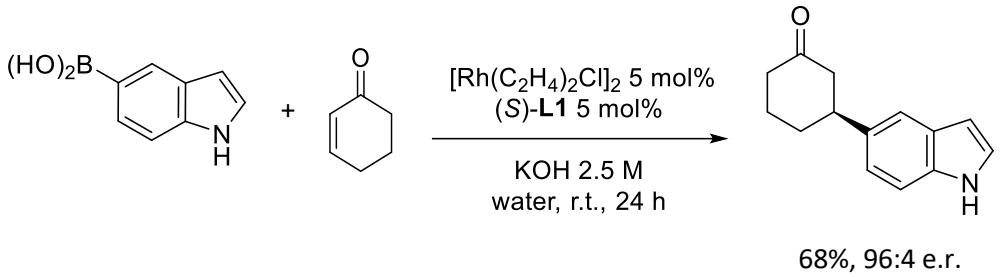


**Scheme 107** The comparable asymmetric reaction in water as a reaction solvent

As outlined in the Introduction, the macro structure of micelles can be altered by the addition of small amounts of organic solvent.[63,64] Methanol, acetone and other organic solvents are commonly used to alter micelle size, offering alternative reactivity, much like changing reaction concentration. Table 10 depicts the effect that adding 10% MeOH to either PTS or TPGS-750-M has on the reactions efficiency and enantiocontrol. Micelle TPGS-750-M is considered a designer surfactant. It is a second generation surfactant, developed from the base structure of PTS. In PTS, the conversion is lowered but a slightly higher enantioenrichment is observed (Table 10, Entry 1). With methanol, TPGS provides a higher conversion than the PTS, but a slightly poorer enantiomeric ratio observed (Table 10, Entry 2). Interestingly, 10% MeCN retained the enantioenrichment of 96:4 while boosting the reaction conversion to 91% (Table 10, Entry 3).

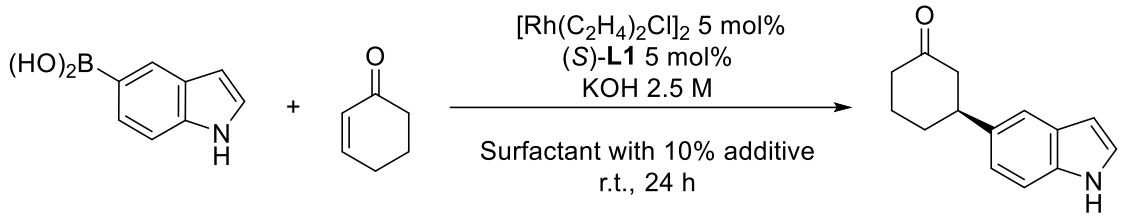


| *Surfactant* | *Additive* | *Conversion* [a] | *e.r.* [b] |
|---|---|---|---|
| PTS | MeOH | 60% | 96:4 |
| TPGS-750-M | MeOH | 73% | 95:5 |
| PTS | MeCN | 91% | 96:4 |

[a] Conversion is based off the relative ratio of starting material to product
[b] Enantiomeric ratio is determined by chiral HPLC on an OD-3 column

**Table 10** The effect of organic solvent additives

Finally, Dr Mackey showcased the fundamental importance of the sulphur-olefin ligand for reaction efficiency. In the absence of the ligand, the reaction proceeded to only 14% conversion even after 48 hours (Scheme 108).

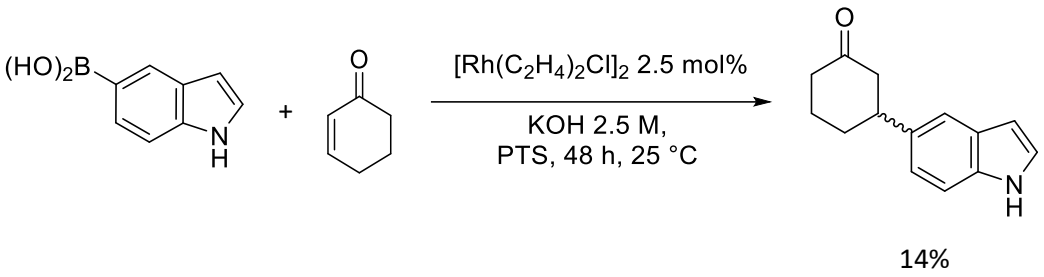


**Scheme 108** Investigation into conjugate additions in the absence of ligand

## 6.4. Reaction Optimisation

The reaction of cyclohexenone with 5-indolyl boronic acid was chosen as the model reaction to optimise this reaction type using similar conditions as those depicted in Table 10. As described in the Introduction, micelle solutions are surfactants which come together to form 'nanoreactor spheres' with a hydrophobic centre and hydrophilic shell.[60] It is inside these hydrophobic centres that the organic chemistry can take place. These nanoreactors create highly concentrated environments and thus, the high concentrations can sometimes obviate the requirement for prolonged reaction times or high temperatures.[60,65] Consequently, investigating the concentration of the micellar solution employed is incredibly important. The PTS solution is a 15 wt% solution in $H_2O$ and a volume of 0.7 mL of this solution in 0.3

mmol of cyclohexenone results in a concentration of 0.4 M for the reaction. With 10% of acetonitrile (MeCN) as an additive, the reaction progressed to 78% at 0.4 M, 91% at 0.8 M and was lowered to 50% at 0.2 M (Table 11, Entries 1-3). Using the concentration of 0.8 M, the catalyst and ligand loadings were lowered to 2.5 mol%. However, the yield of the desired product was reduced (Table 11 Entry 4). Despite the more concentrated system giving higher conversion, the crude material consisted of multiple side-products. The concentration of 0.4 M gave a much cleaner reaction profile and so, 0.4 M remained the preferred reaction concentration. The catalytic loading was also examined at 0.4 M. Initially, the catalyst to ligand ratio was run at 1:1 (5 mol%). When a 1:2 catalyst to ligand ratio (2.5:5 mol%) was employed, an improved conversion to 86% was observed (Table 11 Entry 5).

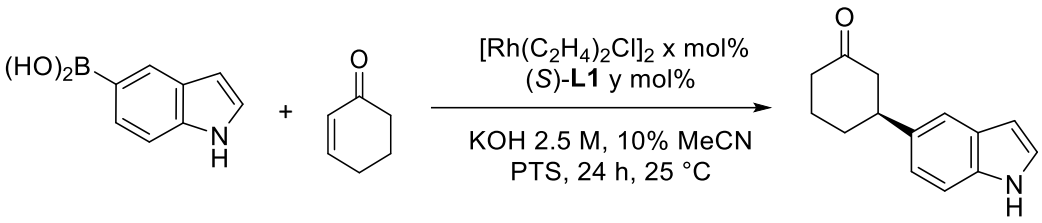


**2**

| ***Entry*** | ***[Rh(C$_2$H$_4$)$_2$Cl]$_2$*** *(mol%)* | ***L1*** *(mol%)* | ***Concentration*** | ***Conversion*** [a] |
|---|---|---|---|---|
| 1 | 5 | 5 | 0.4 M | 78% |
| 2 | 5 | 5 | 0.8 M | 91% |
| 3 | 5 | 5 | 0.2 M | 50% |
| 4 | 2.5 | 2.5 | 0.8 M | 67% |
| 5 | 2.5 | 5 | 0.4 M | 86% |

[a] Conversion was determined by $^1$H NMR spectroscopy using the relative ratio of product to cyclohexenone signals

**Table 11** The screening of micelle concentration in the reaction

A small solvent and additive screening was also carried out in the initial investigations (Table 12). The use of water, PTS or TPGS as the reaction solvent all gave excellent levels of enantioenrichment. Similarly, the use of NaCl, MeCN or MeOH as solvent additives allowed high levels of enantiocontrol to be achieved in the transformation. However, optimal results were observed when PTS was combined with NaCl (Table 12, Entry 2) or 5% of MeCN (Table 12, Entry 5). The use of NaCl as an additive provided a cleaner crude NMR spectrum of the

reaction in comparison to the reaction using MeCN as an additive. Consequently, PTS and NaCl were chosen as the optimal reaction media and additive for the conjugate addition.

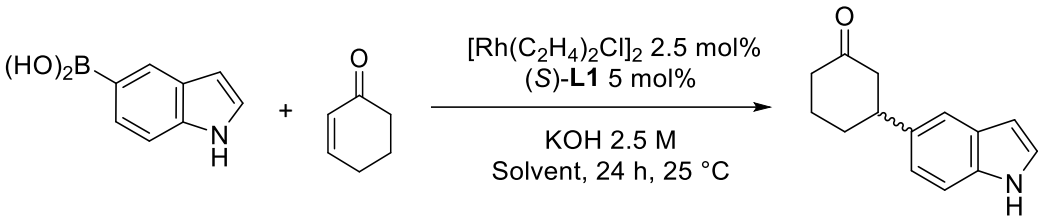


**2**

| *Entry* | *Solvent* | *Additive* | *Conversion* [a] | *e.r.*[b] |
|---|---|---|---|---|
| 1 | PTS | - | 75% | 97:3 |
| 2 | PTS | NaCl (3.0 M) | 90% | 97:3 |
| 3 | TPGS | MeOH (10%) | 73% | 95:5 |
| 4 | $H_2O$ | - | 65% | 96:4 |
| 5 | PTS | MeCN (5%) | 90% | 97:3 |
| 6 | $H_2O$ | NaCl (3.0 M) | 76% | 90:10 |

[a] Conversion was determined by $^1$H NMR spectroscopy using the ratio of product to cyclohexenone
[b] Enantiomeric ratio was determined by chiral HPLC

**Table 12** Investigation into the solvent and additive effect on the reaction

### 6.4.1. General Reaction Parameters

We then investigated the effect of time and temperature on the reaction progress. The model reaction was sampled at various timepoints to view the rate of product formation as well as the corresponding enantiomeric ratio (e.r.). The e.r. of the product remained consistent at 97:3 throughout all timepoints and temperatures trialled. After 1 hour, the product had formed in 55% yield by $^1$H NMR (Table 13, Entry 1). After 8 hours the yield had increased to 72% (Table 13, Entry 2). After 16 hours only a slight increase to 78% was observed (Table 13, Entry 3). At the timepoint of 18 hours the product was formed in 83% (Table 13, Entry 4) and the reaction reached completion after 24 hours where a 90% yield of the desired product was observed (Table 13, Entry 5). Finally, it was shown that the increase of temperature from room temperature to 40 °C allowed the yield to be increased to 95% while retaining the excellent levels of enantioselectivity (Table 13, Entry 6).

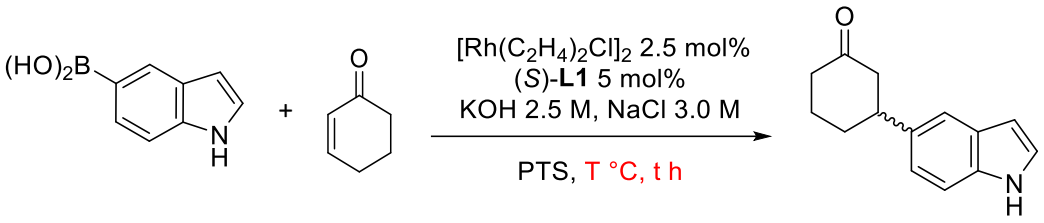


**2**

| ***Entry*** | ***Time*** *(hr)* | ***Temperature*** *(°C)* | ***Yield*** [a] | ***e.r.***[b] |
|---|---|---|---|---|
| 1 | 1 | 20 | 55% | 97:3 |
| 2 | 8 | 20 | 72% | 97:3 |
| 3 | 16 | 20 | 78% | 97:3 |
| 4 | 18 | 20 | 83% | 97:3 |
| 5 | 24 | 20 | 90% | 97:3 |
| 6 | 24 | 40 | 95% | 97:3 |

[a] Yield was determined by $^1$H NMR spectroscopy using 1,3,5-trimethoxybenzene as internal standard
[b] Enantiomeric ratio was determined by chiral HPLC

**Table 13** Screening of time and temperature for the Rh-catalysed conjugate addition of 5-indolyl boronic acid and cyclohexenone

### 6.4.2. Base Screening

We then decided to investigate the effect that the base had on the reaction (Table 14). Sodium hydroxide allowed the product to be formed in a good yield of 86%, albeit with a reduced enantiomeric ratio of 95:5 (Table 14, Entry 1). Use of triethylamine gave an excellent yield and enantiomeric ratio of 91% and 96:4 respectively (Table ***14***, Entry 2). Potassium bifluoride exhibited excellent enantioenrichment of the desired product (98:2 e.r.) but with a reduction in yield (33%) (Table 14, Entry 3). The greatest level of enantioselectivity was observed by the use of potassium fluoride (99:1 e.r.) (Table 14, Entry 4). Despite this high level of enantioenrichment, only a moderate yield of 70% was achieved. Tripotassium phosphate provided the product in an excellent yield of 90% with an enantiomeric ratio of 97:3 (Table 14, Entry 5). Thus, KOH remained the optimal base for this transformation, affording high yields and enantioenrichment of the conjugate addition product **2** (Table 14, Entry 6).

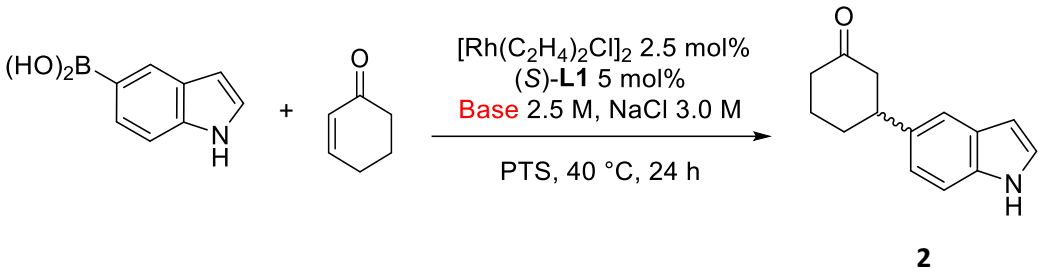


**2**

| ***Entry*** | ***Base*** *(aq. 2.5 M)* | ***Yield*** [a] | ***e.r.*** [b] |
|---|---|---|---|
| 1 | NaOH | 86% | 95:5 |
| 2 | $NEt_3$ | 91% | 96:4 |
| 3 | $KHF_2$ | 33% | 98:2 |
| 4 | KF | 70% | 99:1 |
| 5 | $K_3PO_4$ | 90% | 97:3 |
| 6 | KOH | 95% | 97:3 |

[a] Yield was determined by $^1H$ NMR spectroscopy using 1,3,5-trimethoxybenzene as internal standard
[b] Enantiomeric ratio was determined by chiral HPLC

**Table 14** The base screening of the Rh-catalysed asymmetric conjugate addition of 5-indoly boronic acid and cyclohexenone

### 6.4.3. Investigating the Use of KF

Employing KF as a base in our system led to high levels of enantioenrichment and so, we decided to further explore reaction parameters which could retain the e.r. of 99:1 while increasing the yield of the product. Alternatively, it was hoped that the enantiocontrol could be improved by varying the reaction conditions and increase our level of enantiocontrol. Initially, the equivalents of KF were lowered to try slow the reaction progress and give an increased e.r. However, halving the loading of the base resulted in a drastic drop-off in yield (26%) with no change in the enantioselectivity (Table 15, Entry 1). To try increase the reaction yield, the loading of rhodium catalyst was increased to 5 mol% but interestingly, this also resulted in reduced yield (Table 15, Entry 3). Similarly, when the KF loading was increased to 2 equivalents a yield of 44% was observed after 24 hours (Table 15, Entry 4). Given the success the use of KOH had in achieving high yields of product, it was thought that adding an equimolar amount of KOH and KF may have a synergistic effect on the reaction. However, when this was trialled, the excellent enantiomeric ratio of 99:1 was retained but only a moderate yield of 53% was obtained (Table 15, Entry 5). Finally, as the yield of the reaction could not be increased from 70%, alternative efforts were made to increase the e. r. Firstly,

the reaction temperature was lowered to 0 °C. This expectingly lowered the yield to 33% but, the e.r. remained at 99:1. Lastly, the reaction progress was monitored to see if the initial enantioenrichment was higher early in the reaction compared to later. The reaction was stopped after 1 hour and surprisingly, a good yield of 66% was achieved, albeit with the e.r. of 99:1, unchanged from previous attempts. It was concluded that the yield and e.r. of the product could not be easily improved upon when KF was employed and thus, KOH remained the base of choice for this reaction.

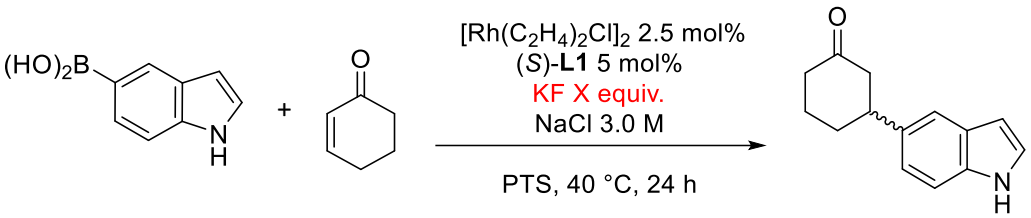


**2**

| ***Entry*** | ***KF*** *(equiv.)* | ***Deviation*** | ***Temp*** *(°C)* | ***Time*** *(h)* | ***Yield*** [a] | ***e.r.*** [b] |
|---|---|---|---|---|---|---|
| 1 | 0.5 | - | 40 | 24 | 26% | 99:1 |
| 2 | 1 | - | 40 | 24 | 70% | 99:1 |
| 3 | 1 | [Rh] – 5 mol% | 40 | 24 | 45% | 99:1 |
| 4 | 2 | - | 40 | 24 | 44% | 99:1 |
| 5 | 1 | KOH – 1 equiv. | 40 | 24 | 53% | 99:1 |
| 6 | 1 | - | 0 | 24 | 33% | 99:1 |
| 7 | 1 | - | 40 | 1 | 66% | 99:1 |

[a] Yield was determined by $^1$H NMR spectroscopy using 1,3,5-trimethoxybenzene as internal standard
[b] Enantiomeric ratio was determined by chiral HPLC

**Table 15** The screening of potassium fluoride and alternate reaction conditions in the model reaction

## 6.5. Investigation into the Chiral Ligand

With conditions optimised for time, temperature, solvent and base, we decided to investigate the final reaction variable; the chiral ligand. As outlined in the introduction, there is a large variety of chiral ligands routinely employed in the field of asymmetric rhodium catalysis. Thus far, we had only examined BINAP and the sulphur-olefin ligand **L1**. In an effort to see if the level of enantioenrichment could be raised with **L1** from an e.r. of 97:3, we

envisaged screening a range of chiral ligands. This list included chiral mono- and bi-phosphines, dienes and derivatised sulphur-olefin based ligands. Many of these ligands were commercially available, but it was required to individually synthesise the sulphur-olefin ligands. With the sulphur-olefin ligand (**L1**) we had utilised thus far, we noticed that the majority of the published protocols use the unoptimised ligand **L1** (Figure 10).[66–68] In a few instances, some functionalisation on the aryl ring of the cinnamaldehyde precursor was reported.[67,69] In one instance, the olefin bond was substituted with a methyl group.[70] In no instance had the sulphur chiral auxiliary been altered from a *t*-butyl group (Figure 10). Understandably, modulation of the aryl ring is the most commonly observed derivatisation, as many functionalised cinnamaldehydes are readily available. However, we were surprised to see how few reports included derivatisation on the olefin or sulphur functionalities, as it is understood that these are the moieties which chelate directly to the metal centre.[67–69] Overall, we hoped to functionalise this sulphur-olefin core to afford novel chiral ligands and potentially increase the enantioselectivity observed in our model reaction.

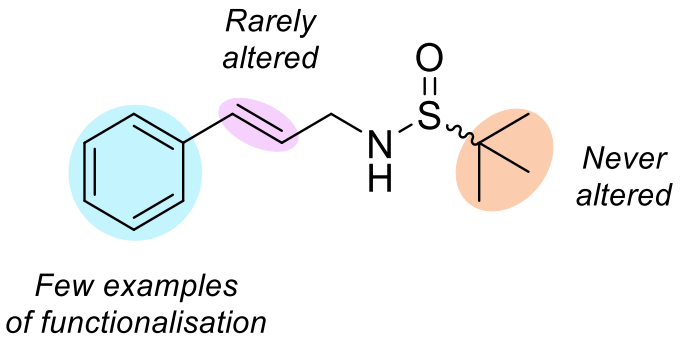


**Figure 10** The literature precedent for this sulphur-olefin ligand functionalisation

### 6.5.1. The Synthesis of Cinnamaldehyde Based Ligands

To synthesise a range of these ligands, various cinnamaldehyde precursors were subjected to a standard reductive amination protocol (Scheme 109). The aldehyde, sulfinamide and titanium ethoxide were added to a flask containing anhydrous THF under an inert atmosphere and heated for 4 hours at reflux. The mixture was subsequently cooled and 2 – 4 equivalents of sodium borohydride was added to reduce the imine formed. The *p*-Me ligand **L3** was synthesised in a moderate yield of 40%. The corresponding *p*-OMe (**L4**), *p*-$NMe_2$ (**L5**) and *p*-F (**L6**) derivatives were furnished in moderate to good yields. The α-methyl ligand **L7** was obtained in a moderate yield of 41%. Extending the chain length of the functional

group on the olefin to a five carbon chain allowed the sulfinamide **L8** to be obtained, albeit in a poor yield of 26%. The olefin could be tethered to the aryl ring as in the case of ligand **L9**, which was afforded in a good yield of 64%. The other position on the olefin was also functionalised as seen with the β-phenyl ligand **L10**, which was synthesised in 54% yield. The imine **L11** was obtained in an excellent yield of 87%. Finally, the chiral sulphur group could be installed as a *p*-tolyl group to give the corresponding sulfinamide **L12** in 26% isolated yield. These isolated yields are not optimised as it was initially only desired to obtain enough material to screen the chiral ligand in the model conjugate addition reaction.

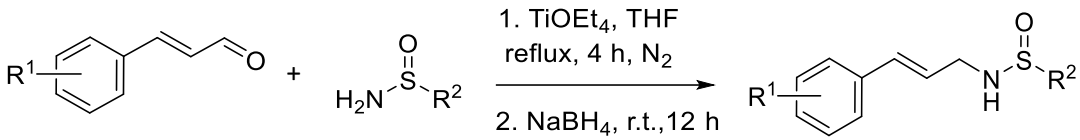


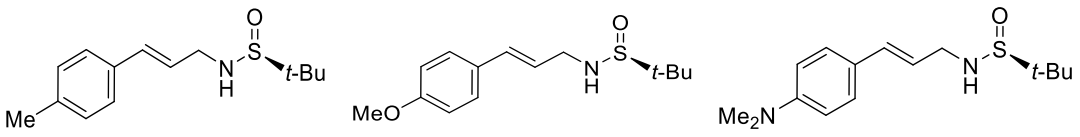

**L3**, 40%



**L4**,74%



**L5**, 49%

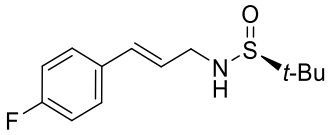

**L6**, 80%

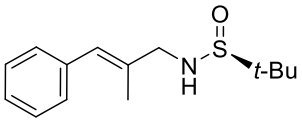

**L7**, 41%

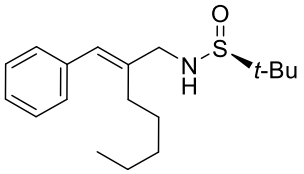

**L8**, 26%

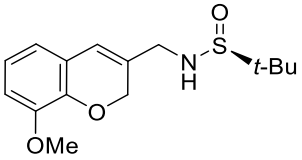

**L9**, 64%

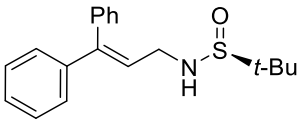

**L10**, 54%

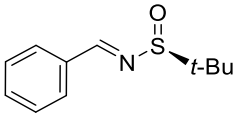

**L11**, 87%

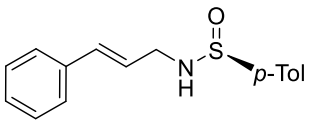

**L12**, 26%

**Scheme 109** The range of sulphur-olefin ligands synthesised

### 6.5.2. Alternative Classes of Chiral Ligands

The range of chiral ligands was then expanded to include a chiral diene and chiral phosphine ligands (Figure 11). It was hoped that this range of ligands would cover a large area of chemical space (BINAP-type ligands, chiral bi-phosphines, mono-phosphines and a chiral diene ligand).

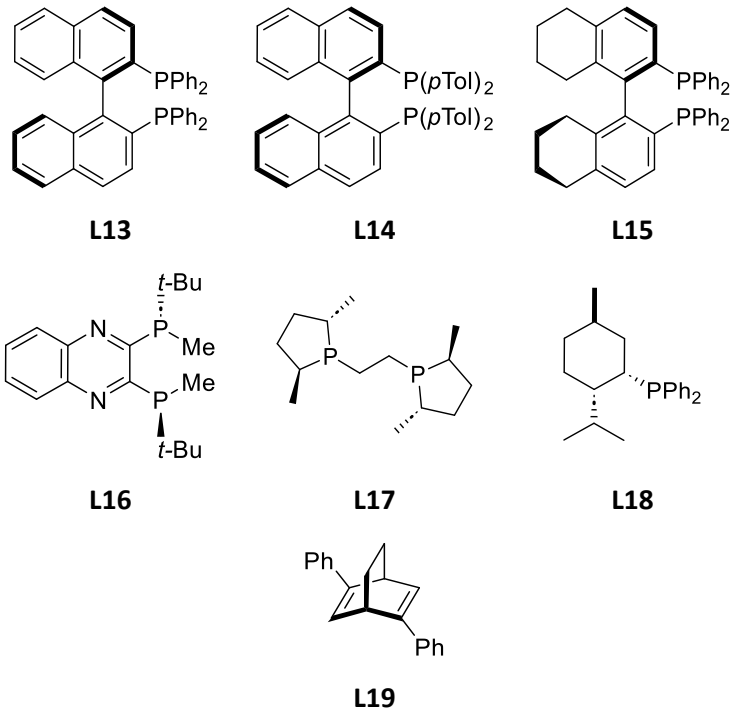


**Figure 11** Alternative ligands obtained to trial in the model reaction

### 6.5.3. Unsuccessful Syntheses of Alternative Chiral Ligands

Through the course of these investigations, alternative sulphur-olefin type ligands were also considered for this transformation. As described in the Introduction, a large number of these ligand classes are reported in the literature and have proven successful with rhodium catalysed reactions. One such ligand is **L20** where the key olefin moiety is in an alternative position in comparison to **L1**.[71,72] To access this ligand, the 3-phenylpropanal aldehyde precursor was treated with formaldehyde in $CH_2Cl_2$ with pyrrolidine in water to yield the conjugated product (Scheme 110). This conjugated compound could then undergo the same reductive amination protocol as with the cinnamaldehyde-based ligands to yield a chiral ligand (Scheme 110). However, the first step concerning the insertion of the double bond on the aldehyde precursor was a poor performing reaction with a very low yield of isolated

product obtained. Alternative conditions were also trialled for this transformation using methanol and propionic acid but similarly, poor conversion to the desired product was observed. Additionally, when the reductive amination protocol was applied to the conjugated intermediate, only trace amounts of product were observed and sufficiently pure material could not be isolated to trial this ligand in the asymmetric 1,4-addition.

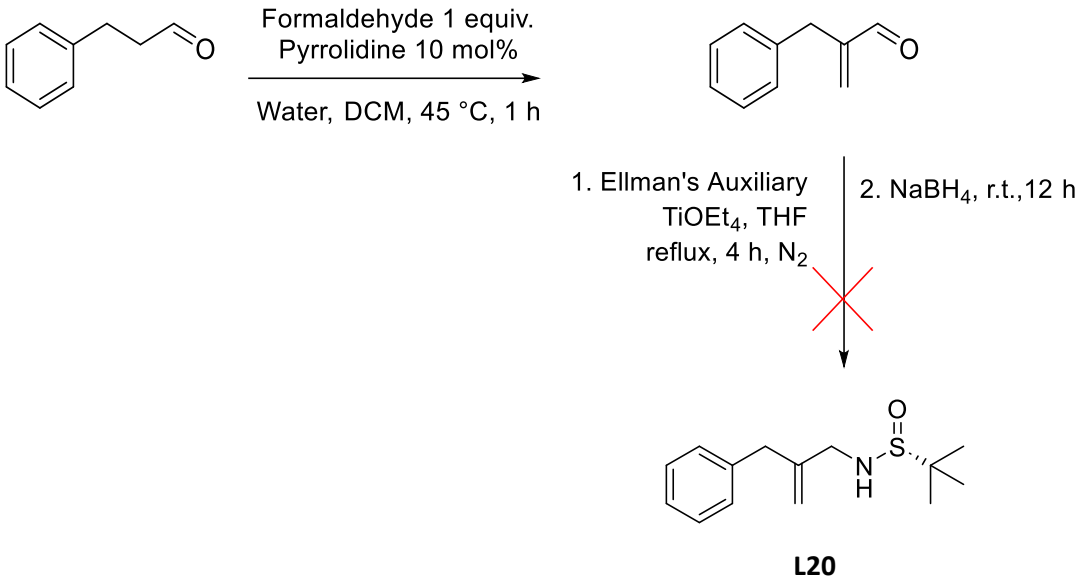


**L20**

**Scheme 110** The unsuccessful synthesis of an alternative sulphur-olefin ligand

Another class of sulphur-olefin ligand was reported in the form of the aziridine **L21** (Scheme 111).[73] In order to access this structure, a sulfinylimine and *S*-allyl tetrahydrothiophenium bromide were required to react under basic conditions. Both the sulphur salt and the sulfinylimine could be prepared successfully. However, the aziridine formation using lithium *t*-butoxide only generated the desired compound in trace amounts (Scheme 111). The use of alternative bases such as caesium carbonate did not improve conversion to product.

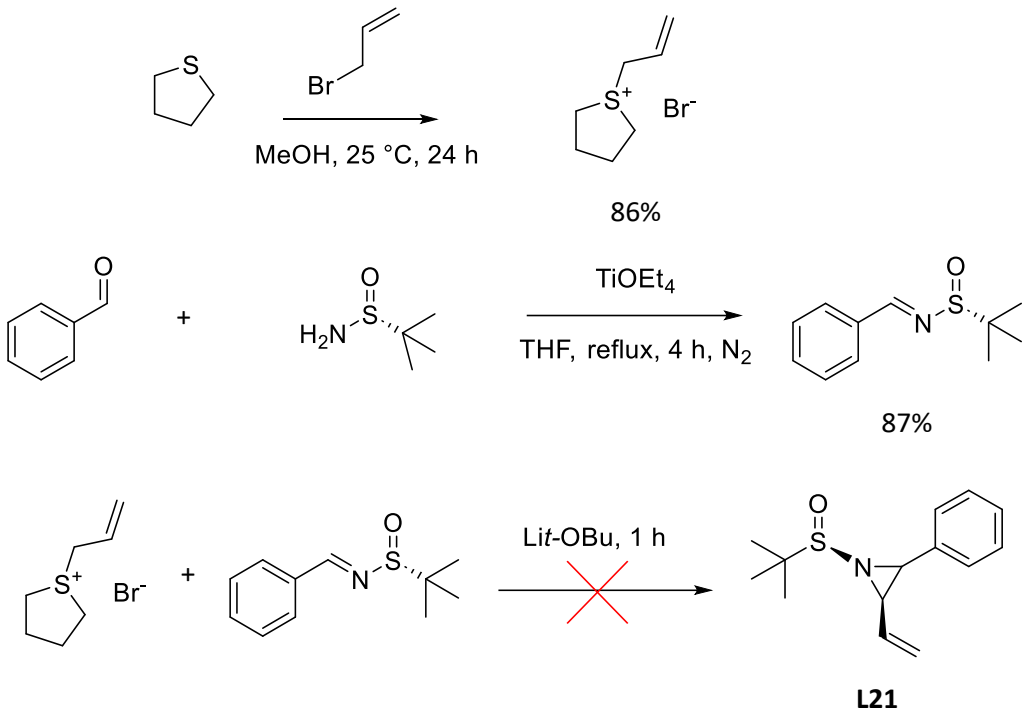


**Scheme 111** Unsuccessful formation of a chiral aziridine ligand

Finally, we attempted to access a naphthyl variant of the model cinnamaldehyde ligand. The pathway to this ligand started with a palladium-catalysed Suzuki-Miyaura reaction with allyl bromide and naphthyl boronic acid to yield the allyl compound. This intermediate could then be oxidised to afford the conjugated aldehyde which could subsequently undergo reductive amination with Ellman's auxiliary. The Suzuki-Miyaura reaction was performed successfully after some moderate optimisation, to provide the allyl intermediate in low yield (15%). However, the oxidation with DDQ only afforded trace amounts of the desired aldehyde and so, the synthesis was not progressed further. Similarly, for the bis-*ortho* methyl derivative, the Suzuki-Miyaura cross-coupling could be performed successfully in moderate yield (28%). However, the oxidation, once again, failed to produce any of the desired aldehyde. A palladium catalysed variant of the DDQ oxidation was also attempted for the bis-*ortho* methyl derivative but no product was obtained under either reaction conditions (Scheme 112).

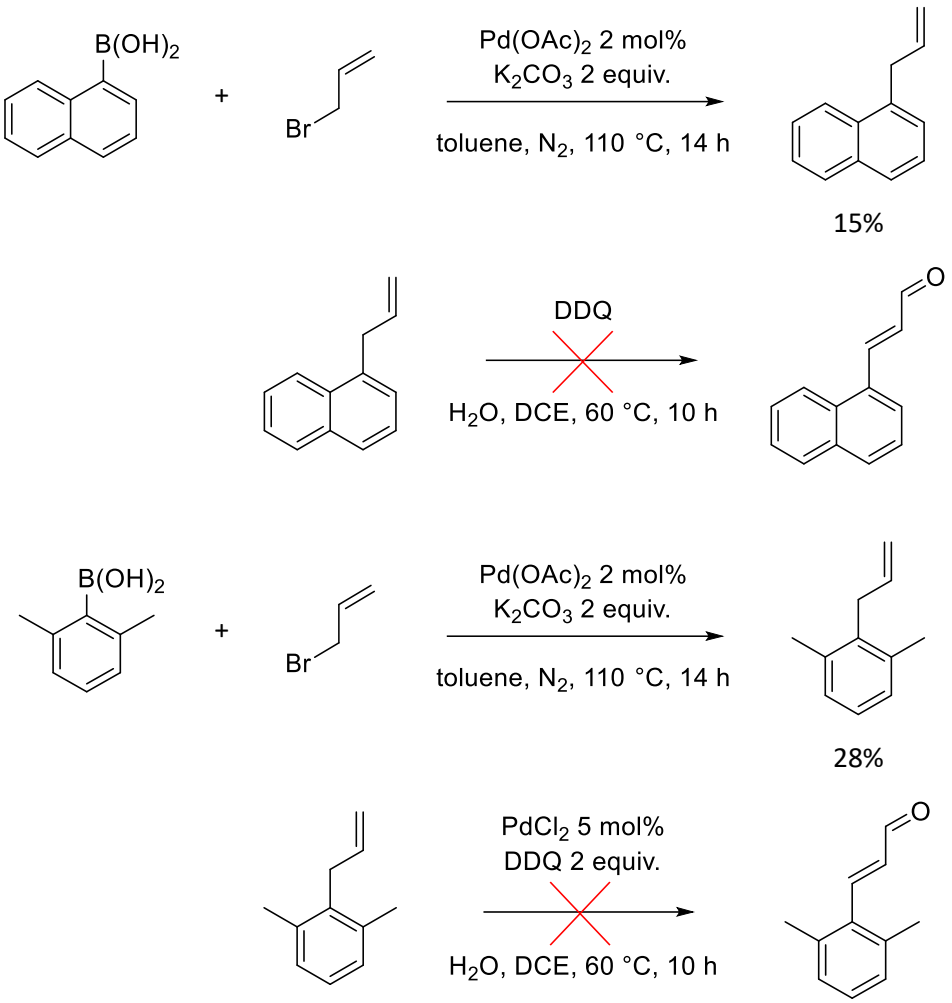


**Scheme 112** The unsuccessful oxidation of cinnamaldehyde precursors for ligand synthesis

### 6.5.4. Chiral Ligand Screening

With the range of ligands to hand, we trialled each ligand in the model reaction of 5-indolyl boronic acid with cyclohexenone (Table 16). This investigation was performed with the currently optimised conditions of KOH, NaCl and PTS for 24 hours at 40 °C with $[Rh(C_2H_4)_2Cl]_2$ as the rhodium catalyst. As a whole, the BINAP-type ligands performed poorly, giving moderate yields and poor enantioenrichment. In the case of $H_8$-BINAP, a nearly racemic product was obtained and in very low yield. The other phosphine ligands proved similarly futile where QuinoxP* and Me-BPE gave poor conversion to the product and very low enantiomeric ratio. Low yields and no enantioselectivity was observed using the mono-phosphine ligand (**L18**) employed in the reaction. The cinnamaldehyde based ligands investigated were functionalised on both the α and β positions of the alkene, the aromatic ring and the chiral sulfinamide itself. It was observed that any functionalisation α to the amide nitrogen on the olefin resulted in a drop in yield and lower enantioenrichment of the

product. Functionalising this position with a methyl group allowed good enantiocontrol to be retained (90:10) but gave a poorer yield (62%). Increasing this chain length to five carbons resulted in only 9% yield of the desired product with a corresponding e.r. of 55:45. When this position was tethered to the aryl ring, in the case of **L9**, the reaction failed to furnish any product. The β position of the alkene showed some tolerance to functionalisation. A phenyl group was successfully attached to the olefin at this position (**L10**) which provided a moderate yield of product (34%) but with a high level of enantioenrichment (95:5). It was found that derivatising the aryl ring of the precursor provided more comparable results to our standard ligand. The *para*-position was functionalised with Me, OMe, $NMe_2$ and F groups. Unfortunately, due to commercial availability or reaction and purification issues, a more comprehensive electronic and steric investigation to this aryl ring could not be conducted. The *p*-Me ligand (**L3**) provided a comparable e.r. to our initial unsubstituted ligand (96:4) albeit with a drop in the yield to 72%. The *p*-OMe derivative (**L4**) enabled high yields of the desired product (94%) but with a lower level of enantioenrichment (93:7). The *p*-$NMe_2$ ligand (**L5**) provided results similar to the *p*-Me ligand exhibiting good yield of 74% and excellent enantioselectivities (97:3). Employing the imine ligand **L11** afforded moderate yield and poor enantioenrichment of the conjugate addition product (39% and 60:40). Altering the chiral auxiliary functional group from a *t*-butyl to a *p*-tolyl moiety in the case of **L12** resulted in both a poorer yield (54%) and e.r. of the desired product (84:16). Finally, employing a commercially available chiral diene (**19**) in the reaction afforded the product in moderate yield (51%) and moderate enantioenrichment (72:28). Thus, the initial, unsubstituted ligand we began with proved to be the best ligand for this transformation.

| Ligand | | Yield [a] | e.r. [b] | Ligand | | Yield | e.r. |
|---|---|---|---|---|---|---|---|
| 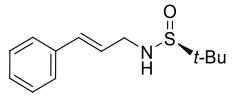 | L**1** | 90% | 97:3 | 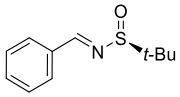 | L**11** | 39% | 60:40 |
| 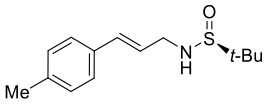 | L**3** | 72% | 96:4 | 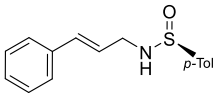 | L**12** | 56% | 84:16 |
| 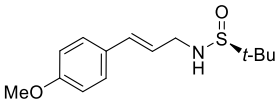 | L**4** | 94% | 93:7 | 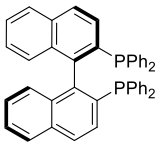 | L**13** | 31% | 63:37 |
| 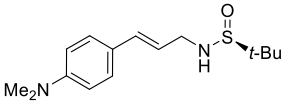 | L**5** | 73% | 97:3 | 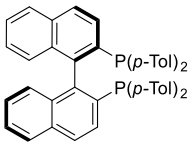 | L**14** | 22% | 62:38 |
| 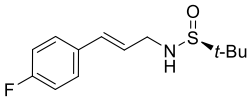 | L**6** | 67% | 90:10 | 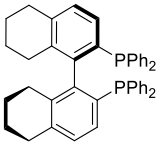 | L**15** | 8% | 50:50 |
| 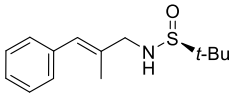 | L**7** | 62% | 90:10 | 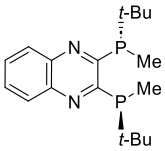 | L**16** | 19% | 59:41 |
| 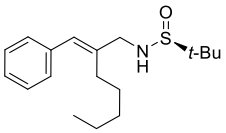 | L**8** | 9% | 55:45 | 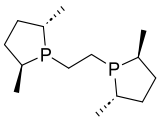 | L**17** | 18% | 51:49 |
| 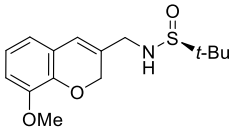 | L**9** | 0% | - | 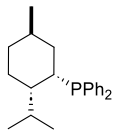 | L**18** | 17% | 56:44 |
| 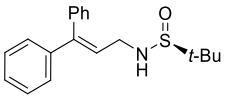 | L**10** | 34% | 95:5 | 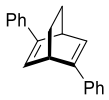 | L**19** | 51% | 72:28 |

[a] Yield was determined *via* $^1$H NMR spectroscopy using 1,3,5-trimethoxybenzene as an internal standard
[b] Enantiomeric ratio was determined by chiral HPLC

**Table 16** The ligand screen of the Rh-catalysed conjugate addition reaction

## 6.6. Pre-Generation of the Catalytic Species

Before applying these conditions to a range of suitable substrates, we wanted to comprehensively investigate reaction conditions which may improve the high level of enantiocontrol observed to date (Scheme 113). Numerous literature protocols call for the pre-generation of an active catalytic species with this type of reaction.[61,74] Firstly, we

investigated potential effects of premixing the rhodium catalyst with the ligand. Thus, 2.5 mol% $[Rh(C_2H_4)_2Cl]_2$ was added to the PTS solution with 5 mol% of **L1**. These species were mixed for 15 minutes before adding the remaining reaction components. The reaction then proceeded under usual conditions. This protocol resulted in a reduced yield of the product (57%) while high levels of enantioenrichment were retained (96:4). Following this, it was decided to allow all reaction components to premix, except for the cyclohexenone substrate. By following a literature precedent for this procedure, everything was added to the reaction flask and mixed for 30 minutes before the Michael-acceptor was added to the reaction mixture. This procedure provided the same level of enantiomeric ratio (97:3) but with a slightly reduced yield relative to our optimal conditions (89%). Thus, we were confident that the most robust protocol was the original method devised.

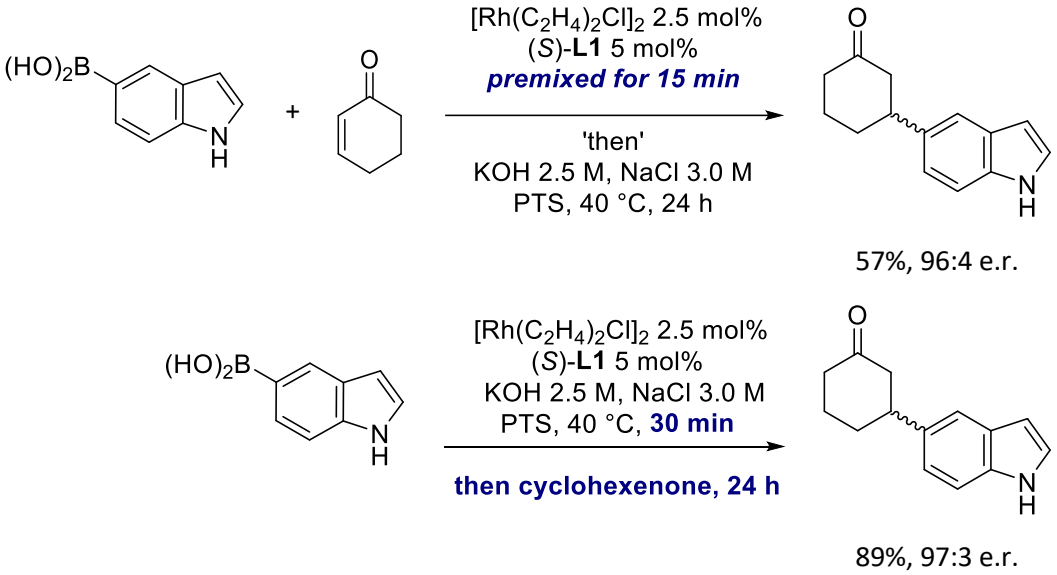


**Scheme 113** The investigation into the pre-generation of active catalytic species for the reaction

## 6.7. Substrate Scope

With these investigations complete, we turned our attention to applying this protocol to a range of indolyl-boronic acids and suitable Michael-acceptors. We started this investigation by employing different cyclic enones with our model 5-indolyl boronic acid. The five-membered ring product **22** could be generated in a good yield of 81% and an excellent enantiomeric ratio of 98.5:1.5. The corresponding cycloheptyl substrate **23** was formed in a moderate yield of 51% but with a high level of enantiocontrol (94:6 e.r.). A lactone moiety was also tolerated at the 5-position, affording the product **24** in a good yield and

enantiomeric ratio (61%, 95:5 e.r.). We next turned our attention to accessing the 4- and 6-substituted products. It was anticipated that the electron deficient nature of these positions would result in a more difficult coupling than the model 5-position.[75] The nucleophilic character of the carbon attached to the boron is known to be improtant in many cases of Rh-catalysed conjugate additions.[46] Pleasingly however, our methodology afforded the desired products in good to excellent yields, with excellent enantioenrichment. Once again, several ring sizes were tolerated. The product with a six-membered ring at the 6-position (**25**) was obtained in good yield and with a good level of enantioenrichment (74%, 97:3 e.r.). The corresponding cyclopentyl product **26** gave a similar yield with a much higher enantioenrichment (72%, 97.5:2.5 e.r.). The cycloheptyl product **27** was furnished in the highest yield to date (94%) with an excellent enantiomeric ratio of 96:4. Determination of stereochemical orientation was achieved through resolution of crystal structures for products **26** and **27** products. The 6-position was also successfully functionalized with a lactone moiety in moderate yield and enantioenrichment to afford **28** (74%, 92:8 e.r.). Similar results were achieved using the 4-indolyl boronic acid starting materials. The cyclohexanone residue was successfully installed at the 4-position to yield **29** in 73% yield and an enantiomeric ratio of 97.5:2.5. A high yield of 87% was afforded for the corresponding cyclopentenone substrate (**30**) with a good enantiomeric ratio of 96.5:3.5. Finally, a cycloheptanone ring was successfully installed at the 4-position (**31**) in a moderate yield of 41%, but with excellent levels of enantioenrichment (97:3 e.r.). A single crystal structure of **31** was also obtained to determine the absolute stereochemistry of the chiral centre created.

Finally, we investigated the 7-position of the indole structure, which is the closest position to the nitrogen of the heteroaromatic ring. The reaction proceeded well and the desired 7-substituted indole **32** was isolated in a moderate 55% yield. However, this product was formed with excellent levels of enantioselectivity (98.5:1.5 e.r.). It was noted that when the cyclohexenone ring was employed with this boronic acid, an undesired product formed. This will be discussed later in Section 'Novel Polycyclic Product Formation'.

We then turned our attention to acyclic enone variants. Despite the success with cyclic enones, early attempts to apply our optimized conditions to acyclic variants gave poorer yields. Moreover, all substrates trialled (**33**–**36**) produced racemic products.

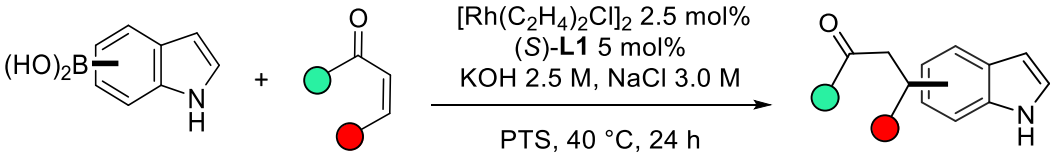


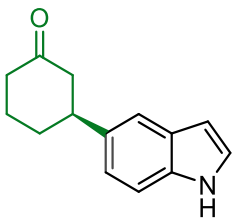

86%, 97:3 e.r.

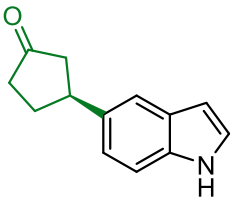

**22**, 81%, 98.5:1.5 e.r.

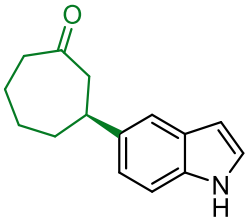

**23**, 51%, 94:6 e.r.

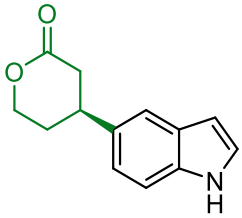

**24**, 61%, 95:5 e.r.

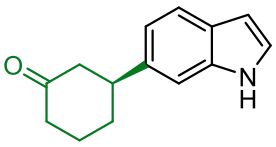

**25**, 74%, 97:3 e.r.

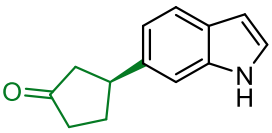

**26**, 72%, 97.5:2.5 e.r.

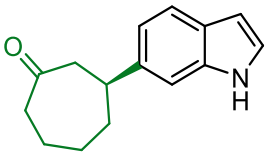

**27**, 94%, 96:4 e.r.

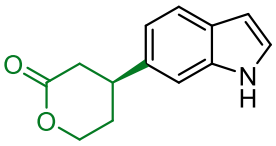

**28**, 74%, 92:8 e.r.

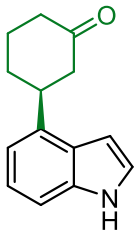

**29**, 73%, 97.5:2.5 e.r.

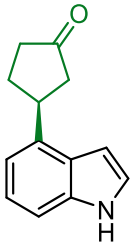

**30**, 87%, 96.5:3.5 e.r.

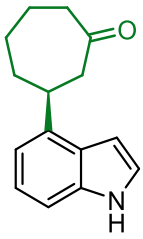

**31**, 41%, 97:3 e.r.

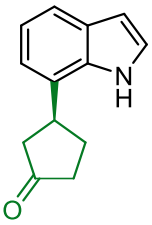

**32**, 55%, 98.5:1.5 e.r.

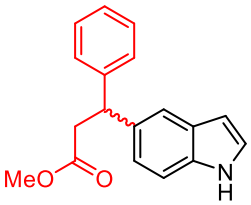


**33**, 23%[a]

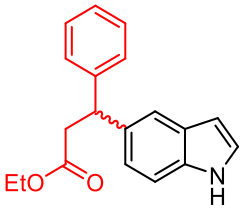


**34**, 20%[a]

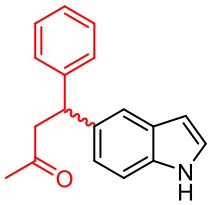


**35**, 81%

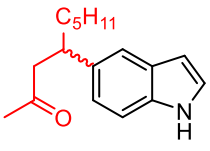


**36**, 42%

All linear enones afforded racemic products

[a] Yield was determined by $^1$H NMR spectroscopy using 1,3,5-trimethoxybenzene as internal standard

### 6.7.1. Single Crystal Structures

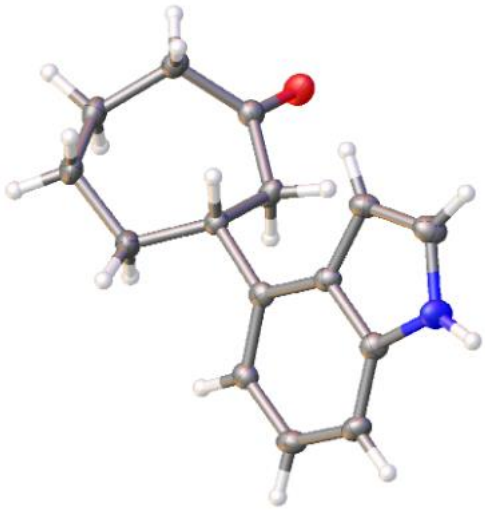

**Figure 12** Single crystal structure obtained for the cycloheptyl substrate **31**

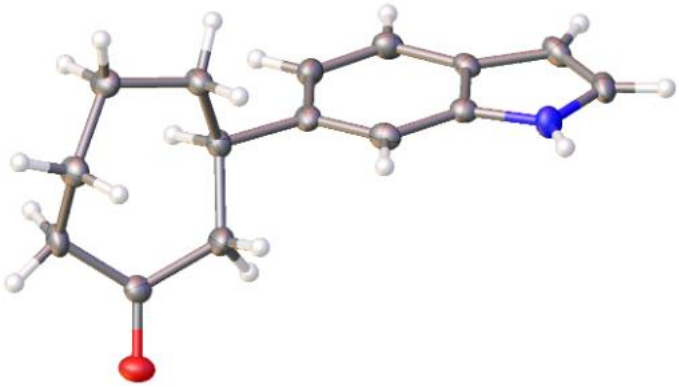

**Figure 13** Single crystal structure obtained for the cycloheptyl structure **27**

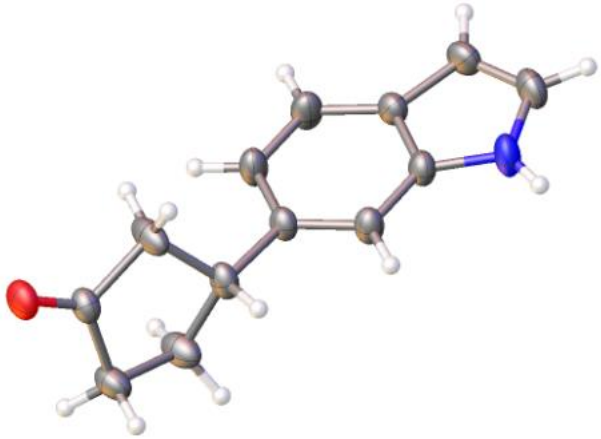

**Figure 14** Single crystal structure obtained for the cyclopentyl substrate **26**

### 6.7.2. Optimisation of Acyclic Enone Substrates

To fully expand the protocol to acyclic enones, further optimisation was required (Table 17, Entry 1). The linear enone **37** was chosen as the model substrate to optimise the reaction parameters (Table 17). Initially, we tried changing the solvent from aqueous micelles to 1,4-dioxane, which allowed a moderate e.r. of 60:40 to be achieved, albeit with a reduction in yield to 60% (Table 17, Entry 2). We then attempted to use a mixture of PTS and dioxane as the reaction solvent but with this, a poor yield of 25% with an e.r. of 55:45 was observed (Table 17, Entry 3). We then trialled BINAP (Table 17, Entry 4) and the chiral diene **19** (Table 17, Entry 5) as chiral ligands in this reaction. Similar levels of enantiomeric excess were observed for BINAP (62:38 e.r.) and the diene ligand (65:35 e.r.). However, the diene enabled a much higher yield of product to be formed (81%). With the best enantioenrichment observed through the use of dioxane as the reaction solvent, we continued to employ organic solvent in place of aqueous media for the remainder of our screening. When the diene was employed in dioxane, full conversion to the desired product was observed and the enantioenrichment was increased to 80:20 e.r. (Table 17, Entry 6). As described previously, a drawback with the use of chiral diene ligands is that they are generally not commercially available. The syntheses of such ligands are often multi-step and arduous, meaning it is difficult to build up a library of ligands to screen for a particular reaction. Given that we could not functionalise this chiral diene ligand, the remaining variable to explore was the rhodium catalyst used in the reaction. Two other rhodium catalysts were employed alongside the chiral diene ligand in dioxane but poor conversion and enantioselectivities was obtained in both cases (Table 17, Entry 7 and 8).

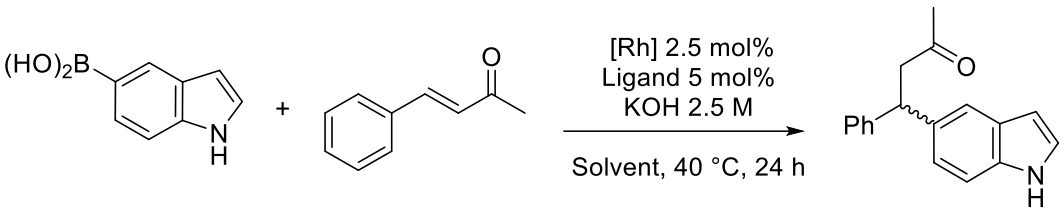


| *Entry* | *Catalyst* *(2.5 mol%)* | *Ligand* *(5 mol%)* | *Solvent* | *Conversion* [a] | *e.r.*[b] |
|---|---|---|---|---|---|
| 1 | $[Rh(C_2H_4)_2Cl]_2$ | 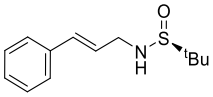 | PTS | 81% | 50:50 |
| 2 | $[Rh(C_2H_4)_2Cl]_2$ | 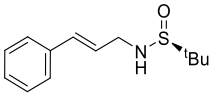 | Dioxane | 60% | 60:40 |
| 3 | $[Rh(C_2H_4)_2Cl]_2$ | 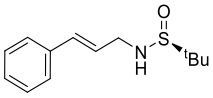 | PTS/Dioxane | 25% | 55:45 |
| 4 | $[Rh(C_2H_4)_2Cl]_2$ | 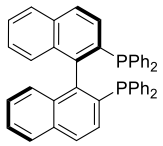 | PTS | 15% | 62:38 |
| 5 | $[Rh(C_2H_4)_2Cl]_2$ | 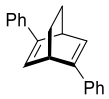 | PTS | 81% | 65:35 |
| 6 | $[Rh(C_2H_4)_2Cl]_2$ | 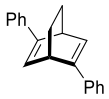 | Dioxane | 100% | 80:20 |
| 7 | $[Rh(coe)_2Cl]_2$ | 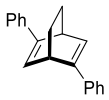 | Dioxane | 35% | 59:41 |
| 8 | $Rh(nbd)_2BF_4$ | 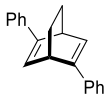 | Dioxane | 12% | 62:38 |

[a] Conversion was determined *via* $^1H$ NMR spectroscopy using the relative ratio of enone to product signals
[b] Enantiomeric ratio was determined by chiral HPLC

**Table 17** The optimisation of linear enones in the asymmetric conjugate addition

Given the influence that the choice of inorganic base had in our initial reaction screening, we decided to explore if screening bases with the chiral diene could increase the enantiomeric ratio of the acyclic products (Table 18). Potassium fluoride was previously found to provide excellent levels of enantiocontrol in the case of cyclic enones. However, the use of KF with acyclic enones gave poorer conversion to product as well as a lower enantiomeric ratio (Table

18, Entry 2). The enantiomeric ratio was found to remain constant when $KHF_2$ and $NEt_3$ were employed. In both cases however, a large reduction in product yield was observed (Table 18, Entry 3 and 4). The use of $K_3PO_4$ allowed excellent conversion to the desired product but as with KOH, the enantiomeric ratio remained at 80:20 (Table 18, Entry 5).

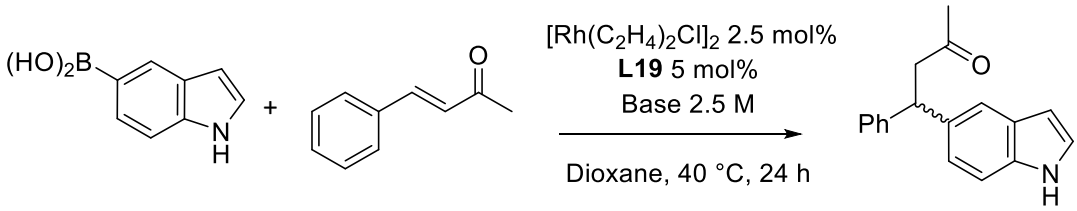


| *Entry* | *Base* *(aq. 2.5 M)* | *Conversion* [a] | *e.r.* [b] |
|---|---|---|---|
| 1 | KOH | 100% | 80:20 |
| 2 | KF | 25% | 69:31 |
| 3 | $KHF_2$ | 5% | 80:20 |
| 4 | $NEt_3$ | 34% | 80:20 |
| 5 | $K_3PO_4$ | 100% | 80:20 |

[a] Conversion was determined *via* $^1$H NMR spectroscopy using the relative ratio of enone to product peaks
[b] Enantiomeric ratio was determined by chiral HPLC

**Table 18** The screening of inorganic bases for the conjugate addition of linear enones

The lack of modularity afforded by the chiral diene ligand meant structural alterations to improve enantioenrichment were not possible. However, we noted that the use of BINAP in the protocol did produce modest levels of enantioselectivity (Table 17, Entry 4). A large advantage associated with chiral phosphine ligands is the diversity of ligands commercially available. A plethora of functionalised chiral phosphines are readily available and so, using this modest 15% yield and 62:38 e.r. as a starting point, we decided to screen a range of chiral phosphine ligands. These reactions were carried out in dioxane as we had established that this solvent enabled the highest conversion to product, alongside the greatest levels of enantioenrichment. The use of QuinoxP* gave an immediate improvement over the chiral diene ligand, and the product was furnished in 81% yield and with an e.r. of 86:14 (Table 19, Entry 1). SegPhos proved to be comparable to QuinoxP* affording the product in 79% and in an e.r. of 87:13 (Table 19, Entry 2). The use of Tol-BINAP provided the product in the highest e.r. observed thus far (91:9 e.r.) and in a very good yield of 87% (Table 19, Entry 3). With this

result, we hypothesised that increasing the electron-density on the phosphorous would correspond with increased levels of enantioselectivity and product yield. Thus, the electron-rich phosphine DTMB-SegPhos was trialled in the reaction. This ligand afforded excellent levels of enantiocontrol giving an e.r. of 98:2 but with a moderate yield of 51% (Table 19, Entry 4). Given the excellent e.r. achieved with DTMB-SegPhos, an attempt was made to increase the product yield by increasing the reaction temperature to 70 °C (Table 19, Entry 5). However, the yield decreased to 29% while retaining the e.r. of 98:2. Another electron-rich phosphine, DM-SegPhos, was employed in the reaction and a good yield of 81% and an excellent e.r. of 95:5 was achieved (Table 19, Entry 6). The ligand DM-BINAP was then trialled under the reaction conditions where an excellent yield and enantiomeric ratio were achieved in 98% and 95:5 respectively (Table 19, Entry 7). Finally, $H_8$-BINAP was employed in the system. Using this ligand, a high yield of 90% was obtained with excellent enantioselectivity (97:3 e.r.) (Table 19, Entry 8). With the use of $H_8$-BINAP, we now had optimised conditions to access linear enones in this asymmetric conjugate addition reaction.

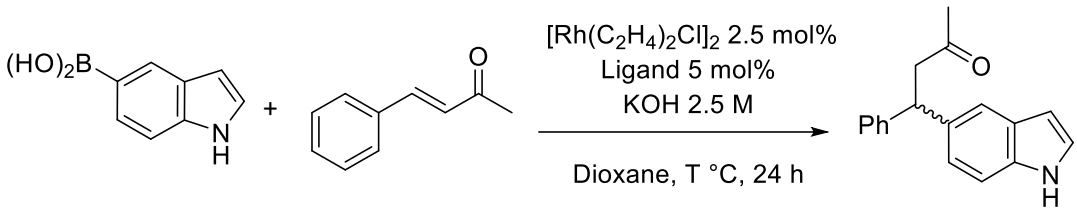


(Table on next page)

| *Entry* | *Ligand* (5 mol%) | *Ligand* | *Temperature* (°C) | *Conversion* [a] | *e.r.*[b] |
|---|---|---|---|---|---|
| 1 | 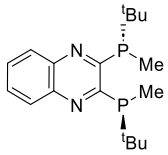 | QuinoxP* | 40 | 81% | 86:14 |
| 2 | 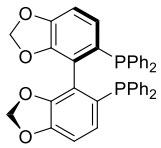 | SegPhos | 40 | 79% | 87:13 |
| 3 | 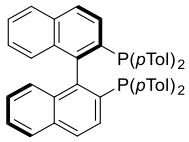 | Tol-BINAP | 40 | 87% | 91:9 |
| 4 | 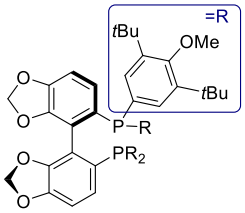 | DTMB-SegPhos | 40 | 51% | 98:2 |
| 5 | 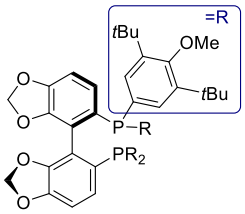 | DTMB-SegPhos | 70 | 29% | 98:2 |
| 6 | 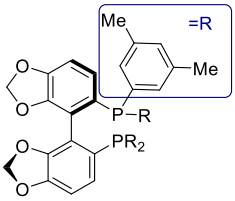 | DM-SegPhos | 40 | 83% | 95:5 |
| 7 | 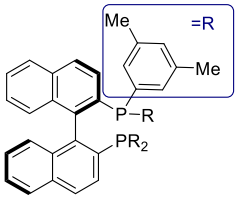 | DM-BINAP | 40 | 98% | 95:5 |
| 8 | 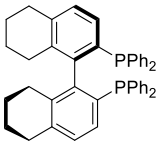 | $H_8$-BINAP | 40 | [90%] | 97:3 |

[a] Conversion was determined *via* $^1$H NMR spectroscopy using the relative ratio of enone to product peaks
[b] Enantiomeric ratio was determined by chiral HPLC
Square brackets indicate that the yield is isolated

**Table 19** The screening of phosphine ligands for the asymmetric conjugate addition of acyclic enones

### 6.7.3. Substrate Scope of Acyclic Enones

Using our optimised conditions with $H_8$-BINAP, we selected some substrates to undergo asymmetric conjugate additions with 5-indolyl boronic acid (Scheme 114). The model substrate yielded the desired product **38** in 90% yield and in an enantiomeric ratio of 96:4. The long-chained product **39** could be generated in a good yield of 80% and with excellent levels of enantioenrichment (96:4 e.r.). A simple, branched enone was successfully subjected to the protocol and gave the product **40** in excellent yield (93%) but unfortunately was not separable on our chiral HPLC and so, the level of enantioselectivity is currently undetermined. Finally, the methyl cinnamate substrate was successfully employed in the reaction providing the ester product **41** in a good yield of 82% and an enantiomeric ratio of 89:11.

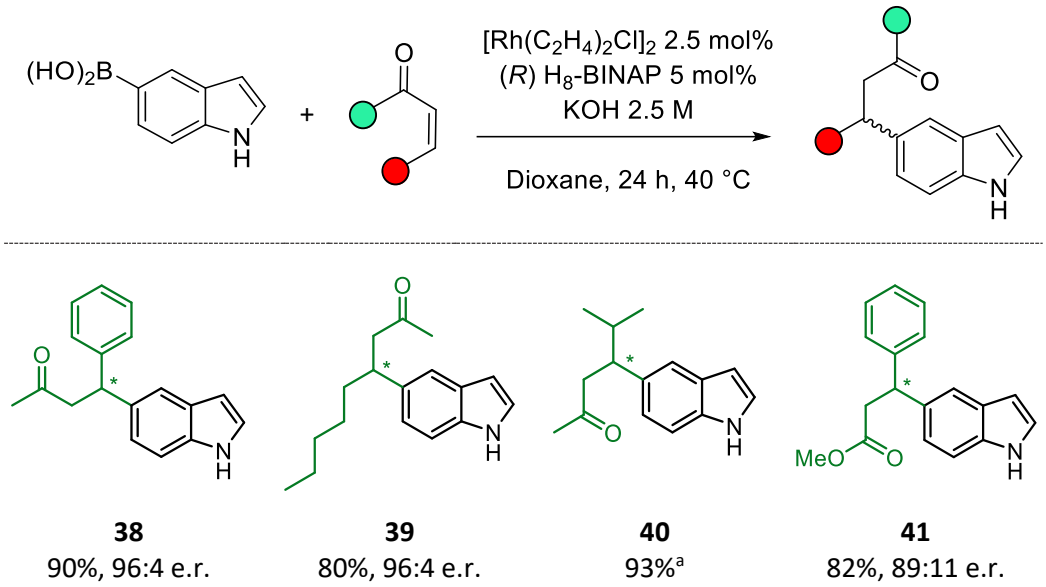


**38** 90%, 96:4 e.r. | **39** 80%, 96:4 e.r. | **40** 93%[a] | **41** 82%, 89:11 e.r.

[a] HPLC method still under development

**Scheme 114** Substrate scope of linear enones with 5-indolyl boronic acid

## 6.8. Novel Polycyclic Product Formation

Previously, when indole-7-boronic acid was reacted with cyclohexanone, the expected product was not formed. When the NMR was analysed, the NH proton peak which was so evident in previous products, was not observed. Usually, this proton is evident downfield of 8 ppm but in this case, a new 1H signal was observed around 2.5 ppm (Figure 15). Additionally, the relevant quaternary carbonyl peak was absent from the $^{13}$C NMR spectrum.

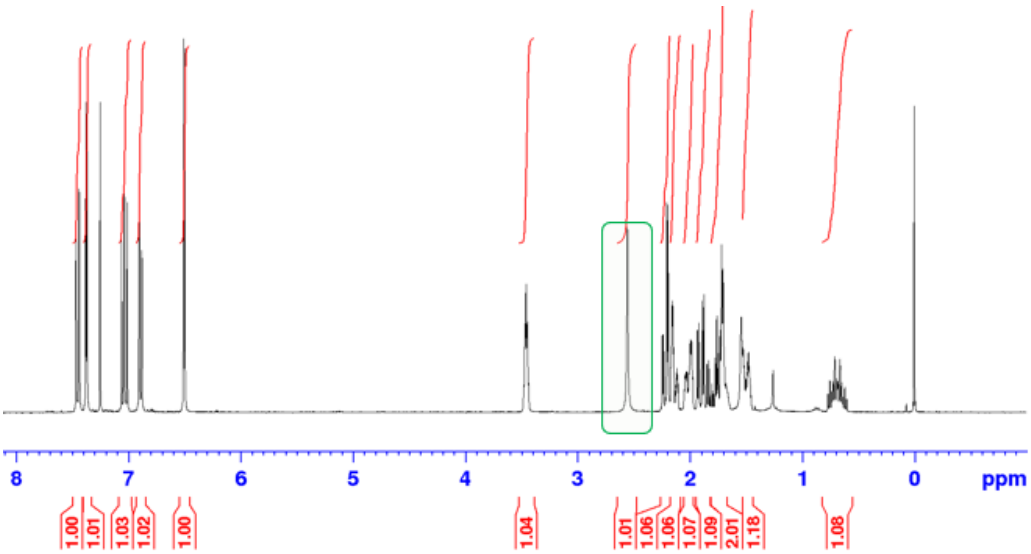


**Figure 15** $^{1}$H NMR spectrum of the isolated product from the conjugate addition reaction of 7-indolyl boronic acid and cyclohexenone

We hypothesised that the conjugate addition happens initially to form the desired product. Then under basic conditions, the indole nitrogen attacks the cyclohexyl carbonyl carbon to form a ring-closed product bearing a tertiary alcohol (Scheme 115). Isolation by column chromatography afforded the product in 65% yield. In fact, when the product was subjected to the chiral HPLC, an enantiomeric ratio of 97:3 was obtained.

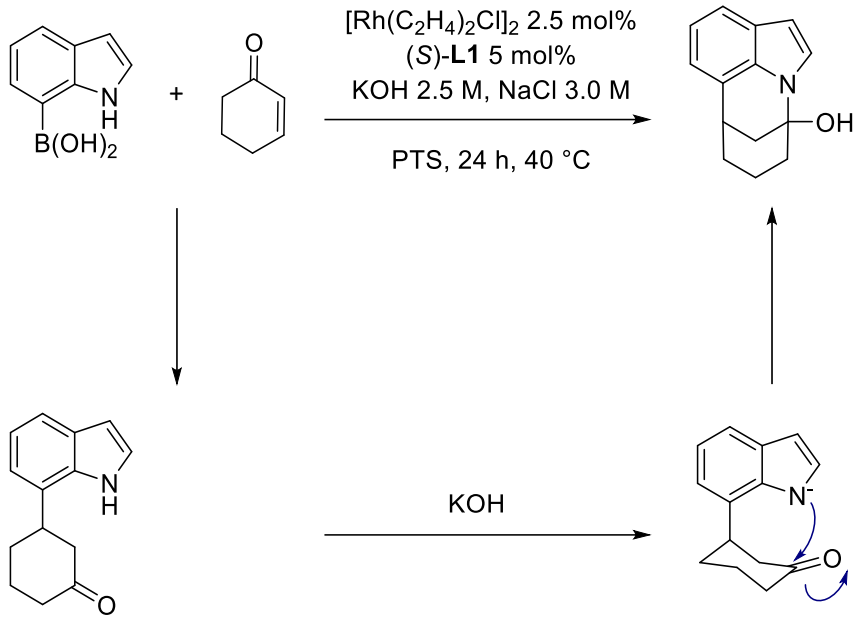


**Scheme 115** Suspected mechanism of product formation for the unexpected cyclised product

The tetracyclic indole based framework formed could be a very efficient means of accessing natural product analogues. Tetracyclic indoles are routinely observed as the core skeleton for a myriad of natural products.[76] Protocols to access polycyclic building blocks in a step-efficient manner would be highly coveted in the field of totally synthesis and drug discovery.[76] Consequently, this reaction may prove very useful.

Overall, a unique tetracyclic, indole-based framework was synthesised in good yield and with an excellent level of enantiocontrol. We believe that the asymmetric rhodium catalysed conjugate addition sets the stereochemistry of the β-position and subsequently, the indole nitrogen atom can only attack from one face.

## 6.9. Application to the 1,2-Addition

With the success observed in the application of indolyl boronic acids in asymmetric rhodium catalysed 1,4-additions, we decided to probe their utility in the corresponding 1,2-addition. Conditions similar to ours were previously published[77] in these asymmetric 1,2-additions. With the same chiral ligand (**L1**), we were able to successfully employ 5-indolyl boronic acid in a 1,2-addition reaction with benzil (**42**) to yield the desired product **43** in 95% yield and an high level of enantioselectivity of 95:5 e.r. (Scheme 116).

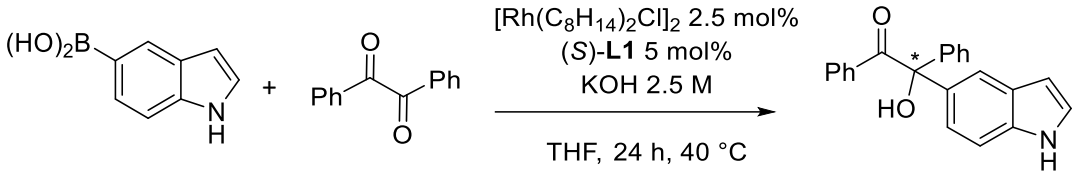


**42** **43**

**Scheme 116** The asymmetric 1,2-addition of benzil with 5-indolyl boronic acid

## 6.10. Cost Improvement Protocols

Despite the success achieved thus far with the methodology, some drawbacks still persisted. In particular, the cost of the reaction components. Micellar solutions have a large variety of structural variability and complexity. As a consequence, the cost of these solutions vary greatly. The PTS micelles employed by us thus far, are more expensive than alternative micelles, routinely used in rhodium catalysis.

### 6.10.1. Investigation of SDS

One particular micellar solvent commonly used is sodium dodecyl sulphate or SDS. SDS is relatively cheap (500 mL/€89) due to its global requirement in biological laboratories and so, we performed our optimised reaction in SDS. Unfortunately, a much lower conversion to the desired product was observed in SDS, albeit with a very good enantiomeric ratio (95:5 e.r.) (Scheme 117).

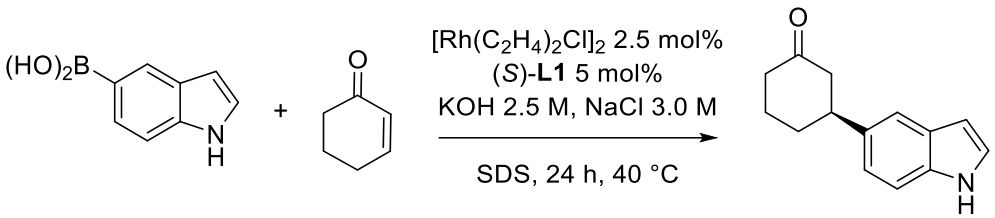


45%, 95:5 e.r.

**Scheme 117** The use of SDS as a reaction solvent as a cheap micellar solution

### 6.10.2. Recyclability Studies using Micelles

As an alternative means of reducing cost of materials, we decided to investigate an advantage of micelles; their recyclability. Work by Lipshutz and co-workers has thoroughly depicted the usefulness of micelles as reaction solvents, and one of these benefits is that they are potentially recyclable.[74] Lipshutz has reported on rhodium-catalysed conjugate

additions in micellar solutions.[64,65,74] Once complete, the reaction mixture could be diluted with organic solvent and the product extracted. The catalyst and ligand remain in the aqueous micellar solution for another transformation. We wished to demonstrate this property and so firstly, we performed our standard reaction. After 24 hours, the reaction mixture was diluted with ethyl acetate and stirred for 5 minutes. The organic layer was then extracted and more indolyl boronic acid and cyclohexenone was added to the aqueous micellar layer. The reaction was then re-run for another 24 hours. The same high level of product conversion was observed after the second run. However, there was a small reduction in the enantiomeric ratio observed (Scheme 118). These results do exhibit the recyclability of micelles and particularly highlight how this method could be used to reduce the waste from the reaction, improve the cost of the reaction and improve the reaction's green metrics.

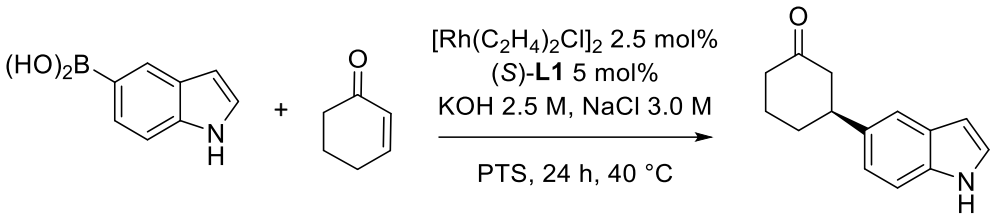


**Run 1**: 95%, 97:3 e.r.

**Run 2**: 94%, 95:5 e.r.

**Scheme 118** The recyclability of the PTS micellar solution in our reaction

## 6.11. Mechanistic Considerations *via* Deuterium Labelling

Fletcher and co-workers recently reported on the asymmetric rhodium-catalysed conjugate additions of piperidines.[45] In this investigation, the authors report how the substrates employed in the reaction can undergo one of two mechanisms. The mechanisms can be differentiated by the site of deuterium incorporation on the product. The most common pathway for these reactions to proceed involves deuteration at the α site to the carbonyl. In Fletcher's case, some substrates incorporated deuterium on the aryl ring of the boronic acid component in a mechanism involving a 1,4-Rh shift. In light of this, we employed both the linear and cyclic enones in deuterium labelling studies with the model 5-indolyl boronic acid. In both cases, deuteration occurred solely at the α-position of the carbonyl ring (Scheme 119). The absence of deuteration on the aryl ring of indole indicates that the mechanism

does not involve a 1,4-Rh shift step (as observed by Fletcher).[45] We envisage a mechanism akin to that described in Figure 16.

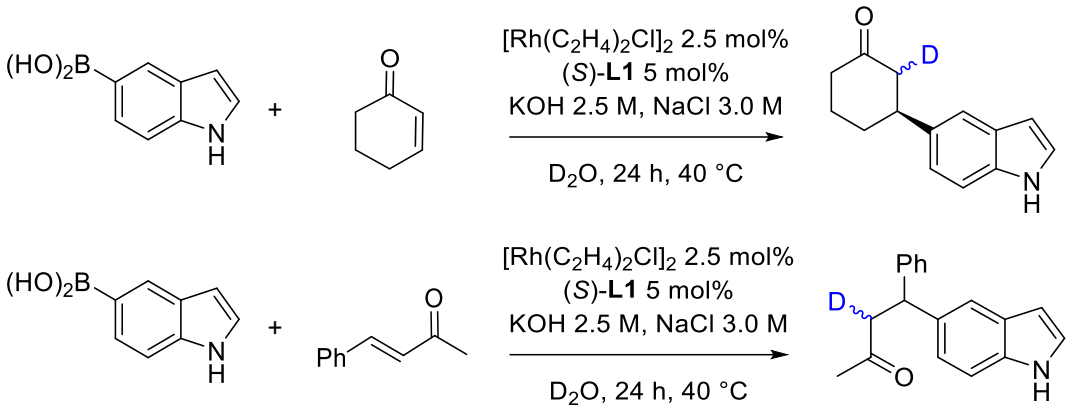


**Scheme 119** Deuterium labelling studies for both substrate classes

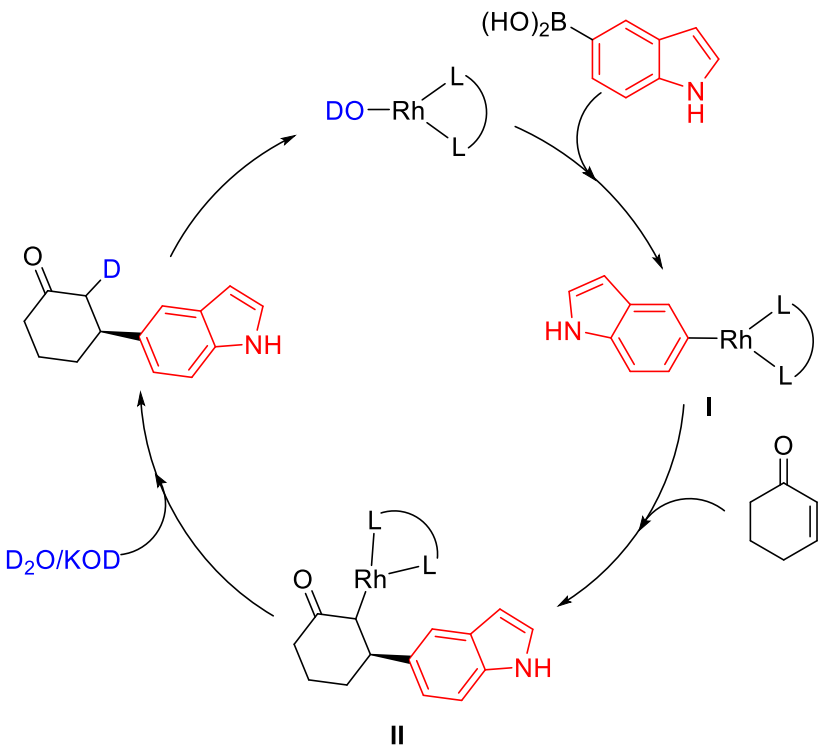


**Figure 16** The proposed mechanism of the Rh-catalysed conjugate addition of indolyl boronic acids

## 6.12. Unsuccessful Substrates

Some substrates were not applicable to our reaction conditions. As outlined in the Introduction to this Chapter, there was a myriad of Michael-acceptor type substrates available to trial in our reaction protocol. The substrates depicted in Figure 17 were tested under our optimised reaction conditions but were unsuccessful. Either a complex reaction mixture was observed by $^{1}$H NMR or no product could be isolated from the reaction mixture. However, we envisage that specific optimisation for each substrate class would enable efficient conversion to the desired product.

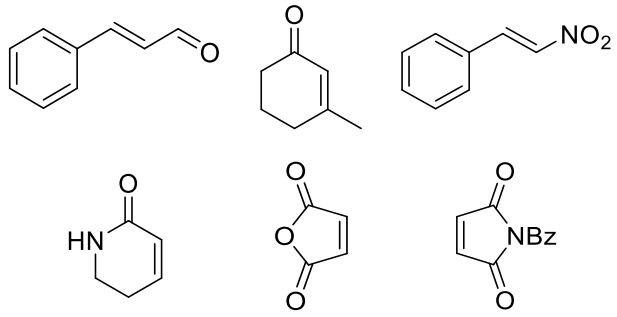


**Figure 17** Unsuccessful substrates

## 6.13. Conclusions & Future Work

The asymmetric rhodium catalysed 1,4-addition of indolyl boronic acids was demonstrated. Using this methodology, a range of cyclic and acyclic enones were successfully installed on the indole carbocyclic backbone with a high level of enantiocontrol. In the case of cyclic substrates, this chemistry was performed in aqueous media, at mild temperature to give good to excellent yields of enantioenriched products. Several single crystal structures were obtained during the course of this work to determine the absolute stereochemistry of the chiral centre. The protocol was optimised to include acyclic enones, which proceeded in good yield and with excellent enantiomeric ratios. This chemistry was expanded to allow indolyl boronic acids undergo 1,2-addition with excellent levels of enantioenrichment. A novel tetracyclic indole scaffold was synthesised *via* an asymmetric conjugate addition and a subsequent intramolecular cyclisation. The polycyclic product, formed through this one-pot, two-step process, was afforded in good yield and with an excellent level of enantiocontrol (65%, 97:3 e.r.). This result could allow for a range of tetracyclic indole frameworks to be accessed through this methodology, enabling efficient means to natural product analogues. The micelle media was recycled and the products could be formed with minimal reduction

of yield and e.r. Finally, mechanistic insight was achieved *via* deuterium labelling. In the case of both substrate classes (cyclic and acyclic enones), the deuterium studies suggested that this protocol follows a documented mechanistic cycle for the conjugate addition reaction of 5-indolyl boronic acids.

Future work for this project could explore the application of these substrates in the 1,2-addition. Furthermore, the failed Michael-acceptor type substrates could be individually optimised to allow a larger breadth of substrate tolerance in the asymmetric functionalisation of the indole carbocyclic backbone. Finally, the tetracyclic indole formed through the use of cyclohexenone and 7-indolyl boronic acid could be expanded upon. Different ring sizes, substitution patterns and bases employed in the system could allow an expansion of these natural product scaffold analogues with high levels of enantioenrichment.

# 7. Experimental

## 7.1. General Information

Solvents and reagents were used as obtained from commercial sources and without purification.

Column chromatography was carried out using 60 Å (35-70 µm) silica. TLC was carried out on precoated silica gel plates (Merck 60 PF254). The developed plates were visualised under UV light.

Melting points were obtained on a uni-melt Thomas Hoover Capillary melting point apparatus.

NMR spectra were run in $CDCl_3$ or $(CD_3)_2SO$ using TMS as the internal standard at 25 °C unless otherwise specified. $^1$H NMR (600 spectra) $^1$H NMR (500 MHz) spectra, $^1$H NMR (400 MHz) spectra and $^1$H NMR (300 MHz) spectra were recorded on Bruker Avance 600, Bruker Avance 500, Burker Avance 400 and Bruker Avance 300 NMR spectrometers respectively. $^{13}$C (150 MHz) spectra, $^{13}$C (125 MHz) spectra, $^{13}$C (100 MHz) spectra and $^{13}$C (75.5 MHz) spectra were recorded on Bruker Avance 600, Bruker Avance 500, Burker Avance 400 and Bruker Avance 300 NMR spectrometers respectively in proton decoupled mode. Chemical shifts $\delta_H$ and $\delta_C$ are expressed as parts per million (ppm), positive shift being downfield from TMS; coupling constants (*J*) are expressed in hertz (Hz). Splitting patterns in $^1$H NMR spectra are designated as s (singlet), br s (broad singlet), d (doublet), dd (doublet of doublets), dt (doublet of triplets), t (triplet), q (quartet) and m (multiplet). For $^{13}$C NMR spectra, the number of attached protons for each signal was determined using the DEPT pulse sequence run in the DEPT-90 and DEPT-135 modes.

Nominal mass spectra were recorded on a Waters Quattro Micro triple quadrupole spectrometer (QAA1202) in ESI mode using 50% acetonitrile–water containing 0.1% formic acid as eluent. High resolution mass spectra (HRMS) were recorded on a Waters LCT Premier Time of Flight spectrometer (KD160) or a Waters Vion IMS mass spectrometer (SAA055 K) in ESI mode using 50% acetonitrile– water containing 0.1% formic acid as eluent. Samples (max. 1 mg) were dissolved in acetonitrile, methanol, water or 10% DMSO/acetonitrile.

The Microanalysis Laboratory, National University of Ireland, Cork, performed elemental analysis using a Perkin-Elmer 240 and Exeter Analytical CE440 elemental analysers.

High performance liquid chromatography was performed using an Agilent 1200 Series HPLC system and a CHIRACEL® OD-3 column, 250 mm × 4.6 mm × 3.0 µm, purchased from Parc d'Innovation. Alternatively in cases where better separation was required, a Phenomenex® Amylose-2 column, 250 mm x 4.6 mm x 3.0 µm was used. Representative samples were prepared for HPLC analysis in hexane;IPA, to a concentration of ca 2 mg/mL. Samples were filtered using PTFE filters (13 mm diameter, 0.2 µm pore size) before analysis.

Example of a HPLC chromatogram obtained:

Compound **31** (see below for crystal data)

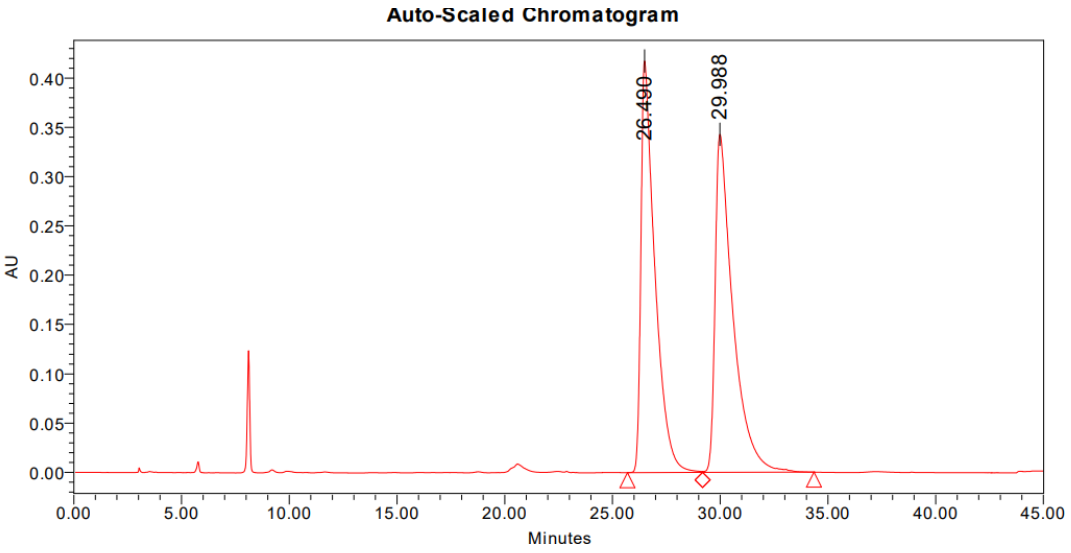


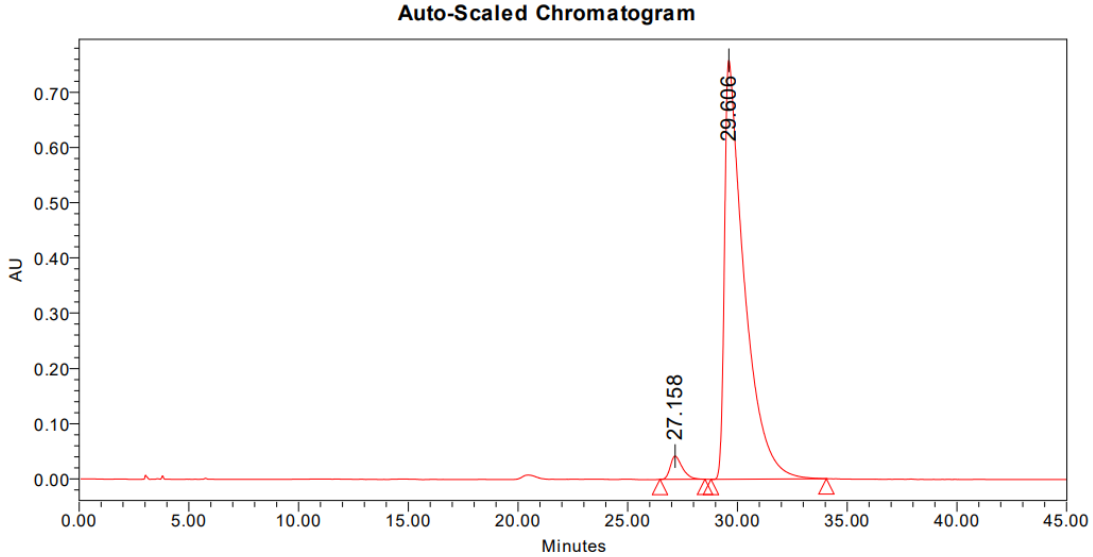

## 7.2. General Procedure for the Synthesis of Cinnamaldehyde-Based Ligands

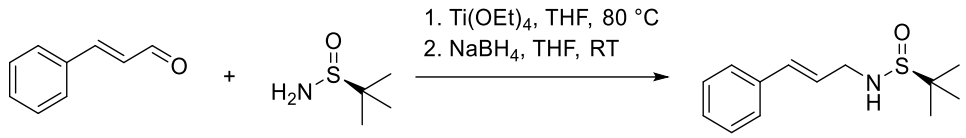


A solution of cinnamaldehyde (1.5 equiv.), (*S*)-tert-butanesulfinamide (1 equiv.) and $Ti(OEt)_4$ (2 equiv.) in 30 mL anhydrous THF was heated to reflux for 4 hours. Then the reaction was cooled to room temperature and $NaBH_4$ (5 equiv.) was added. The mixture was stirred at room temperature for additional 2 hours. When the reaction was complete, methanol was added dropwise until the reaction mixture stopped bubbling. The mixture was poured to 30 mL of brine, stirred and filtered. The filtrate was extracted with ethyl acetate, dried over anhydrous $Na_2SO_4$, and concentrated *in vacuo*. Purification by silica gel column chromatography was subsequently performed using DCM:hexanes as an eluent to yield the title products.

**(*S*,*E*)-*N*-cinnamyl-2-methylpropane-2-sulfinamide (L1)**

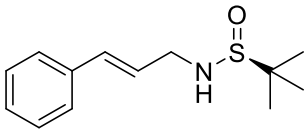


Synthesised according to the General Procedure using cinnamaldehyde (397 mg, 3 mmol, 1.5 equiv.) and (*S*)-tert-butanesulfinamide (241 mg, 2 mmol, 1 equiv.). The reaction mixture was poured to 30 mL of brine, stirred and filtered. The filtrate was extracted with ethyl acetate, dried over anhydrous $Na_2SO_4$, and concentrated *in vacuo*. The resulting residue was purified by silica gel column chromatography using DCM:Ethyl acetate (9:1) as eluent to yield the title product as a yellow solid (213 mg, 45%). Characterisation data is consistent with the literature.[78]

$^1$H NMR (300 MHz, $CDCl_3$) $\delta_H$; 7.41 – 7.35 (m, 2H), 7.34 – 7.28 (m, 2H), 7.27 – 7.23 (m, 1H), 6.58 (d, *J* = 15.8 Hz, 1H), 6.25 (dt, *J* = 15.8, 6.4 Hz, 1H), 4.00 – 3.81 (m, 2H), 3.38 – 3.20 (m, 1H) and 1.24 (s, 9H) ppm. $^{13}$C NMR (75.5 MHz, $CDCl_3$) $\delta_C$; 136.5, 132.6, 128.6, 127.8, 126.5, 55.8, 47.8 and 22.6 ppm.

**(*S,E*)-2-methyl-*N*-(3-(*p*-tolyl)allyl)propane -2-sulfinamide (L3)**

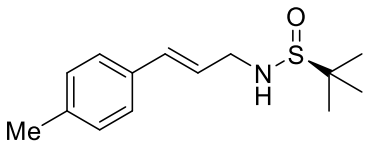

Synthesised according to the General Procedure using *p*-methyl cinnamaldehyde (3.0 mmol, 439 mg, 1.5 equiv.) and (*S*)-tert-butanesulfinamide (2.0 mmol, 241 mg, 1 equiv.). The reaction mixture was poured to 30 mL of brine, stirred and filtered. The filtrate was extracted with ethyl acetate, dried over anhydrous $Na_2SO_4$, and concentrated *in vacuo*. Purification by silica gel column chromatography was subsequently performed using DCM:ethyl acetate (7:3) as eluent to yield the title product as a white solid (200 mg, 40%). Characterisation data is consistent with the literature.[78]

$^1$H NMR (300 MHz, $CDCl_3$) $\delta_H$; 7.26 (d, *J* = 8.0 Hz, 2H), 7.11 (d, *J* = 8.0 Hz, 2H), 6.54 (d, *J* = 15.8 Hz, 1H), 6.19 (dt, *J* = 15.8, 6.4 Hz, 1H), 4.00 – 3.77 (m, 2H), 3.32 (apparent triplet, 1H), 2.32 (s, 3H), 1.23 (s, 9H) ppm. $^{13}$C NMR (75.5 MHz, $CDCl_3$) $\delta_C$; 137.6, 133.7, 132.5, 129.3, 126.4, 125.5, 55.7, 47.9, 22.7, 21.2 ppm. HRMS (ESI) m/z: $[M+Na]^+$ calc. for $C_{14}H_{21}NOSNa^+$ 274.1236, found: 274.1239.

**(*S,E*)-*N*-(3-(4-methoxyphenyl)allyl)-2-methylpropane-2-sulfinamide (L4)**

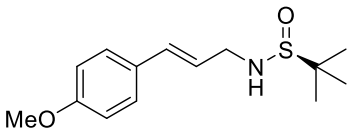

Synthesised according to General Procedure A using *p*-methoxy cinnamaldehyde (3.75 mmol, 607 mg, 1.5 equiv.) and (*S*)-tert-butanesulfinamide (2.5 mmol, 303 mg, 1 equiv.). The reaction mixture was poured to 30 mL of brine, stirred and filtered. The filtrate was extracted with ethyl acetate, dried over anhydrous $Na_2SO_4$, and concentrated *in vacuo*. Purification by silica gel column chromatography was subsequently performed using DCM:ethyl acetate (7:3) to yield the title product as a white solid (495 mg, 74%). Characterisation data is consistent with the literature.[78]

$^1$H NMR (300 MHz, $CDCl_3$) δ; 7.30 (m, 2H), 6.85 (m, 2H), 6.52 (d, *J* = 15.8 Hz, 1H), 6.11 (dt, *J* = 15.8, 6.5 Hz, 1H), 3.99 – 3.82 (m, 2H), 3.80 (s, 3H), 3.25 (apparent triplet, 1H), 1.24 (s, 9H) ppm. $^{13}$C (75.5 MHz, $CDCl_3$) δ; 159.4, 132.2, 129.3, 127.7, 124.2, 114.0, 55.7, 55.3, 48.0, 22.7 ppm. HRMS (ESI) m/z: $[M+Na]^+$ calc. for $C_{14}H_{21}NO_2SNa^+$: 290.11852, found: 290.11849.

**(*S*,*E*)-*N*-(3-(4-(dimethylamine)phenyl)allyl)-2-methylpropane-2-sulfinamide (L5)**

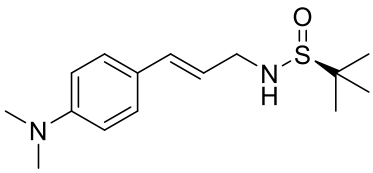

Synthesised according to General Procedure A using (*E*)-3-(4-dimethylamino)phenyl)acrylaldehyde (3.75 mmol, 657 mg, 1.5 equiv.) and (*S*)-tert-butanesulfinamide (2.5 mmol, 303 mg, 1 equiv.). The reaction mixture was poured to 30 mL of brine, stirred and filtered. The filtrate was extracted with ethyl acetate, dried over anhydrous $Na_2SO_4$, and concentrated *in vacuo*. Purification by silica gel column chromatography was subsequently performed using DCM:ethyl acetate (7:3) to yield the title product as a red solid (343 mg, 49%).

$^1$H NMR (300 MHz, $CDCl_3$) $\delta_H$; 7.29 – 7.23 (m, 2H), 6.70 – 6.63 (m, 2H), 6.48 (d, *J* = 15.8 Hz, 1H), 6.04 (dt, *J* = 15.8, 6.7 Hz, 1H), 3.99 – 3.75 (m, 2H), 3.22 (apparent triplet, 1H), 2.96 (s, 6H), 1.23 (s, 9H) ppm. $^{13}$C (75.5 MHz, $CDCl_3$) $\delta_C$; 150.2, 132.8, 127.4, 121.9, 112.4, 55.7, 48.2, 40.5, 22.7 ppm. HRMS (ESI-TOF) *m/z*: $[M+H]^+$ calcd. for $C_{15}H_{25}N_2OS$: 281.1682 found 281.1684.

**(*S*,*E*)-*N*-(3-(4-fluorophenyl)allyl)-2-methylpropane-2-sulfinamide (L6)**

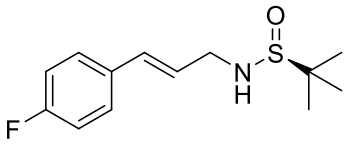

Synthesised according to General Procedure A using (*E*)-3-(4-fluorophenyl)acrylaldehyde (3.75 mmol, 563 mg, 1.5 equiv.) and (*S*)-tert-butanesulfinamide (2.5 mmol, 303 mg, 1 equiv.). The reaction mixture was poured to 30 mL of brine, stirred and filtered. The filtrate was extracted with ethyl acetate, dried over anhydrous $Na_2SO_4$, and concentrated *in vacuo*. Purification by silica gel column chromatography was subsequently performed using 2% MeOH in DCM as eluent to yield the title product as a pale yellow solid (511 mg, 80%). Characterisation data is consistent with the literature.[78]

$^1$H NMR (300 MHz, $CDCl_3$) $\delta_H$; 7.38 – 7.30 (m, 2H), 7.05 – 6.95 (m, 2H), 6.54 (d, *J* = 15.9 Hz, 1H), 6.17 (dt, *J* = 15.9, 6.4 Hz, 1H), 4.01 – 3.79 (m, 2H), 3.29 (apparent triplet, 1H), 1.24 (s, 9H) ppm. $^{13}$C (75.5 MHz, $CDCl_3$) $\delta_C$; 162.3 (d, $^1J_{CF}$ = 248 Hz) 132.6 (d, $^4J_{CF}$ = 3 Hz), 131.3, 127.9 (d, $^3J_{CF}$ = 8 Hz), 126.3 (d, $^4J_{CF}$ = 2.3 Hz), 115.5 (d, $^2J_{CF}$ = 21 Hz), 55.8, 47.8, 22.6 ppm. $^{19}$F (282 MHz, $CDCl_3$) $\delta_F$; 114.1 ppm. HRMS (ESI-TOF) *m/z*: $[M+Na]^+$ calcd. for $C_{13}H_{18}FNOSNa^+$: 278.0985 found 278.0986.

**(*S,E*)-2-methyl-*N*-(2-methyl-3-phenylallyl)propane-2-sulfinamide (L7)**

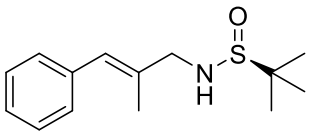

Synthesised according to General Procedure A using α-methyl cinnamaldehyde (0.75 mmol, 110 mg, 1.5 equiv.) and (*S*)-tert-butanesulfinamide (0.5 mmol, 60 mg, 1 equiv.). The reaction mixture was poured to 30 mL of brine, stirred and filtered. The filtrate was extracted with ethyl acetate, dried over anhydrous $Na_2SO_4$, and concentrated *in vacuo*. Purification by silica gel column chromatography was subsequently performed using 100% DCM as eluent to yield the product as a white solid (51 mg, 41%). Characterisation data is consistent with the literature.[70]

$^1$H NMR (300 MHz, $CDCl_3$) $\delta_H$; 7.36 – 7.31 (m, 2H), 7.29 – 7.7.25 (m, 2H), 7.24 – 7.20 (m, 1H), 6.50 (bs, 1H), 3.82 (AB fragment of ABX system *J* = 14.0, 7.5, 5.2 Hz, 2H), 3.33 (m, 1H), 1.91 (d, *J* = 1.1 Hz, 1H), 1.26 (s, 9H) ppm. $^{13}$C NMR (75.5 MHz, $CDCl_3$) $\delta_C$; 137.3, 135.3, 128.9, 128.2, 127.6, 126.6, 55.9, 54.0, 22.7 and 16.3 ppm. HRMS (ESI-TOF) *m/z*: $[M+Na]^+$ calcd. for $C_{14}H_{21}NOSNa^+$: 274.1236 found 274.1246.

**(*S,E*)-*N*-(2-benzylideneheptyl)-2-methylpropane-2-sulfinamide (L8)**

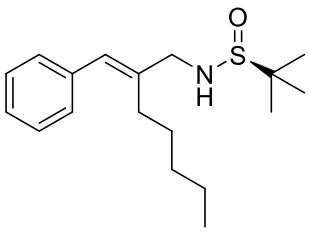

Synthesised according to General Procedure A using (*E*)-2-benzylideneheptanal (3.0 mmol, 202 mg, 1.5 equiv.) and (*S*)-tert-butanesulfinamide (2 mmol, 242 mg, 1 equiv.). The reaction mixture was poured to 30 mL of brine, stirred and filtered. The filtrate was extracted with ethyl acetate, dried over anhydrous $Na_2SO_4$, and concentrated *in vacuo*. Purification by silica gel column chromatography was subsequently performed using DCM:Ethyl acetate (7:1) as eluent to yield the title product as an off-white solid (159 mg, 26%).

$^1$H NMR (300 MHz, $CDCl_3$) $\delta_H$; 7.37 – 7.28 (m, 2H), 7.25 – 7.18 (m, 3H), 6.50 (s, 1H), 3.93 – 3.73 (m, 2H), 3.29 (apparent triplet, 1H), 2.37 – 2.20 (m, 2H), 1.91 – 1.79 (m, 1H), 1.57 – 1.41 (m, 2H), 1.35 – 1.20 (m, 12H including 9H *t*Bu), 0.91 – 0.83 (m, 3H) ppm. $^{13}$C NMR (75.5 MHz, $CDCl_3$) $\delta_C$; 139.9, 137.4, 128.6, 128.2, 127.5, 126.6, 55.9, 51.3, 31.9, 29.0, 27.7, 22.7, 22.4, 13.9 ppm. HRMS (ESI) m/z: $[M+Na]^+$ calc. for $C_{18}H_{29}NOSNa^+$: 330.1862 found 330.1857.

**(*S*)-*N*-((8-methoxy-2*H*-chromen-3-yl)methyl)-2-methylpropane-2-sulfinamide (L9)**

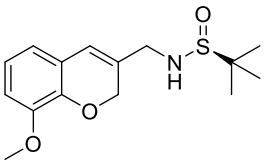

Synthesised according to General Procedure A using 8-methoxy-2*H*-chromene-3-carbaldehyde (3.75 mmol, 715 mg, 1.5 equiv.) and (*S*)-tert-butanesulfinamide (2.5 mmol, 302 mg, 1 equiv.). The reaction mixture was poured to 30 mL of brine, stirred and filtered. The filtrate was extracted with ethyl acetate, dried over anhydrous $Na_2SO_4$, and concentrated *in vacuo*. Purification by silica gel column chromatography was subsequently performed using DCM:Ethyl acetate (1:1) as eluent to yield the title product as a white solid (472 mg, 64%). $^1$H NMR (300 MHz, $CDCl_3$) $\delta_H$; 6.87 – 6.76 (m, 2H), 6.64 (dd, $J$ = 7.1, 1.8 Hz, 1H), 6.40 (apparent triplet, 1H), 4.89 – 4.74 (m, 2H), 3.94 – 3.74 (m, 5H), 3.31 (apparent triplet, 1H), 1.23 (s, 9H) ppm. $^{13}$C NMR (75.5 MHz, $CDCl_3$) $\delta_C$; 147.7, 142.1, 130.9, 122.7, 122.0, 121.2, 119.1, 112.2, 66.9, 56.0, 55.9, 47.7, 22.6 ppm. HRMS (ESI) m/z: $[M+Na]^+$ calc. for $C_{15}H_{21}NO_3SNa^+$: 318.1134 found 318.1141.

**(*S*)-*N*-(3,3-diphenylallyl)-2-methylpropane-2-sulfinamide (L10)**

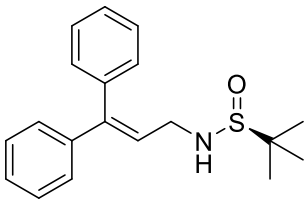

Synthesised according to General Procedure A using 3,3-diphenylacrylaldehyde (2.7 mmol, 561 mg, 1.5 equiv.) and (*S*)-tert-butanesulfinamide (1.8 mmol, 219 mg, 1 equiv.). The reaction mixture was poured to 30 mL of brine, stirred and filtered. The filtrate was extracted with ethyl acetate, dried over anhydrous $Na_2SO_4$, and concentrated *in vacuo*. Purification by silica gel column chromatography was subsequently performed using 1% MeOH in DCM as eluent to yield the title product as an off-white solid (304 mg, 54%). Characterisation data is consistent with the literature.[78]

$^1$H NMR (300 MHz, $CDCl_3$) $\delta_H$; 7.40 – 7.31 (m, 3H), 7.30 – 7.20 (m, 5H), 7.19 – 7.14 (m, 2H) 6.14 (t, *J* = 7.0 Hz, 1H), 3.93 – 3.72 (m, 2H), 3.24 (apparent triplet, 1H), 1.21 (s, 9H) ppm. $^{13}$C NMR (75.5 MHz, $CDCl_3$) $\delta_C$; 144.6, 141.7, 138.9, 129.7, 128.4, 128.2, 127.6, 127.5, 125.6, 55.7, 44.9, 22.6 ppm. HRMS (ESI-TOF) *m/z*: $[M+Na]^+$ calc. for $C_{19}H_{23}NOSNa^+$: 336.1392 found 336.1394.

**(*S,E*)-*N*-benzylidene-2-methylpropane-2-sulfinamide (L11)**

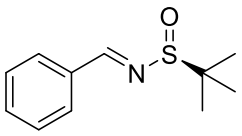

Synthesised according to General Procedure A using benzaldehyde (3.0 mmol, 318 mg, 1.5 equiv.) and (*S*)-tert-butanesulfinamide (2.0 mmol, 241 mg, 1 equiv.). The reaction mixture was poured to 30 mL of brine, stirred and filtered. The filtrate was extracted with ethyl acetate, dried over anhydrous $Na_2SO_4$, and concentrated *in vacuo*. Purification by silica gel column chromatography was subsequently performed using 100% DCM to yield the title product as a pale-yellow oil (364 mg, 87%). Characterisation data is consistent with the literature.[79]

$^1$H NMR (300 MHz, $CDCl_3$) $\delta_H$; 8.59 (s, 1H), 7.87 – 7.83 (m, 2H), 7.55 – 7.43 (m, 3H), 1.27 (s, 9H) ppm. $^{13}$C NMR (75.5 MHz, $CDCl_3$) $\delta_C$; 162.7, 134.1, 132.4, 129.4, 128.9, 57.8, 22.6 ppm. HRMS (ESI) m/z: $[M+Na]^+$ calc. $C_{11}H_{15}NOSNa^+$: for 232.0766 found 232.0765.

**(*S*)-*N*-cinnamyl-4-methylbenzenesulfinamide (L12)**

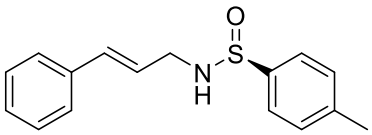

Synthesised according to General Procedure A using cinnamaldehyde (2.25 mmol, 297 mg, 1.5 equiv.) and (*S*)-4-methylbenzenesulfinamide (1.5 mmol, 233 mg, 1 equiv.). The reaction mixture was poured to 30 mL of brine, stirred and filtered. The filtrate was extracted with ethyl acetate, dried over anhydrous $Na_2SO_4$, and concentrated *in vacuo*. Purification by silica gel column chromatography was subsequently performed using 100% DCM to yield the title product as a yellow solid (106 mg, 26%). Characterisation data is consistent with the literature.[80]

$^1$H NMR (500 MHz, $CDCl_3$) $\delta_H$; 7.62 (d, *J* = 8.2 Hz, 2H), 7.34 – 7.20 (m, 7H), 6.49 (d, *J* = 15.8 Hz, 1H), 6.14 (dt, *J* = 15.8, 6.7 Hz, 1H), 4.20 (s, 1H), 3.88 – 3.79 (m, 1H), 3.63 – 3.55 (m, 1H), 2.40 (s, 3H) ppm. $^{13}$C NMR (125 MHz, $CDCl_3$) $\delta_C$; 141.3, 141.1, 136.4, 132.8, 129.6, 128.6, 127.8, 126.4, 126.0, 125.9, 43.3, 21.3 ppm. HRMS (ESI) m/z: $[M+Na]^+$ calc. for $C_{16}H_{17}NOSNa^+$: 294.0923 found 294.0924.

**2-benzylacrylaldehyde**

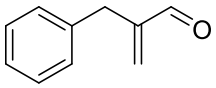

To a mixture of aqueous formaldehyde solution (37% formaldehyde in water, 5 mmol, 1 equiv.) and hydrocinnamaldehyde 95 mmol, 1 equiv.) in *i*PrOH (0.5 mL), was added propionic acid (0.5 mmol, 10 mol%) and pyrrolidine (0.5 mmol, 10 mol%). The reaction mixture was stirred at 45 °C for 2 hours. $NaHCO_3$ was added upon completion and the mixture was extracted with $CH_2Cl_2$ (3 x 10 mL). The extracts were washed with brine, dried using $MgSO_4$ and concentrated *in vacuo*. The resulting residue was purified by flash column chromatography on silica gel using Hexane:DCM (7:3) as the eluent to afford the title product as a pale yellow oil (149 mg, 20%). Characterisation data is consistent with the literature.[81]

$^1$H NMR (300 MHz, $CDCl_3$) $\delta_H$; 9.59 (s, 1H), 7.31 – 7.24 (m, 2H), 7.23 – 7.14 (m, 3H), 6.08 6.05 (m, 1H), 6.03 – 6.00 (m, 1H) and 3.55 (s, 1H) ppm.

**2-allyl-1,3-dimethylbenzene**

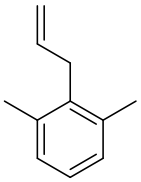

To a Schlenk flask evacuated and refilled with nitrogen, 2,6-dimethyl phenyl boronic acid (650 mg, 5 mmol, 1 equiv.), allyl bromide (1.3 mL, 15 mmol, 3 equiv.), $K_2CO_3$ (1.4 g, 10 mmol, 2 equiv.) and $Pd(OAc)_2$ (22.4 mg, 2 mol%) were added. Freshly distilled toluene (10 mL) was then added and the reaction was heated to 110 °C for 16 hours. After completion, the reaction mixture was cooled and diluted with $CH_2Cl_2$ and filtered through a pad of Celite®. The mixture was then concentrated *in vacuo* and the resulting residue was further purified by column chromatography on silica gel using 100% hexane as the eluent to afford the title product as a clear oil. Characterisation data was consistent with the literature.[82]

$^1$H NMR (300 MHz, $CDCl_3$) $\delta_H$; 7.09 – 7.01 (m, 3H), 6.00 – 5.85 (m, 1H), 5.03 (dq, *J* = 10.1, 1.8 Hz, 1H), 4.89 (dq, *J* = 17.1, 1.8 Hz, 1H), 3.46 – 3.39 (m, 2H) and 2.32 (s, 6H) ppm. Characterisation data is consistent with the literature.

## 7.3. General Procedure for the Rh-catalysed asymmetric 1,4-addition of indolyl boronic acids

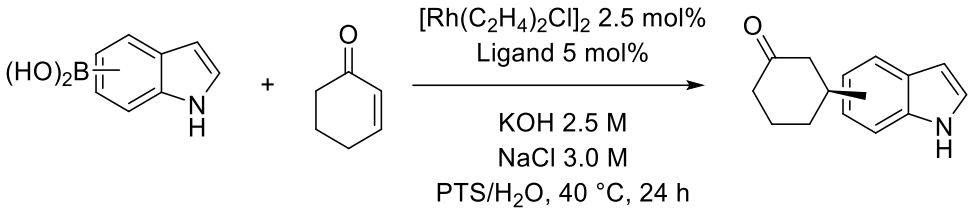


A 10 mL screwcap vial was charged with the appropriate ligand (0.05 equiv., 0.015 mmol), $[Rh(C_2H_4)_2Cl]_2$ (0.025 equiv., 0.0075 mmol) and an indolyl boronic acid (2 equiv., 0.6 mmol, 96 mg). The screwcap vial was then charged with a Michael-acceptor (1 equiv., 0.3 mmol) before being briefly flushed with $N_2$. Solutions of KOH (2.5 M, 0.12 mL) and NaCl (3.0 M, 0.1 mL) in $H_2O$ were then added before the solvent of 15 wt% PTS in $H_2O$ was added (0.7 mL). The screwcap vial was added a magnetic stir-bar and the cap was sealed with parafilm before being added to a multi-reaction heating mantle at 40 °C and 700 rpm. The reaction was then stirred for 24 hours before being cooled to room temperature and diluted with ethyl acetate. The resulting mixture was then passed through a plug of silica before extracting with 3 x 10 mL ethyl acetate and washing with 1 x 10 mL brine and 2 x 10 mL $H_2O$. The resulting solution was dried over $Na_2SO_4$ before concentrating *in vacuo*. The crude product was then purified by column chromatography on silica gel using hexane:ethyl acetate as eluent to yield the final product(s).

**(*S*)-3-(1*H*-indol-5-yl)cyclohexan-1-one (2)**

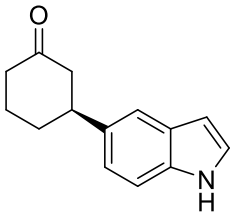

Synthesised according to the General Procedure using cyclohexenone (0.3 mmol, 29 mg, 1 equiv.) and 5-indolyl boronic acid (0.6 mmol, 96 mg, 2 equiv.) to yield the title product as a clear oil (51 mg, 86%, 97:3 e.r.). The enantiomeric ratio was determined by chiral HPLC analysis on a Chiralcel® OD-3 column with hexane:2-propanol (90:10), flow = 1 mL/min at 25 °C and 230 nm. Retention times: 35.5 min, 51.5 min.

$^{1}$H NMR (300 MHz, $CDCl_3$) $\delta_H$; 8.17 (bs, 1H), 7.48 (d, *J* = 0.8 Hz, 1H), 7.34 (d, *J* = 8.5 Hz, 1H), 7.20 (t, *J* = 2.8 Hz, 1H), 7.06 (dd, *J* = 8.5, 1.7 Hz, 1H), 6.52 (m, 1H), 3.16 – 3.05 (m, 1H), 2.70 – 2.53 (m, 2H), 2.52 – 2.33 (m, 2H), 2.21 – 2.08 (m, 1H), 2.00 – 1.87 (m, 1H), 1.87 – 1.73 (m, 1H) ppm. $^{13}$C NMR (75.5 MHz, $CDCl_3$) $\delta_C$; 211.7, 136.1, 134.7, 128.1, 124.7, 121.8, 118.0, 111.6, 102.5, 49.8, 45.0, 41.3, 33.5 and 25.7 ppm. HRMS (ESI-TOF) *m/z*: $[M+H]^+$ calcd. For $C_{14}H_{16}NO^+$: 214.1226, found 214.1229. $[\alpha]_D^{20}$+ 9.21 (c 1.27, $CH_2Cl_2$).

**(*S*)-3-(1*H*-indol-5-yl)cyclohpentan-1-one (22)**

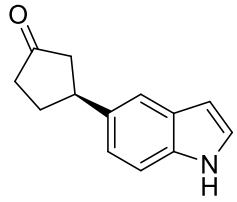

Synthesised according to the General Procedure using cyclopentenone (0.3 mmol, 25 mg, 1 equiv.) and 5-indolyl boronic acid (0.6 mmol, 96 mg, 2 equiv.) to yield the title product as a clear oil (49 mg, 81%, 98.5:1.5 e.r.). The enantiomeric ratio was determined by chiral HPLC analysis on a Chiralcel® OD-3 column with hexane:2-propanol (90:10), flow = 1 mL/min at 25 °C and 230 nm. Retention times: 40.6 min, 41.9 min.

$^{1}$H NMR (300 MHz, $CDCl_3$) $\delta_H$; 8.28 (bs, 1H), 7.50 (apparent doublet, *J* = 0.9 Hz, 1H), 7.33 (d, *J* = 8.4 Hz, 1H), 7.18 (t, *J* = 2.8 Hz, 1H), 7.08 (dd, *J* = 8.4, 1.8 Hz, 1H), 6.52 – 6.49 (m, 1H), 3.57 – 3.42 (m, 1H), 2.75 – 2.63 (m, 1H), 2.53 – 2.22 (m, 4H), 2.11 – 1.94 (m, 1H) ppm. $^{13}$C NMR (75.5 MHz, $CDCl_3$) $\delta_C$; 219.5, 134.8, 134.4, 128.1, 124.9, 121.1, 118.2, 111.3, 102.4, 46.6, 42.4, 39.1 and 31.8 ppm. HRMS (ESI-TOF) *m/z*: $[M+H]^+$ calcd. for $C_{13}H_{14}NO^+$: 200.1069, found 200.1069. $[\alpha]_D^{20}$+ 64.75 (c 0.505, $CH_2Cl_2$).

**(*S*)-3-(1*H*-indol-5-yl)cycloheptan-1-one (23)**

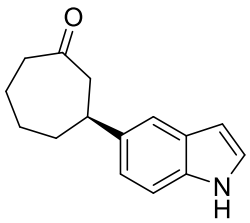

Synthesised according to the General Procedure using cycloheptenone (0.3 mmol, 33 mg, 1 equiv.) and 5-indolyl boronic acid (0.6 mmol, 96 mg, 2 equiv.) to yield the title product as a clear oil (34 mg, 51%, 94:6 e.r.). The enantiomeric ratio was determined by chiral HPLC analysis on a Chiralcel® OD-3 column with hexane:2-propanol (90:10), flow = 1 mL/min at 25 °C and 230 nm. Retention times: 33.6 min, 49.7 min.

$^{1}$H NMR (300 MHz, $CDCl_3$) $\delta_H$; 8.18 (bs, 1H), 7.43 (bm, 1H), 7.31 (d, *J* = 8.4 Hz, 1H), 7.18 (t, *J* = 2.8 Hz, 1H), 7.01 (dd, *J* = 8.4, 1.7 Hz, 1H), 6.51 – 6.47 (m, 1H), 3.06 – 2.93 (m, 2H), 2.77 – 2.66 (m, 1H), 2.64 – 2.56 (m, 2H), 2.19 – 1.94 (m, 3H), 1.88 – 1.68 (m, 2H), 1.59 – 1.44 (m, 1H) ppm. $^{13}$C NMR (75.5 MHz, $CDCl_3$) $\delta_C$; 214.1, 138.7, 134.5, 128.0, 124.6, 121.1, 117.8, 111.2, 102.4, 52.1, 44.0, 42.9, 39.8, 29.4 and 24.3 ppm. HRMS (ESI-TOF) *m/z*: $[M+H]^+$ calcd. For $C_{15}H_{18}NO^+$: 228.1383, found 228.1383. $[\alpha]_D^{20}$+ 32.70 (c 0.685, $CH_2Cl_2$).

**(*S*)-4-(1*H*-indol-5-yl)tetrahydro-2*H*-pyran-2-one (24)**

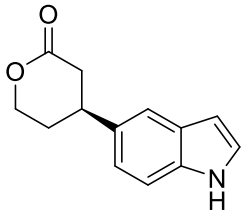

Synthesised according to the General Procedure using 5,6-dihydro-2*H*-pyran-2-one (0.3 mmol, 29 mg, 1 equiv.) and 5-indolyl boronic acid (0.6 mmol, 96 mg, 2 equiv.) to yield the title product as a clear oil (39 mg, 61%, 95:5 e.r.). The enantiomeric ratio was determined by chiral HPLC analysis on a Chiralcel® OD-3 column with hexane:2-propanol (80:20), flow = 1 mL/min at 25 °C and 230 nm. Retention times: 36.5 min, 44.7 min.

$^{1}$H NMR (600 MHz, $CDCl_3$) $\delta_H$; 8.21 (bs, 1H), 7.47 (unresolved doublet, 1H), 7.38 (d, *J* = 8.4 Hz, 1H), 7.23 (t, *J* = 2.7 Hz, 1H), 7.04 (dd, *J* = 8.4, 1.7 Hz, 1H), 6.55 – 6.52 (m, 1H), 4.55 – 4.49 (m, 1H), 4.44 – 4.37 (m, 1H), 3.37 – 3.29 (m, 1H), 2.96 (ddd, *J* = 17.7, 5.9 and 1.6 Hz, 1H), 2.72 (dd, *J* = 17.7, 10.6 Hz, 1H), 2.25 – 2.17 (m, 1H), 2.15 – 2.05 (m, 1H) ppm. $^{13}$C NMR (125 MHz, $CDCl_3$) $\delta_C$; 171.2, 134.9, 134.4, 128.2, 124.9, 120.8, 118.1, 111.5, 102.6, 68.6, 38.2, 37.6 and 30.9 ppm. HRMS (ESI-TOF) *m/z:* $[M+H]^+$ calcd. for $C_{13}H_{14}NO_2^+$: 216.1019 found 216.1016. $[\alpha]_D^{22}$- 17.23 (c 0.125, $CH_2Cl_2$).

**(*S*)-3-(1*H*-indol-6-yl)cyclohexan-1-one (25)**

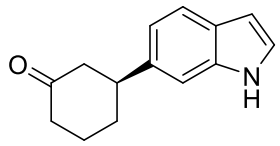

Synthesised according to the General Procedure using cyclohexenone (0.3 mmol, 29 mg, 1 equiv.) and 6-indolyl boronic acid (0.6 mmol, 96 mg, 2 equiv.) to yield the title product as a clear oil (47 mg, 74%, 97:3 e.r.). The enantiomeric ratio was determined by chiral HPLC analysis on a Chiralcel® OD-3 column with hexane:2-propanol (90:10), flow = 1 mL/min at 25 °C and 230 nm. Retention times: 33.2 min, 46.5 min.

$^{1}$H NMR (300 MHz, $CDCl_3$) $\delta_H$; 8.28 (bs, 1H), 7.58 (d, *J* = 8.2 Hz, 1H), 7.19 (apparent doublet, 1H), (dd, *J* = 3.2, 2.4 Hz, 1H), 6.99 (dd, *J* = 8.2, 1.5 Hz, 1H), 6.52 – 6.48 (m, 1H), 3.17 – 3.04 (m, 1H), 2.71 – 2.53 (m, 2H), 2.51 – 2.30 (m, 2H), 2.19 – 2.05 (m, 2H), 1.98 – 1.71 (m, 2H) ppm. $^{13}$C NMR (75.5 MHz, $CDCl_3$) $\delta_C$; 211.8, 138.5, 136.1, 126.7, 124.3, 120.9, 118.9, 108.8, 102.4, 49.6, 45.1, 41.3, 33.3 and 25.3 ppm. HRMS (ESI-TOF) *m/z*: $[M+H]^+$ calcd. For $C_{14}H_{16}NO^+$: 214.1226, found 214.1225. $[\alpha]_D^{20}$+ 11.62 (c 0.31, $CH_2Cl_2$).

**(*S*)-3-(1*H*-indol-6-yl)cyclopentan-1-one (26)**

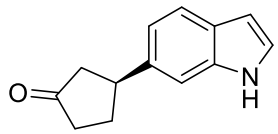

Synthesised according to the General Procedure using cyclopentenone (0.3 mmol, 25 mg, 1 equiv.) and 6-indolyl boronic acid (0.6 mmol, 96 mg, 2 equiv.) to yield the title product as a clear oil (43 mg, 72%, 97.5:2.5 e.r.). The enantiomeric ratio was determined by chiral HPLC analysis on a Chiralcel® OD-3 column with hexane:2-propanol (90:10), flow = 1 mL/min at 25 °C and 230 nm. Retention times: 29 min, 32.7 min.

$^{1}$H NMR (300 MHz, $CDCl_3$) $\delta_H$; 8.21 (bs, 1H), 7.60 (d, *J* = 8.2 Hz, 1H), 7.25 – 7.23 (bm, 1H), 7.18 (dd, *J* = 3.2, 2.4 Hz, 1H), 7.03 (dd, *J* = 8.2, 1.5 Hz, 1H), 6.54 – 6.51 (m, 1H), 3.61 – 3.46 (m, 1H), 2.76 – 2.64 (m, 1H), 2.54 – 2.37 (m, 3H), 2.37 – 2.23 (m, 1H), 2.13 – 1.96 (m, 1H) ppm. $^{13}$C NMR (75.5 MHz, $CDCl_3$) $\delta_C$; 219.1, 137.1, 136.1, 126.7, 124.3, 120.9, 119.2, 108.8, 102.5, 46.4, 42.5, 38.9 and 31.7 ppm. HRMS (ESI-TOF) *m/z*: $[M+H]^+$ calcd. For $C_{13}H_{14}NO^+$: 200.1069, found 200.1066. $[\alpha]_D^{20}$+ 67.50 (c 0.26, $CH_2Cl_2$).

**(*S*)-3-(1*H*-indol-6-yl)cycloheptan-1-one (27)**

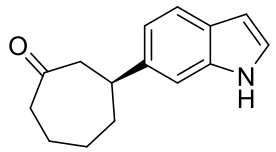

Synthesised according to the General Procedure using cycloheptenone (0.3 mmol, 33 mg, 1 equiv.) and 6-indolyl boronic acid (0.6 mmol, 96 mg, 2 equiv.) to yield the title product as a clear oil (64 mg, 94%, 96:4 e.r.). The enantiomeric ratio was determined by chiral HPLC analysis on a Chiralcel® OD-3 column with hexane:2-propanol (80:20, 0.1% TFA), flow = 1 mL/min at 25 °C and 230 nm. Retention times: 18.3 min, 19.4 min.

$^{1}$H NMR (300 MHz, $CDCl_3$) $\delta_H$; 8.14 (bs, 1H), 7.56 (d, *J* =8.2 Hz, 1H), 7.19 (bs) and 7.16 (dd, *J* = 3.2, 2.4 Hz) (overlapping signals at 7.19 and 7.16 ppm, 2H), 6.96 (dd, *J* = 8.2, 1.5 Hz, 1H), 6.53 – 6.49 (m, 1H), 3.07 – 2.93 (m, 1H), 2.79 – 2.66 (m, 1H), 2.65 – 2.55 (m, 1H), 2.20 – 1.93 (m, 3H), 1.88 – 1.65 (m, 2H), 1.57 – 1.44 (m, 1H) ppm. $^{13}$C NMR (75.5 MHz, $CDCl_3$) $\delta_C$; 213.8, 141.2, 136.0, 126.4, 124.1, 120.8, 118.9, 108.5, 102.5, 51.9, 44.0, 43.0, 39.7, 29.3 and 24.3 ppm. HRMS (ESI-TOF) *m/z*: $[M+H]^+$ calcd. For $C_{15}H_{18}NO^+$: 228.1383, found 228.1386 $[\alpha]_D^{20}$+35.24 (c 0.21, $CH_2Cl_2$).

**(*S*)-4-(1*H*-indol-6-yl)tetrahydro-2*H*-pyran-2-one (28)**

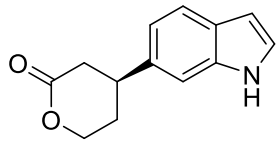

Synthesised according to the General Procedure using 5,6-dihydro-2*H*-pyran-2-one (0.3 mmol, 29 mg, 1 equiv.) and 6-indolyl boronic acid (0.6 mmol, 96 mg, 2 equiv.) to yield the title product as a clear oil (48 mg, 74%, 92:8 e.r.). The enantiomeric ratio was determined by chiral HPLC analysis on a Chiralcel® OD-3 column with hexane:2-propanol (80:20), flow = 1 mL/min at 25 °C and 230 nm. Retention times: 35.0 min, 39.5 min.

$^{1}$H NMR (300 MHz, $CDCl_3$) $\delta_H$; 8.19 (bs, 1H), 7.54 (d, *J* = 8.2 Hz, 1H), 7.16 – 7.11 (m, 2H), 6.90 (dd, *J* = 8.2, 1.5 Hz, 1H), 6.49 – 6.43 (m, 1H), 4.48 – 4.26 (m, 2H), 3.35 – 3.21 (m, 1H), 2.89 (ddd, *J* = 18.0, 6.0, 1.5 Hz, 1H), 2.72 – 2.59 (m, 1H), 2.22 – 2.09 (m, 1H) and 2.09 – 1.93 (m, 1H) ppm. $^{13}$C NMR (75.5 MHz, $CDCl_3$) $\delta_C$; 171.2, 136.8, 136.0, 126.9, 124.6, 121.1, 118.8, 108.6, 102.5, 68.7, 37.9, 37.5 and 30.9 ppm. HRMS (ESI-TOF) *m/z*: $[M+H]^+$ calcd. For $C_{13}H_{14}NO_2^+$: 216.1019, found 216.1016. $[\alpha]_D^{20}$-17.41 (c 0.125, $CH_2Cl_2$).

**(*S*)-3-(1*H*-indol-4-yl)cyclohexan-1-one (29)**

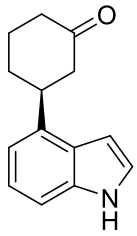

Synthesised according to the General Procedure using cyclohexenone (0.3 mmol, 29 mg, 1 equiv.) and 4-indolyl boronic acid (0.6 mmol, 96 mg, 2 equiv.) to yield the title product as a clear oil (47 mg, 73%, 97.5:2.5 e.r.). The enantiomeric ratio was determined by chiral HPLC analysis on a Chiralcel® OD-3 column with hexane:2-propanol (90:10), flow = 1 mL/min at 25 °C and 230 nm. Retention times: 40.5 min, 48.6 min.

$^{1}$H NMR (300 MHz, $CDCl_3$) $\delta_H$; 8.25 (bs, 1H), 7.30 (d, *J* = 8.1 Hz, 1H), 7.24 – 7.14 (m, 2H), 6.98 (d, *J* = 7.2 Hz, 1H), 6.64 – 6.55 (m, 1H), 3.56 – 3.42 (m, 1H), 2.78 – 2.67 (m, 2H), 2.57 – 2.36 (m, 2H), 2.27 – 2.12 (m, 2H), 2.11 – 1.95 (m, 1H) and 1.94 – 1.77 (m, 1H) ppm. $^{13}$C NMR (75.5 MHz, $CDCl_3$) $\delta_C$; 211.7, 136.4, 135.9, 126.2, 123.9, 122.3, 116.0, 109.6, 100.6, 48.1, 42.1, 41.5, 31.9 and 25.7 ppm. HRMS (ESI-TOF) *m/z*: $[M+H]^+$ calcd. For $C_{14}H_{16}NO^+$: 214.1226, found 214.1227. $[\alpha]_D^{20}$+20.48 (c 0.105, $CH_2Cl_2$).

**(*S*)-3-(1*H*-indol-4-yl)cyclopentan-1-one (30)**

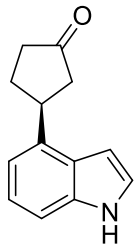

Synthesised according to the General Procedure using cyclopentenone (0.3 mmol, 25 mg, 1 equiv.) and 4-indolyl boronic acid (0.6 mmol, 96 mg, 2 equiv.) to yield the title product as a clear oil (52 mg, 87%, 96.5:3.5 e.r.). The enantiomeric ratio was determined by chiral HPLC analysis on a Phenomenex® Amy-2 column with hexane:2-propanol (91:9), flow = 1 mL/min at 25 °C and 218 nm. Retention times: 20.0 min, 22.0 min.

$^{1}$H NMR (300 MHz, $CDCl_3$) $\delta_H$; 8.33 (bs, 1H), 7.30 (d, *J* = 8.2 Hz, 1H), 7.24 – 7.21 (m, 1H), 7.17 (t, *J* = 7.3 Hz, 1H), 6.97 (d, *J* = 7.3 Hz, 1H), 6.62 – 6.58 (m, 1H), 3.93 – 3.78 (m, 1H), 2.82 – 2.62 (m, 1H), 2.62 – 2.43 (m, 3H), 2.43 – 2.29 (m, 1H) and 2.28 – 2.13 (m, 1H) ppm. $^{13}$C NMR (75.5 MHz, $CDCl_3$) $\delta_C$; 219.3, 135.9, 135.0, 126.7, 124.0, 122.2, 115.9, 109.8, 100.8, 45.2, 39.9, 38.7 and 29.9 ppm. HRMS (ESI-TOF) *m/z*: $[M+H]^+$ calcd. For $C_{13}H_{14}NO^+$: 200.1069, found 200.1069. $[\alpha]_D^{20}$+38.31 (c 0.83 $CH_2Cl_2$).

**(*S*)-3-(1*H*-indol-4-yl)cycloheptan-1-one (31)**

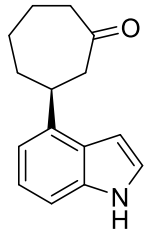

Synthesised according to the General Procedure using cycloheptenone (0.3 mmol, 33 mg, 1 equiv.) and 4-indolyl boronic acid (0.6 mmol, 96 mg, 2 equiv.) to yield the title product as a clear oil (28 mg, 41%, 97:3 e.r.). The enantiomeric ratio was determined by chiral HPLC analysis on a Phenomenex® Amy-2 column with hexane:2-propanol (91:9), flow = 1 mL/min at 25 °C and 218 nm. Retention times: 26.4 min, 29.9 min.

$^{1}$H NMR (500 MHz, $CDCl_3$) $\delta_H$; 8.19 (bs, 1H), 7.20 – 7.17 (m, 1H), 7.14 – 7.12 (m, 1H), 7.07 (t, *J* = 8.0 Hz, 1H), 6.85 (d, *J* = 7.4 Hz, 1H), 6.53 – 6.50 (m, 1H), 3.27 (tt, *J* = 11.4, 2.4 Hz, 1H), 3.00 (dd, *J* = 14.4, 2.4 Hz), 2.72 (dt, *J* = 14.4, 2.4 Hz, 1H), 2.64 – 2.53 (m, 2H), 2.20 – 2.14 (m, 1H), 2.07 – 1.93 (m, 2H), 1.88 – 1.77 (m, 1H), 1.75 – 1.64 (m, 1H), 1.54 – 1.44 (m, 1H) ppm. $^{13}$C NMR (125 MHz, $CDCl_3$) $\delta_C$; 213.04, 137.8, 134.9, 124.8, 122.8, 121.2, 114.9, 108.3, 99.7, 49.5, 42.9, 39.1, 37.0, 28.6 and 23.4 ppm. HRMS (ESI-TOF) *m/z*: $[M+H]^+$ calcd. For $C_{15}H_{18}NO^+$: 228.1383, found 228.1384. $[\alpha]_D^{20}$+43.76 (c 0.945 $CH_2Cl_2$).

**(*S*)-3-(1*H*-indol-7-yl)cyclopentane-1-one (32)**

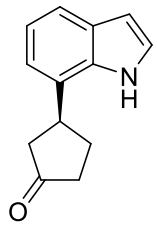

Synthesised according to the General Procedure using cyclopentenone (0.3 mmol, 25 mg, 1 equiv.) and 7-indole boronic acid (0.6 mmol, 96 mg, 2 equiv.) to yield the title product as a clear oil (33 mg, 55%, 98.5:1.5 e.r.) The enantiomeric ratio was determined by chiral HPLC analysis on a Phenomenex® Amy-2 column with hexane:2-propanol (90:10), flow = 1 mL/min at 25 °C and 230 nm. Retention times: 25.8 min, 29.0 min.

$^{1}$H NMR (300 MHz, $CDCl_3$) $\delta_H$; 8.29 (bs, 1H), 7.56 (d, *J* = 7.7 Hz, 1H), 7.27 – 7.19 (m, 1H), 7.15 – 7.02 (m, 2H), 6.63 – 6.56 (m, 1H), 3.81 – 3.69 (m, 1H), 2.82 – 2.67 (m, 1H), 2.60 – 2.44 (m, 3H), 2.43 – 2.30 (m, 1H) and 2.29 – 2.15 (m, 1H) ppm. $^{13}$C NMR (75.5 MHz, $CDCl_3$) $\delta_C$; 218.4, 134.4, 128.1, 125.4, 124.1, 120.1, 119.5, 118.1, 103.4, 44.7, 38.4, 37.6 and 29.4 ppm. $[\alpha]_D^{20}$-28.55 (c 0.33 in $CH_2Cl_2$).

**(*S*)-4-(1*H*-indolo-5-yl)octan-2-one (39)**

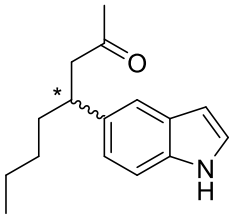

Synthesised according to the General Procedure using (*E*)-oct-3-en-2-one (0.3 mmol, 38 mg, 1 equiv.) and 5-indolyl boronic acid (0.6 mmol, 96 mg, 2 equiv.) to yield the title product as a clear oil (58 mg, 80%, 96:4 e.r.). The enantiomeric ratio was determined by chiral HPLC analysis on a Chiralcel® OD-3 column with hexane:2-propanol (80:20), flow = 1 mL/min at 25 °C and 230 nm. Retention times: 7.1 min, 7.5 min.

$^{1}$H NMR (300 MHz, $CDCl_3$) $\delta_H$; 8.15 (bs, 1H), 7.42 (s, 1H), 7.29 (d, *J* = 8.3 Hz, 1H), 7.16 (t, *J* = 2.7 Hz, 1H), 7.01 (dd, *J* = 8.3, 1.7 Hz, 1H), 6.51 – 6.46 (m, 1H), 3.25 – 3.11 (m, 1H), 2.84 – 2.66 (m, 2H), 1.98 (s, 3H), 1.73 – 1.54 (m, 3H), 1.32 – 1.05 (m, 4H), 0.80 (t, *J* = 7.2 Hz, 3H) ppm. $^{13}$C NMR (75.5 MHz, $CDCl_3$) $\delta_C$; 208.9, 135.9, 134.7, 128.0, 124.4, 121.8, 119.2, 110.9, 102.4, 51.8, 41.7, 36.8, 30.7, 29.7, 22.7 and 13.9 ppm. HRMS (ESI-TOF) *m/z*: $[M+H]^+$ calcd. for $C_{16}H_{22}NO^+$: 244.1695 found 244.1693. $[\alpha]_D^{20}$+ 2.41 (c 0.435 in $CH_2Cl_2$).

**(*S*)-4-(1*H*-indol-5-yl)-4-phenylbutan-2-one (38)**

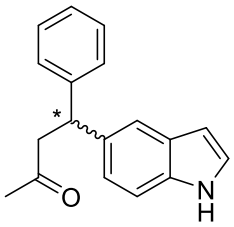

Synthesised according to General Procedure B using (*E*)-4-phenylbut-3-en-2-one (0.3 mmol, 44 mg, 1 equiv.) and 5-indolyl boronic acid (0.6 mmol, 96 mg, 2 equiv.) to yield the title product as a clear oil (71 mg, 90%, 96:4 e.r.).

$^{1}$H NMR (500 MHz, $CDCl_3$) $\delta_H$; 8.08 (bs, 1H), 7.49 (s, 1H), 7.29 – 7.22 (m, 5H), 7.18 – 7.12 (m, 2H), 7.05 (dd, *J* = 8.4, 1.6 Hz, 1H), 6.50 – 6.45 (m, 1H), 4.68 (t, *J* = 7.6 Hz, 1H), 3.29 – 3.16 (m, 2H), 2.06 (s, 3H) ppm. $^{13}$C NMR (125 MHz, $CDCl_3$) $\delta_H$; 207.5, 144.8, 135.4, 134.6, 128.5, 128.0, 127.7, 126.2, 124.5, 122.5, 119.2, 111.2, 102.6, 50.3, 46.3 and 30.7 ppm. HRMS (ESI-TOF) *m/z*: $[M+H]^+$ calcd. for $C_{18}H_{18}NO^+$: 264.1382 found 264.1382. $[\alpha]_D^{20}$ -30.37 (c 0.45 in $CH_2Cl_2$).

**4-(1*H*-indol-5-yl)-5-methylhexan-2-one (40)**

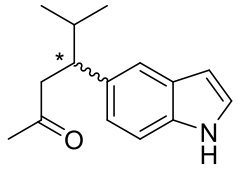

Synthesised according to General Procedure B using (*E*)-5-methylhex-3-en-2-one (0.3 mmol, 34 mg, 1 equiv.) and 5-indolyl boronic acid (0.6 mmol, 96 mg, 2 equiv.) to yield the title product as a clear oil (64 mg, 93%).

$^{1}$H NMR (300 MHz, $CDCl_3$) $\delta_H$; 8.11 (bs, 1H), 7.39 (s, 1H), 7.28 (d, *J* = 8.4 Hz, 1H), 7.16 (t, *J* = 2.8 Hz, 1H), 6.99 (dd, *J* = 8.4, 1.7 Hz, 1H), 6.50 – 6.46 (m, 1H), 3.03 – 2,93 (m, 1H), 2.84 (d, *J* = 7.4 Hz, 2H), 1.94 (s, 3H), 1.92 – 1.81 (m, 1H), 0.96 (d, *J* = 6.6 Hz, 3H), 0.76 (d, *J* = 6.7 Hz, 3H) ppm. $^{13}$C NMR (75.5 MHz, $CDCl_3$) $\delta_C$; 209.1, 134.7, 134.5, 127.8, 124.4, 122.7, 119.9, 110.7, 102.5, 48.5, 48.4, 33.8, 30.6, 20.9 and 20.5 ppm. HRMS (ESI-TOF) *m/z*: $[M+H]^+$ calcd. for $C_{15}H_{20}NO^+$: 230.1539 found 230.1532. $[\alpha]_D^{20}$+12.20 (c 0.25, $CH_2Cl_2$).

**Methyl (*S*)-3-(1*H*-indol-5-yl)-3-phenylpropanoate (41)**

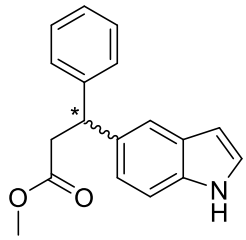

Synthesised according to General Procedure B using methyl cinnamate (0.3 mmol, 49 mg, 1 equiv.) and 5-indolyl boronic acid (0.6 mmol, 96 mg, 2 equiv.) to yield the title product as a clear oil (69 mg, 82%, 89:11 e.r.). The enantiomeric ratio was determined by chiral HPLC analysis on a Chiralcel® OD-3 column with hexane:2-propanol (80:20), flow = 1 mL/min at 25 °C and 230 nm. Retention times: 13.0 min, 14.2 min

$^{1}$H NMR (300 MHz, $CDCl_3$) $\delta_H$; 8.08 (bs, 1H), 7.50 (unresolved doublet, 1H), 7.29 -7.23 (m, 4H), 7.23 – 7.19 (m, 1H), 7.18 – 7.12 (m, 1H), 7.11 (t, *J* = 2.8 Hz, 1H), 7.02 (dd, *J* = 8.4, 1.7 Hz, 1H), 6.49 – 6.44 (m, 1H), 4.66 (t, *J* = 8.0 Hz, 1H), 3.55 (s, 3H), 3.12 (d, *J* = 8.0 Hz, 2H) ppm. $^{13}$C NMR (75.5 MHz, $CDCl_3$) $\delta_C$; 172.7, 144.5, 135.1, 134.6, 128.5, 128.0, 127.7, 126.3, 124.5, 122.4, 119.1, 111.2, 102.6, 51.6, 47.1 and 41.2 ppm. HRMS (ESI-TOF) *m/z*: $[M+H]^+$ calcd. for $C_{18}H_{18}NO_2^+$: 280.1332 found 280.1327. $[\alpha]_D^{20}$-30.07 (c 0.46 in $CH_2Cl_2$).

**(*S*)-2-hydroxy-2-(1*H*-indol-5-yl)-1,2-diphenylethan-1-one (43)**

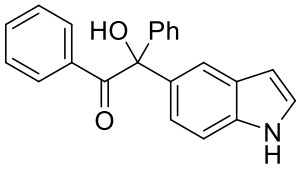


Synthesised according to General Procedure C using benzil (0.3 mmol, 63 mg, 1 equiv.) and 5-indolyl boronic acid (0.6 mmol, 96 mg, 2 equiv.) to yield the title product as a clear oil (93 mg, 95%, 95:5 e.r.). The enantiomeric ratio was determined by chiral HPLC analysis on a Chiralcel® OD-3 column with hexane:2-propanol (90:10), flow = 1 mL/min at 25 °C and 230 nm. Retention times: 23.6 min, 29.7 min.

$^{1}$H NMR (300 MHz, $CDCl_3$) $\delta_H$; 8.20 (bs, 1H), 7.78 – 7.70 (m, 2H), 7.65 – 7.62 (m, 1H), 7.52 – 7.45 (m, 2H), 7.45 – 7.29 (m, 5H), 7.28 – 7.18 (m, 5H), 6.52 – 6.47 (m, 1H), 4.96 (s, 1H). $^{13}$C NMR (75.5 MHz, $CDCl_3$) $\delta_C$; 201.4, 142.5, 135.6, 135.3, 133.7, 132.7, 130.9, 128.5, 128.2, 128.0, 127.9, 127.6, 124.8, 122.7, 120.7, 111.1, 103.3 and 85.5 ppm. HRMS (ESI-TOF) *m/z*: $[M+Na]^+$ calcd. for $C_{22}H_{17}NO_2Na^+$: 350.1151 found 350.1146. $[\alpha]_D^{20}$ -16.29 (c 1.24 in $CH_2Cl_2$).

**8,9,10,11-tetrahydro-7*H*-7,11-methanoazocino[3,2,1-*h*]indol-7-ol**

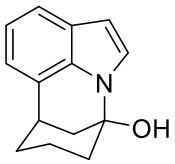


Synthesised according to General Procedure A using cyclohexenone (0.3 mmol, 29 mg, 1 equiv.) and 7-indolyl boronic acid (0.6 mmol, 96 mg, 2 equiv.) to yield the title product as a clear oil (41 mg, 65%).

$^{1}$H NMR (300 MHz, $CDCl_3$) $\delta_H$; 7.45 (dd, *J* = 8.0, 0.9 Hz, 1H), 7.37 (d, *J* = 3.1 Hz, 1H), 7.03 (dd, *J* = 8.0, 7.0 Hz, 1H), 6.89 (d, *J* = 7.0 Hz, 1H), 6.50 (d, *J* = 3.1 Hz, 1H), 3.49 – 3.41 (m, 1H), 2.55 (s, 3H), 2.22 (dd, *J* = 11.9, 3.1 Hz, 1H), 2.17 – 2.09 (m, 1H), 2.06 – 1.96 (m, 1H), 1.88 (td, *J* = 13.0, 4.6 Hz, 1H), 1.81 – 1.67 (m, 2H), 1.53 – 1.45 (m, 1H), 0.79 – 0 .58 (m, 1H) ppm. $^{13}$C NMR (75.5 MHz, $CDCl_3$) $\delta_C$; 135.7, 125.3, 125.1, 121.3, 119.9, 118.3, 117.4, 101.6, 83.8, 41.1, 38.9, 35.7, 32.2 and 19.4 ppm. HRMS (ESI-TOF) *m/z*: $[M+H]^+$ calcd. for $C_{14}H_{16}NO^+$: 214.1226 found 214.1228. $[\alpha]_D^{20}$-78.57 (c 0.56 in $CH_2Cl_2$).

Crystal Data:

| Compound | **31** | **27** | **26** |
|---|---|---|---|
| Formula | $C_{15}H_{17}NO$ | $C_{15}H_{17}NO$ | $C_{13}H_{13}NO$ |
| $D_{calc.}$/ g cm$^{-3}$ | 1.218 | 1.296 | 1.232 |
| $m$/mm$^{-1}$ | 0.593 | 0.081 | 0.078 |
| Formula Weight | 227.29 | 227.29 | 199.24 |
| Colour | clear colourless | clear colourless | clear colourless |
| Shape | block-shaped | plate-shaped | prism-shaped |
| Size/mm$^3$ | 0.34×0.27×0.06 | 0.19×0.16×0.04 | 0.61×0.13×0.05 |
| $T$/K | 100(2) | 100(2) | 100(2) |
| Crystal System | orthorhombic | orthorhombic | monoclinic |
| Flack Parameter | 0.00(5) | 0.2(7) | 0.0(3) |
| Hooft Parameter | -0.00(4) | 0.1(6) | -0.1(3) |
| Space Group | $P2_12_12_1$ | $P2_12_12_1$ | $P2_1$ |
| $a$/Å | 6.89790(10) | 5.4762(2) | 10.0067(3) |
| $b$/Å | 7.22490(10) | 9.2507(4) | 7.5023(2) |
| $c$/Å | 24.8791(3) | 22.9984(9) | 14.3585(4) |
| $a$/° | 90 | 90 | 90 |
| $b$/° | 90 | 90 | 94.993(2) |
| $g$/° | 90 | 90 | 90 |
| V/Å$^3$ | 1239.89(3) | 1165.07(8) | 1073.85(5) |
| $Z$ | 4 | 4 | 4 |
| $Z'$ | 1 | 1 | 2 |
| Wavelength/Å | 1.54184 | 0.71073 | 0.71073 |
| Radiation type | Cu $K_a$ | Mo $K_a$ | Mo $K_a$ |
| $Q_{min}$/° | 3.553 | 2.373 | 2.043 |
| $Q_{max}$/° | 70.154 | 32.203 | 32.187 |
| Measured Refl's. | 11481 | 19681 | 29940 |
| Indep't Refl's | 2337 | 3634 | 6597 |
| Refl's I≥2 $s$(I) | 2324 | 3125 | 5637 |
| $R_{int}$ | 0.0146 | 0.0580 | 0.0272 |
| Parameters | 158 | 154 | 298 |
| Restraints | 0 | 0 | 19 |
| Largest Peak | 0.143 | 0.471 | 0.294 |
| Deepest Hole | -0.148 | -0.270 | -0.257 |
| GooF | 1.073 | 1.044 | 1.064 |

| | | | |
|---|---|---|---|
| $wR_2$ (all data) | 0.0723 | 0.1503 | 0.1169 |
| $wR_2$ | 0.0722 | 0.1422 | 0.1115 |
| $R_1$ (all data) | 0.0281 | 0.0670 | 0.0535 |
| $R_1$ | 0.0281 | 0.0548 | 0.0429 |

Crystal Analysis Experimental

**31**: Single clear colourless block-shaped crystals of **31** recrystallised from a mixture of $CHCl_3$ and hexane by slow evaporation. A suitable crystal with dimensions 0.34 × 0.27 × 0.06 $mm^3$ was selected and mounted on a MITIGEN holder with silicon oil on a ROD, Synergy Custom system, HyPix-Arc 100 diffractometer. The crystal was kept at a steady $T$ = 100(2) K during data collection. The structure was solved with the ShelXT 2014/5 (Sheldrick, 2014) solution program using dual methods and by using Olex2 1.5-alpha (Dolomanov *et al.,* 2009) as the graphical interface. The model was refined with ShelXL 2016/6 (Sheldrick, 2015) using full matrix least squares minimisation on $\boldsymbol{F}^2$.

**27**: Single clear colourless plate-shaped crystals of **27** recrystallised from $CHCl_3$ by slow evaporation. A suitable crystal with dimensions 0.19 × 0.16 × 0.04 $mm^3$ was selected and mounted on a MITIGEN holder with silicon oil on a ROD, Synergy Custom system, HyPix diffractometer. The crystal was kept at a steady $T$ = 100(2) K during data collection. The structure was solved with the ShelXT 2014/5 (Sheldrick, 2014) solution program using dual methods and by using Olex2 1.5-alpha (Dolomanov *et al.,* 2009) as the graphical interface. The model was refined with ShelXL 2016/6 (Sheldrick, 2015) using full matrix least squares minimisation on $\boldsymbol{F}^2$.

**26**: Single clear colourless prism-shaped crystals of **26** recrystallised from $CHCl_3$ by slow evaporation. A suitable crystal with dimensions 0.61 × 0.13 × 0.05 $mm^3$ was selected and mounted on a MITIGEN holder silicon oil on a ROD, Synergy Custom system, HyPix diffractometer. The crystal was kept at a steady $T$ = 100(2) K during data collection. The structure was solved with the ShelXT 2014/5 (Sheldrick, 2014) solution program using dual methods and by using Olex2 1.5-alpha (Dolomanov *et al*., 2009) as the graphical interface. The model was refined with ShelXL 2016/6 (Sheldrick, 2015) using full matrix least squares minimisation on $\boldsymbol{F}^2$.

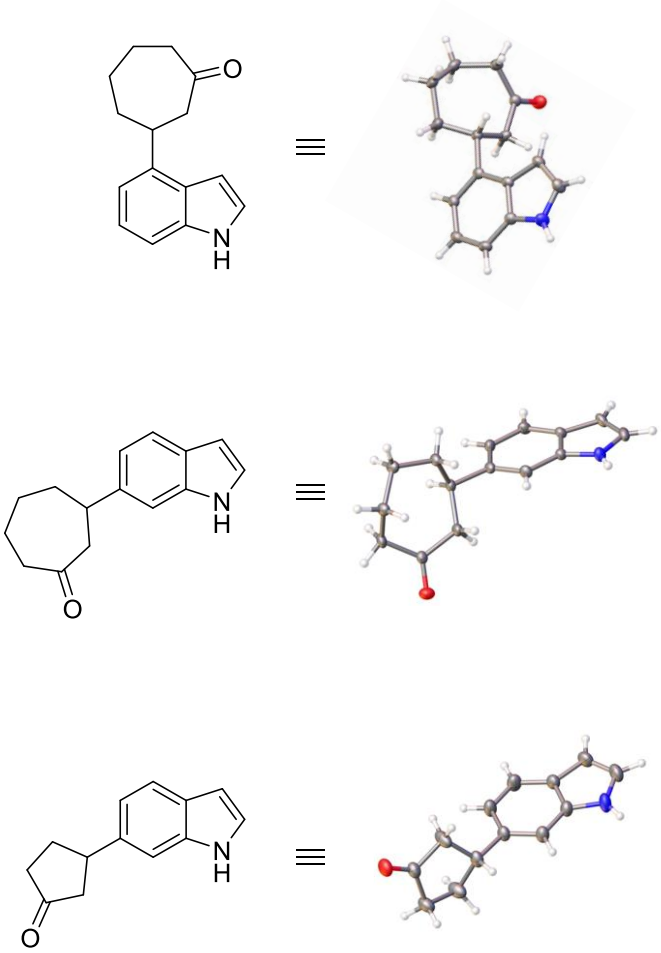

## 8. References


(1) Takao, K. I.; Munakata, R.; Tadano, K. I. *Chem. Rev.* **2005**, *105*, 4779–4807.

(2) Byrne, P. A.; Gilheany, D. G. *Chem. Soc. Rev.* **2013**, *42*, 6670–6696.

(3) Maryanoff, B. E.; Reitz, A. B. *Chem. Rev.* **1989**, *89*, 863–927.

(4) Biffis, A.; Centomo, P.; Del Zotto, A.; Zecca, M. *Chem. Rev.* **2018**, *118*, 2249–2295.

(5) Clayden, J. Greaves, N. Warren, Stuart. in Clayen's Organic Chemistry, *Chapter 22*, Oxford University Press, Oxford, **2012**.

(6) Komnenos, T. *Justus Liebigs Ann Chem* **1883**, *218*, 145–167.

(7) Michael, A. *Journal Fur Praktische Chemie* **1887**, *35*, 349–356.

(8) Kharasch, M. S.; Tawney, P. O. *J. Am. Chem. Soc* **1941**, *63*, 2308–2316.

(9) Lipshutz, B. H.; Kozlowski, J. A.; Breneman, C. M.; Li Li Me-Cu, M. X.; -Cu -Me Lr, M.; Sloan, A. P.; J Am Chem Soc, J. J.; Chem Commun, J. J.; Org, J. J. *J. Am. Chem. Soc.* **1985**, *107*, 3197–3204.

(10) Soai, K.; Yokoyama, S.; Hayasaka, T. *J. Org. Chem.* **1988**, *53*, 4148–4149.

(11) Soai, K.; Hayasaka, T.; Ugajin, S. *Chem. Lett.* **1988**, 1570–1571.

(12) Evans, D. A.; Seidel, D. *J. Am. Chem. Soc.* **2005**, *127*, 9958–9959.

(13) Cacchi, S.; Palmieri, G. *Tetrahedron* **1983**, *39*, 3373–3383.

(14) Cacchi, S.; Misiti, D.; Palmieri, G. *Tetrahedron* **1981**, *37*, 2941–2946.

(15) Ahn, K.-H.; Klassen, B.; Lippard, S. J. *Organometallics* **1990**, *9*, 3178–3181.

(16) Sibi, M. P.; Manyem, S. *Tetrahedron* **2000**, *56*, 8033–8061.

(17) Sawamura, M.; Hamashima, H.; Ito, Y. *J. Am. Chem. Soc.* **1992**, *114*, 8295–8296.

(18) Sakai, M.; Hayashi, H.; Miyaura, N. *Organometallics* **1997**, *16*, 4229–4232.

(19) Takaya, Y.; Ogasawara, M.; Hayashi, T.; Sakai, M.; Miyaura, N. *J. Am. Chem. Soc.* **1998**, *120*, 5579–5580.

(20) Hayashi, T. *Pure Appl. Chem.* **2004**, *76*, 465–475.

(21) Fagnou, K.; Lautens, M. *Chem. Rev.* **2003**, *103*, 169–196.

(22) Hayashi, T.; Takahashi, M.; Takaya, Y.; Ogasawara, M. *J. Am. Chem. Soc.* **2002**, *124*, 5052–5058.

(23) Hayashi, T.; Ueyama, K.; Tokunaga, N.; Yoshida, K. *J. Am. Chem. Soc.* **2003**, *125*, 11508–11509.

(24) Shintani, R.; Okamoto, K.; Hayashi, T. *Org. Lett.* **2005**, *7*, 4757–4759.

(25) Duan, W. L.; Iwamura, H.; Shintani, R.; Hayashi, T. *J. Am. Chem. Soc.* **2007**, *129*, 2130–2138.

(26) Defieber, C.; Paquin, J. F.; Serna, S.; Carreira, E. M. *Org. Lett.* **2004**, *6*, 3873–3876.

(27) Xu, M. H.; Wang, W.; Lin, G. Q. *Org. Lett.* **2000**, *2*, 2229–2232.

(28) Wang, W.; Xu, M. H.; Lei, X. S.; Lin, G. Q. *Org. Lett.* **2000**, *2*, 3773–3776.

(29) Xu, M. H.; Wang, W.; Xia, L. J.; Lin, G. Q. *J. Org. Chem.* **2001**, *66*, 3953–3962.

(30) Jin, S. S.; Wang, H.; Xu, M. H. *Chem. Comm.* **2011**, *47*, 7230–7232.

(31) Takaya, Y.; Ogasawara, M.; Hayashi, T. *Tetrahedron Lett.* **1999**, *40*, 6957–6961.

(32) Cammidge, A. N.; Goddard, V. H. M.; Gopee, H.; Harrison, N. L.; Hughes, D. L.; Schubert, C. J.; Sutton, B. M.; Watts, G. L.; Whitehead, A. J. *Org. Lett.* **2006**, *8*, 4071–4074.

(33) Molander, G. A.; Ellis, N. *Acc. Chem. Res.* **2007**, *40*, 275–286.

(34) Thierig, D.; Umland, F. *Naturwissenschaften* **1967**, *21*, 563–563.

(35) Pucheault, M.; Darses, S.; Genet, J.-P. *Tetrahedron Lett.* **2002**, *43*, 6155–6157.

(36) Pucheault, M.; Darses, S.; Genêt, J. P. *Eur. J. Org. Chem.* **2002**, 3552–3557.

(37) Yamamoto, Y.; Takizawa, M.; Yu, X. Q.; Miyaura, N. *Angew. Chem., Int. Ed. Engl.* **2008**, *47*, 928–931.

(38) Hayashi, T.; Senda, T.; Takaya, Y.; Ogasawara, M. *J. Am. Chem. Soc.* **1999**, *121*, 11591–11592.

(39) Hayashi, T.; Senda, T.; Ogasawara, M. *J. Am. Chem. Soc.* **2000**, *122*, 10716–10717.

(40) Senda, T.; Ogasawara, M.; Hayashi, T. *J. Org. Chem.* **2001**, *66*, 6852–6856.

(41) Chen, G.; Tokunaga, N.; Hayashi, T. *Org. Lett.* **2005**, *7*, 2285–2288.

(42) Shintani, R.; Duan, W. L.; Hayashi, T. *J. Am. Chem. Soc.* **2006**, *128*, 5628–5629.

(43) Dian, L.; Marek, I. *Angew. Chem.* **2018**, *130*, 3744–3748.

(44) Goetzke, F. W.; Hell, A. M. L.; van Dijk, L.; Fletcher, S. P. *Nat. Chem.* **2021**, *13*, 880–886.

(45) Mishra, S.; Karabiyikoglu, S.; Fletcher, S. P. *J. Am. Chem. Soc.* **2023**, *145*, 14221–14226.

(46) Albrecht, F.; Sowada, O.; Fistikci, M.; Boysen, M. M. K. *Org. Lett.* **2014**, *16*, 5212–5215.

(47) Yoshida, K.; Hayashi, T. *Heterocycles* **2003**, *59*, 605.

(48) Chai, G. L.; Zhang, P.; Yao, E. Z.; Chang, J. *J. Org. Chem.* **2022**, *87*, 9197–9209.

(49) Yu, X. Q.; Yamamoto, Y.; Miyaura, N. *Synlett* **2009**, 994–998.

(50) Ye, B.; Yao, J.; Wu, C.; Zhu, H.; Yao, W.; Jin, L.; Dou, X. *ACS Catal.* **2022**, *12*, 2434–2440.

(51) Malapit, C. A.; Luvaga, I. K.; Caldwell, D. R.; Schipper, N. K.; Howell, A. R. *Org. Lett.* **2017**, *19*, 4460–4463.

(52) Cox, P. A.; Leach, A. G.; Campbell, A. D.; Lloyd-Jones, G. C. *J. Am. Chem. Soc.* **2016**, *138*, 9145–9157.

(53) Sravanthi, T. V.; Manju, S. L. *Eur. J. Pharm. Sci.* **2016**, *91*, 1–10.

(54) Sundberg, R. in *The Chemistry of Indoles*, **1970**, pp. 1–92.

(55) Dalpozzo, R. *Chem. Soc. Rev.* **2015**, *44*, 742–778.

(56) Lipshutz, B. H.; Ghorai, S.; Cortes-Clerget, M. *Chem. Eur. J.* **2018**, *24*, 6672–6695.

(57) Shen, T.; Zhou, S.; Ruan, J.; Chen, X.; Liu, X.; Ge, X.; Qian, C. *Adv. Colloid Interface Sci.* **2021**, *287*, 102299.

(58) Lipshutz, B. H.; Isley, N. A.; Moser, R.; Ghorai, S.; Leuser, H.; Taft, B. R. *Adv. Synth. Catal.* **2012**, *354*, 3175–3179.

(59) Khiar, N.; Valdivia, V.; Salvador, Á.; Chelouan, A.; Alcudia, A.; Fernández, I. *Adv. Synth. Catal.* **2013**, *355*, 1303–1307.

(60) Cortes-Clerget, M.; Akporji, N.; Zhou, J.; Gao, F.; Guo, P.; Parmentier, M.; Gallou, F.; Berthon, J. Y.; Lipshutz, B. H. *Nat. Commun.* **2019**, *10*, 2169.

(61) Khiar, N.; Valdivia, V.; Salvador, Á.; Chelouan, A.; Alcudia, A.; Fernández, I. *Adv. Synth. Catal.* **2013**, *355*, 1303–1307.

(62) Salmi, C.; Letourneux, Y.; Brunel, J. M., *Lett. Org. Chem.* **2006**, *3*, 396–401.

(63) Rodríguez, A.; Del Mar Graciani, M.; Angulo, M.; Moyá, M. L. *Langmuir* **2007**, *23*, 11496–11505.

(64) Gabriel, C. M.; Lee, N. R.; Bigorne, F.; Klumphu, P.; Parmentier, M.; Gallou, F.; Lipshutz, B. H. *Org. Lett.* **2017**, *19*, 194–197.

(65) Lipshutz, B. H.; Ghorai, S.; Cortes-Clerget, M. *Chem. Eur. J.* **2018**, *24*, 6672–6695.

(66) Khiar, N.; Salvador, Á.; Chelouan, A.; Alcudia, A.; Fernández, I. *Org. Biomol. Chem.* **2012**, *10*, 2366–2368.

(67) Li, Y.; Xu, M. H. *Chem. Commun.* **2014**, *50*, 3771–3782.

(68) Sipos, G.; Drinkel, E. E.; Dorta, R. *Chem. Soc. Rev.* **2015**, *44*, 3834–3860.

(69) Trost, B. M.; Rao, M. *Angew. Chem. Int. Ed.* **2015**, *127*, 5112–5130.

(70) Borrego, L. G.; Recio, R.; Alcarranza, M.; Khiar, N.; Fernández, I. *Adv. Synth. Catal.* **2018**, *360*, 1273–1279.

(71) Wang, Z.; Xu, M. H. *Org. Biomol. Chem.* **2018**, *16*, 4633–4640.

(72) Wang, H.; Jiang, T.; Xu, M. H. *J. Am. Chem. Soc.* **2013**, *135*, 971–974.

(73) Morton, D.; Pearson, D.; Field, R. A.; Stockman, R. A. *Org. Lett.* **2004**, *6*, 2377–2380.

(74) Lipshutz, B. H.; Isley, N. A.; Moser, R.; Ghorai, S.; Leuser, H.; Taft, B. R. *Adv. Synth. Catal.* **2012**, *354*, 3175–3179.

(75) Prieto, M.; Zurita, E.; Rosa, E.; Muñoz, L.; Lloyd-Williams, P.; Giralt, E. *J. Org. Chem.* **2004**, *69*, 6812–6820.

(76) Wang, Y.; Xie, F.; Lin, B.; Cheng, M.; Liu, Y. *Chem. Eur. J.* **2018**, *24*, 14302–14315.

(77) Zhu, T. S.; Jin, S. S.; Xu, M. H. *Angew. Chem. Int. Ed.* **2012**, *51*, 780–783.

(78) Wu, X.; Ma, W.; Tang, W.; Xue, D.; Xiao, J.; Wang, C. *Chem. Eur. J.* **2022**, *28*, e202201829

(79) Petrone, D. A.; Yoon, H.; Weinstabl, H.; Lautens, M. *Angew. Chem. Int. Ed.* **2014**, *53*, 7908–7912.

(80) Lv, X.; Xiang, Q.; Zeng, Q. *Org. Prep. Proced. Int.* **2014**, *46*, 164–175.

(81) Kudriashova, E. S.; Yarushina, M. A.; Gavryushin, A. E.; Grishin, I. D.; Malysheva, Y. B.; Otvagin, V. F.; Fedorov, A. Y. *Org. Lett.* **2023**, *25*, 4996–5000.

(82) Warsitz, M.; Doye, S. *Chem. Eur. J.* **2020**, *26*, 15121–15125.

# Appendix

EurJOC
European Journal of Organic Chemistry

Research Article
doi.org/10.1002/ejoc.202300790

Chemistry Europe
European Chemical Societies Publishing

www.eurjoc.org

# Access to Electron-Rich Dibenzofurans through $NBu_4OAc$-Mediated Palladium Catalysis

Mark Power,[a] Katrina Mackey,[a] Mark E. Light,[b] David J. Jones,[c] and Gerard P. McGlacken*[a]

Dibenzofuran and its derivatives are ubiquitous and important medicinal and natural products. Many contain electron-rich aryl rings. Forming the key intramolecular Ar–Ar bond using traditional cross-coupling is difficult. The C–H functionalisation (C–H activation) approach is, in principle, far more useful. However, we previously found that the well-established conditions, which promote C–H functionalisation through Concerted Metalation-Deprotonation (CMD), proved unsatisfactory. Herein, we report a Pd-catalysed C–H functionalisation protocol that works with electron-rich arenes. We use tetrabutylammonium acetate ($NBu_4OAc$), which we suspect can act as base, ligand and solvent, rendering this protocol a simple and efficient route to electron-rich dibenzofurans.

## Introduction

The dibenzofuran framework **1**, and its analogues, represent a prominent class of natural products and biologically active entities.[1–3] Consequently, synthetic routes toward dibenzofurans have garnered keen interest from synthetic chemists.[4–16] Retrosynthetic analysis of dibenzofuran reveals two separate intramolecular coupling strategies (Figure 1A): C–C bond formation through a diarylether **2** (Pathway A), or C–O bond formation through a biaryl motif **3** (Pathway B). Direct arylation has been applied successfully to form a decent range of dibenzofurans. Fagnou, in particular, demonstrated the power of the strategy to target C–H bonds in this context.[6–8] The mechanism which evolved from the early studies on this work was termed Concerted Metalation-Deprotonation (CMD) or Ambiphilic Metal-Ligand Assistance (AMLA).[17–19] This mechanistic pathway usually relies on the 'acidity' of the aryl C–H bond and thus, is less applicable to electron-rich substrates. As such, the methodology can be less successful, depending on the electronic properties of the diarylether substituent.[4–16] That said, it should be noted that a number of mechanisms can be envisaged here,[20,21] most recently one which relies on the transmetalation step (rather than the C–H cleavage step) to determine regioselectivity.[22] Recently we reported a methodology on the synthesis of substituted dibenzofurans through a palladium-mediated intramolecular direct arylation of a diarylether utilising a quinoline ligand (Figure 1B).[14] This method proved particularly useful for electron-deficient systems,[23] but the scope of the transformation was very limited for more valuable electron-rich examples. Naturally occurring and medicinally relevant dibenzofuran derivatives frequently contain electron-rich aryl rings and electron-donating groups (Figure 1C)[2,24] and thus, there is a need for practical and robust methodologies that access these highly valuable targets.

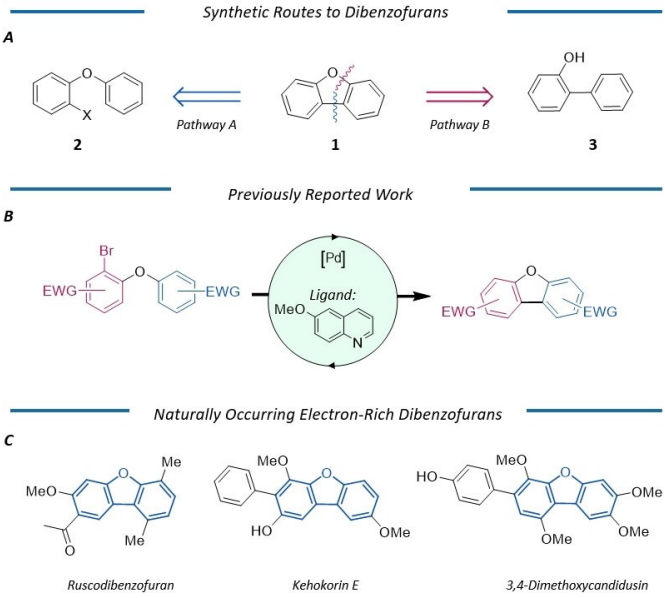


**Figure 1.** Background to dibenzofurans.

More broadly, the optimisation of chemical structures by altering the electron donating and withdrawing properties of substituents is a common approach in medicinal chemistry,

[a] M. Power, Dr. K. Mackey, Dr. G. P. McGlacken
School of Chemistry, University College Cork
Ireland and Analytical and Biological Chemistry Research Facility (ABCRF)
University College Cork
T12 YN60 Cork (Ireland)
E-mail: g.mcglacken@ucc.ie

[b] Dr. M. E. Light
Chemistry Department, University of Southampton
University Road, Southampton SO17 1BJ (United Kingdom)

[c] Dr. D. J. Jones
EaStCHEM School of Chemistry
University of Edinburgh Joseph Black Building
David Brewster Road, Edinburgh, EH9 3FJ (United Kingdom)

Supporting information for this article is available on the WWW under https://doi.org/10.1002/ejoc.202300790

material sciences and numerous other areas of chemical synthesis.[25] Thus, it is important that new methodologies incorporating electron donating and electron withdrawing substituents are developed, to further access the required chemical space. Therefore, even for the most innovative new methodologies, accessing the full breadth of substrate scope is challenging.[26–30]

## Results and Discussion

As mentioned, previous work in our group investigated an intramolecular C–H activation approach to forming dibenzofurans, which faltered when electron-rich substrates were employed.[14] During the evaluation of the substrate scope, we noticed rapid formation of palladium black when electron-rich substrates were used.

We initially considered that the use of a palladium scavenger such as tetrabutylammonium acetate ($NBu_4OAc$) might prevent palladium aggregation, leading to better conversion. We hoped this reagent could also act as a base, avoiding the need for added inorganic base.[31] Indeed, initial investigations improved the yield for electron-rich substrates over our previous results, and good to excellent yields (up to 96% isolated) were observed (Table, entry 1–3). Lowering the temperature of the reaction gave reduced yields (Table 1 entry, 4). With these conditions to hand, we were able to reduce the Pd loading (2.5 mol%) while maintaining excellent yield (Table 1, entry 5). We also investigated the use of tetramethylammonium acetate ($NMe_4OAc$), but this gave lower yield (Table 1, entry 6). Finally, the potentially synergistic use of $NBu_4Cl$ and $K_2CO_3$,[32] was trialled in the system but gave a lower yield of 67% (Table 1, entry 7). Various other conditions were tried but gave inferior results (see Supporting Information for details).

With conditions optimised, we tested this protocol to access a range of dibenzofurans (Scheme 1). It was also important to us that C–H functionalisation could occur on either ring, irrespective of the nature of the substituent, which of course meant that the halogenated aryl ring could also be derivatised. Both these goals were met, and in the case of **5a** and **5b**, C–H functionalisation was enacted on both the halogen-bearing and the halogen-free aryl ring, while also showing tolerance to fluorinated precursors. Another electron-rich substrate was synthesised in **5c** giving an excellent yield and regioselectivity (90% and 96:4). The high yield of **5c** was pleasing to see as this particular substrate was classed as a limitation when investigated using our previously developed methodology. Similarly, the reaction conditions allowed the *m*-methoxy dibenzofuran **5d** to be formed in 94%, with a regioselectivity of 97:3.

Diarylamines were also found to be compatible with the protocol allowing the carbazole motif **5e** to be isolated in 89% yield, in comparison to a moderate yield of 50%, previously reported.[14] Further functionalisation was demonstrated with the acetyl substituted compound **5f** which was furnished in excellent yield (95%). Finally, heterocyclic dibenzofurans were also tolerated and we were delighted to see that benzofuropyridine **5g** was formed, and isolated in 84% yield.

Overall, the methodology successfully handled a range of substrates including electron-deficient, electron-rich and heteroaromatic diarylethers. Importantly, the methodology also functioned well, irrespective of which ring contained the halogen group, providing flexibility as a synthetic tool towards dibenzofuran targets.

Given that this protocol had clearly surpassed our previously published work and given the ubiquity of the dibenzofurans with multiple methoxy groups, we challenged our methodology with highly electron-rich diarylether precursors, reminiscent of naturally occurring dibenzofuran scaffolds.

**Table 1.** Reaction optimisation of the electron-rich model substrate.

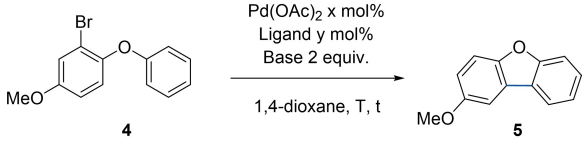


| Entry | Base | $Pd(OAc)_2$ [mol%] | Ligand [mol%] | *t* [h] | Yield[a] [%] |
|---|---|---|---|---|---|
| 1 | $NBu_4OAc$ | 5 | SPhos (10) | 24 | 81 |
| 2 | $NBu_4OAc$ | 5 | $PCy_3.HBF_4$ (10) | 24 | 96[b] |
| 3 | $NBu_4OAc$ | 5 | $PCy_3.HBF_4$ (10) | 16 | 66 |
| 4[c] | $NBu_4OAc$ | 5 | $PCy_3.HBF_4$ (10) | 24 | 41 |
| 5 | $NBu_4OAc$ | 2.5 | $PCy_3.HBF_4$ (5) | 24 | 95[b] |
| 6 | $NMe_4OAc$ | 2.5 | $PCy_3.HBF_4$ (5) | 24 | 74 |
| 7 | $NBu_4Cl$ & $K_2CO_3$ | 2.5 | $PCy_3.HBF_4$ (5) | 24 | 67 |

[a] Measured using $^1H$ NMR spectroscopy with 1,3,5-trimethoxybenzene as an internal standard; [b] compound is isolated after column chromatography; [c] reaction is run at 100 °C instead of 125 °C.

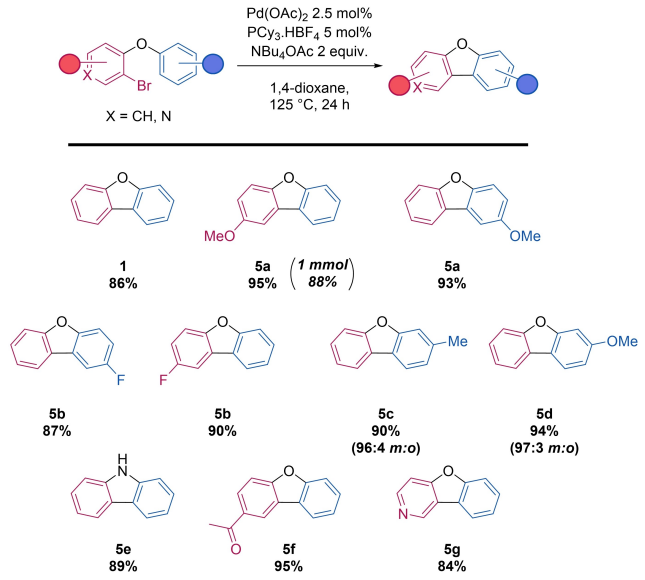


**Scheme 1.** Substrate scope of the intramolecular ring closure to furnish derivatised dibenzofurans.

Research Article
doi.org/10.1002/ejoc.202300790



To a methodology relying on a CMD/AMLA mechanism, we suspected these substrates would represent a significant challenge.[19] However, in our case, product **6a** could be formed in a yield of 91% and surprisingly, even the trimethoxy derivative of **6b** could be formed in 90% yield. Crystal structures were obtained for **6a** and **6b** (Scheme 2). A lower yield of 42% was obtained for substrate **6c**, nevertheless, this is a good, usable yield considering the electronic and steric challenges this substrate poses. An excellent yield of 95% was also observed for the dimethyl substrate **6d** using this protocol.

We next investigated the efficiency of the reaction in the absence of phosphine ligand. Pleasingly $NBu_4OAc$ facilitated the ring closure, giving 70% of product formed using 2.5 mol% of palladium acetate in dioxane (Table 2, entry 1). Building on this initial success, we examined the use of excess $NBu_4OAc$ in the absence of phosphine ligand and solvent. Gratifyingly, we were able to remove the need for both added ligand and added solvent using the organic base neat, obtaining a 93% yield (Table 2 entry 3). This interesting result leads us to believe that the $NBu_4OAc$ can potentially play a tripartite role in the reaction: as solvent, base and ligand. It also exhibits potential for performing these reactions in a green fashion with no requirement for solvent (DMF and NMP are commonly used in these type of protocols), added phosphines, or inorganic base.

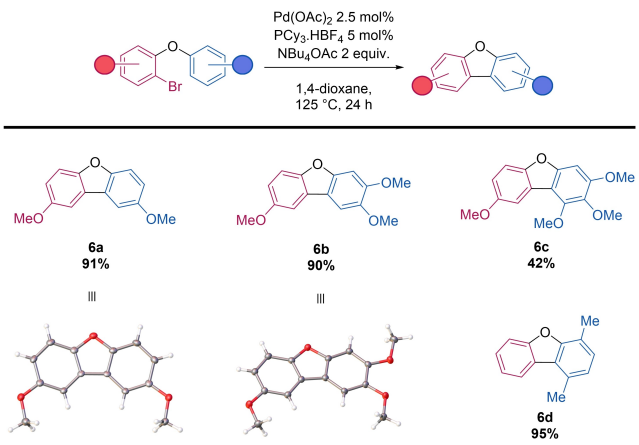


**Scheme 2.** Substrate scope of electron-rich arene precursors.

**Table 2.** Phosphine free and $PBu_4OAc$ investigations.

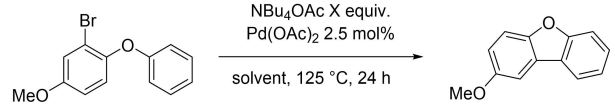


| Entry | Catalyst | Base [equiv.] | Solvent | Yield[a] [%] |
|---|---|---|---|---|
| 1 | $Pd(OAc)_2$ | $NBu_4OAc$ (2) | 1,4-dioxane | 70 |
| 2 | $Pd(OAc)_2$ | $NBu_4OAc$ (5) | Neat | 81 |
| 3 | $Pd(OAc)_2$ | $NBu_4OAc$ (10) | Neat | 93[b] |
| 4[c] | $Pd(OAc)_2$ | $PBu_4OAc$ (2) | 1,4-dioxane | 81 |
| 5 | $PdCl_4(NBu_4)_2$ | $NBu_4OAc$ (2) | 1,4-dioxane | 20 |

[a] Measured using $^1$H NMR spectroscopy with 1,3,5-trimethoxybenzene as an internal standard; [b] yield is isolated after column chromatography; [c] reaction is run for 2 h.

**Table 3.** Comparison of our methodology with the literature conditions.

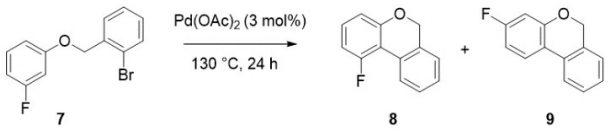


| Entry | Ligand (6 mol%) | Solvent | Base (2 equiv.) | Ratio[a] **8:9** |
|---|---|---|---|---|
| 1- Fagnou[7] | $P^tBu_2Me.HBF_4$ | DMA | $K_2CO_3$ | 6.9:1[b] |
| 2 | $PCy_3.HBF_4$ | 1,4-dioxane | $NBu_4OAc$ | 1:1 |

[a] Ratio is measured by $^1$H NMR spectroscopy; [b] ratio is as reported in the literature – we performed the same reaction and found the same isomer to predominantly form, but in varying ratios.

Finally, Liu and co-workers have shown that an alternative base, in the form of a phosphonium salt, can reduce reaction time as well as temperature in N-aryl coupling reactions.[33] Thus, tetrabutylphosphonium acetate ($PBu_4OAc$) was employed in our reaction, and interestingly within 2 hours, gave the desired product in 81% (Table 2, entry 4). Additionally, Hull and co-workers have shown that tetraalkylammonium salts can form active catalytic species with palladium chloride.[34] This palladate species was trialled in our system but proved inferior, giving only 20% yield (Table 2, entry 5).

Fagnou noted that intramolecular C–H bond functionalisation is not significantly influenced by the electronic nature of the arene, and that this is uncharacteristic of an $S_EAr$ pathway.[35] Indeed he noted that under his (CMD) conditions, in an intramolecular competition experiment, it is the H *ortho* to F that is cleaved (Table 3, entry 1). The same substrate using our conditions, gave a *ca.* 1:1 ratio of both constitutional isomers. Overall it is likely that a different mechanism is operative here, most likely involving electrophilic palladation.[36] Further mechanistic investigations are underway and will be reported in due course.

## Conclusions

In conclusion, we have developed a robust, efficient methodology to synthesise a range of dibenzofurans. In particular, difficult-to-access, electron-rich scaffolds, in good to excellent yields. Tetraalkylammonium salts, particularly $NBu_4OAc$, proved the linchpin, and appears to act as solvent, ligand and base in the reaction.

## Experimental Section

### General Information

Solvents and reagents were used as obtained from commercial sources and without purification. Column chromatography was

carried out using 60 Å (35-70 μm) silica. TLC was carried out on precoated silica gel plates (Merck 60 PF254). The developed plates were visualised under UV light. Melting points were obtained on a uni-melt Thomas Hoover Capillary melting point apparatus. NMR spectra were run in $CDCl_3$ or $(CD_3)_2SO$ using TMS as the internal standard at 25 °C unless otherwise specified. $^1$H NMR (600 spectra) $^1$H NMR (500 MHz) spectra, $^1$H NMR (400 MHz) spectra and $^1$H NMR (300 MHz) spectra were recorded on Bruker Avance 600, Bruker Avance 500, Burker Avance 400 and Bruker Avance 300 NMR spectrometers respectively. $^{13}$C (150 MHz) spectra, $^{13}$C (125 MHz) spectra, $^{13}$C (100 MHz) spectra and $^{13}$C (75.5 MHz) spectra were recorded on Bruker Avance 600, Bruker Avance 500, Burker Avance 400 and Bruker Avance 300 NMR spectrometers respectively in proton decoupled mode. $^{19}$F NMR (376 MHz) and $^{19}$F NMR (282 MHz) spectra were recorded on a Bruker Avance 400 and Bruker Avance 300 NMR spectrometers respectively in proton decoupled mode. Chemical shifts $\delta_H$ and $\delta_C$ are expressed as parts per million (ppm), positive shift being downfield from TMS; coupling constants (*J*) are expressed in hertz (Hz). Splitting patterns in $^1$H NMR spectra are designated as s (singlet), br s (broad singlet), d (doublet), dd (doublet of doublets), dt (doublet of triplets), t (triplet), q (quartet) and m (multiplet). For $^{13}$C NMR spectra, the number of attached protons for each signal was determined using the DEPT pulse sequence run in the DEPT-90 and DEPT-135 modes. Nominal mass spectra were recorded on a Waters Quattro Micro triple quadrupole spectrometer (QAA1202) in ESI mode using 50% acetonitrile–water containing 0.1% formic acid as eluent. High resolution mass spectra (HRMS) were recorded on a Waters LCT Premier Time of Flight spectrometer (KD160) or a Waters Vion IMS mass spectrometer (SAA055 K) in ESI mode using 50% acetonitrile-water containing 0.1% formic acid as eluent. Samples (max. 1 mg) were dissolved in acetonitrile, methanol, water or 10% DMSO/acetonitrile. The Microanalysis Laboratory, National University of Ireland, Cork, performed elemental analysis using a Perkin-Elmer 240 and Exeter Analytical CE440 elemental analysers.

### Experimental Procedure for the synthesis of compounds 1, 5a–g and 6a–d

Diarylether (1 equiv.), $Pd(OAc)_2$ (2.5 mol%), $PCy_3.HBF_4$ (5 mol%), $NBu_4OAc$ (2 equiv.) and 1,4-dioxane (2 mL/mmol) were added to a sealed reaction vial equipped with a magnetic stir bar. The reaction mixture was stirred at 125 °C for 24 hours in a multi-reaction heating mantle. After 24 hours the reaction mixture was cooled to room temperature and diluted with DCM (15 mL), filtered through a pad of Celite® and the solvent was concentrated under reduced pressure. The resulting residue was then purified by column chromatography using hexanes:DCM as eluent on silica gel to elute the title products.

## Supporting Information

Additional references cited within the Supporting Information.[37–48]

## *Acknowledgements*

This research was supported by the Irish Research Council (GOIPG/2019/952) and Science Foundation Ireland, through the Research Frontiers Programme (21/FFP-A/8784) and the Synthesis and Solid State Pharmaceutical Centre (SSPC) (SFI/12/RC/2275 and SFI/ 846 12/RC2275_P2). Open Access funding provided by IReL.

## *Conflict of Interests*

The authors declare no conflict of interest.

## *Data Availability Statement*

The data that support the findings of this study are available in the supplementary material of this article.

**Keywords:** Dibenzofuran · palladium · catalysis, tetraalkylammonium salt · electron-rich

[1] S. R. Patpi, L. Pulipati, P. Yogeeswari, D. Sriram, N. Jain, B. Sridhar, R. Murthy, A. T. Devi, S. V. Kalivendi, S. Kantevari, *J. Med. Chem.* **2012**, *55*, 3911–3922.
[2] B. E. Love, *Eur. J. Med. Chem.* **2015**, *97*, 377–387.
[3] A. Momotake, N. Lindegger, E. Niggli, R. J. Barsotti, G. C. R. Ellis-Davis, *Nat. Methods* **2006**, *3*, 35–40.
[4] J. Liu, A. E. Fitzgerald, N. S. Mani, *J. Org. Chem.* **2008**, *73*, 2951–2954.
[5] Y. Wei, N. Yoshikai, *Org. Lett.* **2011**, *13*, 5504–5507.
[6] L. C. Campeau, P. Thansandote, K. Fagnou, *Org. Lett.* **2005**, *7*,1857–1860.
[7] L. C. Campeau, M. Parisien, A. Jean, K. Fagnou, *J. Am. Chem. Soc.* **2006**, *128*,581–590.
[8] B. Liégault, D. Lee, M. P. Huestis, D. R. Stuart, K. Fagnou, *J. Org. Chem.* **2008**, *73*, 5022–5028.
[9] H. Zhao, K. Yang, H. Zheng, R. Ding, F. Yin, N. Wang, Y. Li, B. Cheng, H. Wang, H. Zhai, *Org. Lett.* **2015**, *17*, 5744–5747.
[10] N. Panda, I. Mattan, D. K. Nayak, *J. Org. Chem.* **2015**, *80*, 6590–6597.
[11] J. W. Lockner, D. D. Dixon, R. Risgaard, P. S. Baran, *Org. Lett.* **2011**, *13*, 5628–5631.
[12] C. Wang, I. Piel, F. Glorius, *J. Am. Chem. Soc.* **2009**, *131*, 4194–4195.
[13] B. Xiao, T. Gong, Z. Liu, D. Luo, J. Xu, L. Liu, *J. Am. Chem. Soc.* **2011**, *133*, 9250–9253.
[14] K. Mackey, D. J. Jones, L. M. Pardo, G. P. McGlacken, *Eur. J. Org. Chem.* **2021**, *2021*, 495–498.
[15] T. Matsuzawa, K. Uchida, S. Yoshida, T. Hosoya, *Org. Lett.* **2017**, *19*, 5521–5524.
[16] S. Prado, V. Toum, B. Saint-Joanis, S. Michel, M. Koch, S. T. Cole, F. Tillequin, Y. L. Janin, *Synthesis* **2007**, *10*, 1566–1570.
[17] P. Gandeepan, T. Muller, D. Zell, G. Cera, S. Warratz, L. Ackermann, *Chem. Rev.* **2019**, *119*, 2192–2452.
[18] Y. Boutadla, D. L. Davies, S. A. Macgregor, *Dalton Trans.* **2009**, 5820–5831.
[19] M. Lafrance, K. Fagnou, *J. Am. Chem. Soc.* **2006**, *128*, 16496–16497.
[20] K. M. Engle, D–H. Wang, J–Q. Yu, *J. Am. Chem. Soc.* **2010**, *132*, 14137–14151.
[21] S. I. Gorelsky, *Coord. Chem. Rev.* **2013**, *257*, 153–164.
[22] D. Kim, G. Choi, W. Kim, D. Kim, Y. K. Kang, H. H. Soon, *Chem. Sci.* **2021**, *12*, 363–373.
[23] The introduction of electronic withdrawing groups (e.g. F and $CF_3$) to heterocyclic systems is an important strategy see R. Filler, Y. Kobayashi, L. M. E. Yagupolskii, *Organofluorine Compounds in Medicinal Chemistry and Biomedical Applications*, Elsevier, Amsterdam, Netherlands, **1993** and S. L. Clarke, G. P. McGlacken, *Tetrahedron* **2015**, *19*, 2906–2913 and citations therein.
[24] W. Zhang, W. Wei, J. Shi, C. Chen, G. Zhao, R. Jiao, *Bioorg. Med. Chem. Lett.* **2015**, *25*, 2698–2701.
[25] S. Dastmalchi, M. Hamzeh-Mivehroud, B. Sokouti in *Quantitative Structure-Activity Relationship, A Practical Approach*, *1st ed.*, Routledge CRC Press, USA, **2021**.
[26] Y.-H. Zhang, B.-F. Shi, J.-Q. Yu, *J. Am. Chem. Soc.* **2009**, *131*, 5072–5074.
[27] M. Li, M. Shang, H. Xu, X. Wang, H–X. Dai, J–Q. Yu, *Org. Lett.* **2019**, *21*, 540–544.

[28] L–Y. Liu, J. X. Qiao, K–S. Yeung, W. R. Ewing, J–Q. Yu, *J. Am. Chem. Soc.* **2019**, *141*, 14870–14977.
[29] R. E. Tundel, K. W. Anderson, S. L. Buchwald, *J. Org. Chem.* **2006**, *71*, 430–433.
[30] M. A. Mantell, M. R. Lasky, M. Lee, M. Remy, M. S. Sanford, *Org. Lett.* **2021**, *23*, 5213–5217.
[31] F. Bellina, M. Lessi, C. Manzini, *Eur. J. Org. Chem.* **2013**, 5621–5630.
[32] T. Jeffrey, *Tetrahedron* **1996**, *52*, 10113–10130.
[33] C. Yang, Y. Fu, Y. Huang, J. Yi, Q. Guo, L. Liu, *Angew. Chem. Int. Ed. Engl.* **2009**, *48*, 7398–7401.
[34] D. G. Kohler, S. N. Gockel, J. L. Kennemur, P. J. Waller, K. L. Hull, *Nat. Chem.* **2018**, *10*, 333–340.
[35] D. Lapointe, K. Fagnou, *Chem. Lett.* **2010**, *39*, 1118–1126.
[36] For a discussion on the mechanism of Direct Arylation see: a) D. Alberico, M. E. Scott, M. Lautens, *Chem. Rev.* **2007**, *107*, 174–238; b) G. P. McGlacken, L. M. Bateman, *Chem. Soc. Rev.* **2009**, *38*, 2447–2464.

Manuscript received: August 1, 2023
Revised manuscript received: September 6, 2023
Accepted manuscript online: September 13, 2023
Version of record online: September 28, 2023

ORGANIC PROCESS RESEARCH & DEVELOPMENT
OPR&D

pubs.acs.org/OPRD

Review

# Organolithium Bases in Flow Chemistry: A Review

Mark Power, Emma Alcock, and Gerard P. McGlacken*

Cite This: *Org. Process Res. Dev.* 2020, 24, 1814−1838

Read Online

ACCESS | Metrics & More | Article Recommendations

**ABSTRACT:** Flow chemistry is a continually emerging and ever-growing area of synthetic organic chemistry. It provides an orthogonal approach to traditional batch chemistry, oftentimes allowing for more efficient routes to desired target molecules. It is generally accepted that flow chemistry offers a valuable change to the process landscape. From a process perspective, there are many advantages associated with flow chemistry over traditional batch chemistry, the most prominent of which is an increased safety profile with the use of highly reactive chemical species, such as organolithiums. These reagents are highly valuable species for the efficient synthesis of pharmaceutical intermediates. Disadvantageously, use of these reagents on commercial scale is severely hindered by the highly energetic nature of the reaction intermediates and their concomitant safety risk. Flow chemistry provides a viable platform for use of these reagents, offering a high degree of control over reaction parameters. In this review, we present a comprehensive account of the published literature implementing the use of organolithium reagents as strong bases for deprotonation reactions in flow systems.

**KEYWORDS:** *flow chemistry, organolithium, base, deprotonation*



## INTRODUCTION

The recent and rapid development of flow chemistry has in many cases led to an orthogonal approach to traditional batch chemistry. The translation of a synthetic protocol from batch to continuous flow, along with the development of new continuous flow chemistry, can have a plethora of benefits, including the development of new reactivity patterns, improved reaction efficiency, and enhanced scalability.[1−3] However, a cornerstone of flow chemistry is its enhanced safety profile. This facet of flow chemistry allows highly reactive reagents to be applied to large-scale reactions, which would not be feasible using flask chemistry. A review by Stevens and co-workers[4] illustrates how many hazardous reagents such as diazo, diazonium, azide, and organometallic species are successfully and safely utilized in continuous processing.

Organometallic species such as organolithium and Grignard reagents are principal species in many organic transformations, but their scale-up is often hindered by their highly reactive nature. Flow chemistry has enabled a safer regime for the employment of organometallics, and reviews by Nagaki,[5] Luisi,[6] and Piccardi[7] have showcased many examples of organometallic chemistry transferred from a flask operation to a flow platform.

Organolithium reagents are among the most reactive and arguably important species in organic synthesis, and their use is widespread across numerous synthetic transformations. The polar C−Li bond allows the reagent to act as a strong base or nucleophile in the formation of new C−C bonds. However, despite the undoubted usefulness of organolithium species in organic synthesis, their safety profile often hinders their scalability. The heat dissipation required when these reagents are used is difficult to achieve, and therefore, their use on an industrial scale has proven to be an onerous task. Additionally, large-scale use of organolithium reagents results in the formation of precipitates, presenting the additional challenge of solubility. A continuous flow chemistry platform provides a viable alternative to traditional batch chemistry for these reactions. The high surface-to-volume ratio available in microreactors offers a means to circumvent a number of problems due to much improved methods of heat dissipation and, in turn, temperature control and energy transfer. Indeed, in certain applications even higher reaction temperatures may be tolerated in flow.

Consequently, the use of organolithium reagents in continuous flow systems is a very topical area of research. Organolithiums can be used to facilitate lithium−halogen exchange reactions or as strong bases in the construction of new molecular entities. The excellent reviews by Nagaki,[5] Luisi,[6] and Piccardi[7] predominantly examine organolithium-mediated lithium−halogen exchange reactions.

This review aims to outline developments concerning the use of organolithium bases in continuous processes. To date, the concept of performing a deprotonation step via an organolithium species in flow chemistry has not been covered in a comprehensive review. Herein we evaluate the existing literature involving the use of organolithium species as strong bases in continuous processes. One of our aims is to describe the rationale and infrastructure behind translating a process

**Special Issue:** Flow Chemistry Enabling Efficient Synthesis

**Received:** March 6, 2020
**Published:** April 30, 2020

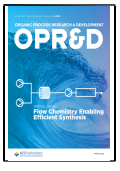





https://dx.doi.org/10.1021/acs.oprd.0c00090
*Org. Process Res. Dev.* 2020, 24, 1814−1838

from batch to continuous flow, as well as detailing the scalability.

This review categorizes the available literature by the organolithium base selected for the scheme, namely, *n*-butyllithium (*n*BuLi), lithium diisopropylamide (LDA), lithium bis(trimethylsilyl)amide (lithium hexamethyldisilazide, LiHMDS), and other organolithium bases, including phenyllithium (PhLi), *sec*-butyllithium (*s*BuLi), and *n*-hexyllithium (*n*HexLi). It is worth noting that the use of *tert*-butyllithium (*t*BuLi) in continuous flow chemistry remains absent in the available literature. The structures of these organolithiums and their respective p$K_a$ values are shown in Figure 1.[8,9] Figure 2 depicts the symbols used throughout to illustrate the variety of flow chemistry components discussed in this review.

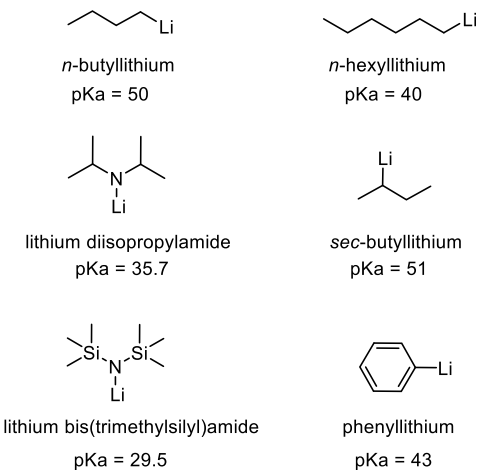


**Figure 1.** Chemical structures of organolithium bases. Quoted p$K_a$ values are of the conjugate acid. The previously published value of 40 for *n*-hexyllithium[8] is surprising low, and is likely to be closer to that of *n*-butyllithium (ca. 50).

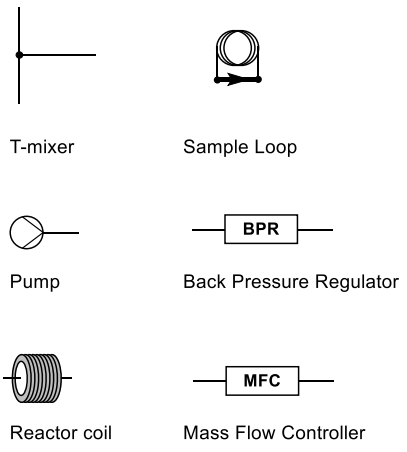


**Figure 2.** Overview of continuous flow symbols.

## N-BUTYLLITHIUM

*n*-Butyllithium is one of the most commonly employed organolithium reagents in organic synthesis.[10] A publication by Ley and co-workers outlines the use of *n*BuLi in the construction of disubstituted alkynes.[11] The authors designed a low-temperature continuous flow platform where *n*BuLi and a variety of monosubstituted aryl alkynes were used to generate a series of disubstituted alkynes. The design of the system involves a series of five reactor coils, arranged to mimic the batch reaction. In batch, this reaction has inherent reactivity issues, resulting in the need for precise temperature control. The intermediate ortho-fluorinated aryllithium species has the tendency to undergo ortho elimination if the temperature is not accurately controlled. This ortho elimination pathway produces an unstable benzyne intermediate, which, coupled with the exothermic nature of this decomposition, presents a potential saftey risk upon scale-up. A flow chemistry system allows for precise reaction and temperature control, consequently removing the undesired ortho elimination pathway and the concurrent safety risk.

This continuous process used three loading loops to supply the five-coil platform with their respective reagents. The alkyne moiety and the organolithium base were both pumped through precooling units before coming together in the first reactor (RX 1) to generate the carbanion intermediate. This intermediate then progressed to meet a suitable electrophile, supplied to the system through a loading loop and a subsequent precooling unit to react in reactor 2 (RX 2). All of the reactors and precooling units were maintained at −40 °C. The authors tested five combinations of substituted aromatic alkynes and electrophile substrates on this platform to successfully afford products of type **1** in yields of 86−90% (Figure 3). Optimization of temperature and *n*BuLi equivalents allowed the substrate scope to be expanded to *N*-methylimidazole and an Evans oxazolidinone auxiliary in yields of 75% and 53%, respectively. Substituted fluoroaromatic substrates were also tolerated when reacted with different electrophiles at −50 °C via fluorine directed ortho lithiation. The authors reported 13 such examples of ortho-substituted aryl products **2** in yields of 62−92% (Figure 4). It is worth noting that the presence of a nitrile group on the fluoroaromatic system meant that only the use of LDA yielded the desired product. It is thought that the steric bulk of LDA was necessary to prevent addition to the nitrile group. These substituted fluoroaromatic substrates were additionally reacted with $CO_2$ at −50 °C to produce carboxylic acids **3** in yields of 64−74% (Figure 5). The nitrile-containing fluoroaromatic once again required LDA to yield the desired product.

In work by Yoshida,[12] "flash chemistry" is used to avoid the issues concerning competing $\beta$-elimination associated with the use of 2-halovinyllithium in batch mode, thereby allowing the creation of synthetically useful substituted alkenes by the use of these unstable intermediates before they decompose. Initially, deprotonation of *trans*-1,2-dichloroethene by *n*BuLi yields 1,2-dichlorovinyllithium. In batch, this step requires cryogenic conditions and is usually performed at −78 °C or below. At 0 °C in batch operation, with a slight excess of *n*BuLi and subsequent addition of benzaldehyde, no conversion to the desired product was attained. A flow scheme was designed to replicate these reaction conditions. The *trans*-1,2-dichloroethene and *n*BuLi were delivered to the system via syringe pumps and then brought together in a T-mixer to react for a short residence time. The resulting carbanion was then progressed to a second T-mixer, where it was mixed with an electrophile stream to generate the desired product. It was noticed that an increase in residence time of the deprotonation step could favor the undesired $\beta$-elimination of the *trans*-1,2-dichlorovinyllithium. Additionally, in continuous flow, a much higher temperature of 0 °C gave optimal results. Lower temperatures resulted in a much reduced yield at a given residence time. Figure 6 illustrates a multistep flow platform


https://dx.doi.org/10.1021/acs.oprd.0c00090
Org. Process Res. Dev. 2020, 24, 1814−1838

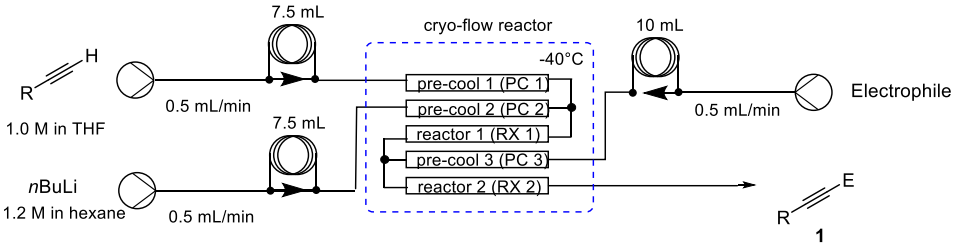


**Figure 3.** Initial five-coil setup for deprotonation and electrophile quench of alkynes, *N*-methylimidazole, and an Evans oxazolidinone auxiliary.

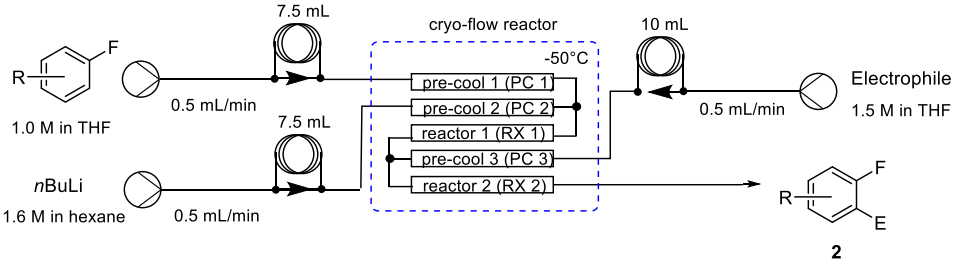


**Figure 4.** Five-coil setup for the synthesis of aromatic building blocks using a fluorine-directed ortho lithiation approach.

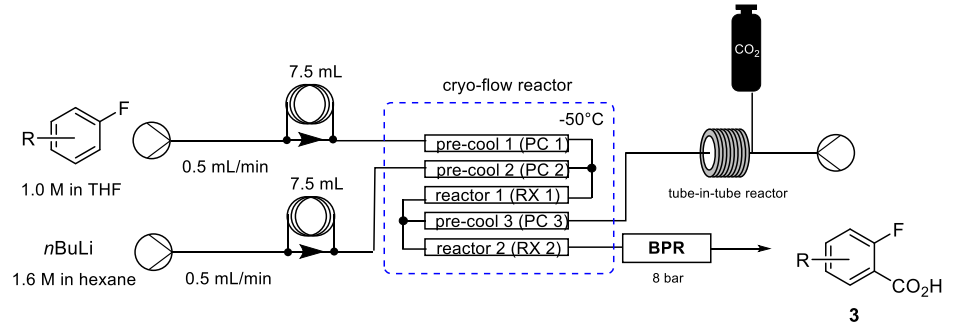


**Figure 5.** Five-coil setup coupled with a tube-in-tube reactor to deliver $CO_2$ as the electrophile for the ortho-lithiated fluoroaromatics.

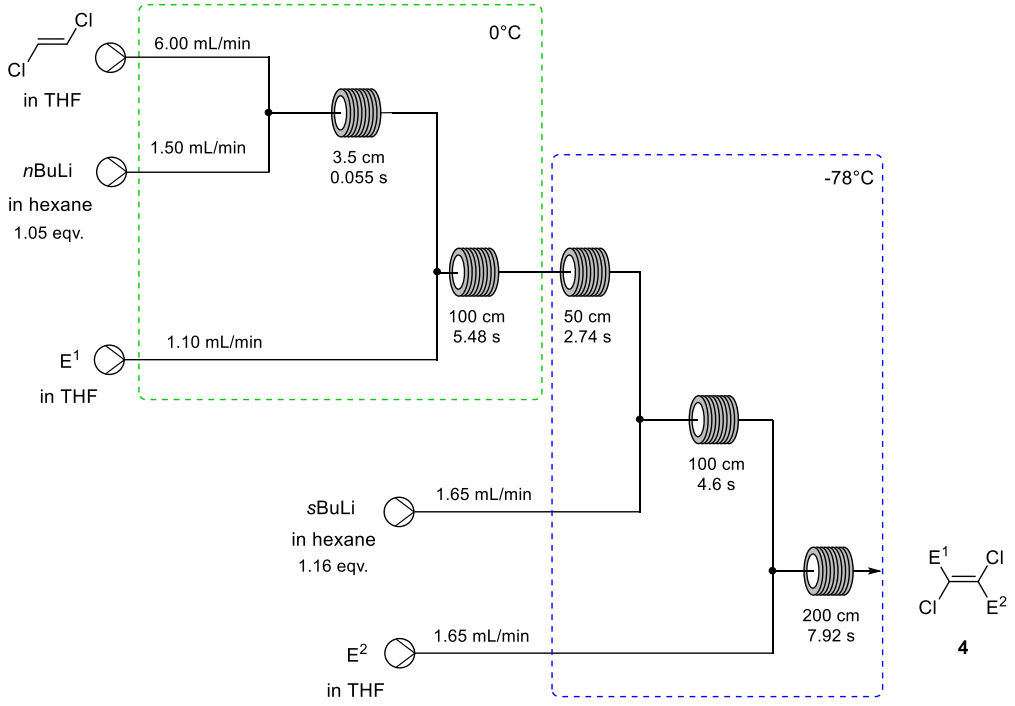


**Figure 6.** Flow platform for the synthesis of disubstituted dichloroalkenes.



https://dx.doi.org/10.1021/acs.oprd.0c00090
Org. Process Res. Dev. 2020, 24, 1814−1838

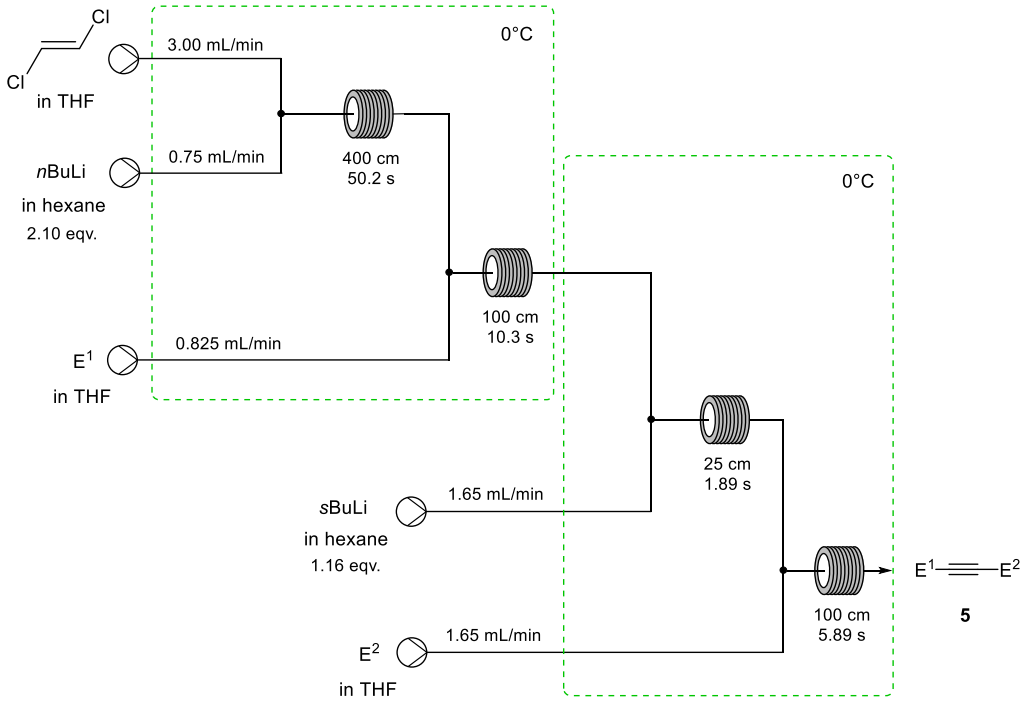


**Figure 7.** Flow platform for the synthesis of asymmetric disubstituted alkynes.

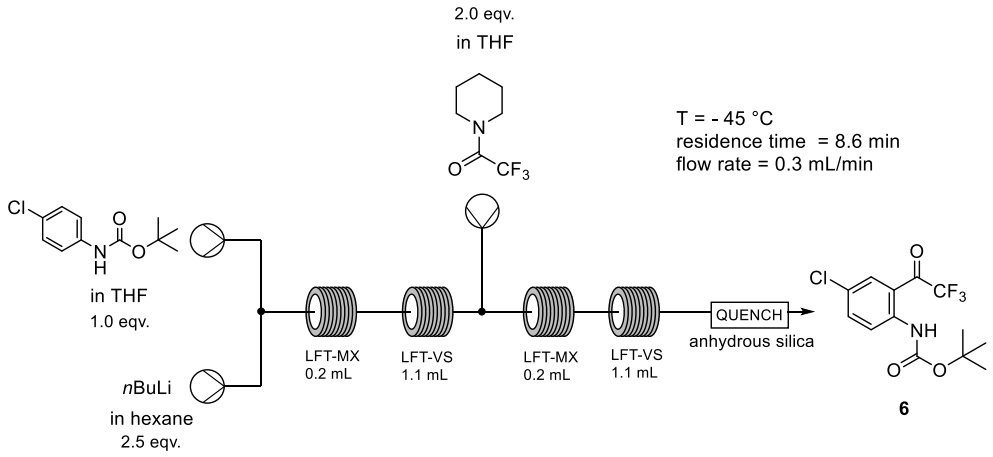


**Figure 8.** Flow system for the synthesis of a key intermediate in the production of efavirenz.

where subsequent deprotonation by *s*BuLi occurs after the electrophilic addition. A variety of electrophiles can be used to quench this intermediate, resulting in the formation of disubstituted dichloroalkene products **4** in yields of 62−73% (Figure 6). It is worth noting that in this scheme, a single deprotonation and substitution using only *n*BuLi and one electrophile was possible, and the authors also synthesized these monosubstituted alkenes in yields of 85−93%.

The authors then turned their attention to synthesizing disubstituted alkynes from *trans*-1,2-dichloroethene using a similar flow setup. The key difference in this procedure was the residence time of the first deprotonation, which was lengthened to 50.2 s to promote *β*-elimination, followed by a subsequent deprotonation by excess *n*BuLi. A quench with different electrophiles resulted in the formation of various disubstituted alkynes of type **5** in yields of 28−91% (Figure 7). The authors established a correlation between the residence time and the yield of either the alkene or alkyne product, where the reaction conditions employed can be manipulated to generate either product in yields of up to 90%.

A publication by Watts and co-workers reported the transfer of the synthesis of efavirenz, a potent non-nucleoside reverse transcriptase inhibitor (NNRTI), from the common batch process to a continuous flow system.[13] The traditional batch synthesis commonly utilizes *s*BuLi[14] or the significantly more hazardous *t*BuLi[15] to facilitate the deprotonation step. Using continuous flow chemistry, *n*BuLi can be used in place of these reagents, offering a much more convenient synthetic route. A continuous process was designed whereby the substrate and organolithium base were reacted to form a lithiated intermediate, which advanced to meet the trifluoroacetylating agent, forming the product **6** in up to 70% yield after an anhydrous silica quench. As an added benefit, the batch process requires *N*,*N*,*N*′,*N*′-tetramethyl-1,2-ethylenediamine (TMEDA) as an additive, while continuous flow circumvents this requirement, consequently simplifying the purification


https://dx.doi.org/10.1021/acs.oprd.0c00090
Org. Process Res. Dev. 2020, 24, 1814−1838

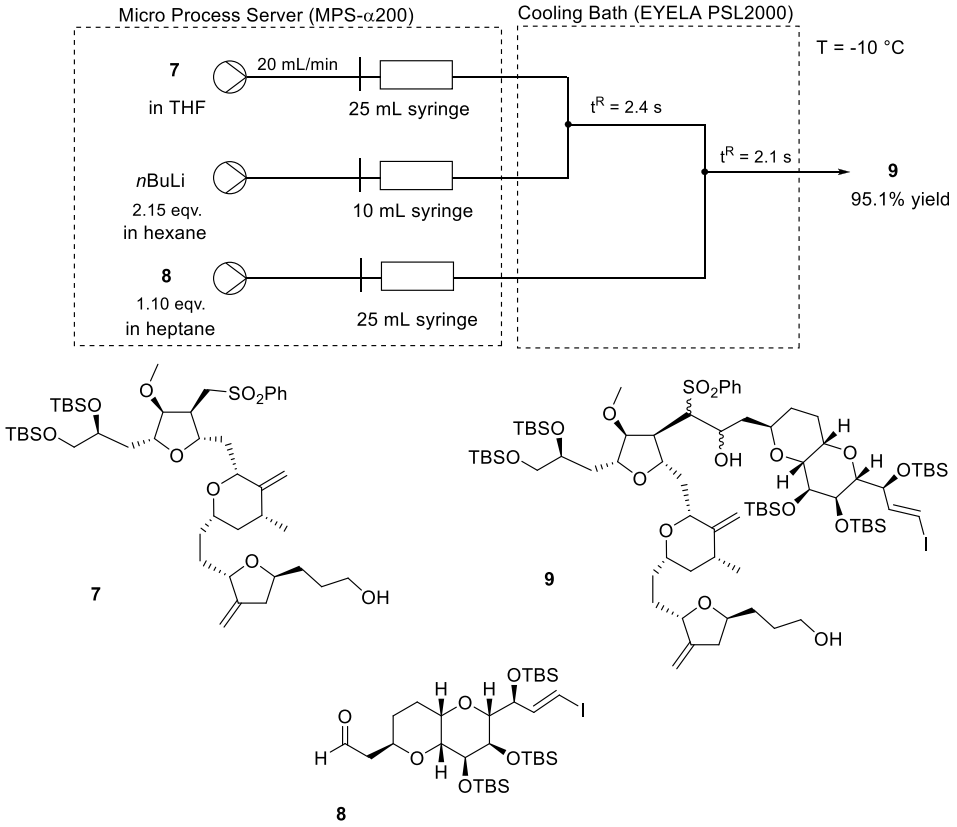


**Figure 9.** Continuous process to facilitate *n*BuLi-mediated coupling in a key step during the synthesis of eribulin mesylate.

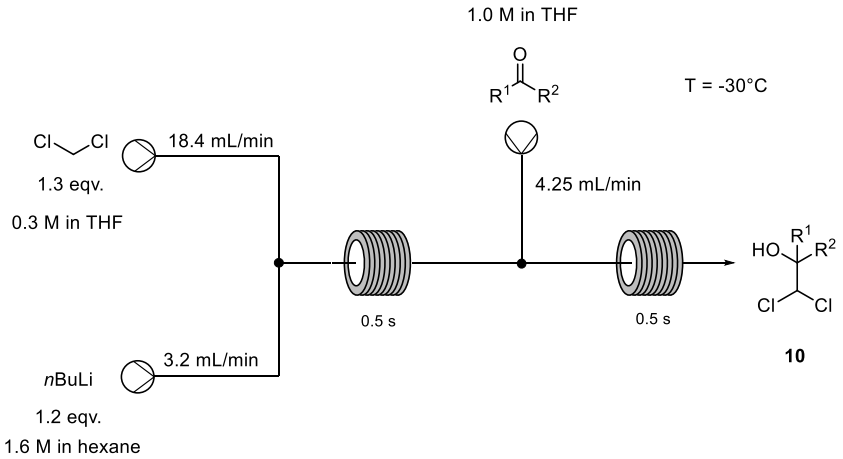


**Figure 10.** Continuous flow synthesis of dichlorocarbinols.

process. Optimization of the reaction conditions resulted in the reaction being conducted at −40 °C with a total residence time of 8.6 min using 2.5 equiv of *n*BuLi and 2 equiv of trifluoroacylating agent. The flow process is outlined with MX plates (used for their mixing structure) and VS plates (simply used to create the desired residence time) (Figure 8).

Similarly, work by Tagami and co-workers employs *n*BuLi in the synthesis of the active pharmaceutical ingredient (API) eribulin mesylate in a continuous flow system.[16] Eribulin mesylate is a fully synthetic derivative of the structurally complex marine natural product halichondrin B, approved by the U.S. Food and Drug Administration in 2010 for the treatment of breast cancer.[17] In batch, the use of *n*BuLi requires cryogenic conditions to complete this step. However, with the continuous flow setup devised by the authors, a more attainable temperature of −10 °C afforded better conversion to product. In the continuous process, a solution of **7** is fed to the system by syringe pumps at 20 mL/min to meet a stream of *n*BuLi supplied by a syringe pump to facilitate deprotonation $\alpha$ to the sulfone. The lithiated species then advances to meet aldehyde **8**, generating the desired product **9** in 95% yield (Figure 9). Advantageously, continuous operation of this process for 87 min led to the same conversion and product quality. Reactions performed at 10 °C initially increased yield to 96.5%, but longer runs led to degradation of the desired product over time.

A 2017 paper by Hafner et al. describes a robust procedure for the generation and subsequent use of thermally unstable


https://dx.doi.org/10.1021/acs.oprd.0c00090
Org. Process Res. Dev. 2020, 24, 1814−1838

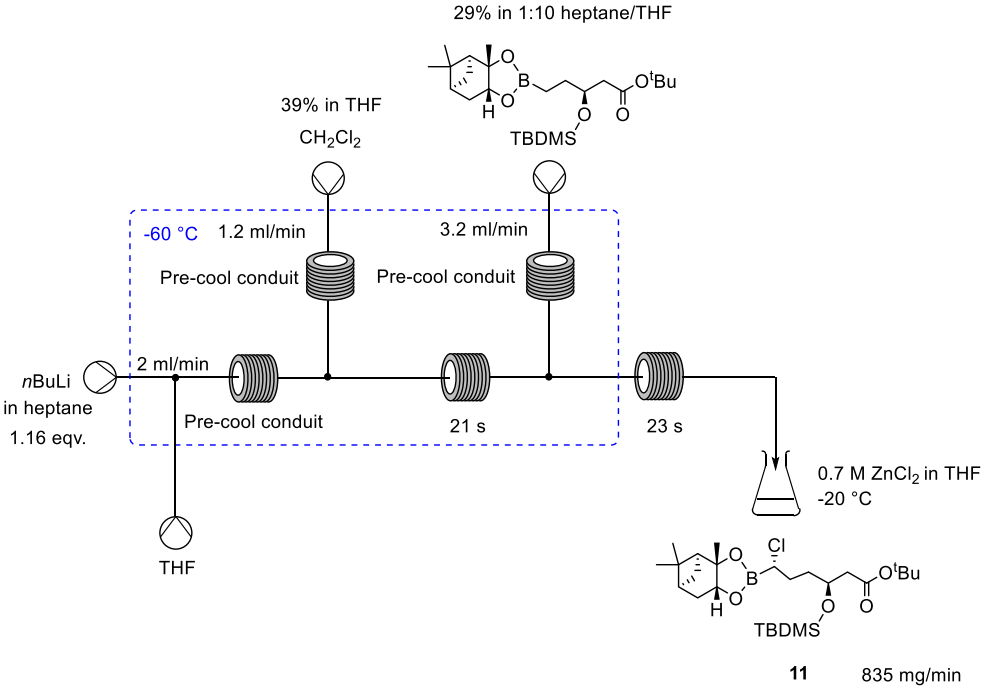


**Figure 11.** Continuous process for a fundamental Matteson homologation step in the synthesis of vaborbactam.

$CHCl_2Li$.[18] The use of $CHCl_2Li$ has been widely reported in the literature, but the thermal instability of the species limits its application to industrial use. Additionally, when an organolithium base such as *n*BuLi is used to generate $CHCl_2Li$, cryogenic conditions of −78 to −100 °C are required to prevent the formation of a carbene species and consecutive degradation pathways. These temperature requirements add to the limitations on using $CHCl_2Li$ on an industrial scale, but applicaion of this reaction to a continuous flow scheme would obviate these limitations. These species serve as synthetically useful building blocks for many organic compounds. The authors devised a flow scheme where dichloromethane (DCM) and *n*BuLi are first supplied to the system by syringe pumps and reacted for a short residence time of 0.5 s to generate $CHCl_2Li$. This lithiated species is then exposed to an electrophile for a residence time of 0.5 s. Initial optimization found that a total residence time of 1 s, 1.3 equiv of DCM, 1.2 equiv of *n*BuLi, and a combined flow rate of ∼20 mL/min run at a temperature of −30 °C allowed the desired product to be successfully obtained in 96% yield when 3-methoxybenzaldehyde was used. Subsequently, a variety of carbonyl-containing compounds were examined, including electron-rich, electron-poor, and heterocylic electrophiles, which afforded the corresponding carbinols with a throughput of 4.25 mmol/min (∼1 g/min) on a multigram scale. The authors also found that carbonyl compounds bearing pendent electrophilic functionalities such as bromine, fluorine, and nitro groups were well-tolerated. These electrophiles proved problematic in batch, displaying a tendency to undergo undesired side reactions or decompose in the presence of the organolithium. The flow protocol was used to generate nine dichlorocarbinols **10** in 82−99% yield (Figure 10). Additionally, $CHCl_2Li$-mediated chain homologation of phenylboronic esters gave $\alpha$-chloroboronic esters in yields of 70−89%.

Similarly, Schuster and co-workers reported the optimization of a continuous flow reaction setup for the synthesis of **11**, a key intermediate of the API vaborbactam.[19] A review by Hughes also outlined a 2016 patent by Rempex for this synthesis.[20] Vaborbactam is a cyclic boronic acid $\beta$-lactamase inhibitor that is commonly used to treat complicated bacterial urinary tract infections. The synthesis of a key intermediate in the process was translated to a flow platform because batch operation required extremely low temperatures and the reaction was sensitive to stoichiometry and mixing effects. An initial batch route involved a complex six-step synthesis furnishing vaborbactam in a yield of 30%.[21] The synthesis involved a Matteson homologation, which required the anion $CHCl_2Li$. DCM is sufficiently deprotonated by *n*BuLi when tetrahydrofuran (THF) is used as a cosolvent to prevent precipitation of *n*BuLi at low temperature. The anion generated is fed into a subsequent reactor to meet the pinanediol boronate, where the Matteson homologation step occurs. Twelve GMP batches of this product were run, affording an average 89% yield to produce 880 kg of product. In batch, this step required temperatures of −95 to −100 °C and gave the desired compound in 75% yield with a diastereomeric ratio (d.r.) of 85:15. The employment of continuous flow technology allowed the temperature to be raised to a more manageable −60 °C. Additionally, the reaction performance in flow resulted in a greatly increased d.r. of 95:5 and a yield of 91%. Finally, the reproducibility of the synthesis in flow was far greater than that of the correpsonding reaction in batch. The flow reaction was performed on a scale to produce 835 mg/min of intermediate **11** in the vaborbactam synthesis (Figure 11).

In the same review, Hughes described the continuous flow synthesis of lifitegrast, an API used to overcome dry eye.[20] In patents granted to SARcode, lifitegrast is prepared from three fragments that are coupled through amide coupling steps.[22] The preparation of one fragment involves a low-temperature carboxylation step. SARcode recently filed a patent outlining the difficulties in batch scale-up, which resulted in lower yields and a tar-like material. To circumvent these issues, a continuous flow platform was designed for this particular


https://dx.doi.org/10.1021/acs.oprd.0c00090
Org. Process Res. Dev. 2020, 24, 1814−1838

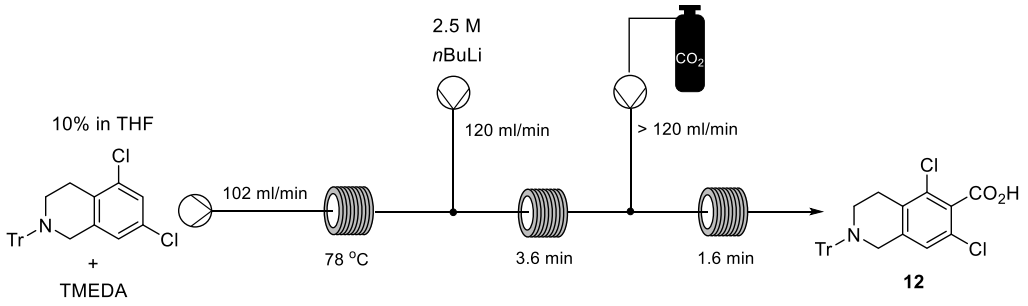


**Figure 12.** Continuous flow carboxylation to yield a central fragment in the synthesis of lifitegrast.

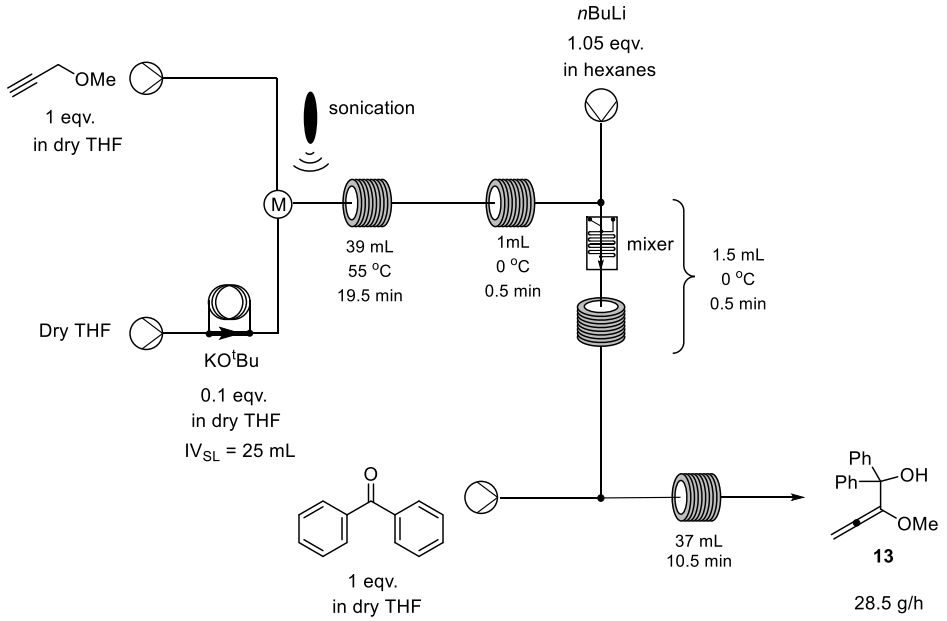


**Figure 13.** Continuous processing of the generation of lithiated methoxyallene and nucleophilic addition to benzophenone.

step.[23] The starting material and TMEDA were introduced together at −78 °C, where they then met a stream of 2.5 M *n*BuLi. The 2.5 M solution was preferentially chosen over the 1.5 M solution of *n*BuLi because it was found to have more consistent lot-to-lot quality. However, the commercially available 2.5 M *n*BuLi contained residues that had to be filtered out before use to avoid precipitates that would cause damage to the pumps. Filters were installed prior to the pumps to allow a steady flow of the feedstock base. Lowering the residence time to 3.6 min as well as increasing the starting material concentration to 10% resulted in a higher conversion upon scale-up. Reaction with $CO_2$ in a subsequent reactor required a residence time of 1.6 min for complete conversion. The patent also noted that the reaction of excess *n*BuLi with $CO_2$ generated valeric acid, which proved to be problematic because it froze in the lines. However, under the optimal conditions, reproducible product yields of 88−91% were achieved in several runs at 4−5 kg scale with a consistent product purity of 97−98%. SARcode prepared a total of 22 kg of carboxylated product **12** (Figure 12). The flow process enabled higher yield, reproducibility, and purity to be achieved on scale.

A publication by Stevens and co-workers addresses the thermal instability and safety concerns associated with the use of methoxyallene, or more specifically, the lithiated species.[24] Use of this lithiated species often provides the most efficient route to targets such as APIs, but these routes are often excluded because of the lack of scale-up potential. Stevens envisioned that the precise control over the reaction parameters and the exquisite heat transfer properties of a flow system would allow a successful translation of the unsafe batch synthesis to a continuous flow platform. Through many rounds of process optimization, a three-step telescoped process was devised. Methyl propargyl ether was pumped by high-performance reciprocating pumps (syringe pumps) to meet a stream of KO$^t$Bu in dry THF, fed to the system through a sample loop, to generate the methoxyallene species with excellent conversion. Subsequently, the methoxyallene species generated was lithiated by a stream of *n*BuLi pumped to the reactor by two parallel syringe pumps. Syringe pumps, alongside sample loops, are often the chosen injection method of organolithium reagents for safety and chemical resistance reasons. As seen with many organolithium deprotonations in flow systems, efficient mixing is the cornerstone to successful conversions. The authors found that a regular T-connector and helical static mixing elements inserted in a tubular reactor afforded the optimal results, leading to conversions of up to 97%. The lithiated methoxyallene progressed to meet a stream of benzophenone, furnishing the desired product **13** in a yield of 94% with a throughput of 28.5 g/h (Figure 13).


https://dx.doi.org/10.1021/acs.oprd.0c00090
Org. Process Res. Dev. 2020, 24, 1814−1838

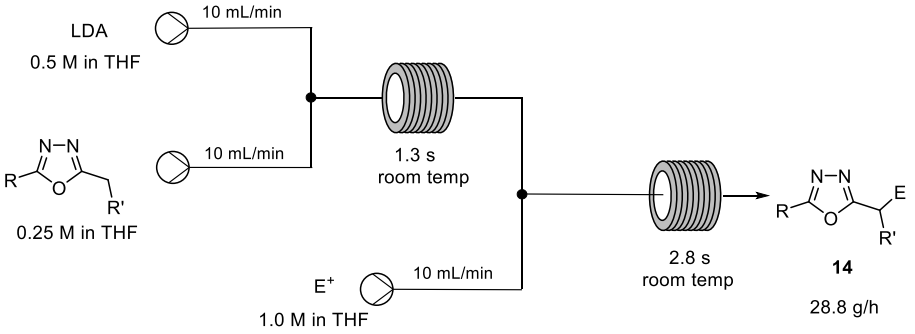


**Figure 14.** Continuous flow system for oxadiazole deprotonation and substitution.

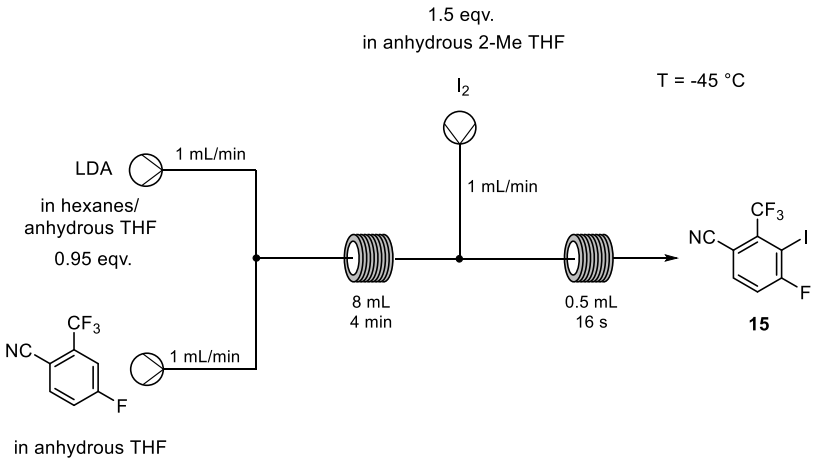


**Figure 15.** Flow synthesis of a tetrasubstituted iodoarene.

## LITHIUM DIISOPROPYLAMIDE

LDA is a strong non-nucleophilic base generated from diisopropylamine and *n*BuLi. Common to most organometallics, the use of LDA often requires cryogenic and carefully controlled reaction conditions.[10] Flow chemistry helps to alleviate issues associated with the use of LDA.

In a publication by Barker and co-workers, the batch and corresponding flow lithiation reactions of 1,3,4-oxadiazoles are reported.[25] These 1,3,4-oxadiazoles are common motifs in bioactive compounds, such as raltegravir and zibotentan. Prior to this paper, it was reported that $\alpha$-lithiation of 1,3,4-oxadiazoles resulted in ring fragmentation.[26] However, the authors in this case reported the $\alpha$-lithiation of 1,3,4-oxadiazoles in batch mode with yields of up to 91%. Since the batch reaction required a temperature of −30 °C, the authors sought to develop a flow setup to achieve less harsh reaction conditions. The reaction was performed initially on a small-scale flow system where the 1,3,4-oxadiazole and LDA solutions were transferred using peristaltic pumps to meet in a reactor coil, producing the lithiated species, which was subsequently quenched in a second reactor coil by a variety of electrophiles, also supplied via peristaltic pumps. In continuous flow, the optimal residence time of 2.8 s achieved complete consumption of starting material and a yield of 86%. Most importantly, the continuous process was successfully performed at a much higher temperature of 0 °C. This temperature proved unsuccessful in batch because of decomposition of the lithiated species. Various electrophiles were well-tolerated, yielding highly functionalized oxadiazoles **14** in yields of up to 86% (Figure 14). These results were then applied to the synthesis of a key synthetic precursor of a cathepsin K inhibitor. An in-flow lithiation−substitution of the substrate 2-methyl-5-phenyl-1,3,4-oxadiazole with pivaldehyde was achieved in 95% yield.

C−H lithiation facilitated by LDA is used to enable the iodination of 4-fluoro-2-(trifluoromethyl)benzonitrile in a publication by Dunn et al.[27] The desired product is a key intermediate in the preparation of a selective androgen receptor modulator API. Both LDA and PhLi (discussed later) were identified as effective bases for the C−H lithiation step. The authors of this paper previously carried out this reaction on a gram scale, where a batch procedure yielded 44% conversion to the 3-iodo product **15**. Increasing the reaction to the kilogram scale was detrimental to the reaction outcome, giving the product in only 11% yield.[28] The moderate to low yields achieved were a result of the formation of multiple byproducts. The authors hypothesized that the lithiated species was unstable under the reaction conditions and decomposed during the longer addition times. Localized hot spots, common to larger-scale reactions, specifically resulting from the exotherm associated with the iodation step, were also thought to negatively impact the yield. A possible solution to this issue involved the use of additional synthetic steps as well as a significant increase in material cost. Therefore, a continuous flow chemistry platform was designed to alleviate the energy transfer issues thought to be hindering the batch reaction. A small-scale reaction set was first performed to investigate the metalation step. Here it became clear that careful control of short reaction times, maintenance of low temperatures during exothermic processes, and precise reaction stoichiometry are key to ensuring optimal yield. The metalation and iodination steps are rapid and possess associated exotherms, so flow


https://dx.doi.org/10.1021/acs.oprd.0c00090
Org. Process Res. Dev. 2020, 24, 1814−1838

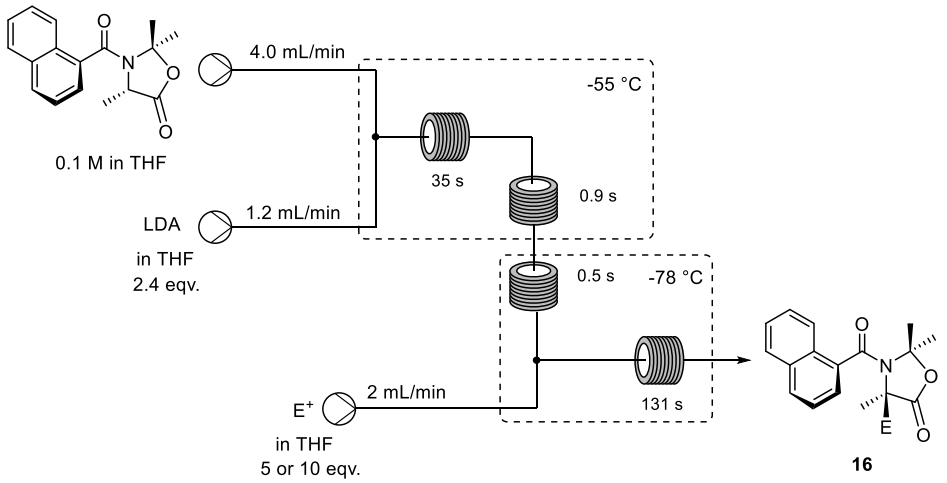


**Figure 16.** Flow deprotonation and alkylation reactions via "memory of chirality".

chemistry was targeted as an alternative approach. In situ NMR and IR were used to study the conversion of the 5-[Li] species to the thermodynamically preferred 3-[Li] species. These mechanistic insights drove the optimization of the second-generation flow process, which utilized standard syringe or HPLC pumps to supply the process with substrate, LDA, and $I_2$ streams, where LDA resulted in a 30:1 preference for the desired 3-[Li] species. This optimized process produced a 67% isolated yield with a throughput of 425 g/L/h (Figure 15). Remarkably, this flow process decreased the time required to synthesize 10 kg of product **15** from over a month to less than a week.

A publication by Alezra and co-workers outlines a three-step synthesis of quaternary $\alpha$-amino acids based on the concept of memory of chirality (MOC).[29] The synthesis involves an intermolecular alkylation of an enolate where the initial chirality of the starting $\alpha$-amino acid is "memorized" only at low temperatures by a chiral conformation of a tertiary aromatic amide. The strict temperature requirements meant that the reaction was extremely difficult to scale. This prompted the authors to develop a flow chemistry platform applicable to the synthesis. A flow chemistry scheme was devised by Alezra and co-workers in a subsequent paper.[30] Initially, the authors investigated an optimization of the two steps in this alkylation reaction in a flow-based system. With ethyl iodoacetate as their alkylating agent, analysis of the reaction parameters revealed the optimum conditions to be a temperature of −55 °C and a residence time of 35 s. The authors next turned their attention to the optimization of the alkylation step, where a variety of electrophiles were screened alongside parameters of temperature and *N*,*N*′-dimethylpropyleneurea (DMPU) addition. A continuous flow process was engineered where three syringe pumps and two T-mixers were used to initially deprotonate the chiral substrate and subsequently trap the anion formed with various electrophiles. Overall, the enantiomeric excess obtained using the flow system was slightly lower than that of the batch method. However, the flow system enabled a residence time of less than 3 min and the use of a superior temperature, allowing the reaction to be considered scalable. Four separate electrophiles were used and gave yields of amino acids **16** between 42 and 99% (Figure 16) and enantiomeric excess (ee) values of 57−89%. A gram-scale synthesis was also conducted with ethyl iodoacetate, and 1.2 g of product was obtained in 82% yield with 89% ee at −70 °C. However, despite the improved utility of the flow reaction, the reaction was found to be more sensitive to the nature of the electrophile in the flow process compared with the batch process.

As a base, LDA was investigated by the Ley group in a search for reactivity patterns not possible in batch mode.[31] The authors decided to focus on homologation reactions using dibromomethane esters. Here the dibromomethane must be cleanly metalated as a key first step. Consuming LDA at −90 °C can take several minutes in this reaction, so short mixing times are undesirable. However, the lithiated dibromomethane species generated from the first step is an unstable species with a short half-life, with decomposition taking place even at temperatures as low as −90 °C. Consequently, generating this species is unsuited to large-scale batch reactions. Flow chemistry was applied to the methodology and displayed efficient mixing with well-controlled residence times, thus alleviating the decomposition issues seen in batch. A continuous process was devised in which $CH_2Br_2$ and LDA were supplied by peristaltic pumps to be precooled in 0.5 mL coils at −90 °C, with LDA delivered via a sample loop. The anion was formed in an initial 8 mL reactor coil over a 4 min residence time and was subsequently reacted with a variety of heterocycles. Pyridines, thiophenes, or isoxazoles were all tolerated in this reaction, and the yields obtained in flow were higher than those of the corresponding batch process. Additionally, heterocycles that were reported to fail under batch conditions were successfully reacted with dibromomethane in a flow system. The authors also focused their attention on developing new reactivity patterns not possible in batch mode involving the use of esters with an $\alpha$-proton. In batch mode, the use of esters with $\alpha$-protons resulted only in starting material. When lithiated dibromomethane was added to an ester, it could be protonated to form dibromoketone **17**, or a second equivalent of base could deprotonate the ester at the $\alpha$-position to form the $\alpha$-dibromoenolate intermediate. However, if an $\alpha$-proton is present in the ester, the second equivalent of base will preferentially remove this over the dibromo proton, and thus, protonation of the kinetic intermediate reforms the starting material. The authors deduced that efficient mixing and suppression of back-mixing would allow the intermediate to exist long enough to be quenched by acid and not react with a second equivalent of base. Furthermore, the precise temperature control enabled by


https://dx.doi.org/10.1021/acs.oprd.0c00090
Org. Process Res. Dev. 2020, 24, 1814−1838

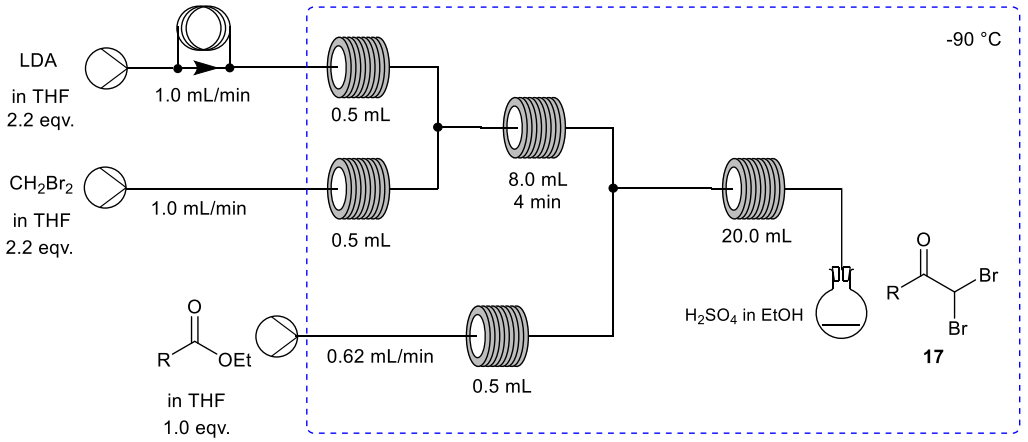


**Figure 17.** Synthesis of dibromoketones using LDA for dibromomethane deprotonation in a flow system.

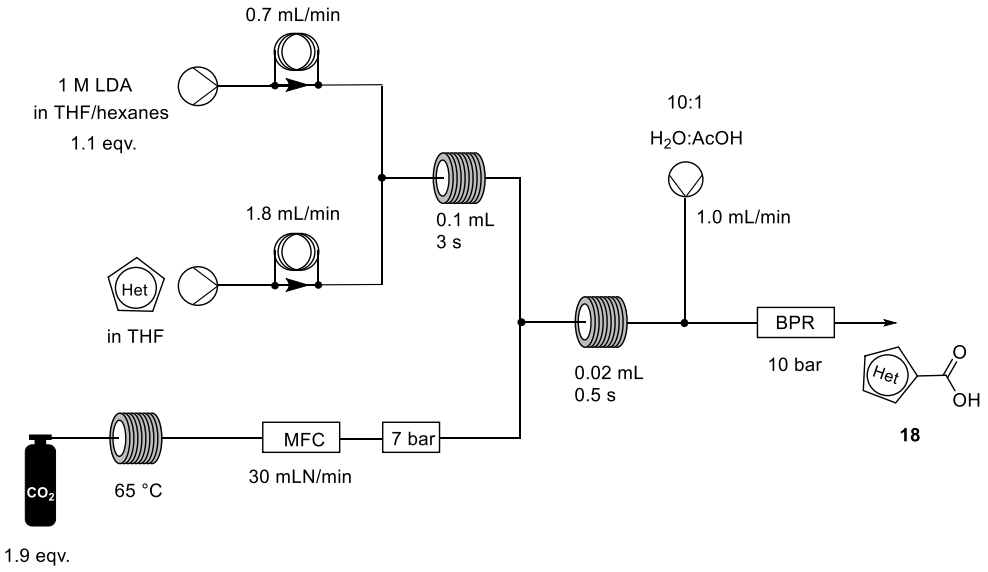


**Figure 18.** LDA-mediated carboxylation of heterocycles in flow.

the flow setup would allow harnessing of unstable intermediates that could not survive in batch. In batch attempts, several runs obtained an optimal yield of 10% of 1,1-dibromo-3-phenylpentan-2-one product. In a continuous flow system, there was an increase in the yield to 49% with 42% recovery of the starting material (Figure 17). Increasing the amount of lithiated dibromomethane species to 4.4 equiv resulted in a dramatic increase in the yield of **17** to 95%. As a result, more complex substrates could be utilized and successfully subjected to these conditions. It was found that substrates that were considered poor in batch were successful in flow, albeit in modest yields. The authors finally demonstrated a scaled example of their chemistry in which 1.74 g of the dibromoketone from $\alpha$-methylcinnamyl ethyl ester was obtained in 25 min in 87% yield.

Kappe and co-workers described a method for the direct lithiation of terminal alkynes and heterocycles with subsequent carboxylation.[32] Their paper outlines the use of two organolithium bases: LiHMDS and LDA. LDA was used for the conversion of heterocyclic substrates to their corresponding carboxylic acids. A flow system was designed where a variety of heterocycles were supplied to the system to meet a stream of LDA. The organolithium base deprotonated the heterocycle after a residence time of 3 s to yield an anion that progressed to meet $CO_2$. The $CO_2$ was introduced to the system through a mass flow controller at a rate of 30 mLN/min and facilitated carboxylation after a residence time of 0.5 s. The carboxylate synthesized was then quenched by a mixture of water and acetic acid (10:1). Attempts to quench the reaction with only water resulted in immediate clogging of the system, so acetic acid was required. Kappe reported that six heterocyclic substrates were tolerated to form products **18** in yields of 43−79% (Figure 18). Increasing the number of equivalents of LDA proved to be an ineffective method of increasing the yield but increasing the number of $CO_2$ equivalents to 1.9 did result in a small increase in yield.

LDA was once again utilized by Kappe and co-workers in a report wherein the authors showcased the ability to monitor a multistep continuous flow process by multiple inline analytical techniques known as process analytical technology (PAT).[33] The authors chose to study a multistep organolithium transformation that involved treating an ester substrate with LDA to yield the corresponding enolate, which was subsequently reacted with an electrophilic aldehyde. The flow microreactor system used for the reaction was coupled to in-line IR spectroscopy, in-line NMR spectroscopy, and online


https://dx.doi.org/10.1021/acs.oprd.0c00090
Org. Process Res. Dev. 2020, 24, 1814−1838

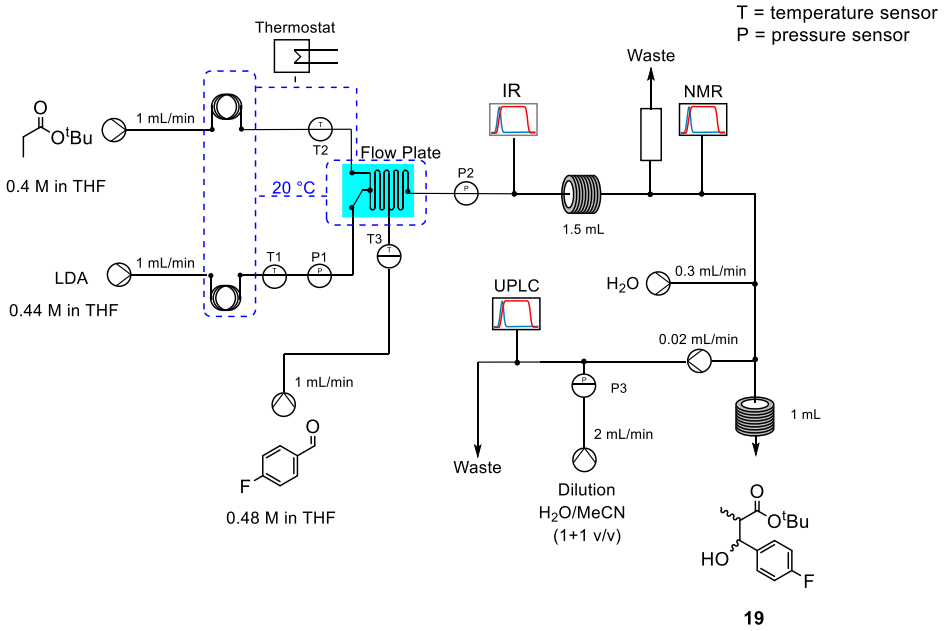


**Figure 19.** Use of PAT instruments in a flow system to optimize ester deprotonation and addition to an electrophile.

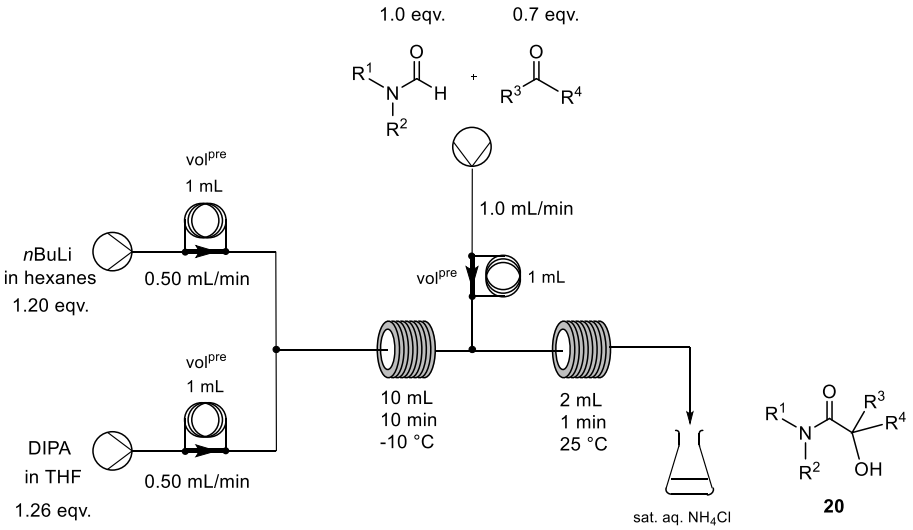


**Figure 20.** Generation of $\alpha$-hydroxy amides in a flow system.

UPLC to allow real-time reaction monitoring. Product quantification was made possible through the use of in-line $^1$H NMR spectroscopy. ReactIR was used to quantify the irreversible deprotonation by LDA. The carbonyl stretch of the starting material can be observed at 1730 cm$^{-1}$ and rapidly disappears because of deprotonation by LDA even at the shortest attempted residence time of 3.9 s. Additionally, a concentration versus response curve for the ester showed its limit of quantification to be ~10% of the initial concentration used, implying that over 90% of the material was successfully deprotonated. As with most flow processes, the authors initially optimized the system through investigation of temperature, LDA loading, and electrophile loading variability, and the process was found to operate most favorably at 20 °C, which was of great benefit in terms of energy savings because cooling was not required. The authors then demonstrated the scale-up possibilities of this platform by operating the process over 70 min to produce **19** with a productivity rate of 4.2 g/h (Figure 19).

## ■ LDA PREPARED IN SITU

LDA is a readily available organometallic reagent, marketed in various solutions and concentrations, allowing for end-user convenience. However, the use of commercial LDA is not without its limitations. Problems with reliable supply and fluctuations in quality and accurate concentration certainly limit the use of commercial LDA. For this reason, LDA is commonly generated in situ by the reaction of *n*BuLi with diisopropylamine (DIPA). In situ generation of LDA results in increased accuracy and reactivity.[34] For production of LDA in a continuous flow system, an additional reactor coil can be added to the setup to pregenerate LDA.

In 2017, Knochel and co-workers utilized the in situ generation of LDA for the formation of $\alpha$-hydroxy amides.[35] They developed an ambient temperature flow method for


https://dx.doi.org/10.1021/acs.oprd.0c00090
Org. Process Res. Dev. 2020, 24, 1814−1838

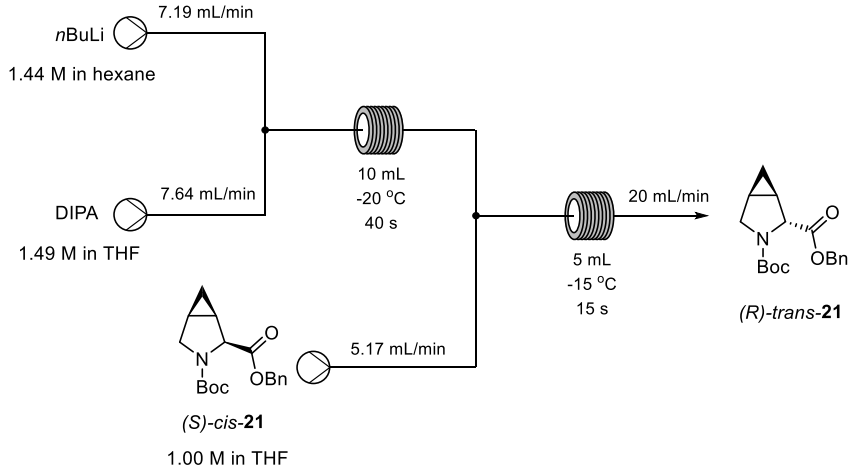


**Figure 21.** LDA-mediated epimerization in a flow system.

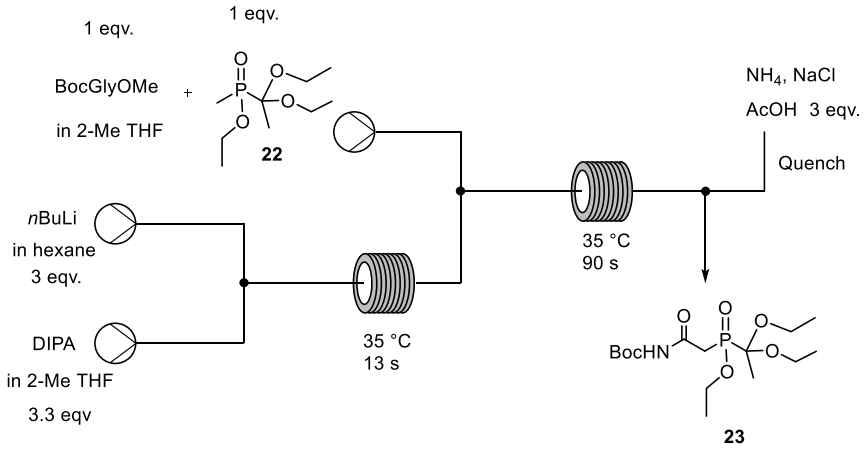


**Figure 22.** Flow platform to facilitate the efficient synthesis of a key intermediate in the steps to AZD6906 synthesis.

nucleophilic amidation and thioamidation to yield carbamoyllithium intermediates. Subsequent reaction of these intermediates with carbonyl-containing compounds successfully furnished $\alpha$-hydroxy amides **20** in good to excellent yields of 58−95% (Figure 20). Ketal, acetal, and aryl halide functionalities were well-tolerated in this reaction. The process was also successfully extended to include the synthesis of $\alpha$-keto amides in moderate to good yields of 61−82% by employing Weinreb amides and structurally related *N*-morpholino amides. Additionally, the lithiation of thioformamides in the presence of *N*-morpholine benzamides provided a reliable route to valuable $\alpha$-keto thioamides in 41−98% yield using this protocol. Furthermore, the authors found that under these optimized flow conditions, no side products derived from lithiation of the electrophile were found.

In similar work published by Ossola and co-workers, a continuous flow system was engineered to promote the epimerization of 3-(*tert*-butoxycarbonyl)-3-azabicyclo[3.1.0]-hexane-2-carboxylic acid. This chemistry, facilitated by the in situ generation of LDA, provides a flow chemistry platform for the synthesis of unnatural amino acids, allowing for known literature procedures to be significantly shortened.[36] The authors outlined numerous methods attempted to successfully epimerize the substrate **21**. LDA was identified as the most suitable organolithium to enable this epimerization. Advantageously, the authors also identified short reaction times as a key factor in the success of the epimerization. Short reaction times of <60 s would be difficult to conduct in batch mode, and a consequential decrease in yield would be expected. A continuous process was envisaged to facilitate the short reaction times necessary for these epimerizations, allowing for process scale-up. *n*BuLi and diisopropylamine were readily mixed at −20 °C to generate LDA, which progressed to meet (*S*)-*cis*-**21** at −15 °C, yielding (*R*)-*trans*-**21** (Figure 21). The authors successfully produced 17 g of (*R*)-*trans*-**21** using this method in 55% yield with a throughput of 55 g/h, demonstrating the scalability of the process.

A paper by Pontén and co-workers at AstraZeneca recently highlighted the use of continuous flow chemistry in the synthesis of the gastroesophageal reflux inhibitor AZD6906.[37] Several problems were encountered throughout the batch synthesis of this API. Initial batch reactions required the use of cryogenic reaction conditions to overcome a potential exotherm and degradation of starting material. This would lead to numerous problems on scale-up. Second, the highly toxic reagent methyldichlorophosphine presented serious safety concerns. Finally, for the batch reaction to proceed, the costly phosphonate reagent **22** was required in 2-fold excess to prevent the acidic protons of the product from quenching the anion created in situ. To overcome these issues, a continuous flow system was devised. It was anticipated that a flow system would prevent exposure of product to the anion formed, therefore removing the requirement for an additional equivalent of **22**. It would also reduce chemist exposure to the


https://dx.doi.org/10.1021/acs.oprd.0c00090
Org. Process Res. Dev. 2020, 24, 1814−1838

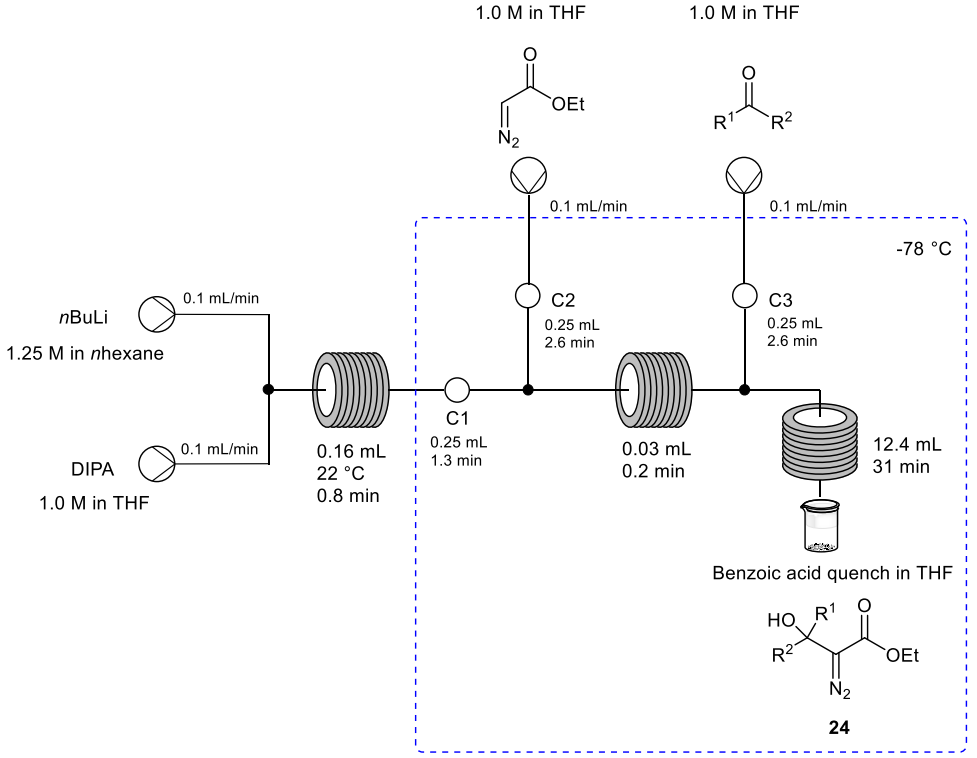


**Figure 23.** Continuous flow lithiation of ethyl diazoacetate.

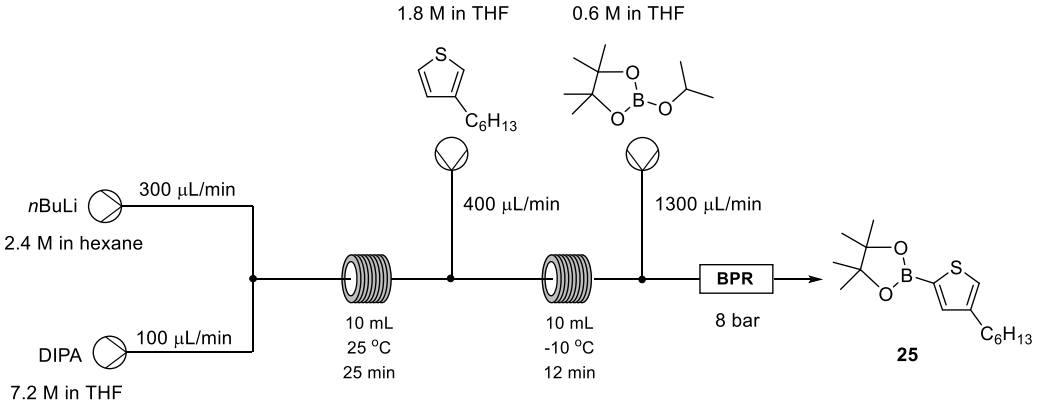


**Figure 24.** Continuous process for the regioselective lithiation−borylation of 3-hexylthiophene.

hazardous methyldichlorophosphine. An optimization period identified a reaction temperature of 35 °C, a residence time of 90 s, and an LDA concentration of 1.25 M to yield the best results while concurrently allowing issues of solubility and clogging to be avoided. The authors discontinued the use of commercial-grade LDA because of interbatch variability. Because the number of equivalents of LDA employed was critical to the reaction, the authors instead turned to generating the 3 equiv of LDA required in situ. This allowed for more consistent reaction results to be achieved and made the previously required degassing process redundant. Under these conditions, 1.3 kg of phosphinate **22** was processed, yielding sufficient amounts of **23** to proceed to the final stage of API synthesis (Figure 22).

Wirth and co-workers reported the optimization of a continuous flow system for the safe and efficient use of ethyl diazoacetate to access tertiary diazoalcohols in good yields.[38] As is common with the use of diazo compounds, the use of ethyl diazoacetate is accompanied by an undesirable safety profile and poor thermal stability.[39] This diazo reagent is commonly combined with LDA to generate highly reactive ethyl lithiodiazoacetate. This lithiated reagent decomposes rapidly even at low temperatures, seriously hindering its use in batch reactions, where low-yielding and varying reaction results are commonly encountered. These authors described a flow chemistry platform using syringe and peristaltic pumps to allow more efficient and safe handling of this chemical species. LDA was generated in-line by combining streams of *n*BuLi and diisopropylamine and subsequently reacted with ethyl diazoacetate to produce the lithiated species. Trapping of this lithiodiazoacetate reagent with various ketones furnished diazo alcohols **24** in yields of 12−71% (Figure 23). In addition to the efficient handling of the unstable lithiodiazoacetate species, the yield of products generated in flow is higher than that in the corresponding batch reaction, providing a much more reliable method.


https://dx.doi.org/10.1021/acs.oprd.0c00090
Org. Process Res. Dev. 2020, 24, 1814−1838

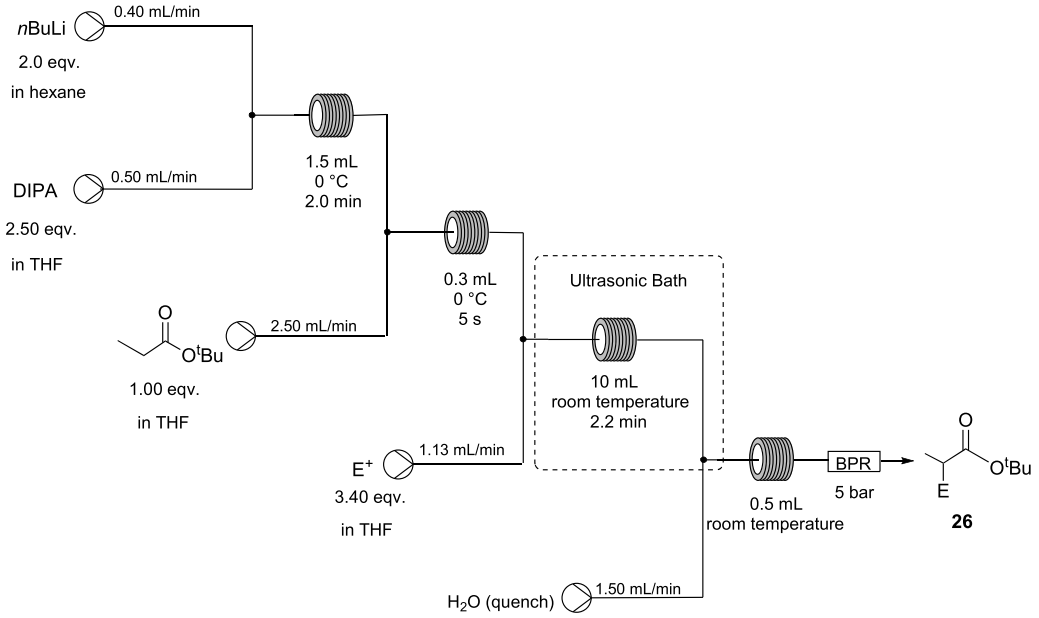


**Figure 25.** Continuous flow process for ester deprotonation and $\alpha$-functionalization.

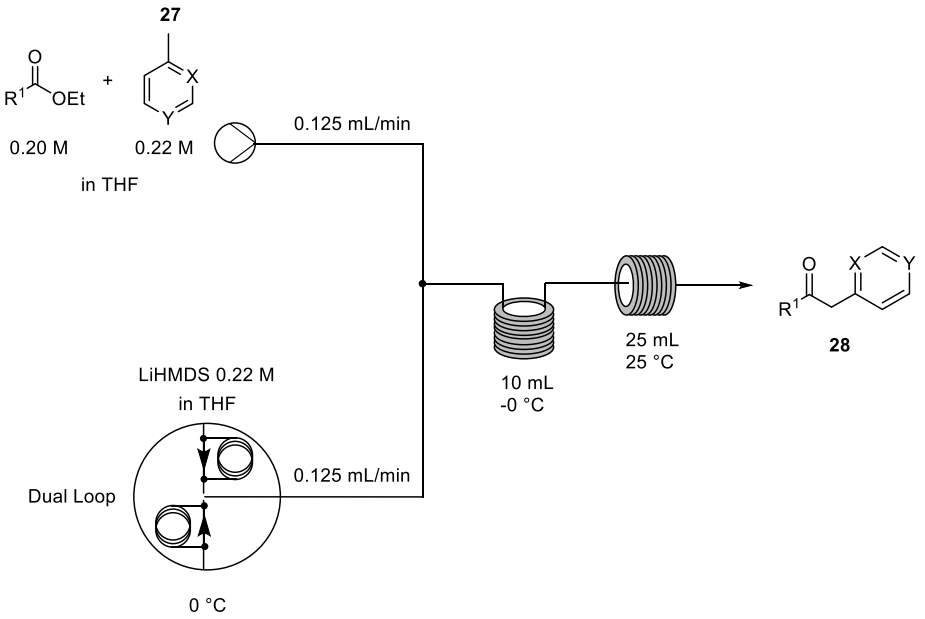


**Figure 26.** LiHMDS-mediated deprotonation and addition to ester substrates.

Work by Wong and co-workers also exploits the in-line generation of LDA for the construction of organic electronic materials. The metalating agent is used in a lithiation−borylation sequence for the generation of thiophene building blocks.[40] These building blocks can then be further functionalized to allow direct access to a range of high-performance organic electronic materials. The authors initially employed *n*BuLi as the base for the process. However, the regioselectivity of the reaction soon became an issue. Generation of mixtures of 2- and 5-substituted products, particularly boronic esters, which proved difficult to separate, prompted the authors to switch to LDA. The steric properties of LDA prompted exclusive lithiation at the 5-position. The authors described a telescoped procedure where LDA is generated in-line and reacted with the thiophene substrate. Subsequent reaction with the boronic ester gave product **25** with high regioselectivity (17:1) in an excellent yield of 88% (Figure 24). The synthesis had a total residence time of 37 min and operated under more efficient temperatures than those observed in batch mode. The flow chemistry platform can be efficiently scaled up without the requirement for cryogenic conditions and without sacrificing the selectivity found in batch.

A final example of in-line LDA generation in a continuous flow system was described by Kappe and co-workers.[41] Their work involved a multistep process to directly functionalize esters at the $\alpha$-position via their enolates (Figure 25). Because of inherent reactivity issues associated with lithium enolates, it was postulated this reaction would be ideally suited to a continuous flow platform. The authors first optimized a reaction sequence using *tert*-butyl propionate, where it was found that with 2 equiv of LDA and a 30 s residence time at a temperature of 0 °C, the desired product was obtained in


https://dx.doi.org/10.1021/acs.oprd.0c00090
Org. Process Res. Dev. 2020, 24, 1814−1838

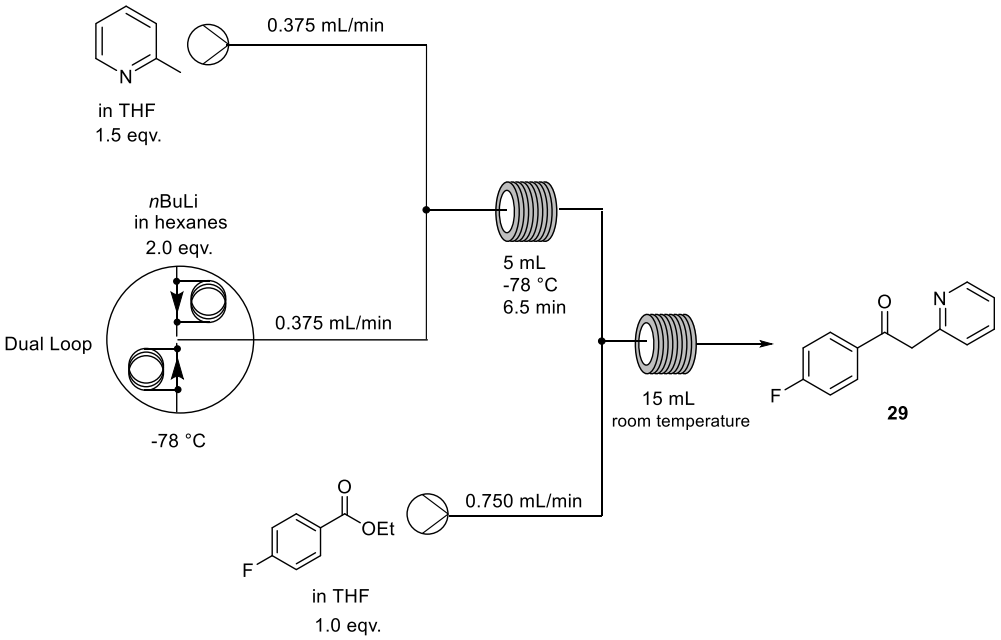


**Figure 27.** *n*BuLi deprotonation using a dual-loop system in the first step of the preparation of a family of casein kinase I inhibitors.

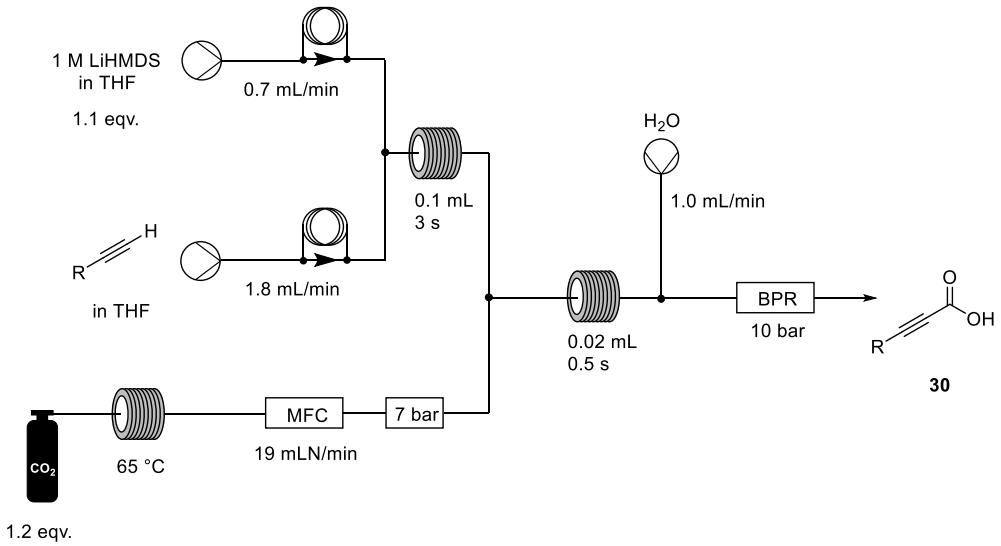


**Figure 28.** Flow process for the carboxylation of alkyne substrates using $CO_2$.

yields of up to 90%. The flow system also incorporated an ultrasound bath in which the section of the flow setup involving the electrophile addition was immersed as a precautionary measure to circumvent issues arising from solid formation. The authors then turned their attention to optimizing a reaction using methyl propionate, which lacks the bulky O$^t$Bu group and consequently has more complex selectivity issues. Homo-Claisen condensation products are a commonly observed byproduct from this reaction. This reaction requires a temperature of −78 °C during the enolate formation step. However, the authors suggested that the reaction is most likely not limited by mass transfer and instead that the poor selectivity results from similar reaction rates for the ester deprotonation reaction and the homo-Claisen condensation reaction. Six examples of $\alpha$-alkylated esters of type **26** were reported to be successfully generated in 29−80% yield. Additionally, scaling of the process was simply achieved by collecting the crude reaction mixture from the output for longer periods of time.

## ■ LITHIUM BIS(TRIMETHYLSILYL)AMIDE

Lithium bis(trimethylsilyl)amide, also called lithium hexamethyldisilazide (LiHMDS), is a lithiated organosilicon compound that is commonly used as a strong, non-nucleophilic base.[42] A publication by Ley and co-workers outlines the synthesis of a family of casein kinase I inhibitors using a continuous flow system.[43] Analogues of imidazo[1,2-*b*]-pyridazine were prepared via a three-step sequence involving the formation of a ketone moiety, $\alpha$-bromination, and subsequent condensation with 3-aminopyridazine to yield a key fragment of the target molecule (Figure 26). The authors designed a scalable multistep assembly to efficiently and directly deliver pure product on a multigram scale. The first step of the three-step sequence involved the use of LiHMDS.


https://dx.doi.org/10.1021/acs.oprd.0c00090
Org. Process Res. Dev. 2020, 24, 1814−1838

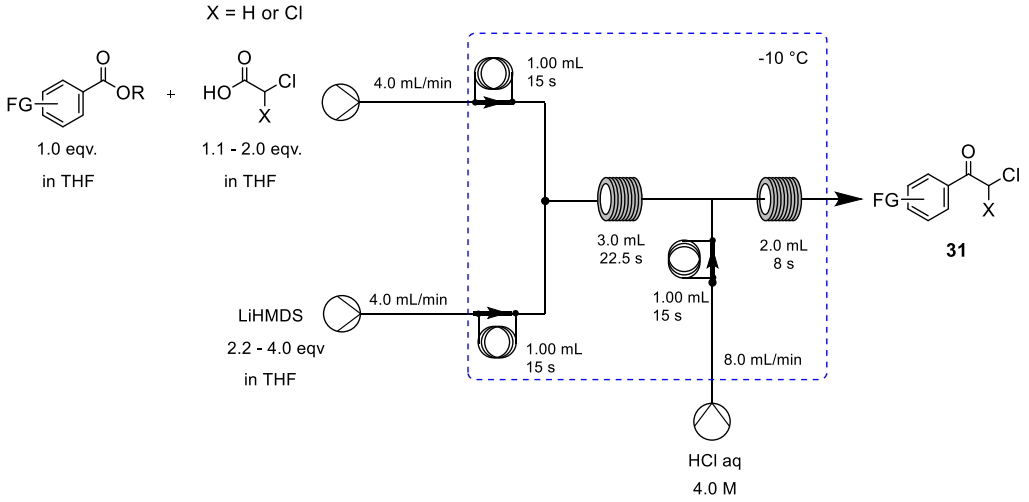


**Figure 29.** Continuous flow chlorohomologation of aromatic esters leading to $\alpha$-chloro- or $\alpha,\alpha'$-dichloroketones.

Using high-pressure pumps, the authors observed difficulties with the use of organolithiums, associated with rapid decomposition and difficulties with exotherm control. To sidestep these issues, a dual-sample-loop injection system was developed. One sample loop served to deliver the organolithium base to the system, while the second loop stored a second loading of base for later injection. This dual sample loop was cooled through submersion in a Dewar flask of water/dry ice before addition. LiHMDS was employed to deprotonate picoline substrates **27**, which reacted with esters to afford products of type **28** (Figure 26). However, LiHMDS was unable to deprotonate a particular 2-picoline substrate, so the authors turned to *n*BuLi. Because of competitive nucleophilic addition of the organolithium to the ester function, the fluorophenyl ester and picoline substrate could not be premixed (Figure 27). Instead, the picoline substrate and *n*BuLi were mixed in a T-mixer and allowed to react in a 5 mL coiled reactor held at −78 °C. The azaenolate generated was then quenched by the ester in a 15 mL reactor coil at ambient temperature. This reaction sequence produced the corresponding ketone **29** in 65% yield on a 50 mmol scale.

A paper previously discussed outlining work by Kappe and co-workers using LDA in continuous flow for the carboxylation of heterocycles also described the application of this system to the carboxylation of alkynes.[32] LiHMDS was the organolithium base used in this reaction to rapidly furnish a variety of carboxylic acids in less than 5 s. Only a slight excess of LiHMDS was required. The LiHMDS and the alkyne were pumped by HPLC pumps and loaded in individual sample loops to meet in a T-mixing unit before passing through a 0.1 mL coiled reactor for a residence time of 3 s to allow lithiation occur. The lithiated alkyne then progressed to a second T-mixer, where $CO_2$ was introduced. The product of the carboxylation then advanced to a third and final T-mixer, where it was quenched by $H_2O$, producing carboxylic acids **30** in good to excellent yields of 66−90% (Figure 28). Both electron-rich and electron-poor aromatic alkynes were well-tolerated, but the phenol and 3-ethynylpyridine substrates tested were unsuccessful because of precipitation of the organometallic intermediate in the reactor.

A paper by Knochel and co-workers described a continuous flow system that uses LiHMDS and chloroacetic acid to enable selective chloromethylenation of functionalized esters.[44] This Claisen homologation reaction was, for the first time, extended to bischloromethylenation using dichloroacetic acid, resulting in a direct route to the underexplored $\alpha,\alpha'$-dichloroketones. The authors reported a flow system capable of producing both $\alpha$-chloro- and $\alpha,\alpha'$-dichloroketones in good to excellent yields in several seconds. The ester and chloroacetic acid are premixed and precooled before being supplied to the system via a peristaltic pump. This mixture is combined with precooled LiHMDS in a T-mixer to generate the lithiated intermediate. This intermediate is then quenched by HCl to produce $\alpha$-chloro- or $\alpha,\alpha'$-dichloroketones **31** (Figure 29). The reaction scheme is highly economical in terms of reagents and reaction time, has a breadth of application across a wide variety of substrates, and demonstrates potential for successful scale-up.

A paper by Kappe and co-workers described a scalable continuous flow system designed for the concise synthesis of $\alpha$-difluoromethylamino acids.[45] The difluoromethyl group ($CHF_2$), delivered by the reagent fluoroform ($CHF_3$), is a moiety found in an increasing number of pharmaceutical and agrochemical products. Fluoroform is an attractive source for the introduction of this motif and is generated on a large scale as a reaction byproduct. Its global warming potential means the release of the gas into the atmosphere is restricted. The organolithium base LiHMDS is employed to deprotonate both an ester substrate and fluoroform, with the latter forming an electrophilic singlet difluorocarbene. This difluorocarbene moiety can then react with the anionic ester substrate, enabling the synthesis of $\alpha$-difluoromethylamino acids **32.** These compounds are potent and selective irreversible inhibitors of their respective $\alpha$-amino acid decarboxylases. This served as motivation for the authors to extend this flow methodology to the synthesis of eflornithine. The authors first performed batch reactions that proved to be unsuccessful, yielding only 2% conversion after 6 h. Resulting from this, the authors turned their attention to developing a continuous flow system to provide a more efficient route to the target. The continuous flow system uses two syringe pumps to feed the ester and LiHMDS into the system. The deprotonation occurs at −30 °C in a 2 mL reactor coil with a residence time of 4 min. Fluoroform is then introduced into the system with the aid of a mass flow controller. The solution is processed through two remaining reactors for a total residence time of 20 min. The


https://dx.doi.org/10.1021/acs.oprd.0c00090
Org. Process Res. Dev. 2020, 24, 1814−1838

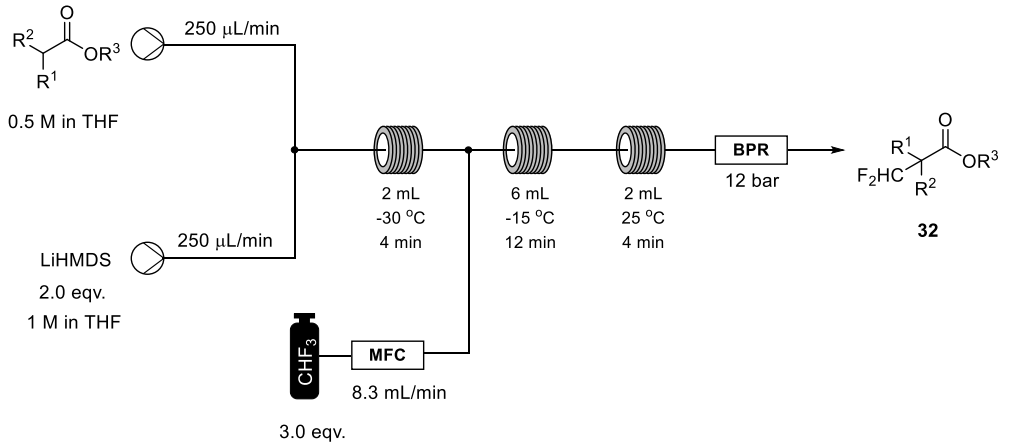


**Figure 30.** Continuous flow $\alpha$-difluoromethylation using fluoroform.

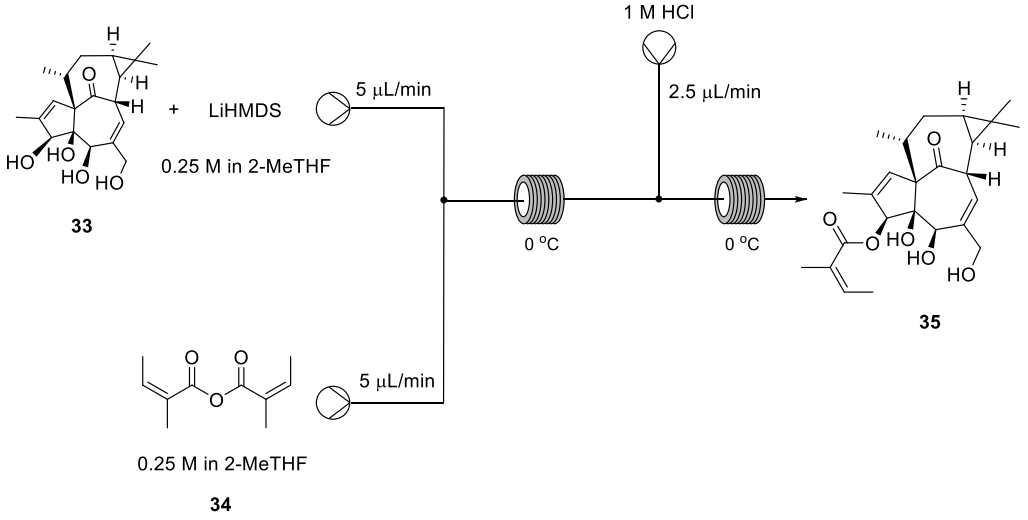


**Figure 31.** Continuous processing of ingenol mebutate.

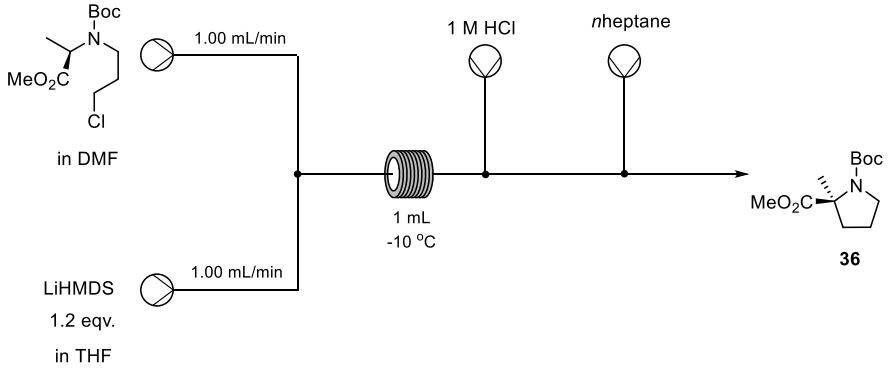


**Figure 32.** Continuous flow processing of asymmetric intramolecular cyclizations via "memory of chirality".

optimum reaction conditions were found to use 2 equiv of base. The process is applicable to several substrates, yielding good results when monoesters, malonates, and amino acids **32** were examined (Figure 30). Although the process is readily scalable, application on an industrial scale would have to involve a plan for removal and, ideally, recycling of excess fluoroform.

A 2017 patent application from Alphora also involves the use of LiHMDS in a continuous flow system toward a more efficient route to ingenol mebutate (**35**),[46] a protein kinase C activator that is approved in the U.S. and Europe for the topical treatment of actinic keratosis, which can potentially develop into skin cancer. The Baran group found that only 1.1 mg of ingenol mebutate could be isolated from 1 kg of plant material.[47] However, ingenol (**33**) itself can be obtained in much larger quantities of 275 mg/kg from the seeds of the plant *Euphorbia lathryis*. Thus, a semisynthesis of ingenol mebutate from ingenol was attempted. Leo Laboratories developed a multistep batch synthesis involving protection and deprotection of the hydroxyl group to provide ingenol


https://dx.doi.org/10.1021/acs.oprd.0c00090
Org. Process Res. Dev. 2020, 24, 1814−1838

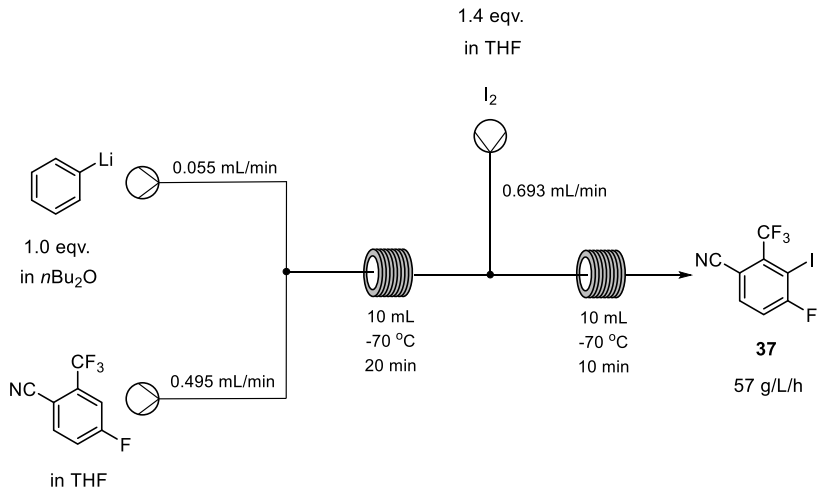


**Figure 33.** Continuous flow synthesis of a key intermediate for API development via PhLi deprotonation.

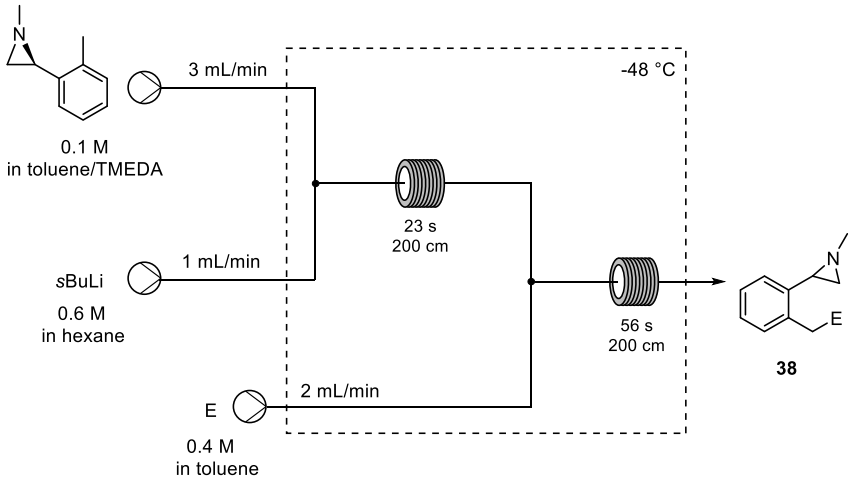


**Figure 34.** Continuous flow system to generate laterally substituted aziridines.

mebutate in 37% yield.[48] In an attempt to streamline the synthesis, Alphora devised a more direct route to ingenol mebutate using a flow chemistry platform. The flow system involved a premixed solution of the organolithium base and ingenol undergoing acylation, facilitated by the use angelic anhydride (**34**) at 0 °C, followed by a 1 M HCl quench at 25 °C (Figure 31). This continuous process allowed for a single-step, protecting-group-free synthesis of ingenol mebutate in 40% yield with much improved regioselectivity for C3.

Finally, work by Vilé et al. identified LiHMDS as the optimal organolithium base for a continuous flow platform that facilitates the enantiospecific cyclization of methyl *N*-(*tert*-butoxycarbonyl)-*N*-(3-chloropropyl)-D-alaninate to 2-methyl-proline derivative **36** via the previously mentioned "memory of chirality" approach.[49] Flow technology was applied to this reaction scheme to improve the scalability and safety profile and to remove the need for cryogenic conditions. Additionally, the authors anticipated improved throughput from a flow-based system. A continuous flow platform was devised in which the substrate was delivered by a HPLC pump to meet 1.2 equiv of LiHMDS in a 1 mL reactor coil at −10 °C for a residence time of 30 s (Figure 32). The reactions were first performed on a 1 g scale, where the use of LiHMDS enabled an isolated yield of **36** of 96% with 97% ee. The authors then scaled the initial 1 g process to run continuously for 6 h with a productivity of 11 g/h to yield 66 g of pure product while preserving the enantioselectivity. The exquisite control of reaction parameters usually required for MOC protocols positions flow approaches as an ideal technology to properly apply these concepts in practice. The designed flow process proved to be superior to the corresponding batch operation, as it operates a temperature of −10 °C, compared with the batch temperature of −60 °C, with a residence time of 30 s, compared with the batch reaction time of 2 h. Additionally, the continuous setup allows the process to be readily scaled to a multigram scale.

## OTHER ORGANOLITHIUM BASES

**Phenyllithium.** Phenyllithium, or lithobenzene, is an alternative to the commonly used organolithium reagents discussed above.[10] Although not as prevalent in the literature as *n*BuLi or LDA, it is often employed to carry out similar reactions. In a previously discussed paper by Dunn et al.,[27] PhLi was also used as an organolithium base to enable the iodation of 4-fluoro-2-(trifluoromethyl)benzonitrile. This process proceeds via C−H lithiation and subsequent treatment with iodine under continuous flow conditions. PhLi was chosen by the authors since it was seen to promote the formation of the 3-iodo isomer to a greater extent than LDA, which resulted in varying amounts of the unwanted 5-iodo


https://dx.doi.org/10.1021/acs.oprd.0c00090
Org. Process Res. Dev. 2020, 24, 1814−1838

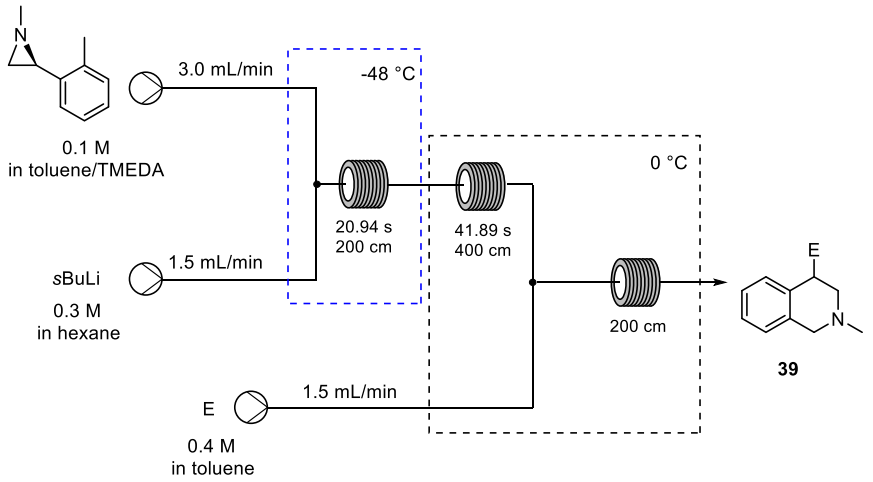


**Figure 35.** Continuous flow system enabling lateral lithiation−thermal isomerization of aziridines.

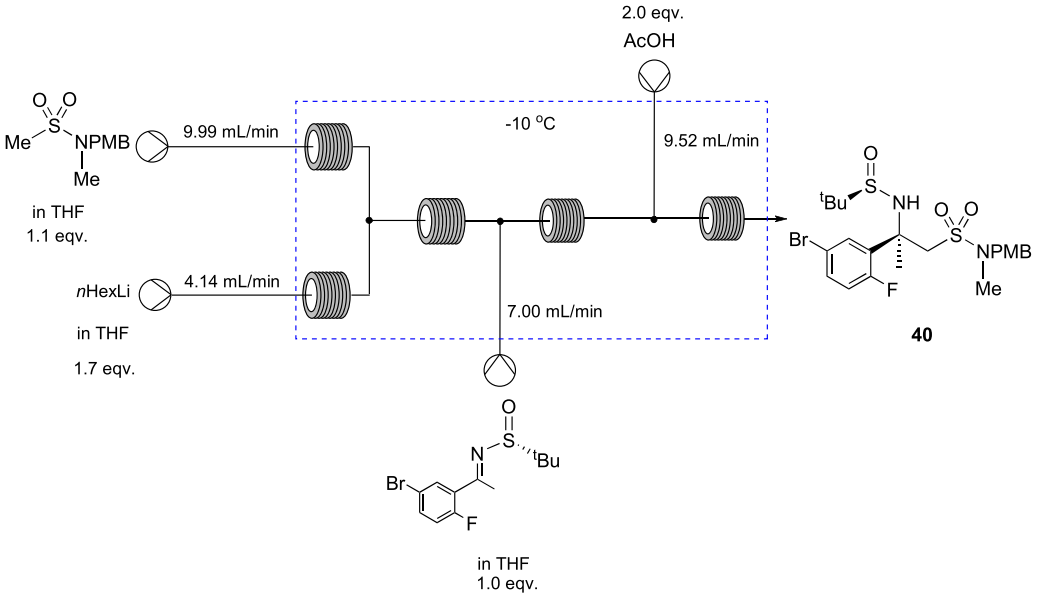


**Figure 36.** Continuous processing of the Mannich-type addition required in the manufacturing of verubecestat.

isomer. The initial continuous process designed by the authors involved mixing of PhLi and 4-fluoro-2-(trifluoromethyl)-benzonitrile in a 10 mL reactor coil at −70 °C for 20 min to facilitate the lithiation step. The lithiated intermediate progressed to meet a stream of $I_2$ delivered by a syringe pump in a second reactor coil for a residence time of 10 min, affording the desired 3-iodo product **37** on a gram scale with a throughput of 57 g $L^{-1}$ $h^{-1}$ in 63% yield (Figure 33). The authors then attempted to run the process on the pilot scale, but progress was hindered by the tendency of PhLi to add to the nitrile, lowering the yield to 50%. Additionally, this caused solid formation during longer runs. Despite these clogging events, 6.85 kg of product was generated over ca. 7 days of continuous processing involving multiple start/stop declogging events.

***sec*-Butyllithium.** *s*BuLi is another organolithium base that is often used in synthesis as a powerful organolithium reagent.[10] *s*BuLi is a stronger base than *n*BuLi but is less nucleophilic. Work by Luisi and cowokers investigated an alternative route to C4-functionalized 1,2,3,4-tetrahydroisoquinolines (THIQs) because of their significant relevance within medicine.[50] A flow chemistry platform consisting of three syringe pumps, two independently sized T-mixers, and two tube reactors was designed to carry out these functionalizations. The enantiopure substrate and *s*BuLi are supplied independently to the system, furnishing the lithiated intermediate. Various electrophiles are then introduced to the system to yield the desired products **38**/**39**. It became apparent to the authors that the reaction was temperature-dependent. Contingent upon the reaction temperature, two possible mechanistic pathways were possible. When the temperature was held at −48 °C for the duration of the reaction, production of a range of laterally substituted aziridines **38** was possible in yields of 48−90% (Figure 34). Subsequent to deprotonation, increasing the temperature to 0 °C allowed for the synthesis of C4-functionalized THIQs **39** in yields of 54−95% (Figure 35). The devised continuous flow process allowed for comprehensive isomer control. Furthermore, it allowed the direct synthesis of THIQs, of which only two known examples exist in batch.

***n*-Hexyllithium.** *n*HexLi is an organolithium base that can usually be used in place of *n*BuLi.[51] It is often used on plant


https://dx.doi.org/10.1021/acs.oprd.0c00090
Org. Process Res. Dev. 2020, 24, 1814−1838

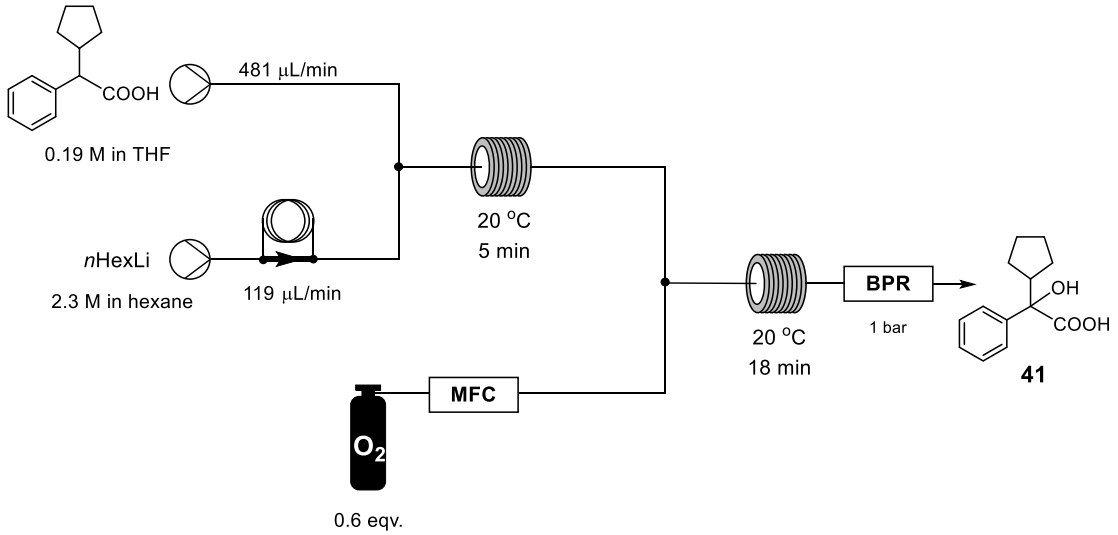


**Figure 37.** Continuous flow platform for *n*HexLi-mediated $\alpha$-lithiation and subsequent oxidation.

scale as a cost-effective and industrially safe organolithium reagent. Additionally, in terms of flow chemistry, liquid byproducts are often easier to deal with than their gaseous counterparts. Thaisrivongs et al. reported the design of a continuous flow chemistry platform for the synthesis of verubecestat, a drug that reached Phase III trials for Alzheimer's disease before being discontinued.[52] The batch synthesis of this drug candidate was problematic from the outset. The protocol proceeds via a Mannich-type addition of a methyl sulfonamide to a chiral Ellman-type sulfinyl ketimine. Excess sulfonamide and cryogenic reaction conditions were required for the batch procedure, even after several optimization attempts. The authors hypothesized that the mixing rate of the reactive species generated in the initial step was the key parameter for optimal conversion to the desired target. It was found that both the nucleophile and lithium anion irreversibly deprotonate the electrophile, competing with the Mannich-type reaction. It was thought a flow system would offer improved mixing and could alter this key parameter, preventing the irreversible deprotonation, by limiting the exposure of the ketimine from its lithiated intermediate. In the development of the continuous platform, the authors investigated the effects of four different variables: (1) mixers, (2) flow rates, (3) residence times, and (4) stoichoimetry. Knowing that lithiation of the substrate was a relatively fast reaction, the authors rationalized that once the two input streams were completely homogenized, *n*HexLi would fully deprotonate the ketimine. Two different integration tees were identified as competent mixers, and ultimately the Koflo Stratos static tube mixer was chosen. Encouraged by successful mixing results, the authors proceeded to devise a scheme in which a third and fourth pump were added to facilitate the Mannich-type reaction and an in-line quench. After optimization, the designed system afforded a yield of 87% and a diastereoselectivity of 92:8 for **40** (Figure 36). Finally, the authors studied the effect of stoichiometry on the reaction, where preliminary batch experiments were used as a foundation for the continuous flow process. Several flow runs showed that when equimolar amounts of all of the reagents were used, only 64% conversion was observed. However, when 1.5 equiv of nucleophile, 1.7 equiv of *n*HexLi, and 1.8 equiv of methyl sulfonamide were employed, optimal conversion was achieved. Additionally, the flow system removed the requirement for cryogenic reaction conditions, and reaction temperatures between −10 and 1 °C offered optimal results. Disappointingly, the authors were met with a challenege when attempting to scale the reaction to kilogram scale. Clogging was observed, and the problem appeared to increase with a rise in temperature. A decomposition event was thought to occur at the point of *n*HexLi mixing with methyl sulfonamide at the increased temperature. To avoid this issue, the heat exchangers and micromixers were cooled to −20 °C, which when coupled with optimized flow rates and stoichiometry enabled the reaction to be successfully run for over 1 h with a constant conversion of 90−91%.

Work by Luisi and co-workers illustrates the use of *n*HexLi in a continuous flow system to generate a dilithium enolate intermediate pivotal in the synthesis of cyclopentyl mandelic acid (CPMA, **41**).[53] The authors describe a telescoped process in which *n*HexLi and phenylcyclopentylacetic acid are mixed in a coiled reactor at 20 °C for a residence time of 5 min to yield the dilithium enolate intermediate. The flow platform designed uses syringe pumps to feed the reagents to the system and a sample loop to deliver *n*HexLi to the system. The intermediate then progresses to meet molecular oxygen in a second coiled reactor at 20 °C to yield the desired product **41** (Figure 37). The optimization initially used a continuous flow setup for each step of the synthesis independently. With the optimized parameters in hand, a telescoped process was examined, yielding a conversion of 57% and an isolated yield of 44%. Minor modifications to the system resulted in an increase in both conversion and isolated yield to 90% and 65%, respectively. This process is superior to the traditional methods employed to access CPMA, as the use of *n*HexLi and less than 10% $O_2$ in $N_2$ allows the platform to be considered industrially safe and scalable.

*tert*-Butyl esters are commonly found moieties in APIs and natural products. Luisi and co-workers reported a concise continuous flow system for the introduction of this functionality into various organic compounds.[54] Aryl and heteroaryl alkynes are reacted with *n*HexLi in a microfluidic system to perform direct *tert*-butoxycarbonylation. *n*HexLi is first reacted with the alkyne substrate, which is then progressed to meet a stream of $(Boc)_2O$, resulting in the generation of


https://dx.doi.org/10.1021/acs.oprd.0c00090
Org. Process Res. Dev. 2020, 24, 1814−1838

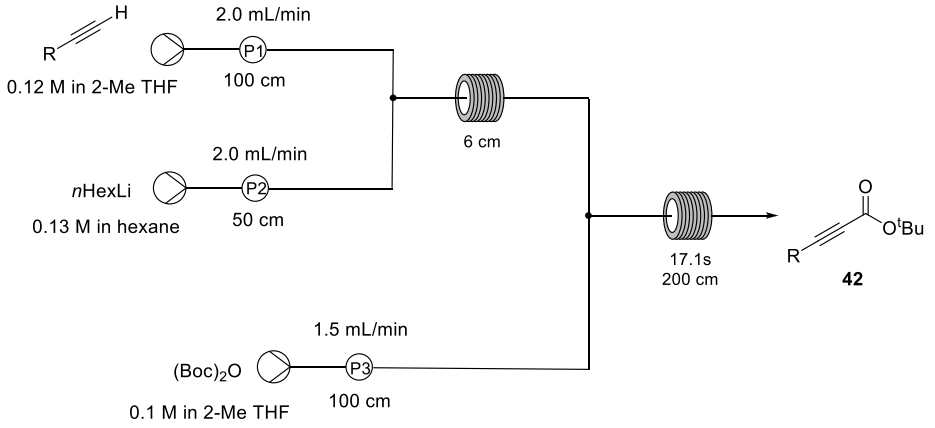


**Figure 38.** Continuous flow system to enable *tert*-butoxycarbonylation of aryl and heteroaryl substrates.

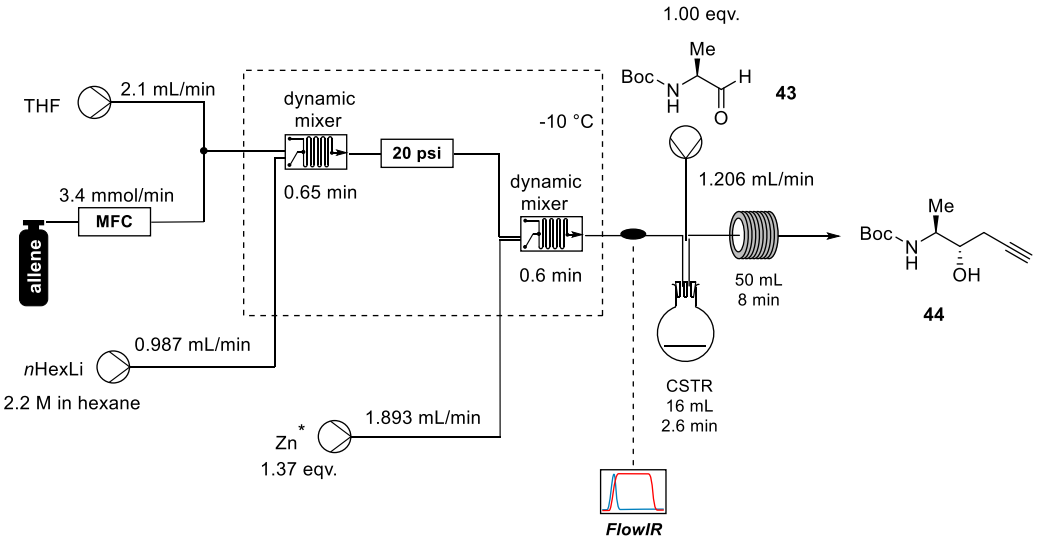


**Figure 39.** Continuous flow platform for lithiation of allene gas to facilitate the generation of homopropargyl *β*-amino alcohol.

esters **42** in yields of 50−95% (Figure 38). This process proceeds at temperatures ranging from −40 to 20 °C. Syringe pumps feed reagents to the system, where they are precooled in P1, P2, and P3. The substrate and *n*HexLi are brought together in a T-mixer before reacting to generate the deprotonated species. The temperature applied to the system is substrate-dependent, and a wide variety of substrates are well-tolerated.

Work by Bio and co-workers used *n*HexLi to facilitate the preparation of a chiral *β*-amino alcohol through asymmetric propargylation in flow.[55] The direct metalation of allene gas is a potentially attractive strategy for propargylation reactions. Allene is an inexpensive and readily available reagent, but its use is accompanied by a serious safety concern. Furthermore, cryogenic conditions are required for the lithiation step. Continuous flow technology affords methodology where allene gas can be utilized efficiently for this reaction protocol. The requirement for cryogenic conditions can be eliminated on account of the improved heat transfer in flow technology. The use of an MFC allows gases to be accurately used in a continuous flow system. The authors found that allene gas could be rapidly dissolved as gas/liquid slugs in THF by controlling the flow rate of the THF delivered by a HPLC pump and that of allene gas delivered by the MFC. The deprotonation step was initially analyzed by FlowIR, where the lithiated allene species appeared as a strong absorbance at 1864 $cm^{-1}$. The formation of the dilithiated allene species became apparent by the appearance of an absorption at 1900 $cm^{-1}$. This species proved to be problematic because it precipitated, resulting in clogging of the reactor, which was noticeable by a sharp increase in system pressure. Slow laminar flow and poor mixing causes a low allene versus *n*HexLi ratio, which was postulated as the cause of this issue. This problem was rectified simply by increasing the amount of allene gas added to the system in combination with the use of high-speed spinning-motioned stir bars, which ensured sufficient mixing and prevented clogging. These modifications enabled the continuous synthesis of allenyllithium at 0 °C for multiple hours. Further optimization identified the most efficient chiral ligand and necessary additive to establish a continuous platform for asymmetric allenylzinc propargylation. The flow process began with the allene/THF dissolution meeting a stream of *n*HexLi to generate the allenyllithium reagent. This was subsequently transmetalated with a chiral zinc complex (Zn*) to furnish a chiral allenylzinc complex, whose formation was monitored by FlowIR. This complex proceeded to meet a solution of enantiopure Boc-L-alaninal (**43**) in a 25 mL continuous stirred tank reactor (CSTR) at room temperature. The authors found that the product d.r. was sensitive to the mode of mixing between the aldehyde and the allenylzinc chiral complex. The


https://dx.doi.org/10.1021/acs.oprd.0c00090
Org. Process Res. Dev. 2020, 24, 1814−1838

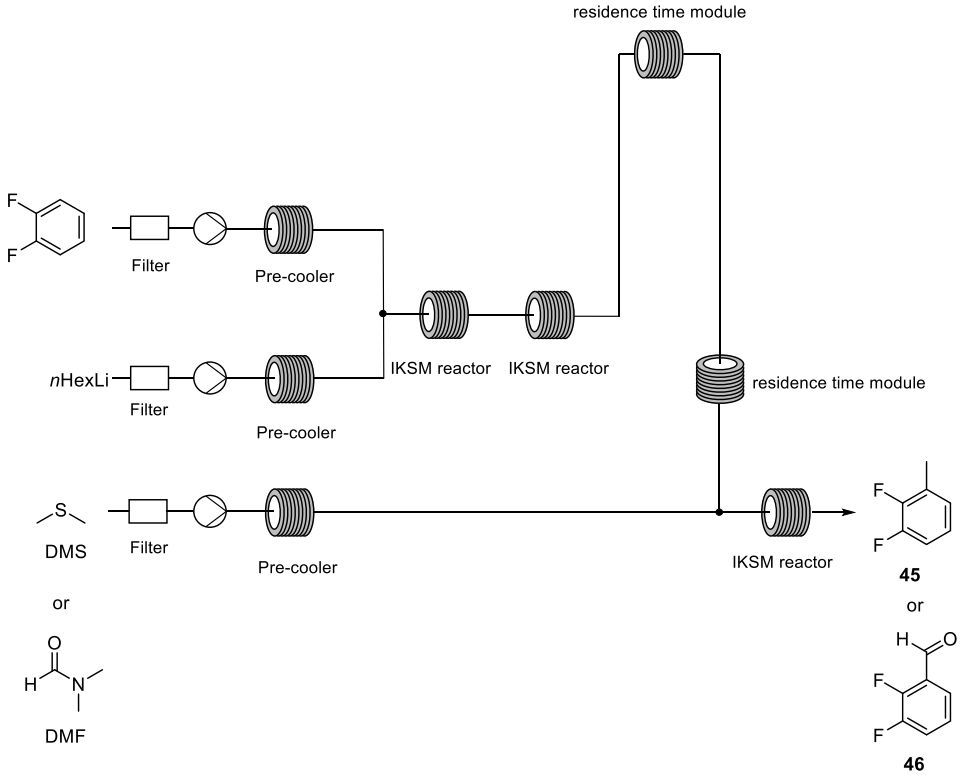


**Figure 40.** LT unit continuous processing of DFT and DFBA.

CSTR was chosen because it produced the optimal d.r. for the reaction. The product was outflowed to a 50 mL tubular reactor to create the desired overall residence time of 10.6 min at ambient temperature to provide for the asymmetric propargylation (Figure 39). This continuous setup produced the desired $\beta$-amino alcohol **44** in 85% yield with a d.r. of 32:1 and a production rate of 15 g/h.

The final example of the use of *n*HexLi in continuous flow involved the scale-up of a robust lab-scale procedure to an industrial scale. A publication by Mleczko and co-workers reported the use of *n*HexLi and fluoroaromatic compounds to generate 2,3-difluorotoluene (DFT, **45**) or 2,3-difluorobenzaldehyde (DFBA, **46**) (Figure 40).[56] DFT is useful as an intermediate for the synthesis of pharmaceuticals and electronics and in the agrochemical industry. However, the lithiated intermediate generated en route is a highly reactive species that is known to participate in several runaway reactions. These authors used preliminary microreactor technology (MRT)-based laboratory experiments as a foundation for scaling DFT and DFBA synthetic processes. MRT was viewed as a preferable route to scale the process because of its superior heat transfer capabilities. Both synthetic routes have significant associated exotherms, leading to potential runaway reactions in a large-scale batch reactor. Thus, the laboratory studies with the fluoroaromatics were performed in a low-temperature (LT) microreactor. The reactions were performed at a temperature of −45 °C with a throughput of 10 g/h. In these reaction runs, DFT and DFBA were successfully synthesized in yields of 95% and 90%, respectively. The authors then repeated these experiments in an industrial standard LT unit. The LT unit used three parallel piston-membrane pumps to minimize pulsations in the continuous process. Temperatures were also measured directly in the product stream, downstream from the reaction modules. Because of the exotherm associated with the process step, the process required a residence time of ∼5 min to efficiently remove the heat produced, particularly in the challenging DFT route. In order to sustain stable operation during the DFT synthesis, the throughput had to be reduced from 1.07 to 0.5 kg/h. Higher throughputs led to runaway reactions in the second stage of the process. Using the optimized conditions in the LT unit gave a yield of 95% for both DFT and DFBA synthesis. Additionally, it was possible to scale the DFBA and DFT processes by factors of 100 and 50, respectively, with no negative impact on performance. Overall, the continuous process was superior to the corresponding batch process. A regioselectivity of 94% was achieved in the continuous process, in contrast to 90% in the batch operation. Furthermore, through the MRT operation approximately 40 kg of product was synthesized in 24 h using a total volume of 3 L. In batch mode, only 20 kg of product could be produced per 400 L batch in 24 h. Finally, a more scalable temperature of −45 °C was required in the continuous flow process, unlike the temperature of −70 °C necessary in batch mode.

## ■ CONCLUSION

Deprotonation chemistry using organolithium bases is a mainstay of organic synthesis. However, many organolithium reagents come with a nonideal safety profile, and typically this type of chemistry is carried out at low temperature (often −78 °C). Thus, scale-up of these protocols in an industrial context is difficult. At the very least, direct synthetic routes that prove highly efficient at small scale are replaced by more convoluted ones on scale-up. Ultimately, predicted issues surrounding scale-up can lead to new chemistries and thus new molecular entities and associated biological activities being unexplored.

Flow chemistry has the potential to avoid most of the pitfalls associated with organolithium chemistry in batch through the


https://dx.doi.org/10.1021/acs.oprd.0c00090
Org. Process Res. Dev. 2020, 24, 1814−1838

use of highly efficient mass and heat transfer, precise control of residence times, and mixing apparatus.

This review aims to underline the importance and associated benefits of continuous processing for the handling and employment of organolithium reagents in organic synthesis, paying specific attention to deprotonation chemistry. The papers cited herein demonstrate how cryogenic conditions are easier to control or can be eliminated in flow processes, leading to reductions in the number of synthetic steps, shorter processing times, more selective reactions, higher conversions, and improved safety profiles. Continuous flow chemistry has also allowed many unsuccessful or so-far-impossible batch mode reactions to be successfully performed.

Flow platforms offer variety within their systemic design where individual system modules can be interchanged for specific reaction control. Different pumps can be used for different reaction requirements. For example, on small scales, syringe pumps used alongside sample loops are often the chosen injection apparatus for organolithium reagents because of their improved safety and chemical resistance profiles. Furthermore, process analytical technology (PAT) tools are becoming more commonly integrated into continuous processes to identify key parameters for reaction success, aiding the efficiency and scalability of a given process. Finally, flow enables efficient telescoping of reaction schemes. In simple yet critically important examples, we see the generation of LDA in situ, which avoids issues around concentration and precipitation associated with the commercially available base.

All that said, it would be remiss to exclude the challenges still faced when using organolithium reagents in continuous flow. Thus, this review also highlights these problems, which include the persistent formation of precipitates, which leads to clogging of reaction systems. Importantly, however, some strategies are emerging to alleviate this problem, such as the filtering of feed stock solutions, accurate temperature control, and the development of clean-in-place techniques.

Additionally, certain elements of established small-scale organolithium batch chemistry are still widely unexplored in flow. For example, powerful asymmetric processes involving lithium (aza)enolates[57−60] have not been investigated in flow. Furthermore, flow chemistry offers the potential to re-engage with the use of *t*BuLi as a reagent. The safety profile of *t*BuLi often causes chemists and industrialists to avoid its use. However, *t*BuLi is a very useful reagent for many organic reactions,[10] and undoubtedly flow chemistry has the potential to add this reagent to our repertoire.

While flow chemistry is now considered a mainstream technology in pharma,[61] the examples depicted in this review showcase how organolithium-base-mediated methodologies, which are often deemed difficult to scale-up because of their safety profile and heat transfer properties, can be cleanly handled and scaled in flow.

## AUTHOR INFORMATION


### Corresponding Author

**Gerard P. McGlacken** − *School of Chemistry, Analytical and Biological Chemistry Research Facility (ABCRF), and Synthesis and Solid State Pharmaceutical Centre (SSPC), University College Cork, Cork T12 YN60, Ireland;* orcid.org/0000-0002-7821-0804; Email: g.mcglacken@ucc.ie

### Authors

**Mark Power** − *School of Chemistry and Analytical and Biological Chemistry Research Facility (ABCRF), University College Cork, Cork T12 YN60, Ireland*

**Emma Alcock** − *School of Chemistry and Analytical and Biological Chemistry Research Facility (ABCRF), University College Cork, Cork T12 YN60, Ireland*

Complete contact information is available at: https://pubs.acs.org/10.1021/acs.oprd.0c00090


### Notes

The authors declare no competing financial interest.

## ACKNOWLEDGMENTS

This work was supported by the Irish Research Council. The authors thank Dr. David Jones and Aobha Hickey for proof-checking.

## REFERENCES


(1) Fitzpatrick, D. E.; Ley, S. V. Engineering Chemistry for the Future of Chemical Synthesis. *Tetrahedron* **2018**, *74*, 3087−3100.

(2) Gérardy, R.; Emmanuel, N.; Toupy, T.; Kassin, V. E.; Tshibalonza, N. N.; Schmitz, M.; Monbaliu, J. C. M. Continuous Flow Organic Chemistry: Successes and Pitfalls at the Interface with Current Societal Challenges. *Eur. J. Org. Chem.* **2018**, *2018*, 2301−2351.

(3) Plutschack, M. B.; Pieber, B.; Gilmore, K.; Seeberger, P. H. The Hitchhiker's Guide to Flow Chemistry. *Chem. Rev.* **2017**, *117*, 11796−11893.

(4) Movsisyan, M.; Delbeke, E. I. P.; Berton, J. K. E. T.; Battilocchio, C.; Ley, S. V.; Stevens, C. V. Taming Hazardous Chemistry by Continuous Flow Technology. *Chem. Soc. Rev.* **2016**, *45*, 4892−4928.

(5) Nagaki, A. Recent Topics of Functionalized Organolithiums Using Flow Microreactor Chemistry. *Tetrahedron Lett.* **2019**, *60*, 150923.

(6) Colella, M.; Nagaki, A.; Luisi, R. Flow Technology for the Genesis and Use of (Highly) Reactive Organometallic Reagents. *Chem. - Eur. J.* **2020**, *26*, 19−32.

(7) Zhao, T.; Micouin, L.; Piccardi, R. Synthesis of Organometallic Compounds in Flow. *Helv. Chim. Acta* **2019**, *102*, e1900172.

(8) Henderson, R. K.; Hill, A. P.; Redman, A. M.; Sneddon, H. F. Development of GSK's Acid and Base Selection Guides. *Green Chem.* **2015**, *17*, 945−949.

(9) Green, P.; Zuev, D. Phenyllithium. In *Encyclopedia of Reagents for Organic Synthesis*; John Wiley & Sons: Chichester, U.K., 2001.

(10) Clayden, J. In *Organolithiums: Selectivity for Synthesis*; Pergamon Press: Oxford, U.K., 2002; p 23.

(11) Newby, J. A.; Blaylock, D. W.; Witt, P. M.; Pastre, J. C.; Zacharova, M. K.; Ley, S. V.; Browne, D. L. Design and Application of a Low-Temperature Continuous Flow Chemistry Platform. *Org. Process Res. Dev.* **2014**, *18*, 1211−1220.

(12) Nagaki, A.; Matsuo, C.; Kim, S.; Saito, K.; Miyazaki, A.; Yoshida, J. Lithiation of 1,2-Dichloroethene in Flow Microreactors: Versatile Synthesis of Alkenes and Alkynes by Precise Residence-Time Control. *Angew. Chem., Int. Ed.* **2012**, *51*, 3245−3248.

(13) Chada, S.; Mandala, D.; Watts, P. Synthesis of a Key Intermediate towards the Preparation of Efavirenz Using *n*-Butyllithium. *J. Flow Chem.* **2017**, *7*, 37−40.

(14) Radesca, L. A.; Lo, Y. S.; Moore, J. R.; Pierce, M. E. Synthesis of HIV-1 Reverse Transcriptase Inhibitor DMP 266. *Synth. Commun.* **1997**, *27*, 4373−4384.

(15) Muchowski, J. M.; Venuti, M. C. Ortho Functionalization of *N*-(*tert*-butoxycarbonyl)aniline. *J. Org. Chem.* **1980**, *45*, 4798−4801.

(16) Fukuyama, T.; Chiba, H.; Kuroda, H.; Takigawa, T.; Kayano, A.; Tagami, K. Application of Continuous Flow for DIBAL-H Reduction and n-BuLi Mediated Coupling Reaction in the Synthesis of Eribulin Mesylate. *Org. Process Res. Dev.* **2016**, *20*, 503−509.

(17) Lin, N. U.; Burstein, H. J. EMBRACE, Eribulin, and New Realities of Advanced Breast Cancer. *Lancet* **2011**, *377*, 878−880.
(18) Hafner, A.; Mancino, V.; Meisenbach, M.; Schenkel, B.; Sedelmeier, J. Dichloromethyllithium: Synthesis and Application in Continuous Flow Mode. *Org. Lett.* **2017**, *19*, 786−789.
(19) Stueckler, C.; Hermsen, P.; Ritzen, B.; Vasiloiu, M.; Poechlauer, P.; Steinhofer, S.; Pelz, A.; Zinganell, C.; Felfer, U.; Boyer, S.; Goldbach, M.; De Vries, A.; Pabst, T.; Winkler, G.; LaVopa, V.; Hecker, S.; Schuster, C. Development of a Continuous Flow Process for a Matteson Reaction: From Lab Scale to Full-Scale Production of a Pharmaceutical Intermediate. *Org. Process Res. Dev.* **2019**, *23*, 1069−1077.
(20) Hughes, D. L. Applications of Flow Chemistry in Drug Development: Highlights of Recent Patent Literature. *Org. Process Res. Dev.* **2018**, *22*, 13−20.
(21) Hecker, S. J.; Reddy, K. R.; Totrov, M.; Hirst, G. C.; Lomovskaya, O.; Griffith, D. C.; King, P.; Tsivkovski, R.; Sun, D.; Sabet, M.; Tarazi, Z.; Clifton, M. C.; Atkins, K.; Raymond, A.; Potts, K. T.; Abendroth, J.; Boyer, S. H.; Loutit, J. S.; Morgan, E. E.; Durso, S.; Dudley, M. N. Discovery of a Cyclic Boronic Acid $\beta$-Lactamase Inhibitor (RPX7009) with Utility vs Class A Serine Carbapenemases. *J. Med. Chem.* **2015**, *58*, 3682−3692.
(22) Zeller, J. R.; Venkatraman, S.; Brot, E. C. A.; Iyer, S.; Hall, M. LFA-1 Inhibitor and Methods of Preparation and Polymorph Thereof. US 9,085,553 B2, July 21, 2015.
(23) Tweedle, S.; Venkatraman, S.; Liu, S.; Zeller, J.; Brot, E.; Hamlin, M.; Newman, M.; McLaws, M.; Rosenberg, J.; Lathbury, D. Continuous Flow Carboxylation Reaction. US 2016/0090361 A1, March 31, 2016.
(24) Seghers, S.; Heugebaert, T. S. A.; Moens, M.; Sonck, J.; Thybaut, J. W.; Stevens, C. V. Design of a Mesoscale Continuous-Flow Route toward Lithiated Methoxyallene. *ChemSusChem* **2018**, *11*, 2248−2254.
(25) Wong, J. Y. F.; Tobin, J. M.; Vilela, F.; Barker, G. Batch Versus Flow Lithiation−Substitution of 1,3,4-Oxadiazoles: Exploitation of Unstable Intermediates Using Flow Chemistry. *Chem. - Eur. J.* **2019**, *25*, 12439−12445.
(26) Micetich, R. G. Lithiation of Five-Membered Heteroaromatic Compounds. The Methyl Substituted 1,2-Azoles, Oxadiazoles, and Thiadiazoles. *Can. J. Chem.* **1970**, *48*, 2006−2015.
(27) Dunn, A. L.; Leitch, D. C.; Journet, M.; Martin, M.; Tabet, E. A.; Curtis, N. R.; Williams, G.; Goss, C.; Shaw, T.; O'Hare, B.; Wade, C.; Toczko, M. A.; Liu, P. Selective Continuous Flow Iodination Guided by Direct Spectroscopic Observation of Equilibrating Aryl Lithium Regioisomers. *Organometallics* **2019**, *38*, 129−137.
(28) Turnbull, P. S.; Cadilla, R. Indolecarbonitriles as Selective Androgen Receptor Modulators. US 9,533,948 B2, January 3, 2017.
(29) Branca, M.; Gori, D.; Guillot, R.; Alezra, V.; Kouklovsky, C. Tertiary Aromatic Amide for Memory of Chirality: Access to Enantioenriched $\alpha$-Substituted Valine. *J. Am. Chem. Soc.* **2008**, *130*, 5864−5865.
(30) Mambrini, A.; Gori, D.; Kouklovsky, C.; Kim, H.; Yoshida, J.; Alezra, V. Memory of Chirality in a Flow-Based System: Enantioselective Synthesis of Quaternary $\alpha$-Amino Acids Using Flow Microreactors. *Eur. J. Org. Chem.* **2018**, *2018*, 6754−6757.
(31) Hartwig, J.; Metternich, J. B.; Nikbin, N.; Kirschning, A.; Ley, S. V. Continuous Flow Chemistry: A Discovery Tool for New Chemical Reactivity Patterns. *Org. Biomol. Chem.* **2014**, *12*, 3611−3615.
(32) Pieber, B.; Glasnov, T.; Kappe, C. O. Flash Carboxylation: Fast Lithiation−Carboxylation Sequence at Room Temperature in Continuous Flow. *RSC Adv.* **2014**, *4*, 13430−13433.
(33) Sagmeister, P.; Williams, J. D.; Hone, C. A.; Kappe, C. O. Laboratory of the Future: A Modular Flow Platform with Multiple Integrated PAT Tools for Multistep Reactions. *React. Chem. Eng.* **2019**, *4*, 1571−1578.
(34) Gupta, L.; Hoepker, A. C.; Singh, K. J.; Collum, D. B. Lithium Diisopropylamide-Mediated Ortholithiations: Lithium Chloride Catalysis. *J. Org. Chem.* **2009**, *74*, 2231−2233.
(35) Ganiek, M. A.; Becker, M. R.; Berionni, G.; Zipse, H.; Knochel, P. Barbier Continuous Flow Preparation and Reactions of Carbamoyllithiums for Nucleophilic Amidation. *Chem. - Eur. J.* **2017**, *23*, 10280−10284.
(36) Bakonyi, B.; Furegati, M.; Kramer, C.; La Vecchia, L.; Ossola, F. Synthesis of All Four Stereoisomers of 3-(tert-Butoxycarbonyl)-3-azabicyclo[3.1.0]hexane-2-carboxylic Acid. *J. Org. Chem.* **2013**, *78*, 9328−9339.
(37) Gustafsson, T.; Sörensen, H.; Pontén, F. Development of a Continuous Flow Scale-Up Approach of Reflux Inhibitor AZD6906. *Org. Process Res. Dev.* **2012**, *16*, 925−929.
(38) Müller, S. T. R.; Hokamp, T.; Ehrmann, S.; Hellier, P.; Wirth, T. Ethyl Lithiodiazoacetate: Extremely Unstable Intermediate Handled Efficiently in Flow. *Chem. - Eur. J.* **2016**, *22*, 11940−11942.
(39) Clark, J. D.; Shah, A. S.; Peterson, J. C.; Patelis, L.; Kersten, R. J. A.; Heemskerk, A. H.; Grogan, M.; Camden, S. The Thermal Stability of Ethyl Diazoacetate. *Thermochim. Acta* **2002**, *386*, 65−72.
(40) Seyler, H.; Haid, S.; Kwon, T. H.; Jones, D. J.; Bäuerle, P.; Holmes, A. B.; Wong, W. W. H. Continuous Flow Synthesis of Organic Electronic Materials − Case Studies in Methodology Translation and Scale-up. *Aust. J. Chem.* **2013**, *66*, 151−156.
(41) von Keutz, T.; Strauss, F. J.; Cantillo, D.; Kappe, C. O. Continuous Flow Multistep Synthesis of $\alpha$-Functionalized Esters via Lithium Enolate Intermediates. *Tetrahedron* **2018**, *74*, 3113−3117.
(42) Wu, G.; Huang, M. Organolithium Reagents in Pharmaceutical Asymmetric Processes. *Chem. Rev.* **2006**, *106*, 2596−2616.
(43) Venturoni, F.; Nikbin, N.; Ley, S. V.; Baxendale, I. R. The Application of Flow Microreactors to the Preparation of a Family of Casein Kinase I Inhibitors. *Org. Biomol. Chem.* **2010**, *8*, 1798−1806.
(44) Ganiek, M. A.; Ivanova, M. V.; Martin, B.; Knochel, P. Mild Homologation of Esters through Continuous Flow Chloroacetate Claisen Reactions. *Angew. Chem., Int. Ed.* **2018**, *57*, 17249−17253.
(45) Köckinger, M.; Ciaglia, T.; Bersier, M.; Hanselmann, P.; Gutmann, B.; Kappe, C. O. Utilization of Fluoroform for Difluoromethylation in Continuous Flow: A Concise Synthesis of $\alpha$-Difluoromethyl-Amino Acids. *Green Chem.* **2018**, *20*, 108−112.
(46) Jordan, R. W. Continuous Flow Process for the Preparation of Ingenol-3-mebutate. US 9,758,464 B2, September 12, 2017.
(47) Jørgensen, L.; McKerrall, S. J.; Kuttruff, C. A.; Ungeheuer, F.; Felding, J.; Baran, P. S. 14-Step Synthesis of (+)-Ingenol from (+)-3-Carene. *Science* **2013**, *341*, 878−882.
(48) Höberg, T.; Grue-Sorenson, G.; Liang, X.; Horneman, A. M.; Petersen, A. K. Method of Producing Ingenol-3-angelate. US 9,676,698 B2, June 13, 2017.
(49) Vilé, G.; Schmidt, G.; Richard-Bildstein, S.; Abele, S. Enantiospecific Cyclization of Methyl N-(Tert-Butoxycarbonyl)-N-(3-Chloropropyl)-D-Alaninate to 2-Methylproline Derivative via 'Memory of Chirality' in Flow. *J. Flow Chem.* **2019**, *9*, 19−25.
(50) Giovine, A.; Musio, B.; Degennaro, L.; Falcicchio, A.; Nagaki, A.; Yoshida, J.; Luisi, R. Synthesis of 1,2,3,4-Tetrahydroisoquinolines by Microreactor-Mediated Thermal Isomerization of Laterally Lithiated Arylaziridines. *Chem. - Eur. J.* **2013**, *19*, 1872−1876.
(51) Rathman, T. L. Hexyllithium. In *Encyclopedia of Reagents for Organic Synthesis*; John Wiley & Sons: Chichester, U.K., 2001.
(52) Thaisrivongs, D. A.; Naber, J. R.; McMullen, J. P. Using Flow To Outpace Fast Proton Transfer in an Organometallic Reaction for the Manufacture of Verubecestat (MK-8931). *Org. Process Res. Dev.* **2016**, *20*, 1997−2004.
(53) De Angelis, S.; Hone, C. A.; Degennaro, L.; Celestini, P.; Luisi, R.; Kappe, C. O. Sequential $\alpha$-Lithiation and Aerobic Oxidation of an Arylacetic Acid—Continuous-Flow Synthesis of Cyclopentyl Mandelic Acid. *J. Flow Chem.* **2018**, *8*, 109−116.
(54) Degennaro, L.; Maggiulli, D.; Carlucci, C.; Fanelli, F.; Romanazzi, G.; Luisi, R. A Direct and Sustainable Synthesis of Tertiary Butyl Esters Enabled by Flow Microreactors. *Chem. Commun.* **2016**, *52*, 9554−9557.
(55) Li, H.; Sheeran, J. W.; Clausen, A. M.; Fang, Y.; Bio, M. M.; Bader, S. Flow Asymmetric Propargylation: Development of


https://dx.doi.org/10.1021/acs.oprd.0c00090
*Org. Process Res. Dev.* 2020, 24, 1814−1838

Continuous Processes for the Preparation of a Chiral β-Amino Alcohol. *Angew. Chem., Int. Ed.* **2017**, *56*, 9425−9429.
(56) Laue, S.; Haverkamp, V.; Mleczko, L. Experience with Scale-Up of Low-Temperature Organometallic Reactions in Continuous Flow. *Org. Process Res. Dev.* **2016**, *20*, 480−486.
(57) McSweeney, C. M.; Foley, V. M.; McGlacken, G. P. The asymmetric Alkylation of Dimethylhydrazones; Intermolecular Chirality Transfer Using Sparteine as Chiral Ligand. *Chem. Commun.* **2014**, *50*, 14817−14819.
(58) Cano, R.; Zakarian, A.; McGlacken, G. P. Direct Asymmetric Alkylation of Ketones: Still Unconquered. *Angew. Chem., Int. Ed.* **2017**, *56*, 9278−9290.
(59) Job, A.; Janeck, C. F.; Bettray, W.; Peters, R.; Enders, D. The SAMP-/RAMP-Hydrazone Methodology in Asymmetric Synthesis. *Tetrahedron* **2002**, *58*, 2253−2329.
(60) Franklin, A. S.; Paterson, I. Recent Developments in Asymmetric Aldol Methodology. *Contemp. Org. Synth.* **1994**, *1*, 317−338.
(61) Porta, R.; Benaglia, M.; Puglisi, A. Flow Chemistry: Recent Developments in the Synthesis of Pharmaceutical Products. *Org. Process Res. Dev.* **2016**, *20*, 2−25.

## ■ NOTE ADDED AFTER ASAP PUBLICATION

This paper orginally published ASAP on 5/14/20. The caption for Figure 1 has been modified and the new version of the paper was reposted on 5/29/20.



https://dx.doi.org/10.1021/acs.oprd.0c00090
*Org. Process Res. Dev.* 2020, 24, 1814−1838

Reaction Chemistry & Engineering

ROYAL SOCIETY OF CHEMISTRY

COMMUNICATION

View Article Online
View Journal | View Issue



Cite this: *React. Chem. Eng.*, 2023, **8**, 1839

Received 17th April 2023,
Accepted 29th April 2023

DOI: 10.1039/d3re00229b

rsc.li/reaction-engineering



# The α-alkylation of ketones in flow†

Ella Cooper,‡ Emma Alcock,‡ Mark Power and Gerard McGlacken *

**The α-deprotonation and alkylation of ketones is a fundamental transformation in organic chemistry. However, the apparent simplicity of this process belies its complexity. Oftentimes experimental conditions are non-ideal, and yields are low. Herein, we directly target these issues, and provide a continuous flow methodology which leads to excellent yields, reduces reaction time, avoids cryogenic temperatures, minimises exposure to alkyllithiums/alkylhalides, and can be scaled-out.**

The α-deprotonation and alkylation of ketones is a fundamental transformation in organic chemistry, taught at undergraduate level.[1] Ketone lithium enolates are utilised in particular,[2] and are applied 'pervasively'[3] both in academia[2] and industry.[4] The abundance of commercially available ketones which are potentially enolisable (>10 000)[5] bolsters the applicability of simple alkylation protocols.

Although a conceptually simple transformation, the practical α-alkylation of a ketone (Fig. 1) is plagued with issues. Firstly, the transformation can be low yielding.[6–8] This is usually as a result of either: i) incomplete enolisation, ii) incomplete alkylation or iii) problematic side reactions. Aldol-type reactions/condensations, *O*-alkylation, dialkylation and persistent presence of starting ketone, are the most common issues. To alleviate these problems and effect some control over the reactivity of highly energetic lithium enolate intermediates, cryogenic reaction conditions (usually −78 °C) are employed. Efficient ketone alkylation remains a key goal and a highly rewarding endeavour for organic chemists.[9]

Seminal reports by Enders and Corey[10] described an alternative approach for the synthesis of α-substituted ketones. In this work, *N*,*N*-dimethylhydrazones (DMHs) were used as ketone surrogates allowing access to a range of α-substituted ketones in good yields. Despite the widespread application of the DMH strategy,[11] the use of dimethylhydrazine in stoichiometric quantities, and issues around the formation of toxic by-products formed upon ketone reinstatement, makes this alternative protocol a very unattractive choice. The classic Stork enamine protocol[12] has advantages, but again is not a direct alkylation of ketones.

Overall, we envisaged that the direct alkylation of ketones could be improved upon, and a number of the issues (*vide supra*) could be obviated by using continuous flow technology. In addition to the challenges associated with the previously discussed issues, reactor clogging due to aggregation of organometallic speciation,[13,14] was a concern of ours, but we anticipated that use of a peristaltic pump, at least during the process of alkylation and LiBr formation, would obviate these issues.

Listed as one of IUPACs top emerging technologies in chemistry in 2019,[15] continuous flow chemistry has emerged from an enabling technology to a new platform for improved chemistry. The development of continuous flow chemistry

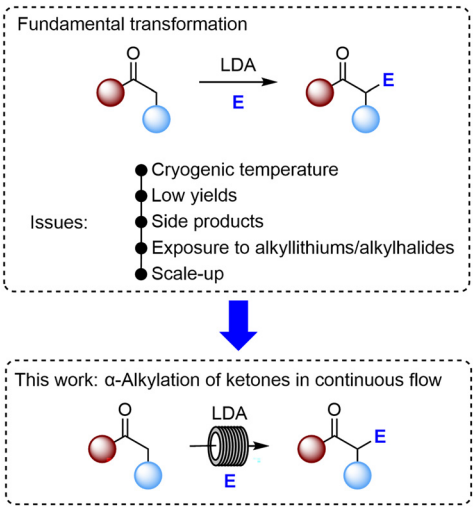


**Fig. 1** The α-alkylation of ketones: issues alleviated in continuous flow.

*School of Chemistry and Analytical and Biological Chemistry Research Facility, University College Cork, T12 YN60 Cork, Ireland. E-mail: g.mcglacken@ucc.ie*

† Electronic supplementary information (ESI) available. See DOI: https://doi.org/10.1039/d3re00229b

‡ Authors contributed equally.

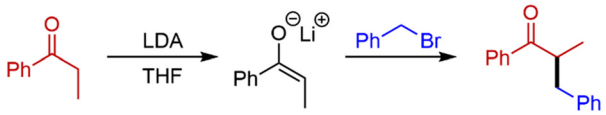


Scheme 1 The α-alkylation of propiophenone using BnBr.

can provide a plethora of benefits, including the discovery of new reactivity patterns, improved reaction efficiency, enhanced safety, and scalability.[16–20] Pioneering work by Yoshida[21] encapsulates these benefits *via* the use of organolithiums in flow.[22]

An excellent report by Kappe involving the continuous flow alkylation of esters has been reported.[23] Specific issues "especially in the case of enolates derived from ketones" was noted by Kappe. The pointed divergent reactivity of ketones and esters (related to the comparatively lower p$K_a$[24] and higher electrophilicity[25] of ketones) requires new methodology/engineering development, and a scale-out for both reactions in flow has yet to be reported to the best of our knowledge.

Herein, we document a successful continuous flow methodology for the synthesis of α-alkylated ketones in good to excellent yields. Numerous advantages over the corresponding batch reaction are detailed and include: i) reduced reaction times; ii) elimination of cryogenic conditions, iii) increased safety profile; and iv) facile scale-out.

## Results and discussion

Initially, deprotonation of propiophenone using LDA[26] and α-alkylation using benzyl bromide (BnBr) was chosen as the model system for our optimisation (Scheme 1). In batch, this transformation uses temperatures as low as −78 °C, and reaction times of up to 20 hours. This is a problematic reaction and, in our hands, we achieve variable yields of 25–45% in batch.

Our initial continuous flow set-up consisted of two reaction zones: i) enolate formation and ii) electrophilic addition. The ketone substrate was delivered to the system *via* a commercially available HPLC/piston pump (Vapourtec R-series). With the aid of a second HPLC/piston pump, a solution of commercially available LDA was added to the system *via* a sample loop. The alkylating agent was introduced *via* a peristaltic pump (Vapourtec R-series). A 10 mL dual-core cooled reactor coil and a 10 mL heated reactor coil were used for all reactions. PFA reactor tubing was utilised, and the reagents were sequentially mixed using Teflon T-mixers (Table 1). An anhydrous, inert atmosphere and a pressure of 7 bar was maintained throughout.

Initially, RC 1 was set at a temperature of −15 °C and RC 2 was set to room temperature (rt) (Table 1, entry 1). Disappointingly however, these conditions resulted in no observed α-benzylated product. Subsequently, we decreased the temperature of RC 1, and increased the temperature of RC 2 (Table 1, entry 2), which gave a steady state yield of 15%. Gratifyingly, a continual increase of the temperature of

Table 1 Optimisation parameters for the α-alkylation of propiophenone using benzyl bromide[a]

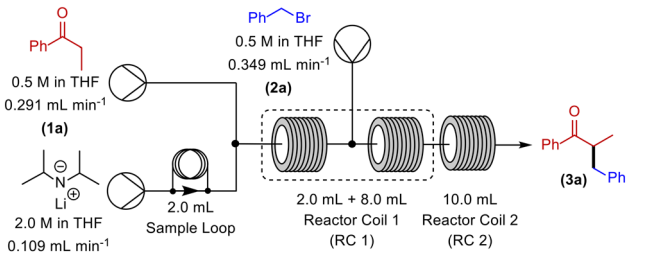


| Entry | RC 1 temp (°C) | RC 2 temp (°C) | Residence time (min) | Steady state[b] (yield%) |
|---|---|---|---|---|
| 1 | −15 | rt | 5 | 0 |
| 2 | −70 | 75 | 5 | 15 |
| 3 | −45 | 75 | 5 | 39 |
| 4 | −30 | 75 | 5 | 53 |
| 5 | −15 | 75 | 5 | 64 |
| 6 | 0 | 75 | 5 | 70 |

[a] Unless otherwise noted, conditions are as follows: 1 equiv. of propiophenone, 1.5 equiv. of LDA, 1.2 equiv. of BnBr. [b] Determined by use of $^1$H NMR with 1,3,5-trimethoxybenzene as internal standard.

RC 1 to 0 °C (Table 1, entries 2–6) culminated in a yield of 70% of α-benzylated product, at steady state.

With these partially optimised reaction conditions in hand, we made two further alterations to our reaction conditions. Firstly, due to decreased volatility, we changed the alkylating agent employed to *p-tert*-butylbenzyl bromide (for comparison, in our hands, we achieved a 44% yield in batch using this electrophile). Secondly, we altered the configuration of the dual-core cooled reactor (RC 1) from (2 mL + 8 mL) configuration to (8 mL + 2 mL) configuration. This configurational swap allowed for a greater residence time for the enolate formation step, which we hoped would result in an increased yield of α-benzylated product. Using our previously optimised conditions, we initiated these reactions with the temperature of RC 1 set to 0 °C, which resulted in a 60% yield of α-benzylated product at steady state (Table 2, entry 1). Further increasing the temperature of RC 1 to room temperature resulted in a slight increase in the yield (Table 2, entry 2). In addition, the yield was further increased by lowering the equivalents of LDA (Table 2, entry 3). Extending the residence time from 5 min to 7.5 min resulted in a significant increase in the yield, to 80%, of α-benzylated product (Table 2, entry 4). Prolonging the residence time further to 10 min, gave a 90% steady state yield of α-benzylated ketone (Table 2, entry 5). However, any further increase in the residence time did not result in any improvement in yield (Table 2, entry 6).

With the optimised reaction conditions in hand, we next sought to examine a small range of ketones and electrophiles tolerated within this methodology (Table 3). Initially, the reactions of a range of electrophiles, including benzyl and allylhalides were examined in the α-alkylation reaction of propiophenone (Table 3, entries 1–6). Pleasingly, in all cases, good to excellent yields (75–92%) of α-alkylated products

**Table 2** Optimisation parameters for the α-alkylation of propiophenone using *p*-*tert*-butylbenzyl bromide[a]

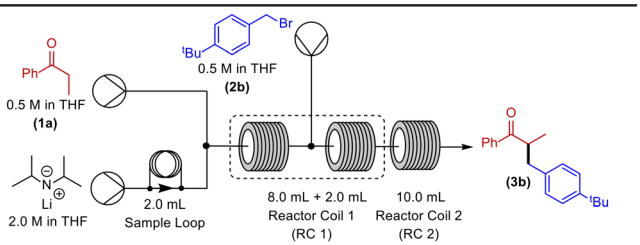


| Entry | LDA (equiv.) | Electrophile (equiv.) | RC 1 temp (°C) | Residence time (min) | Steady state[b] (yield%) |
|---|---|---|---|---|---|
| 1 | 1.5 | 1.2 | 0 | 5 | 60 |
| 2 | 1.5 | 1.2 | rt | 5 | 63 |
| 3 | 1.2 | 1.5 | rt | 5 | 70 |
| 4 | 1.2 | 1.5 | rt | 7.5 | 80 |
| 5 | 1.2 | 1.5 | rt | 10 | 90 |
| 6 | 1.2 | 1.5 | rt | 15 | 60 |

[a] Unless otherwise noted, conditions are as follows: 1 equiv. of propiophenone, RC 2 temperature set to 75 °C. [b] Determined by use of $^1$H NMR with 1,3,5-trimethoxybenzene as internal standard.

were obtained at steady state. Altering the ketone substrate proved equally successful, with excellent yields obtained at steady state (92% & 95%) for the reaction of 2-phenyl acetophenone with both benzyl and allylhalides (Table 3, entries 7 & 8). Finally, we examined the reactivity of 3-pentanone in this methodology. This is a particularly difficult substrate to undergo α-alkylation and can produce very low yields.[27] Gratifyingly, a good yield of 55% of the α-benzylated 3-pentanone was achieved at steady state (Table 3, entry 9). No evidence for the formation of additional side-products, for example, dialkylated product, was observed for this substrate. Finally, further purification is often not needed, but steady state yields translated very well to isolated yields (Table 3). In the case of cyclohexanone, the yield using flow chemistry is lower (34%) than that in batch (49%) (see ESI†), and investigations are ongoing to improve yields using symmetric ketones.

Having demonstrated the versatility of this protocol, our next challenge was to scale-out our reaction to generate an appreciable quantity of α-alkylated ketone using this methodology. The α-allylation of 2-phenyl acetophenone was chosen as the reaction to conduct these investigations (Scheme 2). Our previously optimised reactor configuration was altered to include a 10 mL sample loop, allowing for a significantly increased loading of LDA to our system. All other reaction parameters remained unchanged. Pleasingly, a yield of 96% of α-alkylated ketone at steady state[28] was achieved for this reaction, over a 45 min collection time.

## Conclusion

In conclusion, we provide an efficient methodology for the alkylation of ketones in continuous flow. Conveniently, commercial LDA can be used as a base in the deprotonation

**Table 3** α-Alkylation substrate scope using optimised parameters

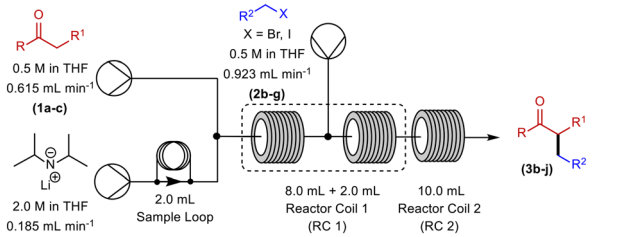


| Entry | Ketone | Electrophile | Product | Steady state[a] (yield%) | Isolated[b] (yield%) |
|---|---|---|---|---|---|
| 1 | 1a | 2b | 3b | 90 | 81 |
| 2 | 1a | 2c | 3c | 75 | 70 |
| 3 | 1a | 2d | 3d | 85 | 72 |
| 4 | 1a | 2e | 3e | 87 | 71 |
| 5 | 1a | 2f | 3f | 92 | 75 |
| 6 | 1a | 2g | 3f | 80 | 71 |
| 7 | 1b | 2b | 3g | 92 | 85 |
| 8 | 1b | 2f | 3h | 95 | 80 |
| 9 | 1c | 2b | 3i | 55 | 53 |

[a] Determined by use of $^1$H NMR with 1,3,5-trimethoxybenzene as internal standard. [b] Isolated yield after purification by column chromatography on $SiO_2$.

of several exemplar ketones along with a good variety of alkylhalides. The continuous flow protocol with good to excellent yields, provides numerous advantages over the corresponding batch reaction, including the avoidance of cryogenic temperatures, reduction in reaction time, lessening of side product formation and a convenient scale-out (>3 g of material in 45 min).

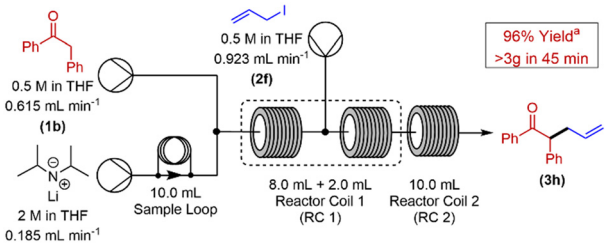


**Scheme 2** Continuous flow set-up for the scale out of 2-phenyl acetophenone α-allylation. [a]Determined by use of $^1$H NMR with 1,3,5-trimethoxybenzene as internal standard.

## Conflicts of interest

Vapourtec flow company helped in the early development of these reactions.

## Acknowledgements

Funding was provided through the IRC Enterprise Partnership Scheme (IRC EPSPG/2021/130) co-funded by Pfizer, Ringaskiddy, Ireland as the Industry Partner. We thank the Science Foundation Ireland (SFI/21/FFP-A/8784), and the Synthesis and Solid State Pharmaceutical Centre (SSPC) (SFI/12/RC/2275 and SFI/12/RC2275_P2). We thank D. Guthrie, C. Guthrie and R. C. Moses at Vapourtec for advice, and time on their instruments. We thank Dr Kishore Kumar for proof-reading this manuscript.

## Notes and references

1 J. E. McMurry, *Organic Chemistry*, Cengage Learning, Boston, 2015.
2 (*a*) B. M. Trost and I. Flemming, *Comprehensive Organic Synthesis*, Paragamon, Amsterdam, 1991; (*b*) J. Plaquevent, D. Cahard, F. Guillen and J. Green, *Science of Synthesis*, Georg Thieme Verlag, 2005, vol. 26, pp. 463–511; (*c*) A. R. Katritzky and R. J. K. Taylor, *Comprehensive Organic Functional Group Transformations II*, Elsevier, Amsterdam, 2005.
3 L. R. Liou, A. J. McNeil, A. Ramirez, G. E. S. Toombes, J. M. Gruver and D. B. Collum, *J. Am. Chem. Soc.*, 2008, **130**, 4859–4868.
4 (*a*) R. W. Dugger, J. A. Ragan and D. H. B. Ripin, *Org. Process Res. Dev.*, 2005, **9**, 253–258; (*b*) V. Farina, J. T. Reeves, C. H. Senanayake and J. J. Song, *Chem. Rev.*, 2006, **106**, 2734–2793; (*c*) G. Wu and M. Huang, *Chem. Rev.*, 2006, **106**, 2596–2616.
5 T. J. Donohoe, B. S. Pilgrim, G. R. Jones and J. A. Bassuto, *Proc. Natl. Acad. Sci. U. S. A.*, 2012, **109**, 11605–11608.
6 B. M. Trost and E. Keinan, *Tetrahedron Lett.*, 1980, **21**, 2591–2594.
7 B. M. Trost and J. Xu, *J. Am. Chem. Soc.*, 2005, **127**, 2846–2847.
8 B. M. Stoltz, N. B. Bennett, D. C. Duquette, A. F. G. Goldberg, Y. Liu, M. B. Loewinger and C. M. Reeves, in *Comprehensive Organic Synthesis II*, ed. P. Knochel, Elsevier, Amsterdam, 2014, pp. 1–55.
9 F. Mo and G. Dong, *Science*, 2014, **345**, 68–72.
10 (*a*) E. J. Corey and D. Enders, *Tetrahedron Lett.*, 1976, **17**, 11–14; (*b*) E. J. Corey and D. Enders, *Tetrahedron Lett.*, 1976, **17**, 3–6; (*c*) E. J. Corey and S. Knapp, *Tetrahedron Lett.*, 1976, **17**, 4687–4690.
11 R. Lazny and A. Nodzewska, *Chem. Rev.*, 2010, **110**, 1386–1434.
12 G. Stork, R. Terrell and J. Szmuszkovicz, *J. Am. Chem. Soc.*, 1954, **76**, 2029–2030.
13 T. Noël, J. R. Naber, R. L. Hartman, J. P. McMullen, K. F. Jensen and S. L. Buchwald, *Chem. Sci.*, 2011, **2**, 287–290.
14 S. L. Poe, M. A. Cummings, M. P. Haaf and D. T. McQuade, *Angew. Chem., Int. Ed.*, 2006, **45**, 1544–1548.
15 F. Gomollón-Bel, *Chem. Int.*, 2019, **41**, 12–17.
16 M. B. Plutschack, B. Pieber, K. Gilmore and P. H. Seeberger, *Chem. Rev.*, 2017, **117**, 11796–11893.
17 R. Porta, M. Benaglia and A. Puglisi, *Org. Process Res. Dev.*, 2016, **20**, 2–25.
18 M. Colella, A. Nagaki and R. Luisi, *Chem. – Eur. J.*, 2020, **26**, 19–32.
19 M. Baumann, T. S. Moody, M. Smyth and S. Wharry, *Org. Process Res. Dev.*, 2020, **24**, 1802–1813.
20 A. Hafner, P. Filipponi, L. Piccioni, M. Meisenbach, B. Schenkel, F. Venturoni and J. Sedelmeier, *Org. Process Res. Dev.*, 2016, **20**, 1833–1837.
21 J.-I. Yoshida, *Basics of Flow Microeactors Synthesis*, Springer, Tokyo, 2015.
22 M. Power, E. Alcock and G. P. McGlacken, *Org. Process Res. Dev.*, 2020, **24**, 1814–1838.
23 T. von Keutz, F. J. Strauss, D. Cantillo and C. O. Kappe, *Tetrahedron*, 2018, **74**, 3113–3117.
24 F. G. Bordwell and J. A. Harrelson Jr, *Can. J. Chem.*, 1990, **68**, 1714–1718.
25 H. Neuvonen, K. Neuvonen, A. Koch, E. Kleinpeter and P. Pasanen, *J. Org. Chem.*, 2002, **67**, 6995–7003.
26 We also generated LDA *in situ* in flow from *n*-BuLi and diisopropylamine and used it in the formation of α-benzylated propriophenone from propiophenone and BnBr. However the yield was lowered to 42%. Overall, it proved advantageous and more convenient to use titrated commercial LDA, as we observed no reliability issues.
27 G. A. Molander and C. del Pozo Losada, *J. Org. Chem.*, 1997, **62**, 2935–2943.
28 The product was sufficiently pure at this stage (see ESI† for details and spectra).